University of Alberta
Department of Civil &
Environmental Engineering

Structural Engineering Report No. 225

An Analysis of the Cyclic Behaviour of Steel Gusset Plate Connections

by

Scott Walbridge

Gilbert Y. Grondin

and

Roger J.J. Cheng

September, 1998

An Analysis of the Cyclic Behaviour of Steel Gusset Plate Connections

by

Scott Walbridge

Gilbert Y. Grondin

Roger J.J. Cheng

Structural Engineering Report 225

Department of Civil and Environmental Engineering
University of Alberta
Edmonton, Alberta

September 1998

ABSTRACT

This report summarizes a numerical investigation of the cyclic behaviour of gusset plate connections conducted using the finite element program ABAQUS. This numerical investigation consisted of two phases. In the first phase. models were constructed of previously tested gusset plate connections. incorporating framing members. nonlinear material behaviour. initial imperfections and bolt slip. In the second phase. the gusset plate models developed in the first phase were modified to include brace members. A parametric study was then conducted to examine the interaction between the gusset plate and the brace member and to determine the effect of load sequence on the behaviour of these models.

Based on the results of this investigation. conclusions are presented regarding: (1) the effects of various parameters on the cyclic behaviour of gusset plate connections. and (2) the potential of the "weak gusset plate – strong bracing member" concept proposed by Rabinovitch and Cheng (1993).

ACKNOWLEDGEMENTS

Funding for this research was provided through the Natural Sciences and Engineering Research Council, the University of Alberta, and the C.W. Carry for Steel Research.

TABLE OF CONTENTS

LIST OF TABLES

LIST OF FIGURES

1. INTRODUCTION

1.1 General

Several lateral load resisting systems have been developed for steel structures including concentrically braced frames (CBF's), eccentrically braced frames (EBF's), moment resisting frames (MRF's) and shear walls. Of these, concentrically braced frames (CBF's) are among the most commonly used due to their structural efficiency and the relative ease with which they may be designed, constructed, and repaired (Redwood and Jain, 1992). During the life of a structure, the lateral load resisting system may be called upon to dissipate energy imparted to the structure by earthquakes or strong winds. Although generally considered inferior to EBF's in terms of their energy dissipation potential, CBF's can be designed to dissipate significant amounts of energy. CBF's consist of beams and columns for resisting gravity loads, braced with inclined lateral bracing members that can adopt several configurations including diagonal bracing, cross-bracing, or chevron bracing (see Figure 1.1). Gusset plates are commonly used in CBF's to connect the lateral bracing members to the beams and columns (see Figure 1.2).

Due to the complex behaviour of the gusset plate in this type of system, the design of gusset plate connections has traditionally involved highly simplified methods (see Whitmore, 1952; Hardash and Bjorhovde, 1984; Thornton, 1984). Although these methods have proven to be adequate, it is believed that the factor of safety associated with their usage is highly variable (Kulak et al., 1987). Up until recently the majority of

the research on gusset plates has focused on elastic stress distributions or the inelastic behaviour of gusset plates loaded monotonically in tension. Relatively little attention has been given to compressive or cyclic behaviour.

Typically, CBF's are designed to dissipate energy through yielding or buckling of the brace members. The remaining members and connections are designed to carry the forces that are present in the structure at the load level that causes the brace member to yield or buckle. This design approach embodies the philosophy of capacity design (Redwood and Jain, 1992). A recent study of gusset plate behaviour carried out at the University of Alberta (Rabinovitch and Cheng, 1993) showed that under cyclic loading the tensile capacity of the gusset plate remains stable and the post-buckling compressive capacity of the gusset plate, although less than the load required to buckle the gusset plate initially, tends to stabilize after a few cycles. Based on these observations, a design approach that would take advantage of the energy dissipation potential of the gusset plate was proposed. This approach, referred to as the "weak gusset plate – strong brace member" concept, consists of designing the gusset plate as the weak element rather than the brace member.

A better understanding of the cyclic behaviour of gusset plates will facilitate the development of gusset plate design guidelines that better reflect their true behaviour. This may allow for the design of gusset plate connections with a more consistent safety index than is generally associated with the current design approach. It is also felt that a better understanding of the energy dissipation characteristics of gusset plate connections

under cyclic loading may lead to an alternative CBF design approach that takes advantage of the energy dissipation potential of the gusset plate.

1.2 Objectives

The objectives of the numerical investigation presented in this report are:

(1) to develop and validate finite element models that accurately predict the behaviour of steel gusset plate connections under monotonic and cyclic loading; and,

(2) to expand the finite element models developed in (1) to include brace members and to use these subassembly models to study the effects of gusset plate – brace member interaction and load sequence on the behaviour of steel gusset plate connections under cyclic loading.

1.3 Scope

The scope of the work presented in this report has been limited to the study of steel gusset plates geometrically similar to those tested previously at the University of Alberta. These gusset plates were corner gusset plates, either 500 mm x 400 mm or 550 mm x 450 mm, ranging in thickness from 6.18 mm to 13.3 mm. The factors affecting the behaviour of gusset plate connections that are the focus of this investigation include gusset plate thickness, material properties, bolt behaviour, and the usage of gusset plate edge stiffeners. In the later part of this investigation (the parametric study), load sequence and

the effect of gusset plate – brace member interaction are also examined. The aspects of the connection behaviour that are the focus of this study include general behaviour (both pre- and post-buckling) and energy dissipation characteristics.

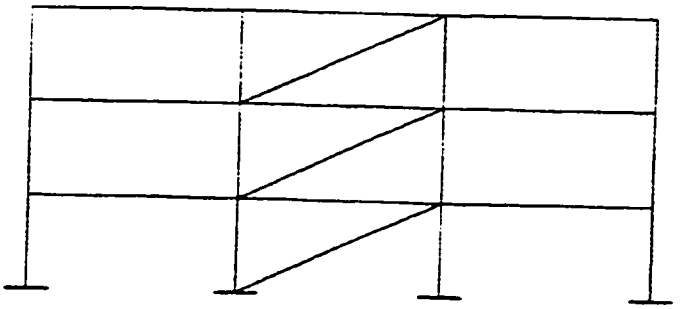

a) Diagonal Bracing

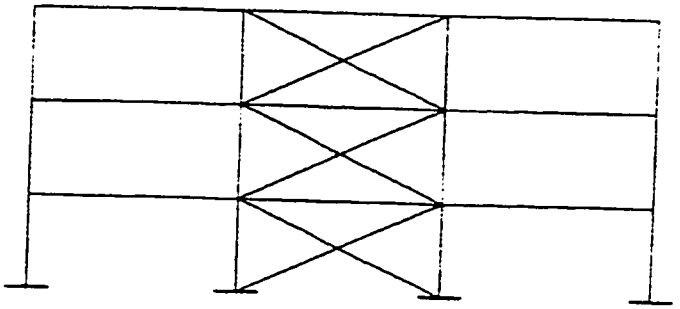

b) X-bracing

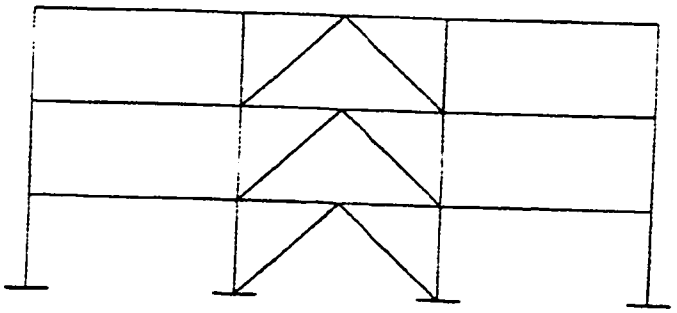

c) Chevron Bracing

Figure 1.1 - Various configurations for concentric braced frames.

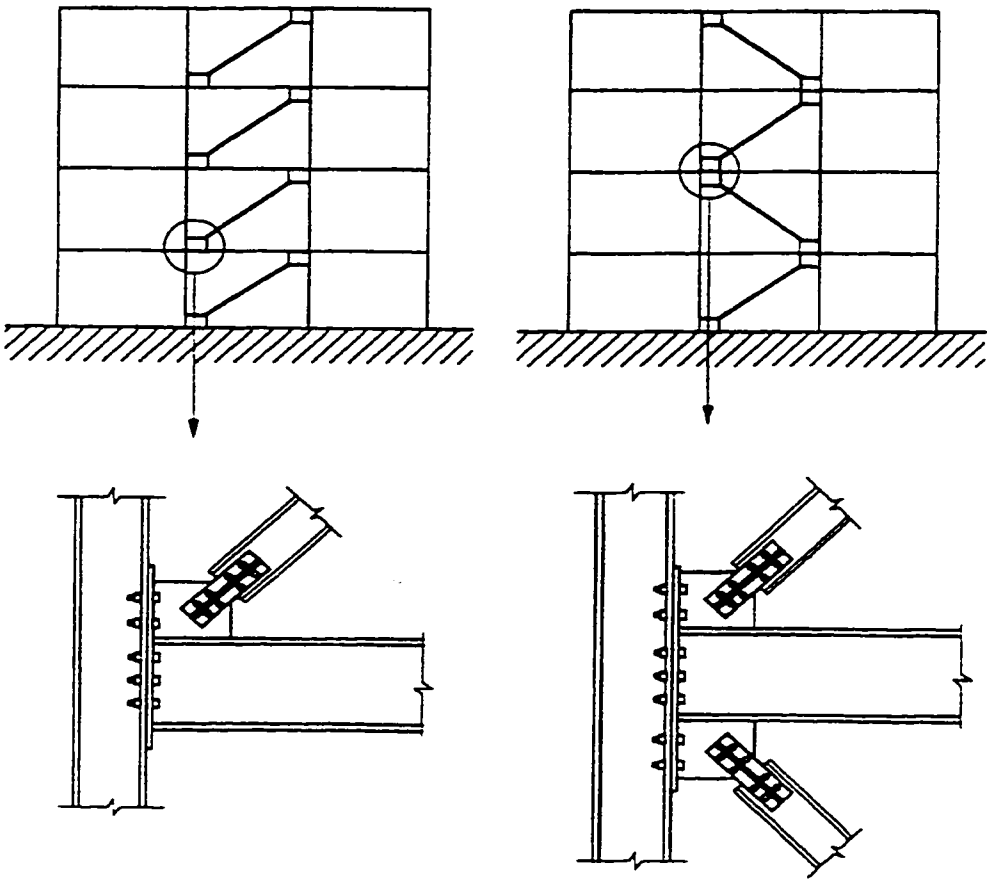

Figure 1.2 - Typical concentric braced frames.

2. LITERATURE REVIEW

2.1 Elastic Behaviour of Gusset Plates

In 1952, Whitmore reported the results of an experimental investigation in which he studied the stress distribution in a gusset plate connection detail commonly found in Warren truss type bridges. The main objectives of Whitmore's investigation were to determine the location and magnitude of the peak stress in the gusset plate, and to develop a practical method for estimating this peak stress for use in structural design.

Whitmore's experimental investigation primarily involved the measurement of strains in quarter scale aluminum gusset plate models loaded in the elastic range. Whitmore also studied stress distributions on masonite and bakelite gusset plate models using stresscoats and photoelastic methods. He determined that the location of the peak stress in the gusset plate usually occurs near the last row of fasteners in the gusset-to-brace connection. He also determined that the direct, bending and shear stress distributions across critical sections of the gusset plate did not compare well with values determined using the previously popular beam method. The beam method did, however, provide a conservative estimate of the peak stress.

Based on the results of his investigation, Whitmore proposed a method for predicting the peak stress in a gusset plate for a given brace load. He proposed that the peak stress could be estimated by taking the brace load and dividing it by an area equal to the plate

thickness times what later became known as the "Whitmore effective width". The Whitmore effective width is defined as the distance between two lines radiating outward at 30 degree angles from the first row of bolts in the gusset-to-brace connection along a line running through the last row of bolts (see Figure 2.1). Whitmore showed that the resulting stress corresponded well with test results.

In 1957, Irvan carried out a similar investigation with an aluminum model of a double gusset plate Pratt truss connection detail. Once again, his investigation showed that stress distributions computed with the beam method did not match well with test results. Irvan proposed a method of determining the peak stress that was similar to the Whitmore method.

Hardin (1958), Davis (1967), Varsarelyi (1971) also investigated the stresses in gusset plates loaded in the elastic range. Hardin's experimental investigation confirmed Irvan's conclusions regarding the beam method and supported Irvan's method for determining the magnitude of the peak stress in the gusset plate. Davis and Varsarelyi carried out finite element investigations of the elastic stresses in gusset plates. In general, these investigations confirmed the findings of the experimental investigations regarding the stresses in gusset plates loaded in the elastic range.

2.2 Inelastic Behaviour of Gusset Plates

2.2.1 Monotonic Loading

Chakrabarti and Bjorhovde (1983) studied the behaviour and strength of gusset plates loaded beyond the elastic range, in monotonic tension. Current design practices (including a yield criterion based on the Whitmore method) were evaluated using test results.

The test program conducted by Chakrabarti and Bjorhovde involved six gusset plate specimens loaded in monotonic tension. Two gusset plate thicknesses (9.6 mm (3/8 in.) and 3.2 mm (1/8 in.)) and three brace angles (30, 45 and 60 degrees) were tested. Due to limitations of the testing equipment, only the 3.2 mm specimens were loaded to failure.

Chakrabarti and Bjorhovde found that the primary failure mode for the test specimens was tearing of the gusset plate across the last row of bolt holes in the gusset-to-brace connection. Tearing of the gusset-to-frame fasteners was found to occur in specimens where the Whitmore effective width intercepted the boundaries of the plate. Based on their test results, Chakrabarti and Bjorhovde concluded that a yield criterion based on the Whitmore method (i.e. with yield occurring at the brace load that causes the Whitmore peak stress to exceed the yield strength of the material) was appropriate for the design of gusset plates. Recommendations for future work included further study of the influence of plate boundaries, including the use of stiffeners along the free edges.

Hardash and Bjorhovde (1984) developed an ultimate strength design procedure for gusset plates loaded in monotonic tension. Based on the results of tests on 42 gusset plate specimens tested at the University of Arizona, the University of Illinois and the University of Alberta, a block shear model was proposed. It was found that the ultimate strength can be taken as the sum of the ultimate tensile strength of the gusset plate between the bolts in the last row of bolts and the shear strength along the connection length. This can be expressed as:

$$R_n = F_u S_{net} t + 1.15 F_{eff} L t \qquad (2.1)$$

where F_u is the ultimate tensile strength of gusset plate material. S_{net} is the net width of gusset-to-brace connection as shown in Figure 2.2. L is the length of gusset-to-brace connection (see Figure 2.2). t is the gusset plate thickness, and F_{eff} is a uniform effective shear stress given as:

$$F_{eff} = (1-C_1)F_y + C_1 F_u \qquad (2.2)$$

where F_y is the yield strength of the gusset plate material and C_1 is given as:

$$C_1 = 0.95 - 0.047L \text{ (with L in inches)} \qquad (2.3)$$

The mode of failure that was found to be most prevalent in this test program was tensile tearing along the last row of bolt holes.

In an article published in 1984, Thornton took an in-depth look at a steel gusset plate connection design example, demonstrating the application of an intuitive, lower bound solution method for determining the ultimate capacity of the connection in tension and in compression. Thornton defined a lower bound solution as one in which: (1) equilibrium is satisfied, and (2) all stresses are below yield. He qualified this definition by adding that members must be stocky enough to preclude buckling.

Thornton used the block shear method in his example to check the tear-out strength of the gusset plate connection and proposed a lower bound method for determining compressive strength of the gusset plate. Thornton's proposed method for determining compressive strength uses a unit strip with a characteristic length equal to the largest of L1, L2, or L3 (see Figure 2.3) and an effective length factor, k = 0.65, from which the elastic buckling capacity of the unit strip is calculated. Multiplying this capacity by the Whitmore width gave what Thornton said should be a conservative estimate of the compressive strength of the gusset plate. Thornton suggested that a shorter effective length (such as the average of lengths L1, L2, and L3) might be more appropriate for approximating the buckling strength of the gusset plate.

Using simple statics, Thornton demonstrated that it may not be critical for the centerline of the diagonal brace to pass through the center of the beam-column connection.

especially in high-rise structures where diagonal braces carry primarily lateral loads and are typically much smaller than the beams and columns. This means that under certain conditions gusset plate connections can be designed to be more compact (see Figure 2.4).

Williams and Richard (1986) performed analytical and experimental work to develop design procedures for gusset plate connections in diagonal braced frames. Their work focused on the distribution of forces in the gusset-to-frame and gusset-to-brace fasteners. A finite element analysis of several CBF connections was performed to study these forces. A procedure for developing two dimensional fastener elements was developed. The procedure involves the following steps:

(1) isolate the fastener from the real structure.

(2) design fastener tests to duplicate the forces and deformations that occur in the real structure.

(3) perform fastener tests to obtain force-deformation data.

(4) fit curves to the test data. and use the fitted curves as input parameters for nonlinear spring elements.

The nonlinear behaviour of the gusset plate material was modeled in this investigation. A linear-elastic material model was used for the framing members. however. to ensure that yielding was confined to the gusset plate and fasteners.

Williams and Richard found that frame action had a significant effect on the gusset-to-frame fastener force distributions. A comparison of models that included the frame members and models that did not suggested (according to Williams and Richard) that the frame should be incorporated in finite element models of this type.

Factors that were found to have little effect on fastener force distributions included: compressive versus tensile brace loads, brace configuration, beam and column properties, gusset-to-frame fastener type, and brace eccentricity. Factors that were found to have a significant effect on fastener force distributions included: gusset plate aspect ratio, brace load, and brace angle. Gusset plates were found to cause beam-to-column connections to act rigidly. Fastener force distributions were found to be more uniform in the more compact gusset plates, where small amounts of in-plane eccentricity were permitted (i.e. the centerline of the diagonal brace was not made to pass through the center of the beam-to-column connection). Fastener force design equations were proposed.

Williams and Richard also included linear elastic buckling in their investigation. A method for estimating compressive capacity was proposed in which the buckling load is calculated using Thornton's unit strip approach in conjunction with column design equations. This buckling load is then compared with the yield load predicted using the Whitmore effective width and the lesser of the two is taken to be the compressive capacity of the gusset plate. To increase compressive capacity, it was proposed that gusset plate thickness be increased, gusset plate dimensions be reduced, or gusset plate free edge stiffeners be incorporated.

Gross (1990) presented findings from monotonic tests on three variations of a particular gusset plate connection detail. The tests were conducted to study:

(1) the influence of framing members on the strength and behaviour of the gusset plate connection:

(2) the effect of in-plane connection eccentricity on the gusset plate capacity and on the forces transferred to the framing members; and

(3) the difference between a gusset plate connection made to the column flange as opposed to one made to the column web.

Gross found that the yield load determined using the Whitmore method seemed to correspond well with the observed yield load. Thornton's method for estimating the compressive strength of the gusset plate was found to be sufficiently conservative when an effective length factor, k, of 0.5 was used. He also found that his compact specimens (with in-plane eccentricity) had a higher buckling load than the less compact specimen (designed to have no in-plane eccentricity). The orientation of the column (i.e. gusset plate connected to column flange vs. gusset plate connected to column web) had little effect on the buckling load.

Hu and Cheng (1987) and Yam and Cheng (1993) carried out tests to study the buckling behaviour of gusset plate connections under monotonic compressive loading. These tests are described in section 2.3.

2.2.2 Cyclic Loading

Compared to the information that is available on the cyclic behaviour of the brace members in braced frames, the amount of work that has been done to investigate the cyclic behaviour of gusset plates is quite small.

Jain, Goel and Hanson (1978) studied the effect of gusset plate bending stiffness and bracing member length on the cyclic behaviour of bracing members. The focus of their investigation was on the behaviour of the brace member, however some observations were made regarding the interaction between the brace member and the gusset plate. Their investigation included 18 tests on different gusset plate – brace member combinations. In all cases the brace member was a 25.4 mm x 25.4 mm x 2.76 mm steel hollow structural section. Three different gusset plates were used and the length of the brace member was varied. Figure 2.5 shows a typical gusset plate – brace member specimen tested by Jain, Goel and Hanson (1978). All of the gusset plates were designed to have a yield strength greater than the yield strength of the brace member. The flexural stiffness was computed for all gusset plates and brace members, and the ratio, R, of the gusset plate flexural stiffness to the brace member flexural stiffness was computed for each specimen, as well as an effective brace member slenderness (kL/r). Jain, Goel and Hanson concluded that there is no advantage in making the flexural stiffness of the gusset plate greater than the flexural stiffness of the brace member (i.e. $R > 1.0$). However, for a given brace member length, the effect of increasing the flexural stiffness of the gusset plate is to decrease the effective brace member slenderness, by decreasing the effective

length factor, k. This has the same effect as reducing the brace member length, which results in an improvement in the cyclic behaviour of the brace member.

Astaneh, Goel and Hanson (1981) studied the cyclic behaviour of brace members connected to gusset plates. Again, the focus of their investigation was on brace member behaviour. In-plane and out-of-plane buckling of the brace members was investigated. Figure 2.6 shows a typical specimen. As can be seen in this figure, the brace members were composed of back-to-back double angles tied with stitches. Astaneh, Goel and Hanson expressed concerns regarding the current code design procedures. Practical design procedures for improving brace member ductility and energy dissipation characteristics were proposed. For brace members that buckle out-of-plane, they stress the importance of designing the gusset plates so that they accommodate the formation of plastic hinges, allowing brace buckling to take place without tearing of the connection. Their test program involved 16 specimens with gusset plates connected by bolts and fillet welds.

Rabinovitch and Cheng (1993) carried out tests to study the behaviour of gusset plate connections under cyclic loading. These tests are described in the next section.

2.3 Tests at the University of Alberta

This section presents the results of three experimental investigations conducted at the University of Alberta to study the behaviour of gusset plate connections. Hu and Cheng

(1987) investigated the buckling behaviour of thin corner gusset plates loaded monotonically in compression. Yam and Cheng (1993) carried out a similar investigation with thicker gusset plate specimens that exhibited inelastic behaviour prior to buckling. Rabinovitch and Cheng (1993) extended the Yam and Cheng test program to include the effect of cyclic loading on the behaviour of corner gusset plates. Some of the results from the investigations of Yam and Cheng (1993) and Rabinovitch and Cheng (1993) were used to validate the finite element model developed for this report. These results are summarized.

2.3.1 Hu and Cheng (1987)

Hu and Cheng (1987) studied the buckling behaviour of gusset plate connections loaded monotonically in compression. Their test program focused on the effects of plate thickness, geometry, boundary conditions, eccentricity and reinforcement. This test program included 14 tests on six thin gusset plate specimens. A parametric study was subsequently performed using the finite element method.

Hu and Cheng found that thin gusset plates tended to buckle at a load much lower than the yield load predicted using the Whitmore effective width. In general, either sway or local buckling modes were observed depending on the out-of-plane brace restraint conditions. The parametric study indicated that an increase in the stiffness of the gusset-to-brace splice plate should result in an increase in the buckling strength of the gusset plate up to a splice plate thickness of two to four times the gusset plate thickness. It was

recommended that gusset plate connections of this type should be designed so that the distance between the end of the splice plate and the gusset-to-frame boundaries is kept to a minimum. It was also recommended that the interaction between the gusset plate and the brace member be investigated.

2.3.2 Yam and Cheng (1993)

Yam and Cheng (1993) presented the results of a test program designed to study the compressive behaviour and ultimate strength of gusset plate connections. The parameters studied in this investigation included: gusset plate thickness and size, brace angle, out-of-plane brace restraint conditions, moments in the framing members and out-of-plane eccentricity of the brace load. The specimens tested by Yam and Cheng were stockier than those tested by Hu and Cheng, and, as a result, tended to show significantly more inelastic behaviour prior to buckling. Figure 2.7 shows one of the test frames used by Yam and Cheng with a typical specimen in place.

Yam and Cheng found that the compressive capacity of the specimens that they tested was almost directly proportional to the thickness of the gusset plate. They also found that the effect of beam and column moments on the compressive capacity of the specimens was small, although these moments did have some effect on the measured strain distributions in the gusset plate. Yam and Cheng found Thornton's method to give a conservative estimate of compressive capacity. They recommended that a parametric

study be performed to determine "important design variables" so that a rational design procedure may be developed.

Some of the results of the gusset plate tests done by Yam and Cheng were used to validate the finite element models developed for the numerical investigation described in Chapter 3. The test results for these specimens are summarized in Table 2.1. Axial load versus out-of-plane displacement plots for these specimens are presented in Figure 2.8.

2.3.3 Rabinovitch and Cheng (1993)

Rabinovitch and Cheng carried out a test program to study the cyclic behaviour of steel gusset plate connections. The effects of gusset plate thickness, geometry, edge stiffeners, and bolt slip were studied. The test frame used by Rabinovitch and Cheng was intended to model a CBF connection for which the gusset plate was designed to buckle before the brace member. The beam, column and gusset plate subassembly was free to slide out-of-plane while the brace member was restrained. It was assumed that infinite rotational restraint was provided by the brace (i.e. the brace was assumed to have a much greater bending stiffness than the gusset plate). This meant that yielding and buckling of the gusset plate dissipated all of the energy introduced by the cyclic load. The beam and column forces, which would be present in an actual frame, were ignored. Figure 2.9 shows the test frame used by Rabinovitch and Cheng with a typical specimen in place. Five full-scale specimens were tested.

Rabinovitch and Cheng found that cyclic loading causes the compressive strength of the gusset plate to drop to a stable post-buckling level. but has little effect on the tensile strength. The addition of edge stiffeners was shown to significantly improve the post buckling compressive strength and the energy dissipation characteristics of the gusset plates tested. A parametric study was recommended to improve edge stiffener design.

Some of the results of the gusset plate tests performed by Rabinovitch and Cheng were used to validate the finite element model developed for the numerical investigation described in Chapters 3 and 4. The test results by Rabinovitch and Cheng that were used for the validation of the finite element model are summarized in Table 2.2. Axial load vs. axial deflection hysteresis plots for these specimens are presented in Figure 2.10.

2.4 Current Design Practice

As mentioned previously. CBF's are typically designed to dissipate energy imparted to the structure through yielding or buckling of the brace members. The remaining members and connections are designed so that they are able to carry the forces that are present in the structure at the load level that causes the brace members to yield or buckle. Thus. gusset plates in a CBF are typically designed to resist a tensile load equivalent to the load required to yield the lateral bracing member in tension. This forms the basis for plate thickness selection. The number of bolts required in the connection is usually the main factor determining the in-plane dimensions of the gusset plate. Under compressive

load an approach such as the one proposed by Thornton is typically used to ensure that the gusset plate does not buckle before the lateral bracing member.

Clauses pertaining to the design of gusset plate connections in CAN/CSA-S16.1-94 – Limit States Design of Steel Structures (1995) are for the most part performance oriented rather than prescriptive in nature. Several clauses in CAN/CSA S16.1 (1995) are, however, worthy of note:

1) Clause 13.4.3 recommends that the tensile resistance of a gusset plate should be determined using the CAN/CSA S16.1 (1995) block shear formulas. These formulas are essentially a variation of the block shear formulas proposed by Hardash and Bjorhovde (1984).
2) Clause 27.4.4.1 recommends that eccentricities in bracing connections be minimized. This is good engineering practice, although Thornton (1984) showed that it is not essential to eliminate eccentricity all together.
3) Clause 27.4.4.2 recommends minimum strengths for brace connections in tension. In zones with heavy seismic activity (velocity and acceleration related seismic zones of 3 or higher), the minimum strength is governed by capacity design, i.e. the factored resistance of the connection must exceed the yield strength of the brace member. In lighter seismic zones, this criterion is relaxed somewhat.
4) Clause 27.4.4.3 recommends that gusset plates be detailed in such a manner as to avoid brittle fracture when the brace member buckles, either in-plane or out-of-plane. The recommendations of this clause (and the associated commentary) fall in line with

the recommendations of Astaneh, Goel and Hanson (1981). Rabinovitch and Cheng (1993) suggest that these recommendations may not apply for corner gusset plates such as the ones they tested and in fact, that detailing corner gusset plates in accordance with these recommendations may actually hinder their performance.

CAN/CSA-S16.1-94 recommends that seismic design of structures be done in accordance with the National Building Code of Canada (NRCC, 1995). CAN/CSA-S16.1–94 provides criteria for classifying CBF's into three ductility categories: ductile, nominally ductile, or a third category for which no special provisions are made for ductility. These categories affect the design seismic loads assessed in accordance with the National Building Code of Canada.

The National Building Code of Canada (NRCC, 1995), section 4.1.9, gives guidelines for seismic design of structures. Most of this section is related to the assessment of the lateral design loads for the seismic design of structures. The magnitude of these lateral loads depends on, among other things, the ductility of the structure and the earthquake zone in which the structure is located. A discussion of how this building code and others handle the seismic design of CBF's can be found in Redwood and Jain (1992).

Table 2.1 - Summary of Yam and Cheng (1993) specimens.

Specimen	Plate Size (mm)	Material Properties			Performance	
		Modulus of Elasticity (MPa)	Yield Strength (MPa)	Ultimate Strength (MPa)	Ultimate Tensile Load (kN)	Ultimate Compressive Load (kN)
GP1	500 x 400 x 13.3	207600	295	501	-	1956
GP2	500 x 400 x 9.8	210200	305	465	-	1356
GP3	500 x 400 x 6.5	196000	275	467	-	742

Table 2.2 - Summary of Rabinovitch and Cheng (1993) specimens.

Specimen	Plate Size (mm)	Material Properties			Performance	
		Modulus of Elasticity (MPa)	Yield Strength (MPa)	Ultimate Strength (MPa)	Ultimate Tensile Load (kN)	Ultimate Compressive Load (kN)
A1	550 x 450 x 9.32	206000	449	537	1794	1682
A2	550 x 450 x 6.18	206000	443	530	1340	1128
A3	550 x 450 x 9.32 *	206000	449	537	1884	2004
A4	550 x 450 x 6.18 *	206000	443	530	1265	1149

* *stiffened edges*

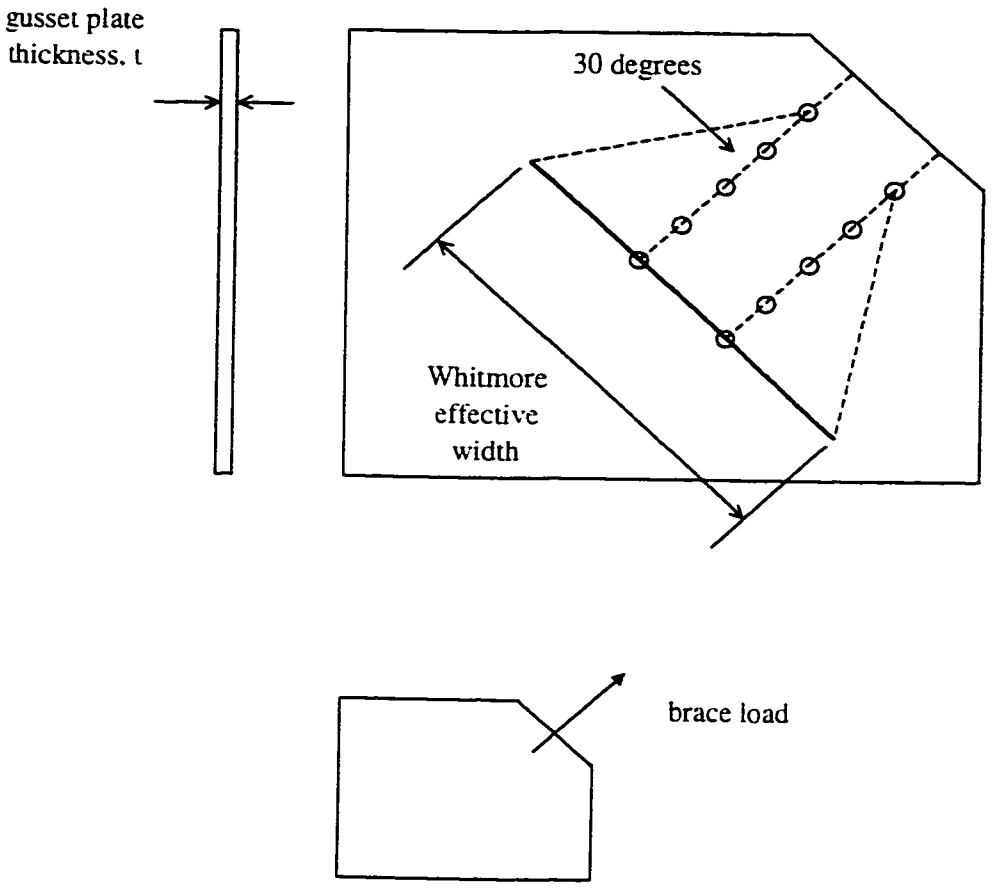

peak stress = (brace load) / ((Whitmore effective width) x (t)

Figure 2.1 - Explanation of Whitmore method for predicting peak stress in gusset plate.

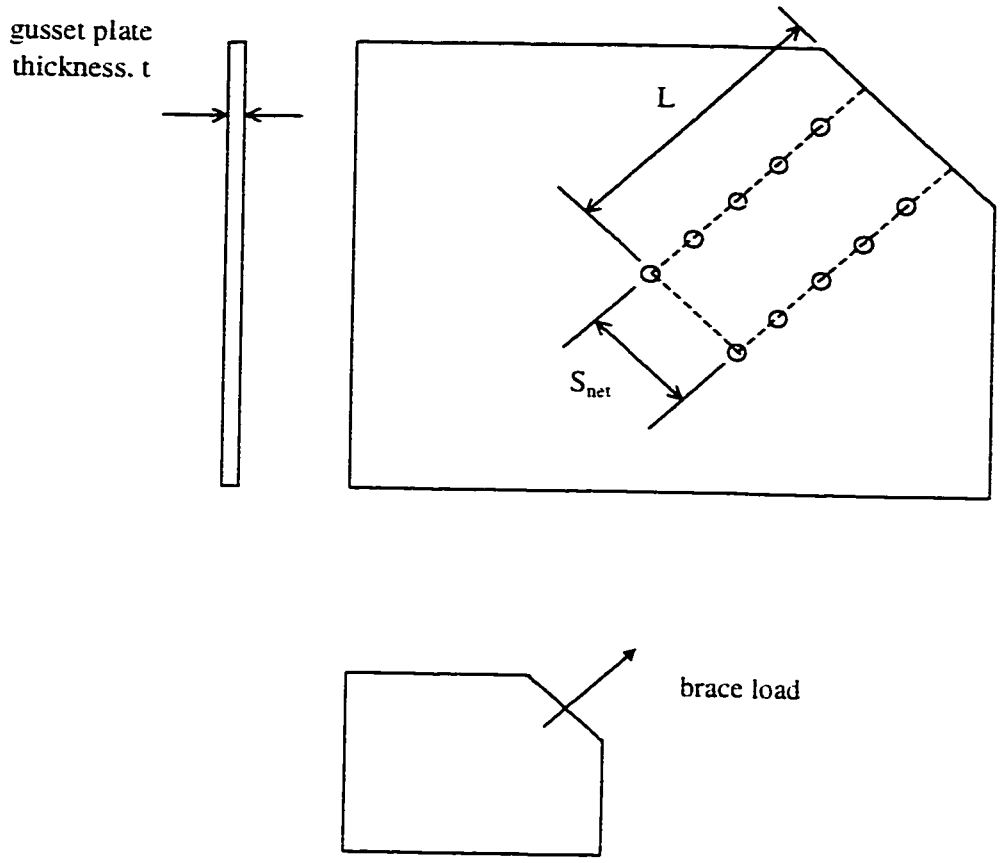

$$F_{eff} = (1-C_1)F_y + C_1F_u$$

$$C_1 = 0.95 - 0.047L$$

$$\text{brace load}^* = F_uS_{net}t + 1.15F_{eff}Lt$$

** to cause gusset plate tear-out failure*

Figure 2.2 - Explanation of block shear method for predicting tear-out strength of gusset plate.

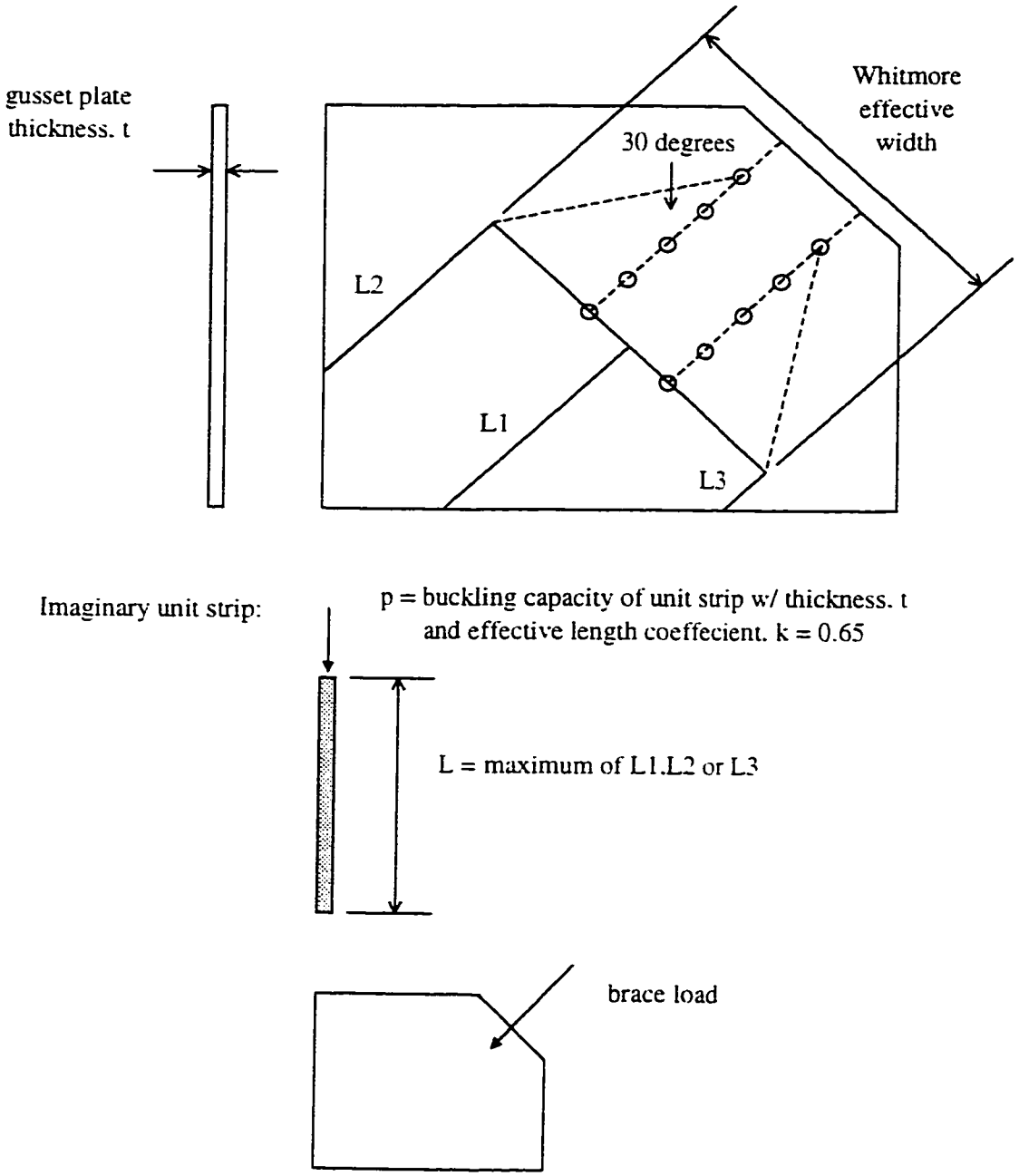

Figure 2.3 - Explanation of Thornton method for predicting buckling capacity of gusset plate.

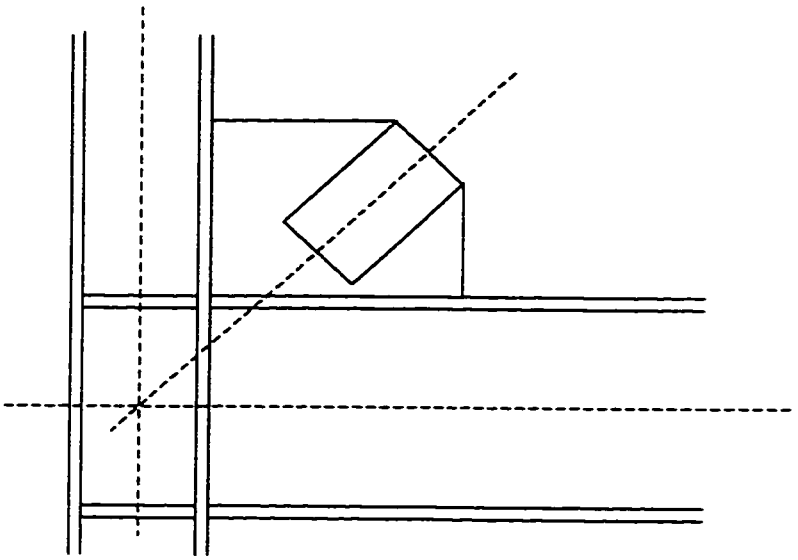

(a) gusset plate connection detail with no in-plane connection eccentricity

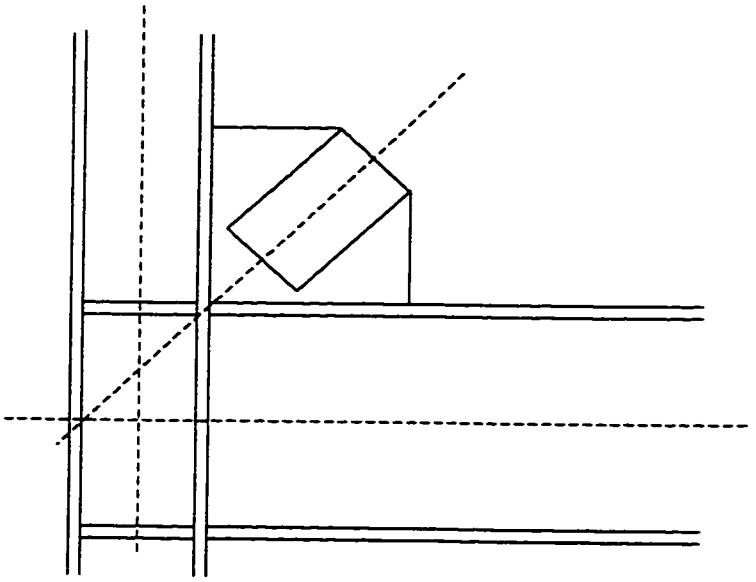

(b) "compact" gusset plate connection detail with in-plane connection eccentricity

Figure 2.4 - Explanation of in-plane connection eccentricity.

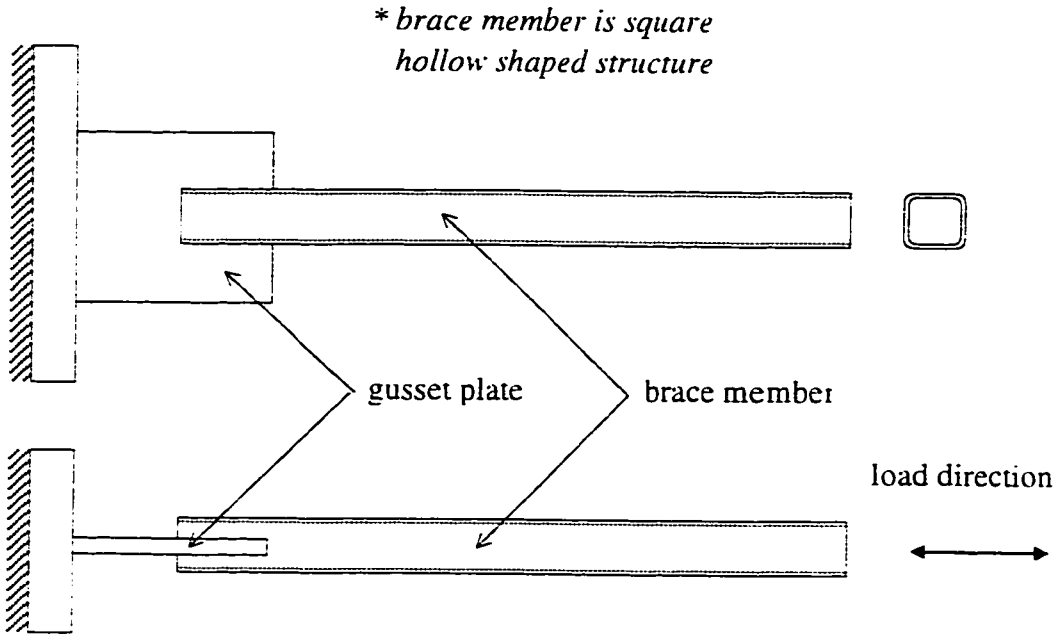

Figure 2.5 - A typical test specimen from Jain, Goel and Hanson, 1978.

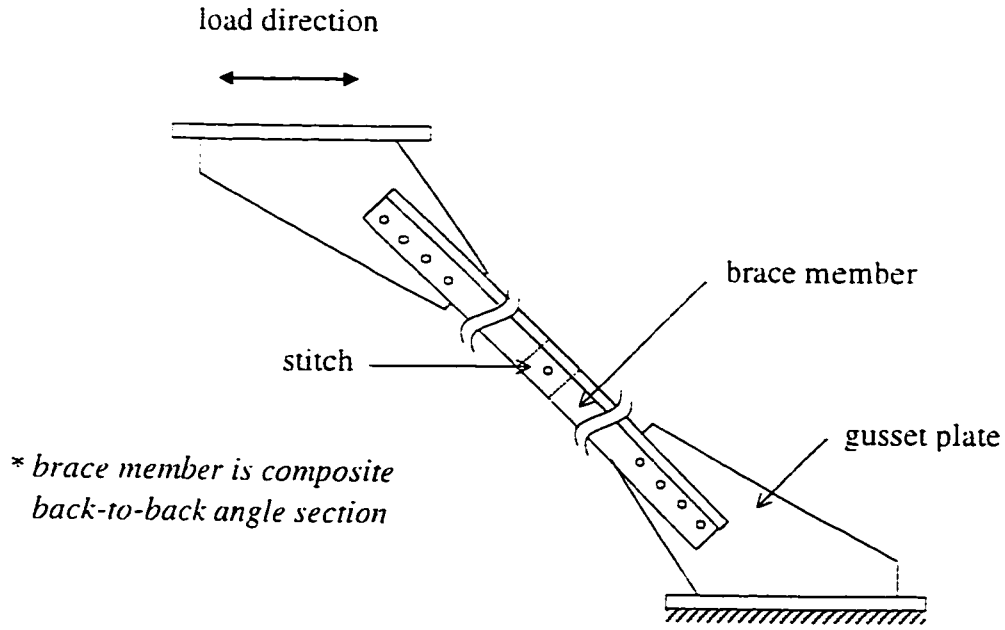

Figure 2.6 - A typical test specimen from Asteneh, Goel and Hanson, 1981.

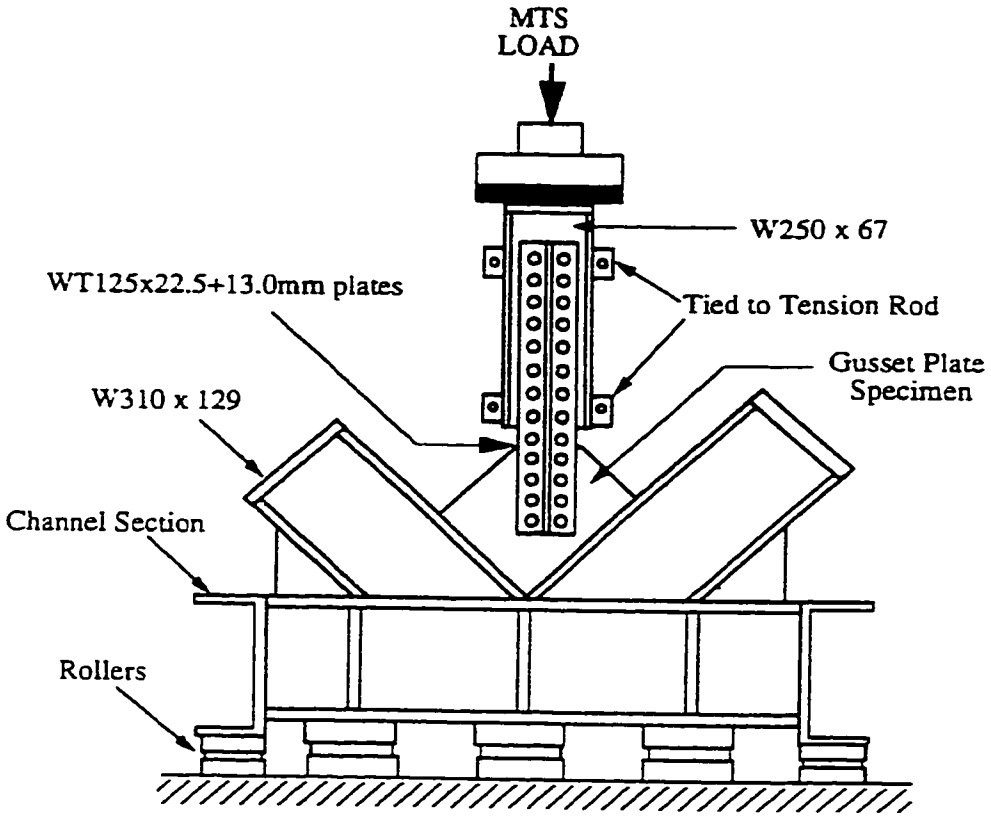

Figure 2.7 - One of the test frames used by Yam and Cheng, 1993.

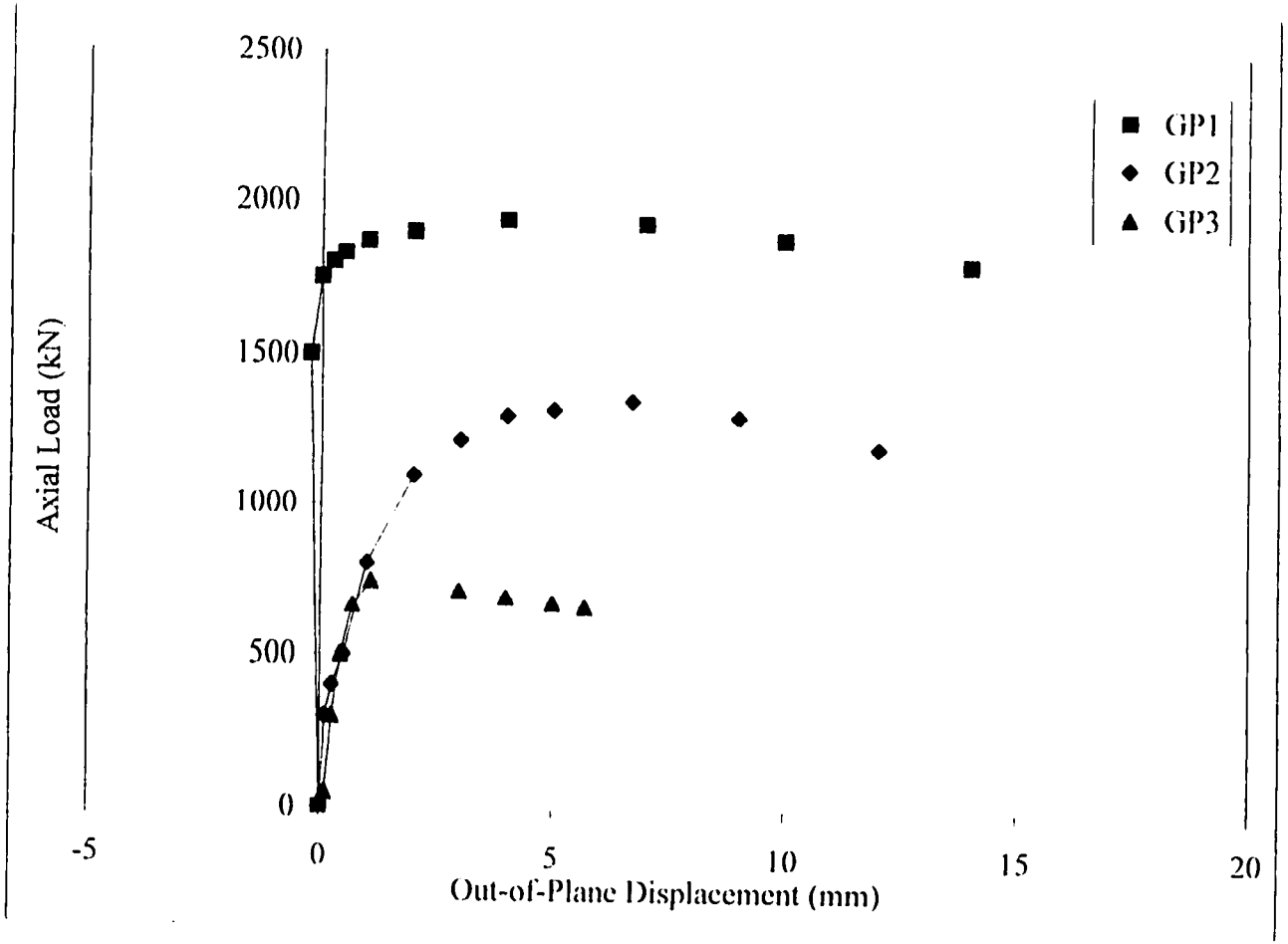

Figure 2.8 - Axial load versus out-of-plane displacement plots for Yam and Cheng (1993) specimens.

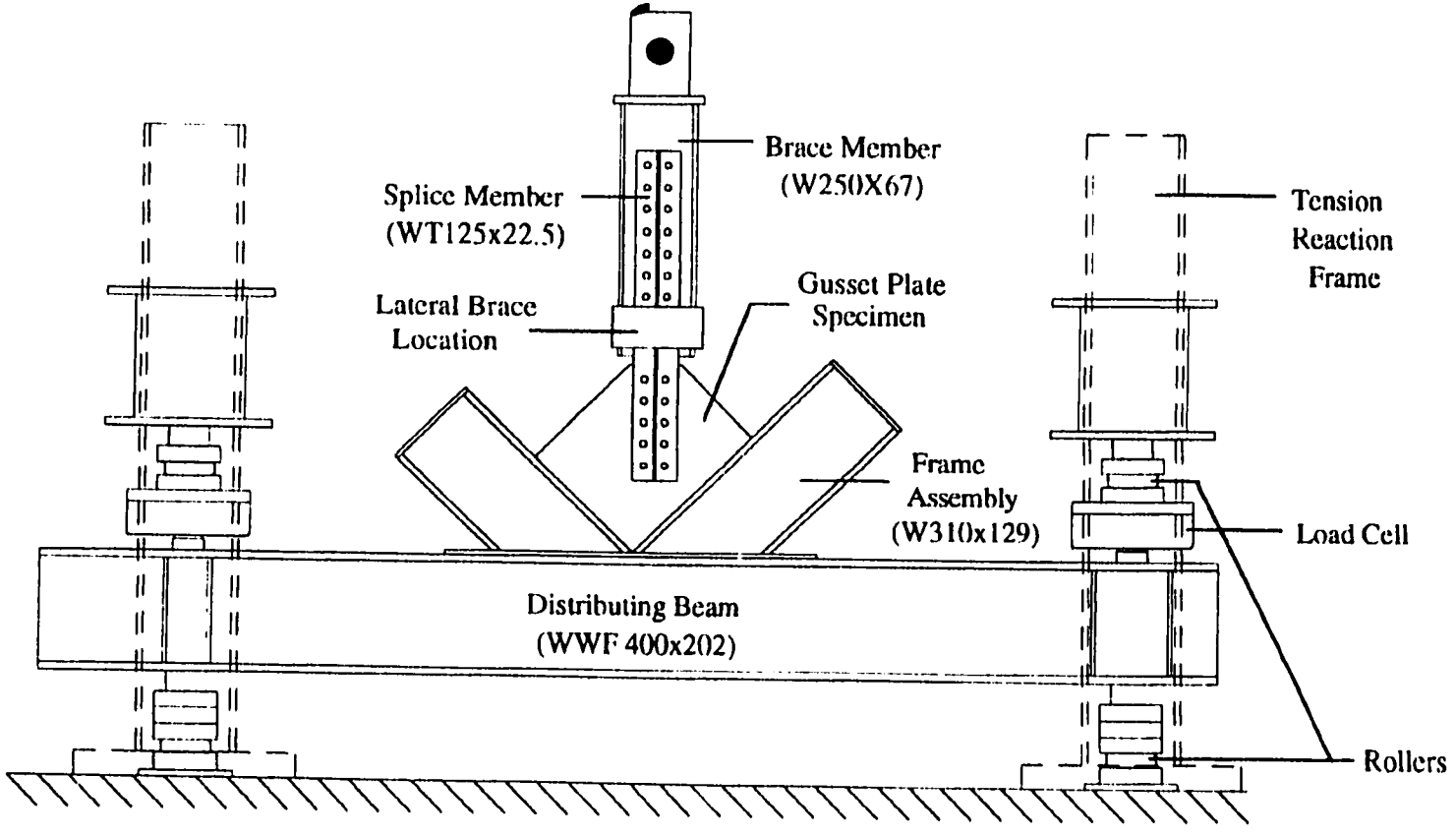

Figure 2.9 - Test frame used by Rabinovitch and Cheng, 1993.

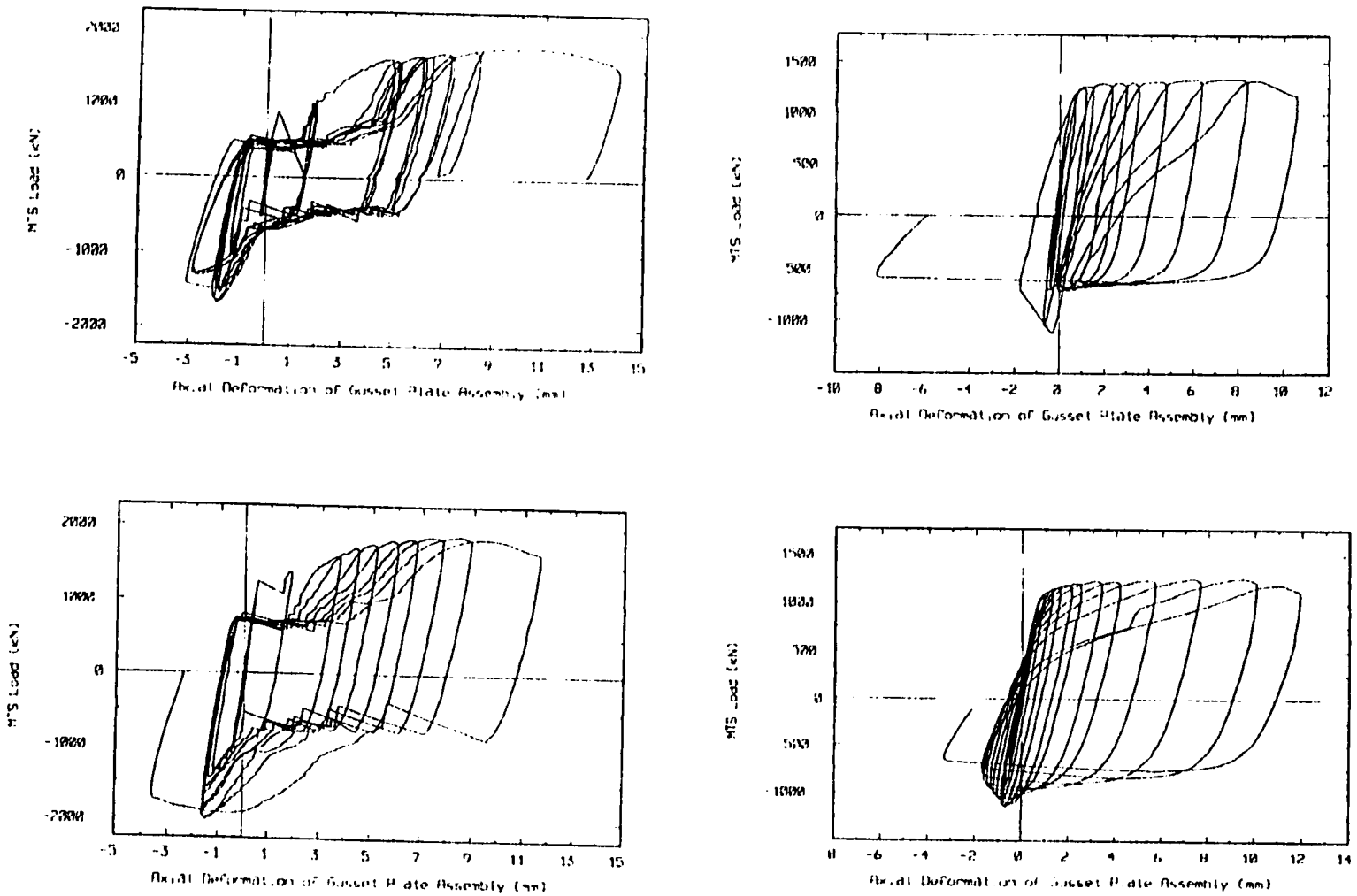

Figure 2.10 - Axial load vs. axial displacement hysteresis plots for Rabinovitch and Cheng (1993) specimens.

3. FINITE ELEMENT ANALYSIS

3.1 Introduction

In the next 3 chapters, a numerical investigation of the behaviour of gusset plate connections, performed using the finite element program ABAQUS (1995), version 5.5, will be described and the results of the investigation presented. The investigation was comprised of two phases. In the first phase, finite element models were developed to predict the behaviour of gusset plate connections under monotonic and cyclic loading. In this phase, the models were validated with data from the experimental investigations of Yam and Cheng (1993) for gusset plates under monotonic compressive loading, and Rabinovitch and Cheng (1993) for gusset plates under cyclic loading. In the second phase of the investigation, the finite element models were expanded to include brace members and a parametric study was conducted, using these subassembly models, to study the effects of gusset plate – brace member interaction and load sequence on the behaviour of steel gusset plate connections under cyclic loading.

This chapter focuses on the development of the finite element models used in the first phase of the investigation. The validation of these models will be presented and discussed in Chapter 4. The parametric study is presented in Chapter 5. The basic steps involved in the first phase of the investigation were as follows:

(1) A linear elastic mesh study of a gusset plate connection was performed to determine the level of mesh refinement required to ensure convergence.

(2) Inelastic behaviour was incorporated in the gusset plate connection models from (1). and the models were loaded monotonically in tension well beyond first yield. In this step. the effects of mesh refinement. material strain hardening. framing member stiffness and fastener (bolt) model were studied.

(3) The gusset plate connection models from (2) were modified to model the behaviour of the gusset plate connection loaded monotonically in compression. In this step. initial imperfections were incorporated in the model and the effects of mesh refinement. material strain hardening. framing member stiffness and fastener (bolt) model were studied.

(4) The gusset plate connection models from (3) were used to model some of the cyclic loading tests conducted by Rabinovitch and Cheng (1993). In this step. a simple fastener model was developed that incorporated bolt slip. and gusset plate edge stiffeners were added to some of the models.

Since no monotonic tension test results were available for the gusset plate connections modeled in the first phase of the investigation. the models in (2) were validated by comparing peak tensile loads from the analysis with peak tensile loads from the cyclic loading tests conducted by Rabinovitch and Cheng (1993). The gusset plate models in (3) were validated against results from the monotonic compression loading tests conducted by Yam and Cheng (1993). Since in-plane displacements were not measured in the early tests conducted by Yam and Cheng. axial load vs. out-of-plane displacement

behaviour is used as a basis for comparison. The models in (4) were validated with results from the cyclic loading tests conducted by Rabinovitch and Cheng (1993).

3.2 Linear Elastic Mesh Study

The main purpose of the linear elastic mesh study was to determine the level of mesh refinement required to ensure convergence. In this step, four different finite element meshes were used to model Rabinovitch and Cheng (1993) Specimen A2 (see Figure 3.1). For each mesh, the ABAQUS shell element S4R was used to model the gusset plate and the splice members. The bolts were modeled as rigid links, connecting the nodes in the gusset plate and the splice members that corresponded with the bolt locations. Linear elastic material properties were assigned to all gusset plate and splice member elements. The modulus of elasticity used in the linear elastic material model was 206000 MPa, based on results of material tests performed by Rabinovitch and Cheng (1993) (see Table 2.2). The framing members were assumed to be infinitely rigid in this step. Thus, rotational and translational degrees of freedom at the nodes along the connected edges of the gusset plate model were fully restrained. The load was applied through the nodes along the loaded edges of each splice member. In order to model the rigid brace member boundary conditions assumed in the Rabinovitch and Cheng (1993) tests, full rotational restraint was imposed at the loaded splice member nodes. A tensile load, equal to half of the yield load predicted using the Whitmore method, was applied to each gusset plate connection model. Figure 3.2 shows a typical gusset plate model used for the linear elastic mesh study. The splice members are shown in Figure 3.3. Looking at the

coordinate system in Figure 3.2 it can be seen that the gusset plate lies in the 1-2 plane. In this report, "in-plane" displacement refers to displacement in the 1-2 plane. "Out-of-plane" displacement refers to displacement in the coordinate 3 direction. The same system is used to refer to restraints. For each analysis in this step, displacements of the loaded nodes, the peak principal stress in the gusset plate, and contour plots of principal stresses in the gusset plate were obtained. The models that were constructed for the linear elastic mesh study were given designations from MS1 to MS4. Descriptions of these models can be found in Table 3.1.

3.3 Inelastic Analysis

3.3.1 Monotonic Tension Loading

For this portion of the analysis, nonlinear material behaviour was taken into consideration so that the behaviour of the gusset plate could be investigated beyond the elastic range. Elastic-perfect plastic and isotropic strain hardening material models were developed (see Figures 3.4(b) and 3.4(c) for examples) based on results from tension coupon tests performed by Rabinovitch and Cheng (1993). Since true stress versus plastic strain material properties are used in ABAQUS, tension coupon test data had to be converted accordingly.

In order to investigate the behaviour of the gusset plate beyond the elastic range, the four gusset plate models developed previously for the linear elastic mesh study were modified

to incorporate the nonlinear material models described above. This resulted in eight new gusset plate models (MT1 to MT8 in Table 3.1): four levels of mesh refinement and two material models. In order to study the effects of mesh refinement beyond first yield, models with the same material properties, but different levels of mesh refinement were compared. In order to study the effects of strain hardening, models with the same level of mesh refinement but different material models were compared. In this manner, the effect of mesh refinement could be compared using either material model, and likewise, the effect of strain hardening could be determined for any level of mesh refinement. The boundary and loading conditions were the same as those described in the previous section.

Subsequent to the investigation of mesh refinement and strain hardening, the second finest mesh (Mesh 3 in Figure 3.1(c)) was adopted and modified to evaluate the effects of: (1) the assumption of rigid framing members and (2) the rigid fastener model. To model the framing members more realistically, the beam and column assembly used by Rabinovitch and Cheng (1993) was modeled and attached to the previously developed gusset plate mesh (see Figure 3.5). The beam and column assembly was modeled with S4R shell elements. These elements were assigned linear elastic material properties to ensure that yielding was confined to the gusset plate. To study the effect of the rigid fastener model, a more realistic bolt model was developed using ABAQUS SPRING2 elements. The SPRING2 element links a global degree of freedom at one node with a global degree of freedom at another node. For this model, two springs were required (one for each in-plane displacement degree of freedom) to link each of the two splice members

to the gusset plate at each bolt location. The spring stiffness assigned to the SPRING2 elements for this step was taken from a double shear load-displacement plot presented by Wallaert et al. (1965). The stiffness value was taken as the initial slope of the "typical" A490 bolt behaviour plot in this paper. This value was computed to be 253000 N/mm. ABAQUS models that were constructed to study the behaviour of gusset plate connections loaded monotonically in tension were designated MT1 to MT20. Descriptions of these models can be found in Table 3.1.

3.3.2 Monotonic Compression Loading

In order to conduct the analysis for monotonic compression loading, initial imperfections had to be incorporated into the gusset plate model. Since no measurements of initial imperfections were taken for any of the specimens tested by Yam and Cheng (1993) or Rabinovitch and Cheng (1993), it was necessary to use a trial and error approach to obtain an initial imperfection shape and magnitude that gave analytical results consistent with the experimental results. Initial imperfections of various shapes and magnitudes were studied, so that the effects of varying initial imperfection shape and magnitude could be ascertained. As shown in Figure 3.6, the three shapes that were studied were: (1) a one quarter sine wave shape; (2) a full sine wave shape; and (3) a shape constructed by taking the buckled configuration from a monotonic compression analysis performed with shape (1) and scaling it down to achieve the desired initial imperfection magnitude. Initial imperfection magnitude was defined for this study as the maximum out-of-plane initial imperfection of any node in the gusset plate. The three initial imperfection

magnitudes used for this comparison were 0.05 mm, 0.5 mm, and 5 mm. No attempt was made to correlate initial imperfection magnitude with gusset plate thickness. For Rabinovitch and Cheng Specimen A2, these magnitudes corresponded to 0.81, 8.1 and 81 percent of the plate thickness (6.18 mm). For Yam and Cheng Specimen GP3, these magnitudes corresponded to 0.77, 7.7 and 77 percent of the gusset plate thickness (6.5 mm).

The other factor that had a significant effect on the behaviour of gusset plate connections loaded monotonically in compression was the manner in which out-of-plane restraint was assumed to be imparted to the gusset plate by the splice members due to clamping. The two cases that were considered for this study were:

(1) no out-of-plane (clamping) restraint imparted by the splice members (i.e. the out-of-plane displacements of the splice member nodes and the gusset plate nodes between the splice members were independent (except at the bolt locations)), and
(2) full out-of-plane (clamping) restraint imparted by the splice members (i.e. the out-of-plane displacements of the splice member nodes and the gusset plate nodes between the splice members were linked).

These cases were thought to be reasonable lower and upper bounds of the actual level of restraint taking place. Both cases were run with the quarter sine wave initial imperfection shape shown in Figure 3.6(a) at three imperfection magnitudes (0.05, 0.5, and 5 mm). The effects of initial imperfection shape, initial imperfection magnitude and the out-of-

plane restraint imparted by the splice members were studied using models of Specimen GP3 from Yam and Cheng (1993). Since GP3 was almost identical to Specimen A2 from Rabinovitch and Cheng it was felt that the findings from the mesh study for Specimen A2 could be applied to Specimen GP3. Thus, only one mesh was developed for Yam and Cheng Specimen GP3. This mesh was essentially identical to Mesh 2 shown in Figure 3.1(b). The boundary conditions in this step were the same as in the previous two steps.

Finite element models of Rabinovitch and Cheng Specimen A2 were used to study the effects of mesh refinement, framing member stiffness, and fastener (bolt) model on the monotonic compressive behaviour of the gusset plate connection. An initial imperfection shape and magnitude was chosen (the quarter sine wave shape shown in Figure 4.6 (a) with a magnitude of 0.5 mm) based on the results from the study of Specimen GP3. Full out-of-plane (clamping) restraint was assumed to be imparted by the splice members.

Based on the results from the studies of Specimens GP3 and A2, models were constructed of Specimens GP1, GP2 and GP3 from the test program of Yam and Cheng (1993). A quarter sine wave initial imperfection shape with a magnitude of 2.0 mm was assumed. It was also assumed that the splice members imparted full out-of-plane restraint to the gusset plate and flexible framing members were incorporated into the model. This configuration closely predicted the ultimate buckling loads for each of the three specimens. The models that were constructed to study the behaviour of gusset plate connections loaded monotonically in compression were designated MC1 to MC27. These models are described in Table 3.2.

3.3.3 Cyclic Loading

This step involved the modeling of Specimens A1, A2, A3, and A4 from Rabinovitch and Cheng (1993). These models incorporated the features that were determined to be critical in the monotonic loading studies. Cyclic loading sequences were imposed in order to model test loading conditions. The elastic-perfect plastic material model was used in the gusset plate models developed for the cyclic loading study.

To model Rabinovitch and Cheng Specimens A1 and A3, bolt slip had to be considered. In order to do this, ABAQUS SPRING2 elements, with nonlinear load-displacement behaviour were used at the bolt locations. Although ABAQUS allows the user to give SPRING2 elements nonlinear load versus displacement attributes, these elements cannot model inelastic behaviour. Thus, in order to model the cyclic bolt slip that took place during the testing of these specimens, the superposition of several spring elements was necessary (see Figure 3.7). Essentially, the 3 Springs in Figure 3.7 were turned "on" or "off" to force the effective spring (the superposition of the "on" springs at any given time) to follow the desired load versus displacement path. This procedure is conceptualized in Figures 3.8(a) to 3.8(d). In Figure 3.8(a), Spring 1 is "on": the bolt is loaded in the positive direction until slip occurs and the bolt bears up against the edge of the bolt hole. Note, that the positive direction is the direction corresponding to a positive (tensile) brace load. Once the desired positive gusset plate displacement is reached, Spring 2 is turned on, resulting in an "effective" spring corresponding to the solid line in Figure 3.8(b). The bolt is then loaded in the negative direction until the bolt slips again

and bears against the opposite edge of the bolt hole (see Figure 3.8(b)). Once the desired negative gusset plate displacement is reached, Spring 2 is turned "off" and Spring 3 is turned "on" resulting in the "effective" spring corresponding to the solid line in Figure 3.8(c). The bolt is then reloaded in the positive direction until one full cycle is completed. If desired, the cycle is repeated. The path of the "effective" spring through one entire cycle is shown in Figure 3.8 (d). It was necessary to design this bolt slip modeling procedure so that turning springs "on" or "off" would not result in any sudden changes in the "effective" spring force at the bolt node. This model achieves this, as long as the sequence described above is followed. If a bolt does not slip or only slips partially (i.e. doesn't bear up against the edge of the bolt hole) in a given cycle then the procedure fails. The slopes of the elastic portions of the spring load versus displacement plots in Figures 3.7 and 3.8 have been reduced for clarity. Since it was determined at this point that the use of an elastic bolt did not have a significant effect on monotonic gusset plate behaviour, no attempt was made to base these slopes on measured load versus displacement behaviour. Rather, values much greater than those used in the elastic bolt model were chosen, essentially resulting in rigid bolt behaviour. As for the amount of slip which was allowed in the model, a trial-and-error approach was used to find the value which resulted in the best match between the overall model behaviour and the Rabinovitch and Cheng Specimen A1 and A3 test results. A value of 2.5 mm turned out to work the best. This value can be thought of as the assumed average difference between the bolt diameter and the bolt hole diameter. Due to the tediousness of the bolt slip model procedure (described above) and the limitations of the procedure in its current

form, only a few cycles of the Rabinovitch and Cheng Specimen A1 and A3 tests were modeled.

Specimens A3 and A4 from Rabinovitch and Cheng (1993) were essentially identical to Specimens A1 and A2 with the exception of the addition of gusset plate edge stiffeners. These edge stiffeners were modeled in ABAQUS with S4R shell elements. According to Rabinovitch and Cheng these stiffeners were fabricated from the same steel as the gusset plates. Thus, the shell thickness and material model assigned to the stiffener elements were the same as for the gusset plate elements. A typical gusset plate connection model with edge stiffeners is shown in Figure 3.9. The finite element models that were constructed to study the behaviour of gusset plate connections loaded cyclically were designated CL1 to CL4. Descriptions of these models can be found in Table 3.2.

Table 3.1 - Summary of finite element models (part 1).

Model	Specimen	Mesh	Material Model	Initial Imperfection Shape	Initial Imperfection (mm)	Special
(a) - Linear Elastic Mesh Study Models						
MS1	R/C - A2	1	elastic	-	-	-
MS2	R/C - A2	2	elastic	-	-	-
MS3	R/C - A2	3	elastic	-	-	-
MS4	R/C - A2	4	elastic	-	-	-
(b) - Monotonic Tension Loading Models						
MT1	R/C - A2	1	elastic-plastic	-	-	-
MT2	R/C - A2	1	strain hardening	-	-	-
MT3	R/C - A2	2	elastic-plastic	-	-	-
MT4	R/C - A2	2	strain hardening	-	-	-
MT5	R/C - A2	3	elastic-plastic	-	-	-
MT6	R/C - A2	3	strain hardening	-	-	-
MT7	R/C - A2	4	elastic-plastic	-	-	-
MT8	R/C - A2	4	strain hardening	-	-	-
MT9	R/C - A2	3	elastic-plastic	-	-	flexible framing members
MT10	R/C - A2	3	strain hardening	-	-	flexible framing members
MT11	R/C - A2	3	elastic-plastic	-	-	elastic bolt model
MT12	R/C - A2	3	strain hardening	-	-	elastic bolt model
MT13	R/C - A1	3	strain hardening	-	-	flexible framing members
MT14	R/C - A2	3	strain hardening	-	-	flexible framing members
MT15	R/C - A3	3	strain hardening	-	-	flexible framing members
MT16	R/C - A4	3	strain hardening	-	-	flexible framing members
MT17	R/C - A1	3	elastic-plastic	-	-	flexible framing members
MT18	R/C - A2	3	elastic-plastic	-	-	flexible framing members
MT19	R/C - A3	3	elastic-plastic	-	-	flexible framing members
MT20	R/C - A4	3	elastic-plastic	-	-	flexible framing members

R/C - Rabinovitch and Cheng

Table 3.2 - Summary of finite element models (part 2).

Model	Specimen	Mesh	Material	Initial Imperfection Shape	Initial Imperfection (mm)	Special
(a) - Monotonic Compression Loading Models						
MC1	Y/C - GP3	-	strain hardening	shape 1	0.05	full splice member restraint
MC2	Y/C - GP3	-	strain hardening	shape 1	0.5	full splice member restraint
MC3	Y/C - GP3	-	strain hardening	shape 1	5	full splice member restraint
MC4	Y/C - GP3	-	strain hardening	shape 2	0.05	full splice member restraint
MC5	Y/C - GP3	-	strain hardening	shape 2	0.5	full splice member restraint
MC6	Y/C - GP3	-	strain hardening	shape 2	5	full splice member restraint
MC7	Y/C - GP3	-	strain hardening	shape 3	0.05	no splice member restraint
MC8	Y/C - GP3	-	strain hardening	shape 3	0.5	no splice member restraint
MC9	Y/C - GP3	-	strain hardening	shape 3	5	no splice member restraint
MC10	Y/C - GP3	-	strain hardening	shape 1	0.05	full splice member restraint
MC11	Y/C - GP3	-	strain hardening	shape 1	0.5	full splice member restraint
MC12	Y/C - GP3	-	strain hardening	shape 1	5	full splice member restraint
MC13	R/C - A2	1	strain hardening	shape 1	0.5	-
MC14	R/C - A2	2	strain hardening	shape 1	0.5	-
MC15	R/C - A2	3	strain hardening	shape 1	0.5	-
MC16	R/C - A2	4	strain hardening	shape 1	0.5	-
MC17	R/C - A2	3	strain hardening	shape 1	0.5	flexible framing members
MC18	R/C - A2	3	strain hardening	shape 1	0.5	elastic bolt model
MC19	Y/C - GP1	-	elastic-plastic	shape 1	1	flexible framing members
MC20	Y/C - GP1	-	strain hardening	shape 1	1	flexible framing members
MC21	Y/C - GP2	-	elastic-plastic	shape 1	1	flexible framing members
MC22	Y/C - GP2	-	strain hardening	shape 1	1	flexible framing members
MC23	Y/C - GP3	-	elastic-plastic	shape 1	1	flexible framing members
MC24	Y/C - GP3	-	strain hardening	shape 1	1	flexible framing members
MC25	Y/C - GP1	-	strain hardening	shape 1	2	flexible framing members
MC26	Y/C - GP2	-	strain hardening	shape 1	2	flexible framing members
MC27	Y/C - GP3	-	strain hardening	shape 1	2	flexible framing members
(b) - Cyclic Loading Models						
CL1	R/C - A1	3	elastic-plastic	shape 1	2	bolt slip
CL2	R/C - A2	3	elastic-plastic	shape 1	2	-
CL3	R/C - A3	3	elastic-plastic	shape 1	2	bolt slip, edge stiffeners
CL4	R/C - A4	3	elastic-plastic	shape 1	2	edge stiffeners

R/C - Rabinovitch and Cheng
Y/C - Yam and Cheng

shape 1 - quarter sine wave shape
shape 2 - full sine wave shape
shape 3 - buckled configuration shape

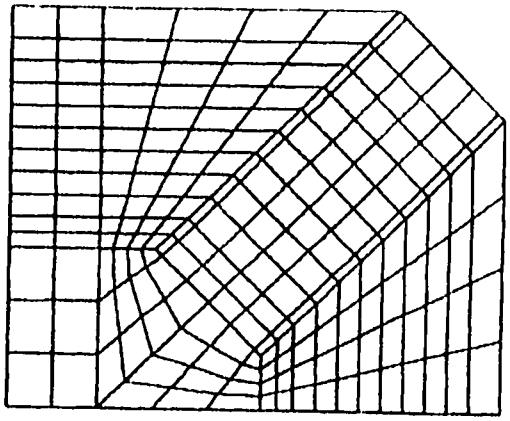

(a) - Mesh 1.

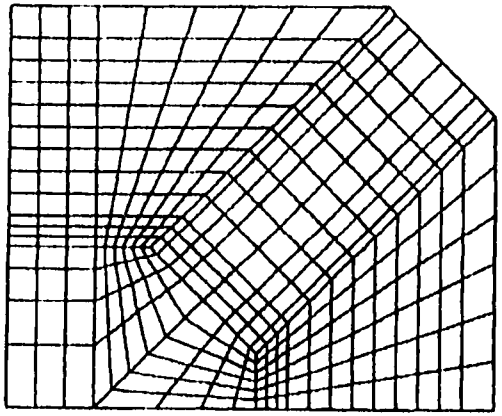

(b) - Mesh 2.

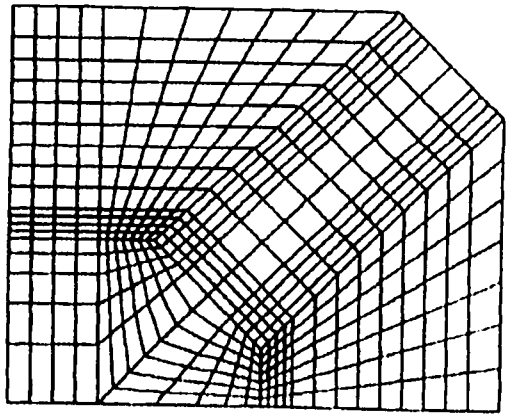

(c) - Mesh 3.

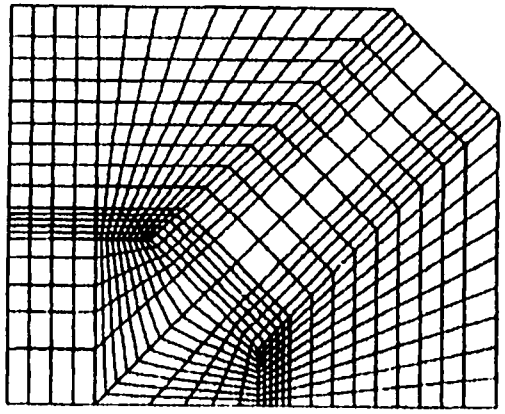

(d) - Mesh 4.

Figure 3.1 - Gusset plate meshes used for linear elastic mesh study.

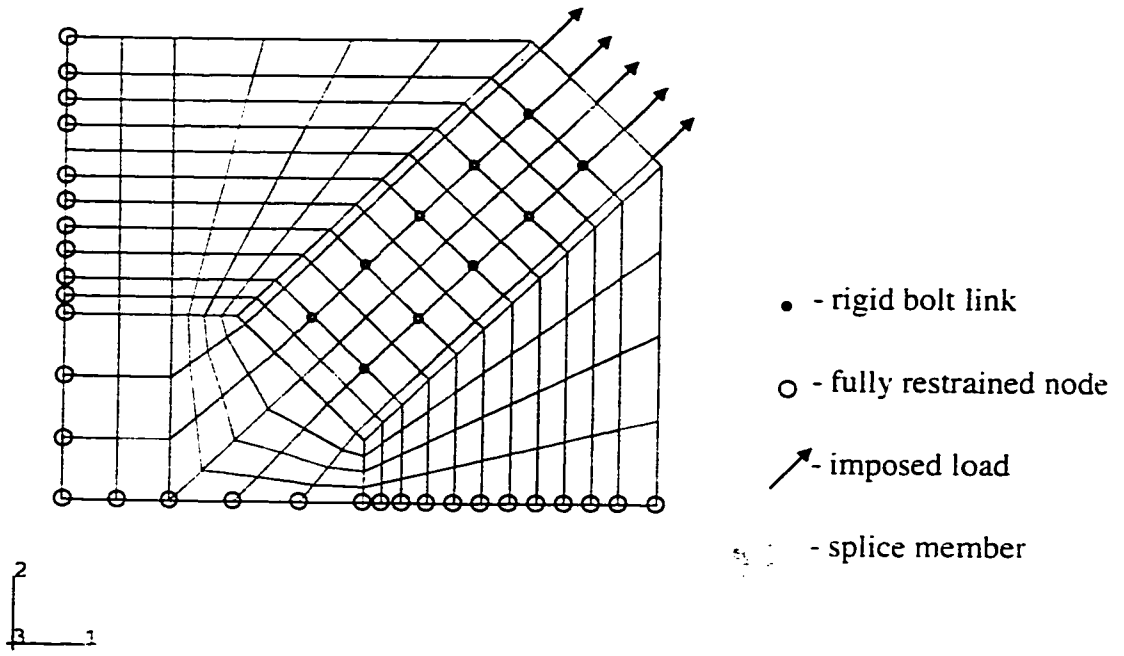

Figure 3.2 - ABAQUS gusset plate connection model.

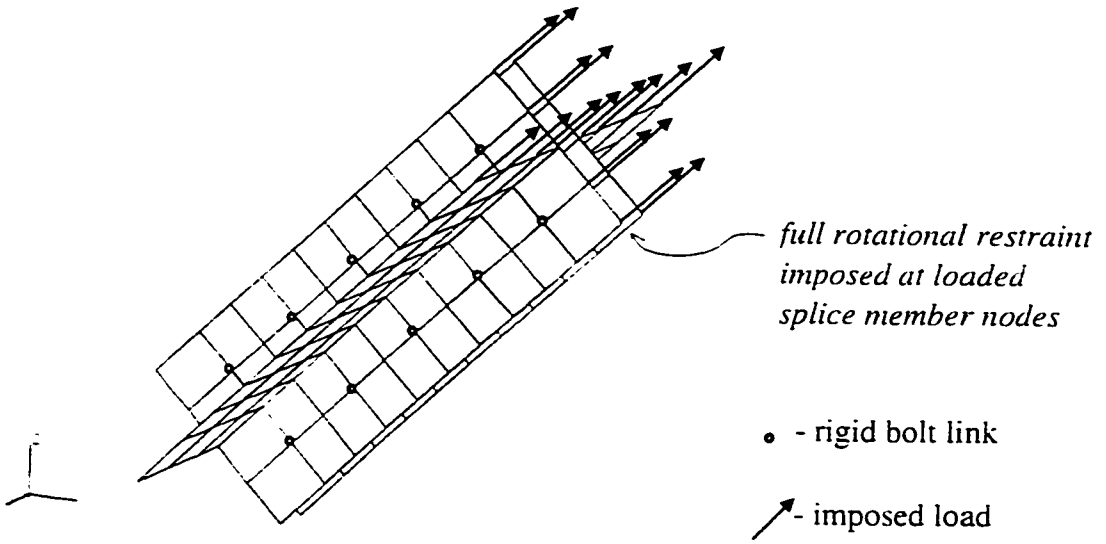

Figure 3.3 - ABAQUS splice member model.

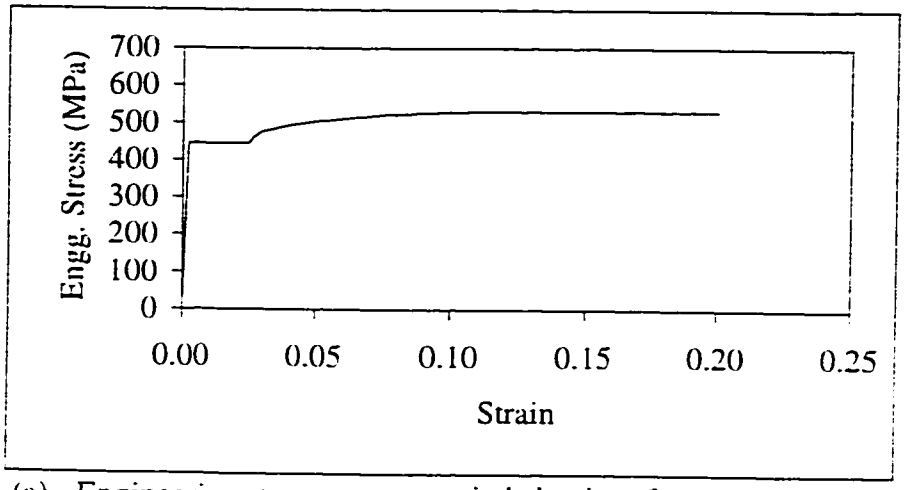

(a) - Engineering stress versus strain behaviour from tension coupon test.

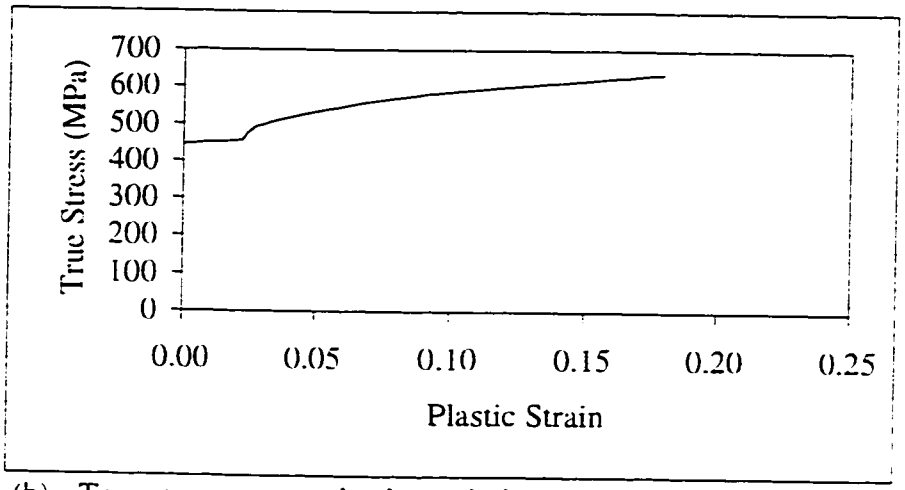

(b) - True stress versus plastic strain isotropic strain hardening model.

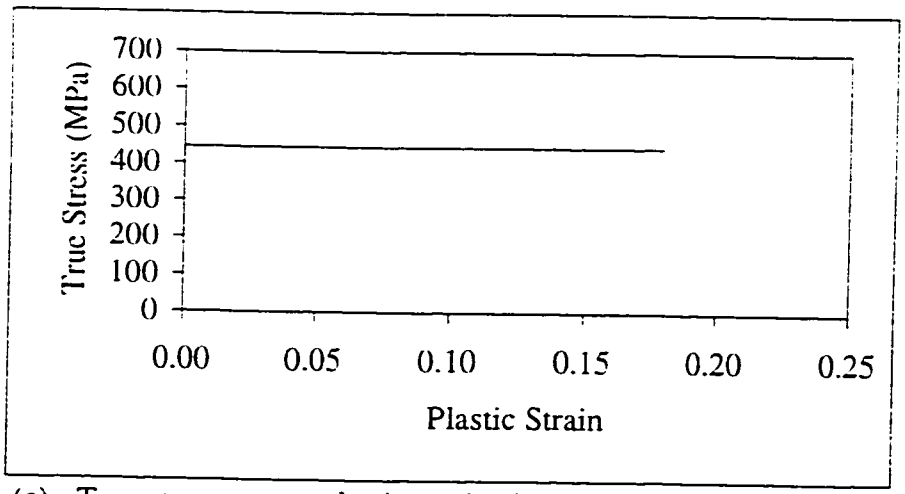

(c) - True stress versus plastic strain elastic - perfect plastic model.

Figure 3.4 - Material models for Rabinovitch and Cheng (1993) Specimen A2.

Side View:

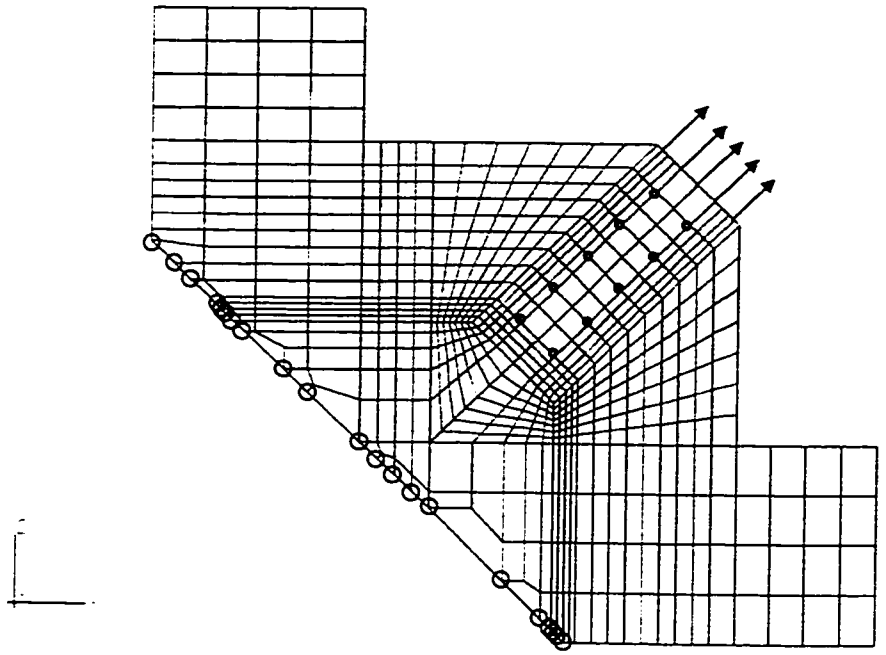

Isometric View:

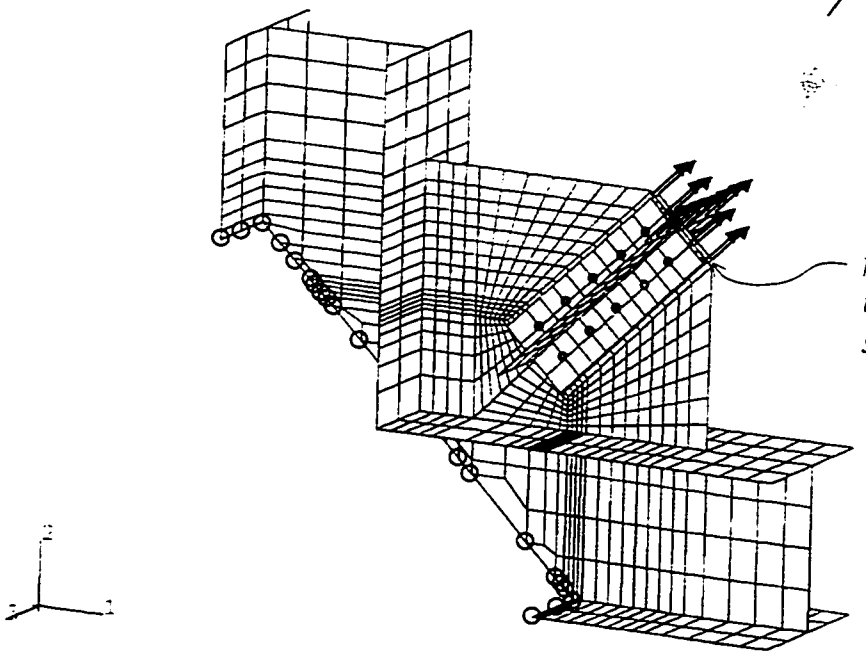

Figure 3.5 - ABAQUS gusset plate connection model with flexible framing members.

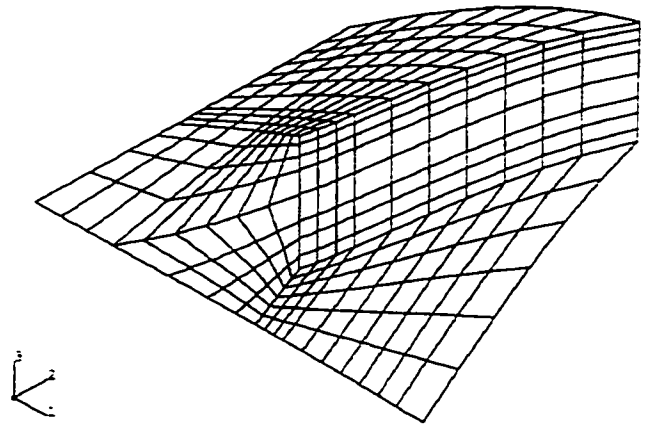

(a) - quarter sine wave shape

** shapes have been amplified for clarity*

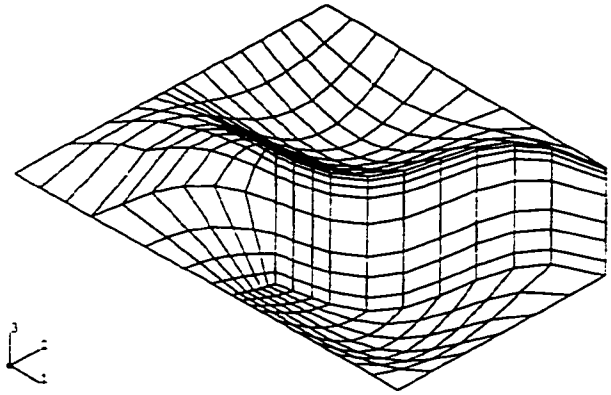

(b) - full sine wave shape

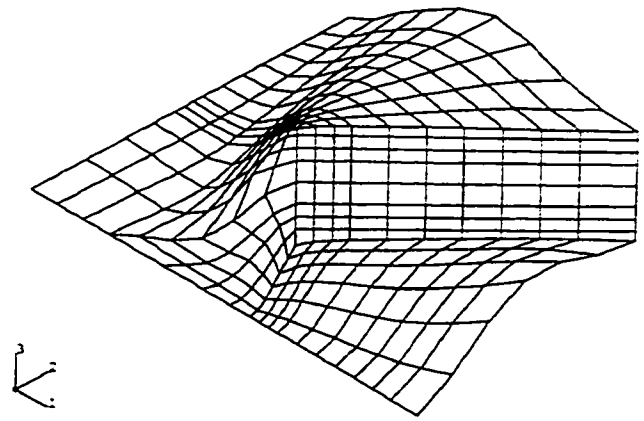

(c) - buckled configuration shape

Figure 3.6 - Initial imperfection shapes.

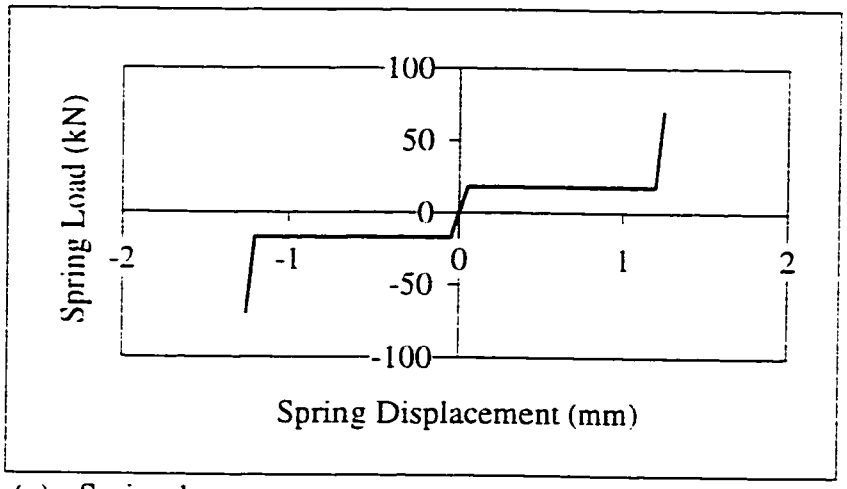

(a) - Spring 1.

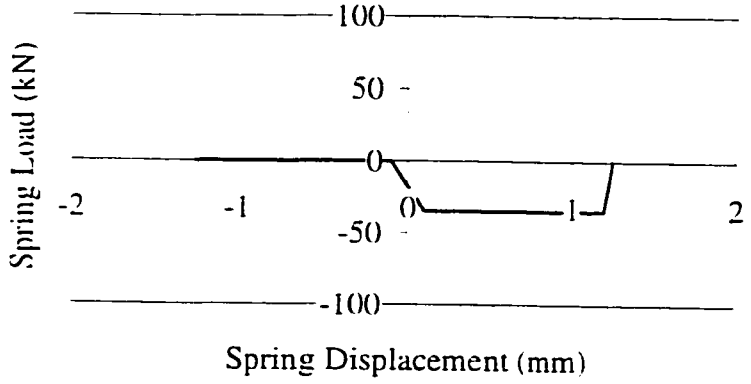

(b) - Spring 2.

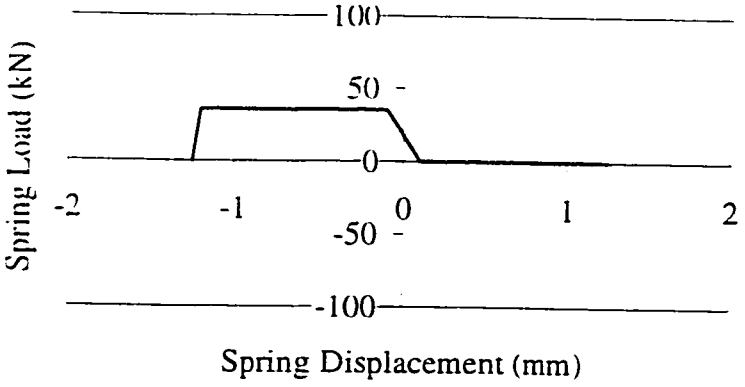

(c) - Spring 3.

Figure 3.7 - Springs used in bolt slip model.

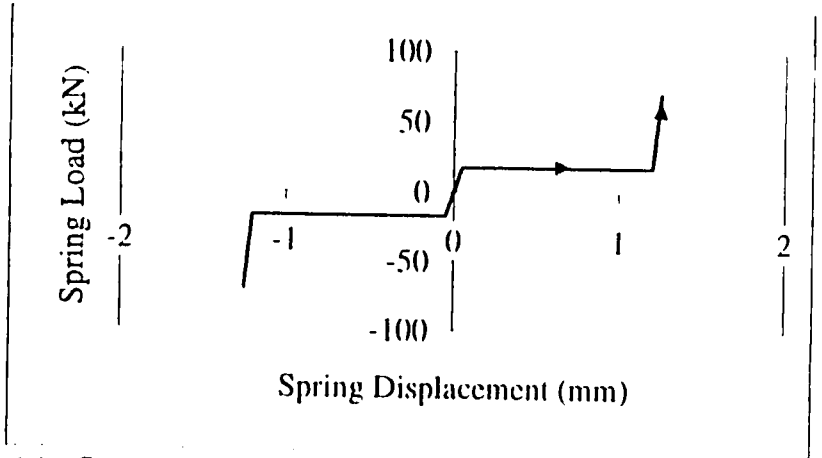

(a) - Step 1: Spring 1.

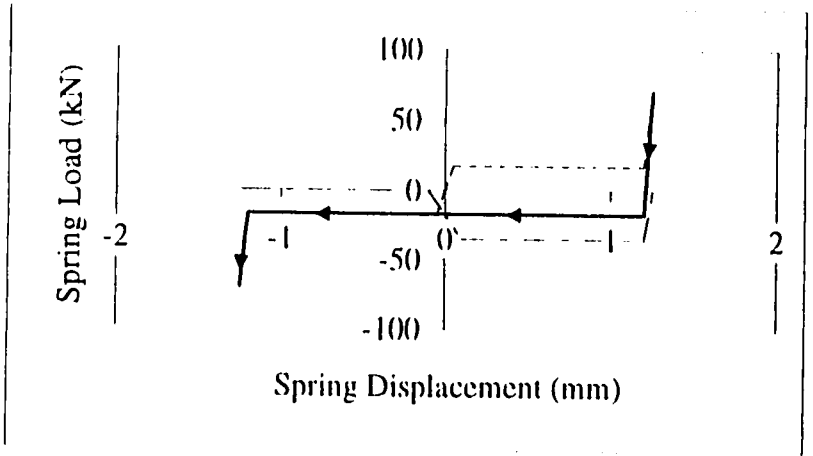

(b) - Step 2: Spring 1 + Spring 2.

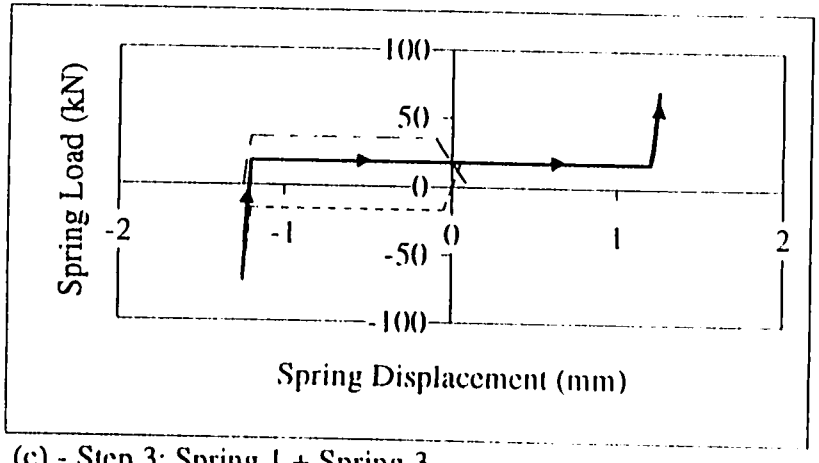

(c) - Step 3: Spring 1 + Spring 3.

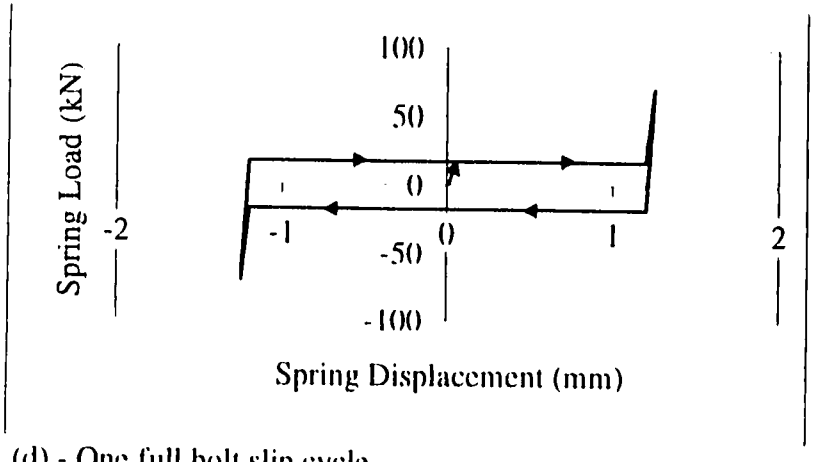

(d) - One full bolt slip cycle.

* *Note: dashed lines represent springs that are "on", solid line represents the "effective" spring (i.e. the sum of the "on" springs).*

Figure 3.8 - Conceptualization of steps in spring superposition sequence for bolt slip model.

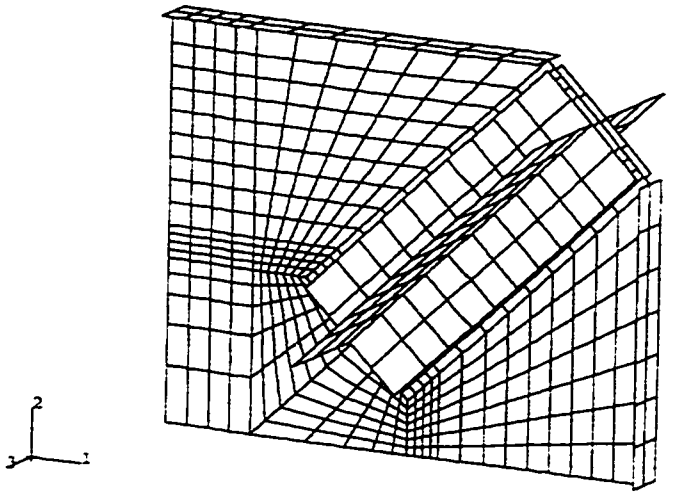

Figure 3.9 - ABAQUS gusset plate connection model with free edge stiffeners.

4. VALIDATION OF THE FINITE ELEMENT MODELS

4.1 Introduction

The results of the first phase of the numerical investigation are presented in this chapter. The numerical models developed in the previous chapter are validated by comparison with the experimental results from Yam and Cheng (1993) and Rabinovitch and Cheng (1993).

4.2 Linear Elastic Mesh Study

A mesh study was conducted using a linear elastic model to investigate the stress distribution in a gusset plate and to determine the level of mesh refinement that would be required for modeling the gusset plate connection under monotonic and cyclic loading. For the linear elastic mesh study, a predetermined load was applied to each model. Axial displacement and principal stress output was compared for the various meshes. Axial displacement output was used primarily, however, in selecting the sufficient level of mesh refinement.

As described in the previous chapter, four different meshes, with the number of shell elements ranging from 206 to 596, were investigated. Table 4.1 and Figure 4.1 compare axial displacements, U(in-plane), and maximum principal stresses, SP(max), for the four levels of mesh refinement. The axial displacements can be seen to converge to a constant

value as the level of mesh refinement is increased. The third finest mesh (Mesh 2 in Figure 3.1(b)) appears to be adequate for predicting displacements in the elastic range. Refinement beyond this point appears to have little effect on axial displacement.

The principal stress contour plots for each level of mesh refinement, shown in Figure 4.2, indicate that the highest stresses and maximum stress gradients occur near the last row of bolts. Principal stress contour plots appear to match with experimental and analytical results from other researchers (Irvan, 1963, Yam and Cheng, 1994).

In Table 4.1 (or Figure 4.1), SP(max) can be seen to be increasing as the mesh is refined. In Figure 4.2 it is apparent that the principal stresses away from the bolts are converging. Since simple rigid links were used to model the bolts, it was felt that a precise value of SP(max) (determined using this simplified bolt model) would not be a value that could be related directly to the stresses in the actual connection. Since it was the general load versus displacement behaviour of the gusset plate that was of most interest in this study, no attempt was made to refine the mesh to achieve convergence of SP(max).

4.3 Inelastic Analysis

4.3.1 Monotonic Tension Loading

In order to investigate the behaviour of the gusset plate connection loaded monotonically in tension up to and beyond yield, the models developed for the linear elastic mesh study

were modified to incorporate nonlinear material behaviour. At this level, the effects of mesh refinement, material strain hardening, framing member stiffness and fastener (bolt) model were studied.

Figure 4.3 shows a typical deformed configuration of a gusset plate model loaded monotonically in tension. As can be seen in this figure, most of the element distortion is occurring in the elements just beyond the last row of bolts in the gusset plate.

For the levels of mesh refinement investigated, the effect of mesh refinement on monotonic tension load-displacement behaviour appears to be small. Figure 4.4 shows that as the mesh is refined, the ultimate tensile capacity of the model decreases slightly. The difference between subsequent refinements appears to diminish as the mesh is refined. The second finest mesh (Mesh 3 in Figure 3.1(c)) was selected for the remaining monotonic tension analysis.

In studying the effects of mesh refinement, framing member stiffness, and fastener (bolt) model, models with both inelastic material models were constructed. In Figures 4.4 to 4.6, the models that used the isotropic strain hardening material model are shown as solid lines and the models that used the elastic - perfect plastic material model are shown as dashed lines. Looking at any one of these figures, it can be seen that the effect of strain hardening on the load versus displacement behaviour of the gusset plate model is essentially an increase in ultimate tensile capacity.

Comparison of MT5 with MT9 and MT6 with MT10 in Figure 4.5 indicates that the effects of incorporating realistic, flexible framing members are: (1) a reduction in ultimate tensile capacity, and (2) a reduction in tensile stiffness in the elastic range. For modeling the cyclic behaviour of gusset plates (see Section 4.3.3) and for the subsequent parametric study (see Chapter 5), it was felt that these effects were significant enough to warrant the inclusion of flexible framing members in the models.

Figure 4.6 shows the effect of incorporating the elastic fastener (bolt) model on the load versus deflection characteristics of the gusset plate model loaded monotonically in tension. A comparison of MT5 with MT11 and MT6 with MT12 indicates that the result is only a slight reduction in stiffness. The effect on the ultimate load is negligible. The rigid bolt model was used in subsequent gusset plate models unless otherwise specified.

Table 4.2 compares ultimate loads from the monotonic tension loading analysis with ultimate tensile loads from the cyclic tests conducted by Rabinovitch and Cheng (1993). Table 4.2 shows a good correlation between the test and predicted ultimate load when the elastic-perfect plastic material model is used. When the isotropic strain hardening model is used, the analysis tends to overestimate the ultimate tensile capacity of the gusset plate. There are several possible explanations for this:

1) In Table 4.2, the peak tensile load from a cyclic test is being compared with the peak tensile load from a monotonic analysis. It is possible that the tensile capacity of the cyclically loaded gusset plate is reduced somewhat due to cycling. Although this may

be part of the reason, results from cyclic analysis of the same gusset plate connections (see Section 4.3.3) suggest that cycling does not significantly reduce the tensile capacity of the gusset plate.

2) In this investigation, no attempt was made to model the tearing of the gusset plate observed in the specimens tested by Rabinovitch and Cheng (1993). Again, although this may account for some of the difference, it is believed that tearing only occurred in the later stages of the tests, after the ultimate capacity of the gusset plate was reached.

3) The analytical model used in this investigation did not take into account the gusset plate material removed at the bolt hole locations. As explained in Chapter 3, the bolts in this analysis were modeled as either rigid or elastic links, and the gusset plate mesh was continuous at the bolt locations. The gross connection length, L, for the Rabinovitch and Cheng (1993) specimens was 330 mm and 22 mm (7/8") bolts were used. The net connection length was therefore only 221 mm (assuming 24 mm bolt holes), which represents a 33 percent reduction in the area along the shear planes used in the block shear model proposed by Hardash and Bjorhovde (1984). It would seem reasonable to assume that this would result in the numerical model overestimating the tensile capacity of the gusset plate. By accounting for this reduction in the gusset plate material with either an "effective" yield stress or a reduced gusset plate thickness, a closer result would have been achieved with the strain hardening material model. This was accomplished indirectly with the use of the elastic-perfect plastic material model, and this may be the reason why the elastic perfect-plastic material model gave better results.

Figures 4.7 and 4.8 show axial load versus displacement plots for finite element models of Rabinovitch and Cheng (1993) Specimens A1 to A4 (with and without strain hardening). In these figures, the envelopes from the cyclic tests conducted by Rabinovitch and Cheng are each represented with two lines: (1) a sloped line corresponding to the initial stiffness of the gusset plate specimen, and (2) a horizontal line corresponding to the ultimate capacity of the gusset plate specimen (in tension). In these figures, it can be seen that the initial stiffness of the gusset plate model is less than the stiffness of the corresponding test specimen in all cases. It is suspected that this is partly due to the frictional restraint between the splice members and the gusset plate, which was present in the test specimens but was not modeled in the analysis. The horizontal lines in Figures 4.7 and 4.8 correspond with the test ultimate loads presented in Table 4.2.

4.3.2 Monotonic Compression Loading

In this part of the analysis, initial imperfections were incorporated into the model and monotonic behaviour in compression was investigated. The effects of initial imperfection (shape and magnitude), of mesh refinement, material strain hardening, framing member stiffness and fastener (bolt) model were investigated.

Figure 4.9 shows the typical buckled configuration of a gusset plate model loaded in compression. The out-of-plane deformation apparent in this figure usually occurs suddenly and is usually associated with a sudden drop in the axial load.

As mentioned previously, it was necessary to adopt a trial and error approach for modeling the initial imperfections since initial imperfections were not measured during any of the test programs. Figure 4.10 shows the axial load versus displacement plots for models MC1 to MC3. These are models of Yam and Cheng Specimen GP3, each with initial imperfection shape (1) (the quarter sine wave shape shown in Figure 3.6) and initial imperfection magnitudes of 0.05, 0.5, and 5.0 mm. As can be seen in this figure, initial imperfection magnitude has a significant effect on ultimate compressive capacity. In general, the larger the initial imperfection magnitude, the lower the predicted compressive capacity. Initial imperfection magnitudes of 0.05, 0.5, and 5.0 mm resulted in predicted compressive capacities of 850, 786, and 628 kN respectively. The actual peak compressive load achieved by Specimen GP3 was 742 kN. Although predicted compressive capacity was quite sensitive to the assumed initial imperfection magnitude, this parameter resulted in only a slight reduction in the post buckling compressive load sustained by each of the gusset plate models.

It was found that initial imperfection shape is much less critical than initial imperfection magnitude. Figure 4.11 compares the effect of using different initial imperfection shapes for three different initial imperfection magnitudes (0.05, 0.5, and 5.0 mm). It can be seen that for a given initial imperfection magnitude, the difference between the axial load versus displacement plots for models with different initial imperfection shapes is small. As expected, shape (3) (the buckled configuration shape in Figure 3.6) tended to give slightly lower predicted compressive loads. Shapes (1) and (2) gave almost identical

results. Unless otherwise specified. the quarter sine wave shape (shape (1)) was adopted from this point forth because it seemed to be a realistic initial imperfection shape and it was a fairly simple one to generate.

The degree of out-of-plane (clamping) restraint imparted to the gusset plate by the splice members has a significant effect on the compressive behaviour of the gusset plate model. Full restraint and no restraint cases were modeled. Figures 4.12(a) and 4.12(b) show buckled configurations for the full restraint and no restraint cases. It can be seen that for the no restraint case. the buckled gusset plate actually passes through the plane of the inside splice member. The buckled configuration for the full restraint case is much closer to what was observed in tests. The axial load versus axial displacement plots for the models with full restraint and no restraint are presented in Figure 4.13 for three initial imperfection magnitudes. A comparison of the predicted capacities with the test result indicates that the ultimate compressive capacities of the models with full restraint are in better agreement. For the full restraint case. the predicted capacities range from 628 to 850 kN depending on initial imperfection magnitude. Even with a 0.05 mm initial imperfection magnitude. the maximum compressive capacity achieved with the no restraint case was only 554 kN. This value is significantly less than the actual compressive capacity of Specimen GP3 (742 kN), suggesting that the level of out-of-plane restraint imparted by the splice members must have been significant. The full restraint case is used in subsequent monotonic compression and cyclic models.

The effect of mesh refinement on the load response of the gusset plate is illustrated in Figure 4.14. Meshes 3 and 4 give almost identical results up to the peak load, indicating convergence. A relatively small discrepancy between the two meshes is observed in the post buckling range. This difference between the two meshes was not considered significant enough to warrant the use of the finer mesh.

As shown in Figure 4.15, the effect of incorporating the realistic, flexible framing members appears to be a slight reduction in the stiffness of the gusset plate connection model. However, the stiffness of the framing members appears to have little or no effect on ultimate capacity.

The effect of using an elastic bolt model versus a rigid one is a slight reduction in the stiffness of the gusset plate connection model, as shown in Figure 4.16. Again, the bolt model used does not affect the ultimate capacity.

Load versus axial displacement response is presented in Figure 4.17 for models of three gusset plates (GP1, GP2, and GP3 from Yam and Cheng (1993)) analyzed with both inelastic material models. It can be observed from Figure 4.17 that the effect of strain hardening on the capacity of the gusset plate model loaded in compression is small. However, the effect of strain hardening on the stiffness of the model once yielding begins can be significant depending on the gusset plate thickness and material yield strength. It appears that for thinner gusset plates, with higher material yield strengths, buckling occurs when most of the gusset plate is still in the elastic range, and therefore the model

is less sensitive to strain hardening (gusset plate models MC23 and MC24 in Figure 4.17). For stockier gusset plates with lower material yield strengths the effect of strain hardening on the stiffness of the model once yielding begins is more significant.

A 2 mm quarter sine wave (shape (1)) initial imperfection results in a good correlation between analytical and experimental results for Yam and Cheng (1993) Specimens GP1, GP2 and GP3. Table 4.3 compares the predicted ultimate capacities with the corresponding test results for these specimens. Figure 4.18 shows a comparison between the analytical and experimental axial load versus out-of-plane displacement plots for these specimens. As mentioned in Chapter 2, Yam and Cheng used MTS (test machine) head displacement readings as a measure of axial displacement during the tests. The MTS head displacement readings included displacements associated with portions of the test frame (as well as the testing machine itself) which were outside of the boundaries modeled in the analysis. For this reason analytical axial load versus axial displacement plots do not compare well with test results based on MTS head displacement.

The effect of gusset plate thickness on the axial load versus displacement behaviour can be seen in Figures 4.17 and 4.18. Test specimens GP1, GP2, and GP3 (with gusset plate thicknesses equal to 13.3, 9.8, and 6.5 mm, respectively) from Yam and Cheng (1993) were modeled. The figures show a reduction in stiffness and buckling resistance as the gusset plate thickness is reduced. As mentioned above, the thickness of the gusset plate is also a factor determining the amount of yielding that takes place before buckling occurs

(i.e. a stockier gusset plate will exhibit a greater amount of inelastic deformation prior to buckling).

4.3.3 Cyclic Loading

In this step, the finite element models developed above were used to model the cyclic loading tests conducted by Rabinovitch and Cheng (1993). A simple fastener model was developed that incorporated bolt slip (for Specimens A1 and A3 from Rabinovitch and Cheng (1993)), and edge stiffeners were added to the appropriate models (Specimens A3 and A4).

Specimen A2 from Rabinovitch and Cheng was the simplest specimen to model since there was no need to model bolt slip or edge stiffeners. Figure 4.19 presents a comparison between the predicted axial load versus displacement hysteresis (model CL2) and the experimental hysteresis for this specimen. As can be seen in this figure, the finite element model seems to predict the hysteresis envelope on the tension side with each cycle quite well. On the compression side, the finite element model captures the buckling load and the subsequent decay of the post-buckling compressive capacity with each cycle.

Using combinations of nonlinear springs to model bolt slip, a limited number of cycles were modeled for Specimens A1 and A3 from Rabinovitch and Cheng. The bolt slip model (described in Chapter 3) is based on the assumption that all of the bolts slip in each cycle, and therefore is not suitable for modeling the earlier cycles. Figure 4.20 and

Figure 4.21 show a comparison between predicted and experimental hysteresis plots for Specimens A1 and A3 from Rabinovitch and Cheng. Because of the limitations of the analytical process, these test specimens were analyzed for only a few cycles of loading. A good correlation was found between the predicted behaviour and the test results.

Figure 4.21 and Figure 4.22 show predicted and experimental hysteresis plots for Specimens A3 and A4 from Rabinovitch and Cheng. Specimens A3 and A4 were identical to Specimens A1 and A2 with the exception of the addition of edge stiffeners for Specimens A3 and A4. The effect of edge stiffeners on cyclic behaviour appears to be a reduction in the rate of decay of the buckling load with consecutive cycles. This can be observed both in the test results and the finite element analysis results.

The manner in which the cyclic load is applied to the model appears to have a significant effect on how well the test results are matched. For the initial cycles, Rabinovitch and Cheng used load control to cycle the specimens between loads corresponding to different fractions of the Whitmore yield load. The finite element model matches these cycles best when load control is employed. In this range, slight differences in the stiffness of the specimen and the model mean that the axial displacements for a given axial load can be quite different. For this reason, displacement control was not appropriate in this range. Displacement control does, however, work better for the higher displacement cycles. Once the gusset plate yields (or buckles), small changes in load can lead to large displacements and therefore load control becomes difficult. On the compression side it is

important to monitor the load versus out-of-plane hysteresis, as this seems to be a good measure of the extent of buckling that has taken place.

Table 4.4 compares the ultimate tensile and compressive loads for Specimens A2 and A4 by Rabinovitch and Cheng with the ultimate loads predicted by the finite element models. This table shows excellent agreement between measured and predicted ultimate capacities in tension and compression, with test to predicted ratios ranging from 1.03 to 1.08.

Figures 4.23 and 4.25 compare the measured energy dissipated (per cycle) for Specimens A2 and A4 with the energy dissipated (per cycle) by the corresponding finite element models (CL2 and CL4). Figures 4.24 and 4.26 compare cumulative energy dissipation for the same specimens. The cumulative energy dissipation plots show that the finite element predictions are slightly greater than the measured values for both test specimens. This is likely due to the fact that the elastic – perfect plastic material model was used in the cyclic loading study. As mentioned in the previous section, the effect of strain hardening on ultimate compressive capacity is small. However, the effect of this parameter on the stiffness of the model (in compression) once yielding begins is significant. For Specimen A2 especially, it was found that larger displacements needed to be imposed on the compression side just to cause buckling to occur as observed during the test. This meant that more energy was being dissipated in this portion of each cycle. Figure 4.23 shows that most of the difference between the two cumulative curves for Specimen A2 and model CL2 occurs in cycles 3, 4, and 5. In these cycles, higher displacements had to be imposed on the compression side to cause the gusset plate model

to buckle in the same cycle as the test specimen. In subsequent cycles, the energy dissipated (per cycle) matches quite well. A possible solution to this problem would be to use the elastic - perfect plastic material model with an "effective" yield stress that results in the model buckling at the correct axial displacement. Comparing Figures 4.24 and 4.26 the benefits of using gusset plate edge stiffeners on energy dissipation are apparent.

Figure 4.27 compares out-of-plane cyclic behaviour for Specimens A2 and A4 and finite element models CL2 and CL4. In general, it can be seen that the finite element models did not displace as far out-of-plane as the test specimens did. This having been said, it appears that the finite element model captures the general out-of-plane behaviour quite well, including the "residual" out-of-plane displacement apparent in the post buckling cycles (i.e. the small amount of out-of-plane displacement apparent even when the gusset plate is yielded in tension).

4.5 Conclusions

The following conclusions can be drawn from the first phase of this investigation:

(1) Monotonic and cyclic behaviour of gusset plate connections can be modeled reasonably accurately using the finite element method. The accuracy with which the gusset plate behaviour is modeled could potentially be improved with the use of an effective material model to account for factors, such as in-plane clamping friction,

and the loss of gusset plate material at the bolt hole locations. that were not included in the gusset plate model. However, this would require further investigation.

(2) For the gusset plate connections modeled. it was found that Mesh 2 in Figure 3.1(b) with initial imperfection shape (1) (quarter sine wave shown in Figure 3.6). with a magnitude of 2.0 mm. an elastic-perfect plastic material model. a rigid bolt model. flexible framing members and full out-of-plane (clamping) restraint imparted to the gusset plate by the splice member works the best.

(3) Although bolt slip was successfully modeled. the limitations of the procedure in its current form. as well as the highly variable nature of the bolt slip phenomenon. make the bolt slip model impractical for inclusion in a parametric study at this time.

Table 4.1 - Linear elastic mesh study – summary of results.

Finite Element Model	Mesh Number	Number of Elements	SP(max) (MPa)	U(in-plane) (mm)
MS1	Mesh 1	206	176.2	0.2715
MS2	Mesh 2	336	209.6	0.2900
MS3	Mesh 3	454	245.8	0.2896
MS4	Mesh 4	596	261.9	0.2903

** Note:* *- SP(max) = maximum principal stress value*
- U(in-plane) = in-plane displacement
- Mesh numbers correspond to gusset plate meshes shown in Figure 3.1

Table 4.2 - Monotonic tension loading – comparison with test results of Rabinovitch and Cheng (1993).

Test Specimen	Measured Capacity (kN)	Finite Element Model	Mesh Number	Material Model	Ultimate Capacity (kN)	Test / Predicted Ratio
A1	1794	MT13	Mesh 3	ish	2344	0.77
		MT17	Mesh 3	e-pp	1923	0.93
A2	1340	MT14	Mesh 3	ish	1520	0.88
		MT18	Mesh 3	e-pp	1245	1.08
A3	1884	MT15	Mesh 3	ish	2376	0.79
		MT19	Mesh 3	e-pp	1928	0.98
A4	1265	MT16	Mesh 3	ish	1533	0.83
		MT20	Mesh 3	e-pp	1248	1.01

** Note:* *- ish = isotropic strain hardening*
- e-pp = elastic - perfect plastic
- Mesh numbers correspond with gusset plate meshes shown in Figure 3.1

Table 4.3 - Monotonic compression loading – comparison with test results of Yam and Cheng (1993).

Test Specimen	Measured Capacity (kN)	Finite Element Model	Ultimate Capacity (kN)	Test / Predicted Ratio
GP1	1956	MC20	2073	0.94
GP2	1356	MC22	1342	1.01
GP3	742	MC24	711	1.04

Table 4.4 - Cyclic loading – comparison with test results of Rabinovtich and Cheng (1993).

(a) - Tension

Test Specimen	Measured Capacity (kN)	Finite Element Model	Ultimate Capacity (kN)	Test : Predicted Ratio
A2	1340	CL2	1243	1.08
A4	1265	CL4	1225	1.03

(b) - Compression

Test Specimen	Measured Capacity (kN)	Finite Element Model	Ultimate Capacity (kN)	Test : Predicted Ratio
A2	1128	CL2	1094	1.03
A4	1149	CL4	1120	1.03

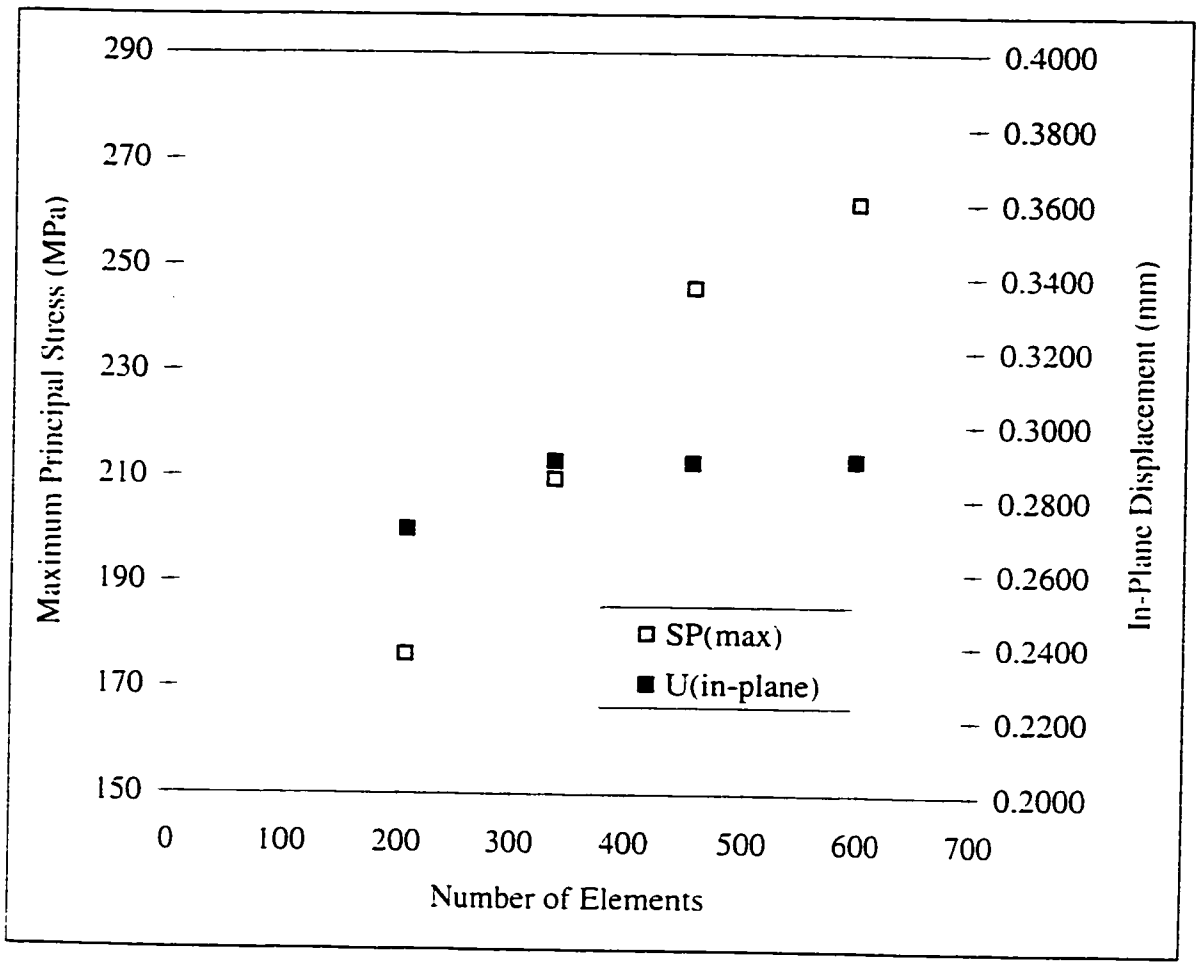

* *Note:* - *SP(max) = maximum principal stress value*
- *U(in-plane) = in-plane displacement*

Figure 4.1 - Linear elastic mesh study – summary of results.

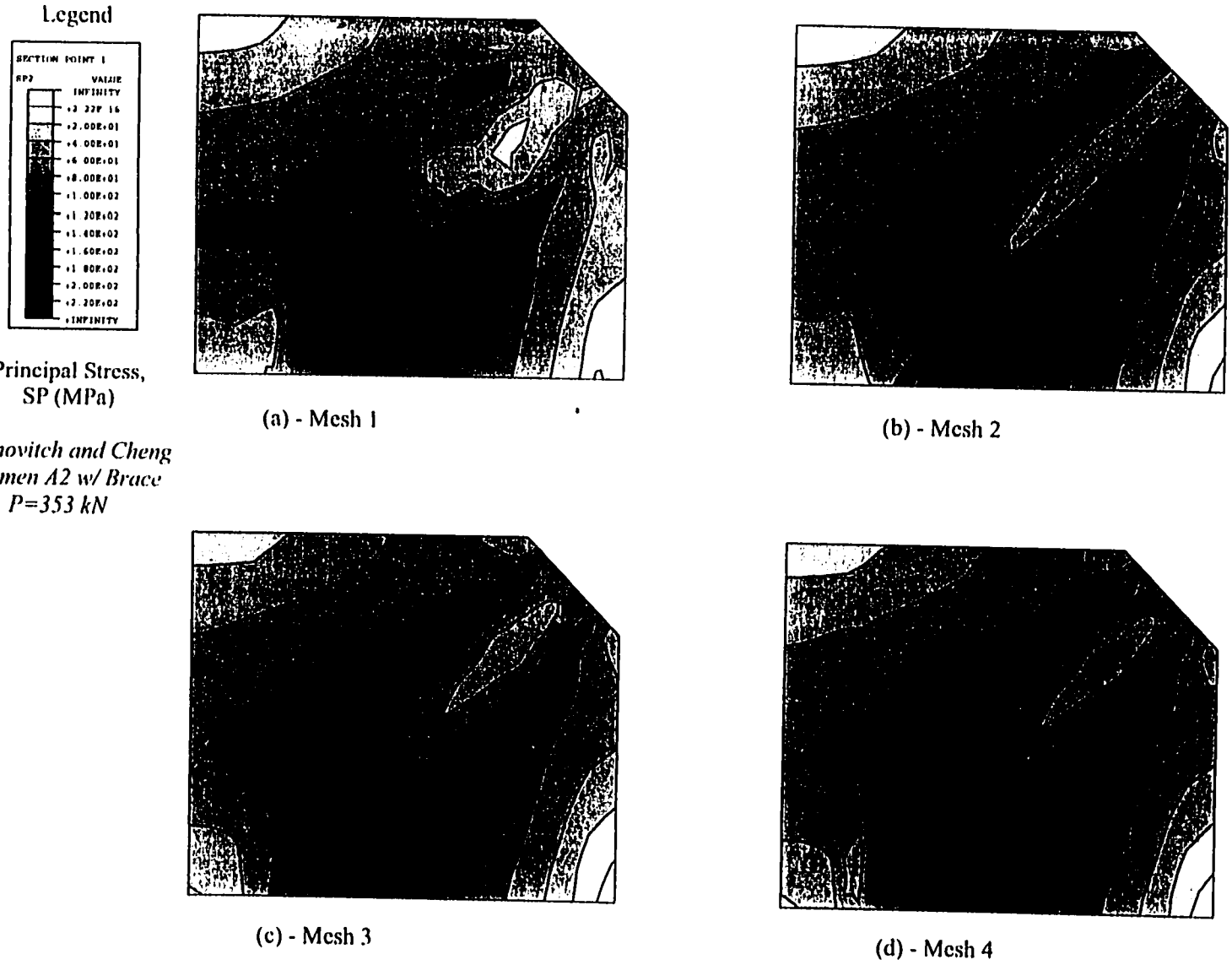

Figure 4.2 - Principal stress contour plots from linear elastic mesh study.

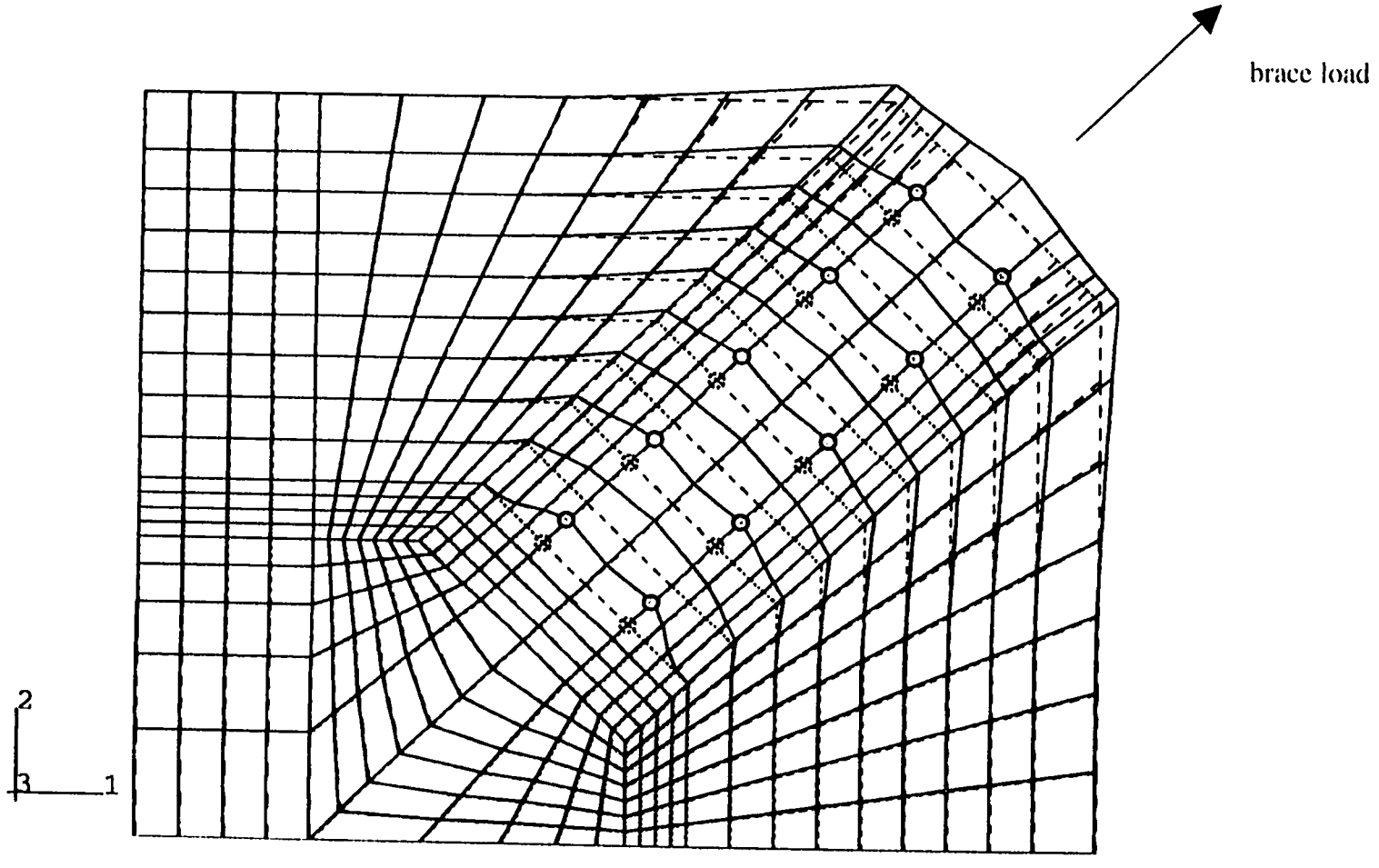

Figure 4.3 - Typical deformed configuration of gusset plate model loaded monotonically in tension.

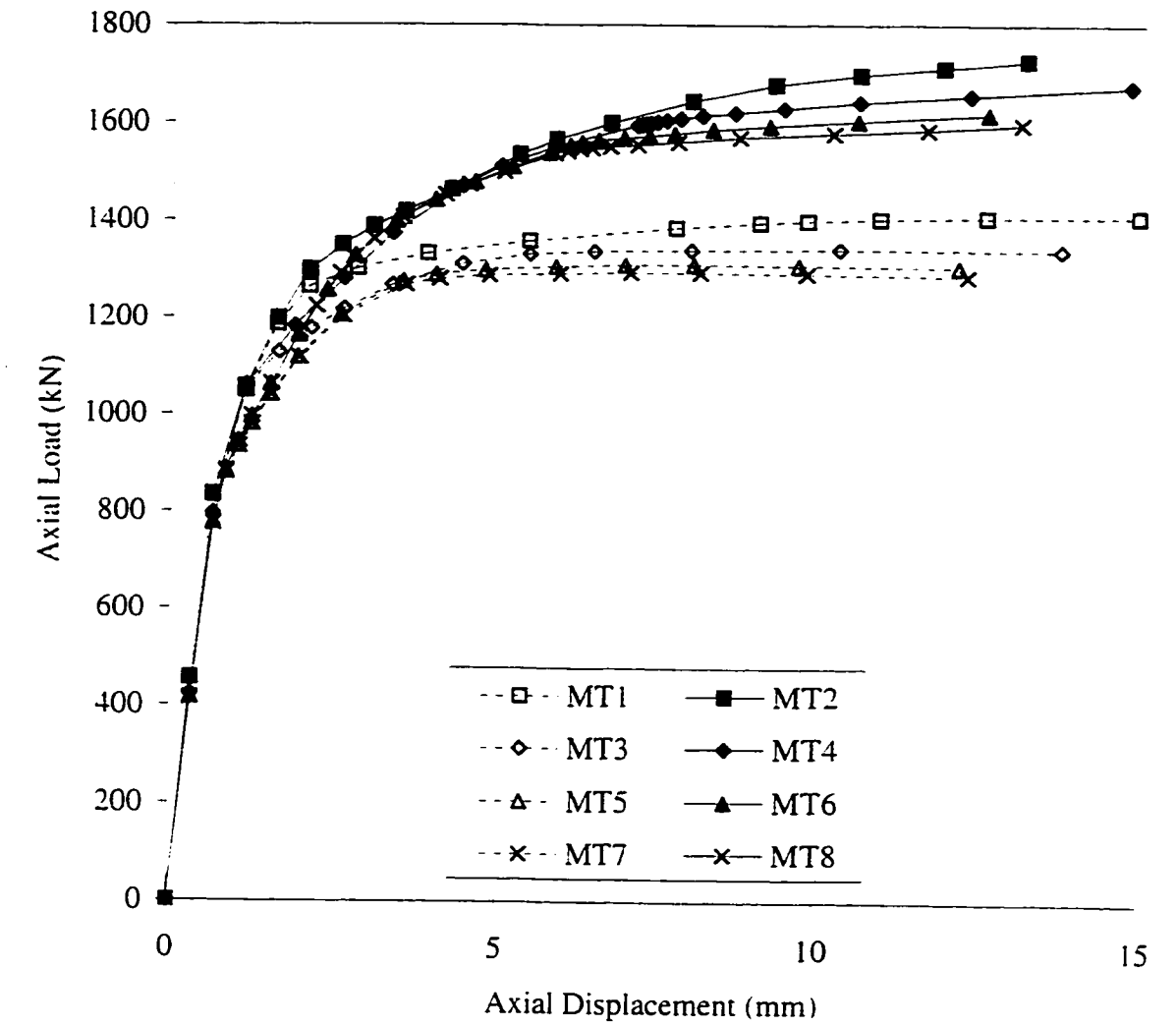

Model Description:

MT1 - *Mesh 1, elastic - perfect plastic material model*
MT2 - *Mesh 1, isotropic strain hardening material model*
MT3 - *Mesh 2, elastic - perfect plastic material model*
MT4 - *Mesh 2, isotropic strain hardening material model*
MT5 - *Mesh 3, elastic - perfect plastic material model*
MT6 - *Mesh 3, isotropic strain hardening material model*
MT7 - *Mesh 4, elastic - perfect plastic material model*
MT8 - *Mesh 4, isotropic strain hardening material model*

Figure 4.4 - Monotonic tension loading – effect of mesh refinement.

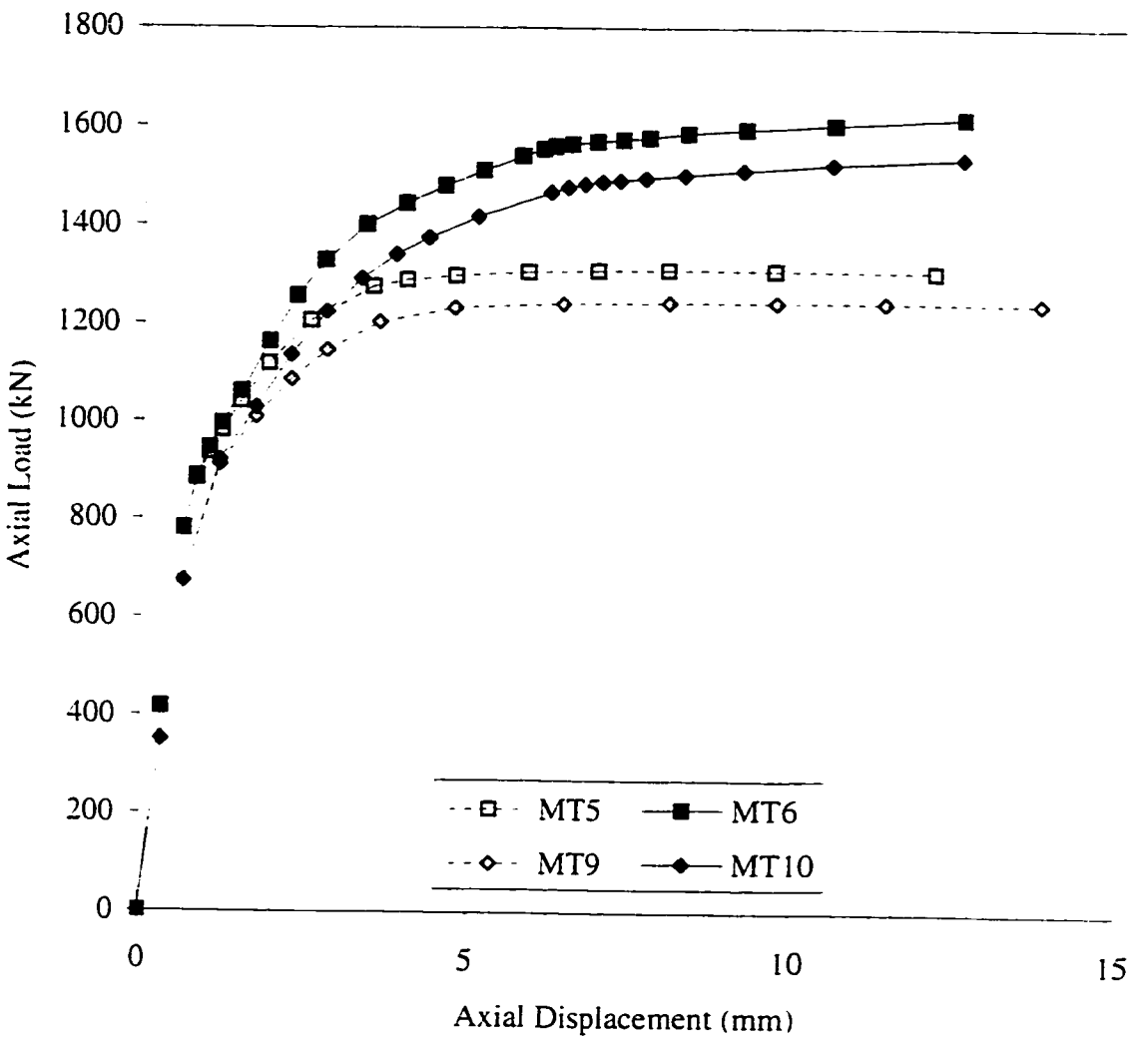

Model Description:

MT5 - *elastic - perfect plastic material model, rigid framing members*
MT6 - *isotropic strain hardening material model, rigid framing members*
MT9 - *elastic - perfect plastic material model, flexible framing members*
MT10 - *isotropic strain hardening material model, flexible framing members*

Figure 4.5 - Monotonic tension loading – rigid vs. flexible framing members.

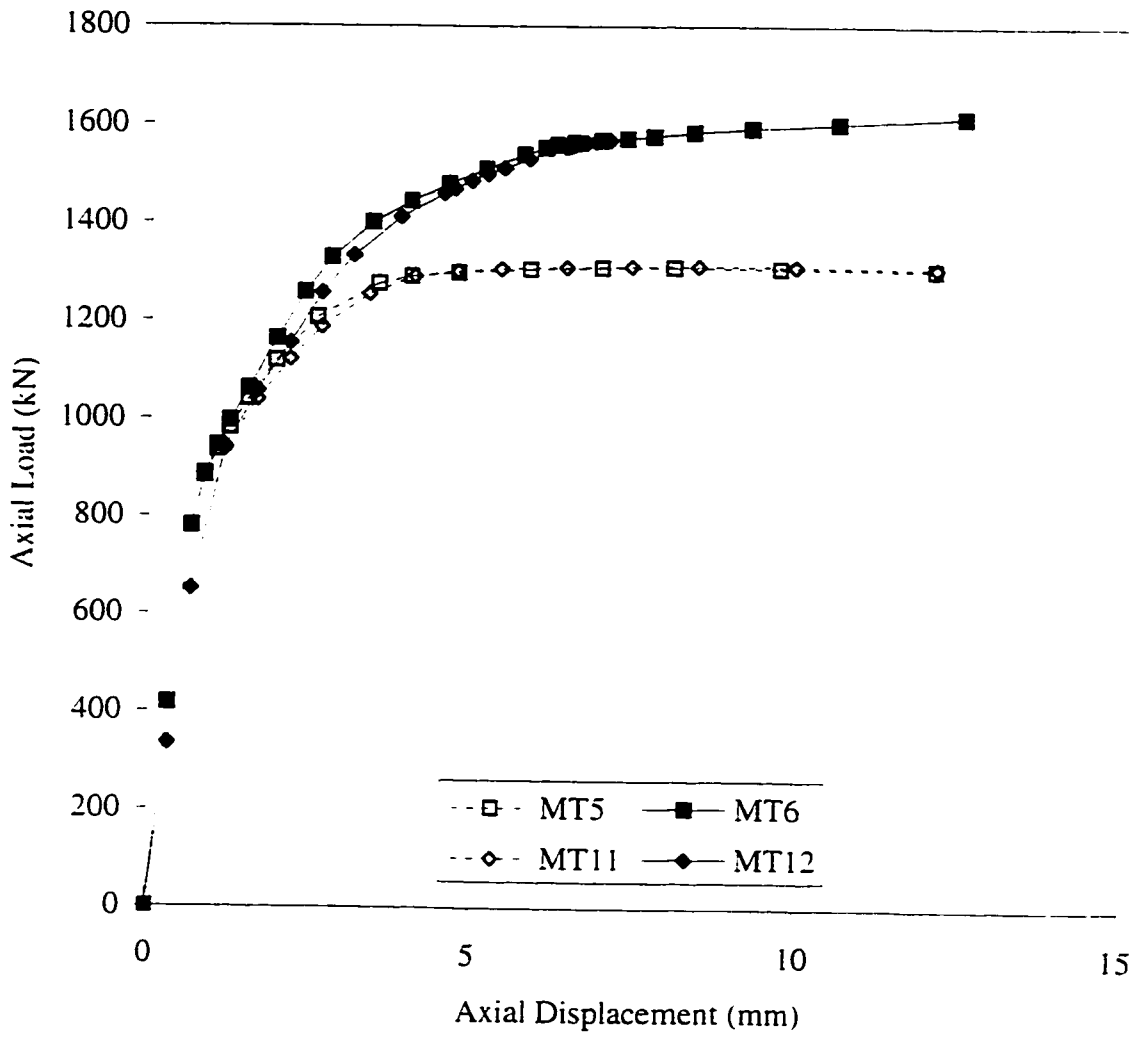

Model Description:

MT5 - *elastic - perfect plastic material model, rigid bolt model*
MT6 - *isotropic strain hardening material model, rigid bolt model*
MT11 - *elastic - perfect plastic material model, elastic bolt model*
MT12 - *isotropic strain hardening material model, elastic bolt model*

Figure 4.6 - Monotonic tension loading – effect of fastener (bolt) model.

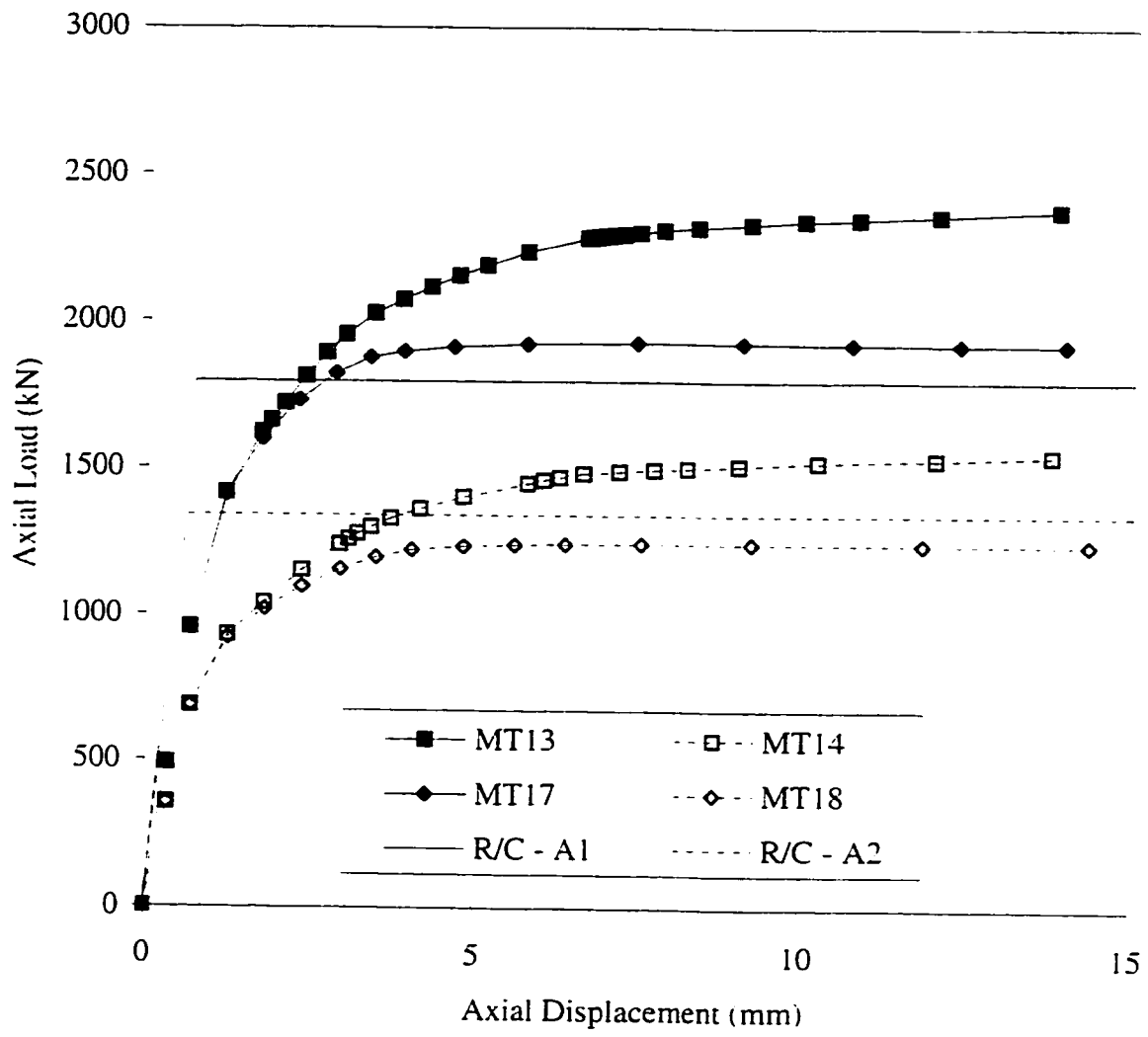

Model Description:

MT13 - *R/C - A1 model with isotropic strain hardening material model*
MT14 - *R/C - A2 model with isotropic strain hardening material model*
MT17 - *R/C - A1 model with elastic - perfect plastic material model*
MT18 - *R/C - A2 model with elastic - perfect plastic material model*

R/C - A1 - *two line representations of the hysteresis envelopes from*
R/C - A2 *tests conducted by Rabinovitch and Cheng (1993). The two lines represent initial stiffness and ultimate tensile capacity.*

Figure 4.7 - Monotonic tension loading – comparison with Rabinovitch and Cheng Specimens A1 and A2.

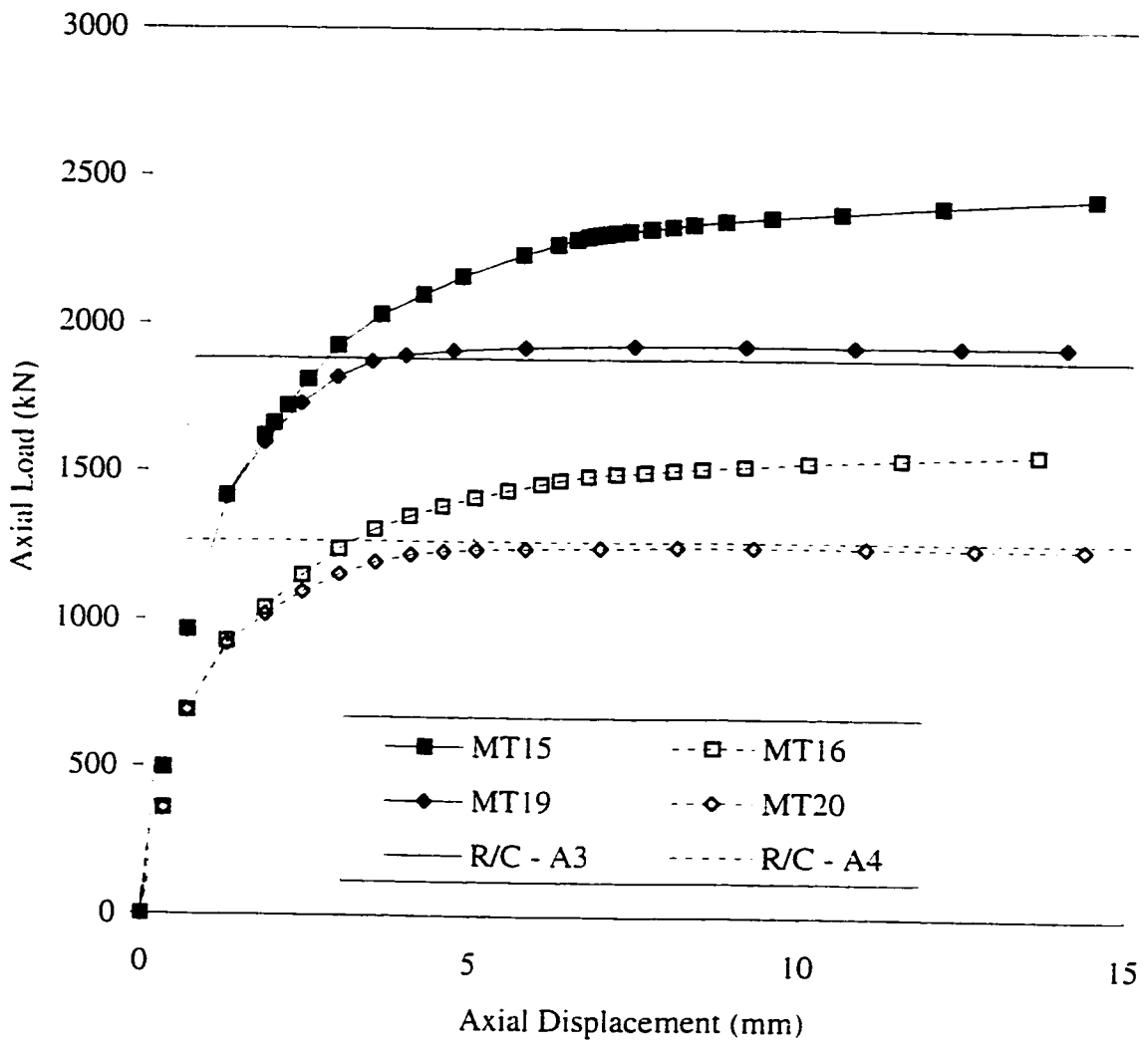

Model Description:

MT15 - *R/C - A3 model with isotropic strain hardening material model*
MT16 - *R/C - A4 model with isotropic strain hardening material model*
MT19 - *R/C - A3 model with elastic - perfect plastic material model*
MT20 - *R/C - A4 model with elastic - perfect plastic material model*

R/C - A3 - *two line representations of the hysteresis envelopes from*
R/C - A4 *tests conducted by Rabinovitch and Cheng (1993). The two lines represent initial stiffness and ultimate tensile capacity.*

Figure 4.8 - Monotonic tension loading – comparison with Rabinovitch and Cheng Specimens A3 and A4.

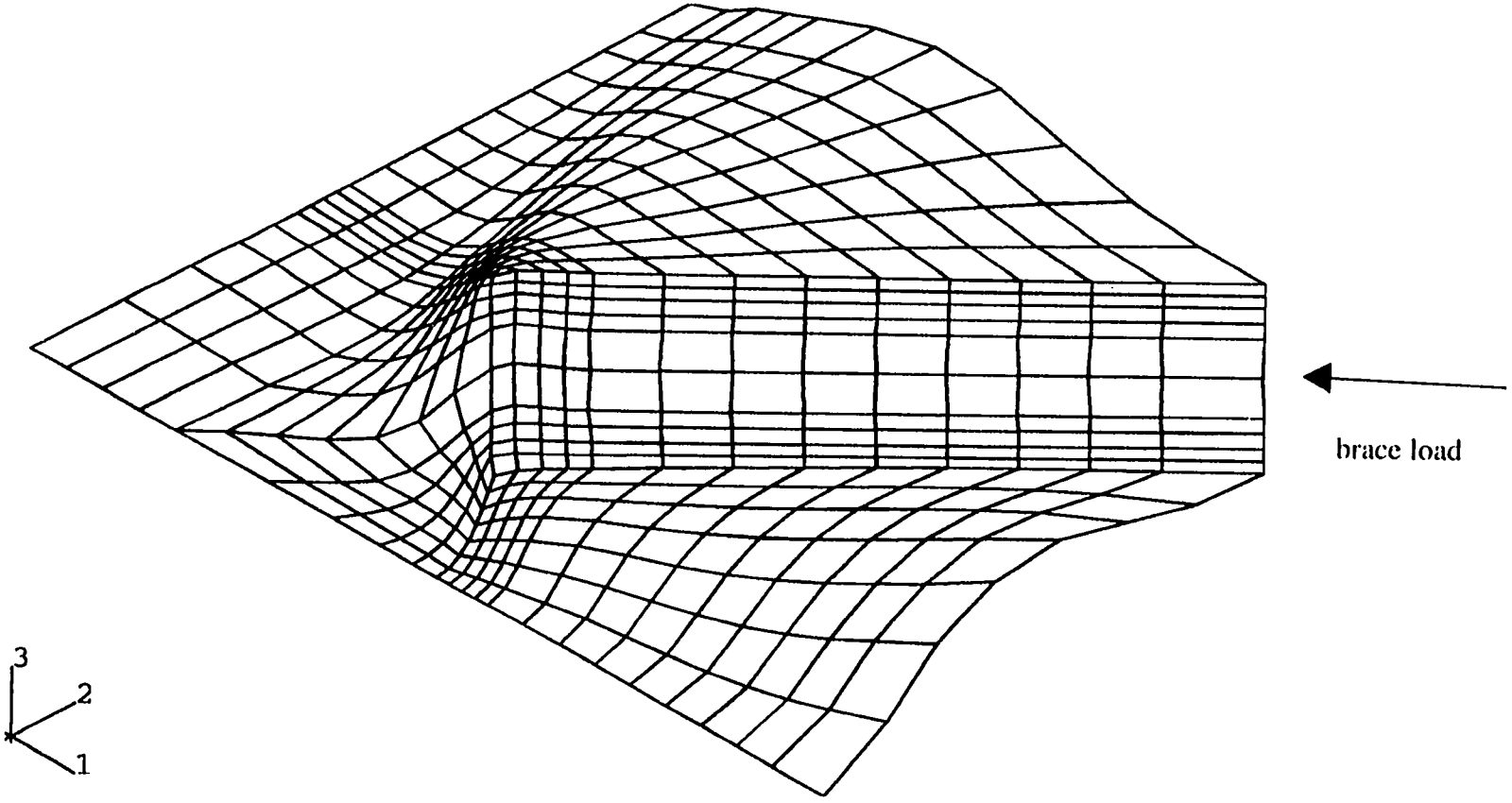

Figure 4.9 - Typical buckled configuration of gusset plate model loaded monotonically in compression.

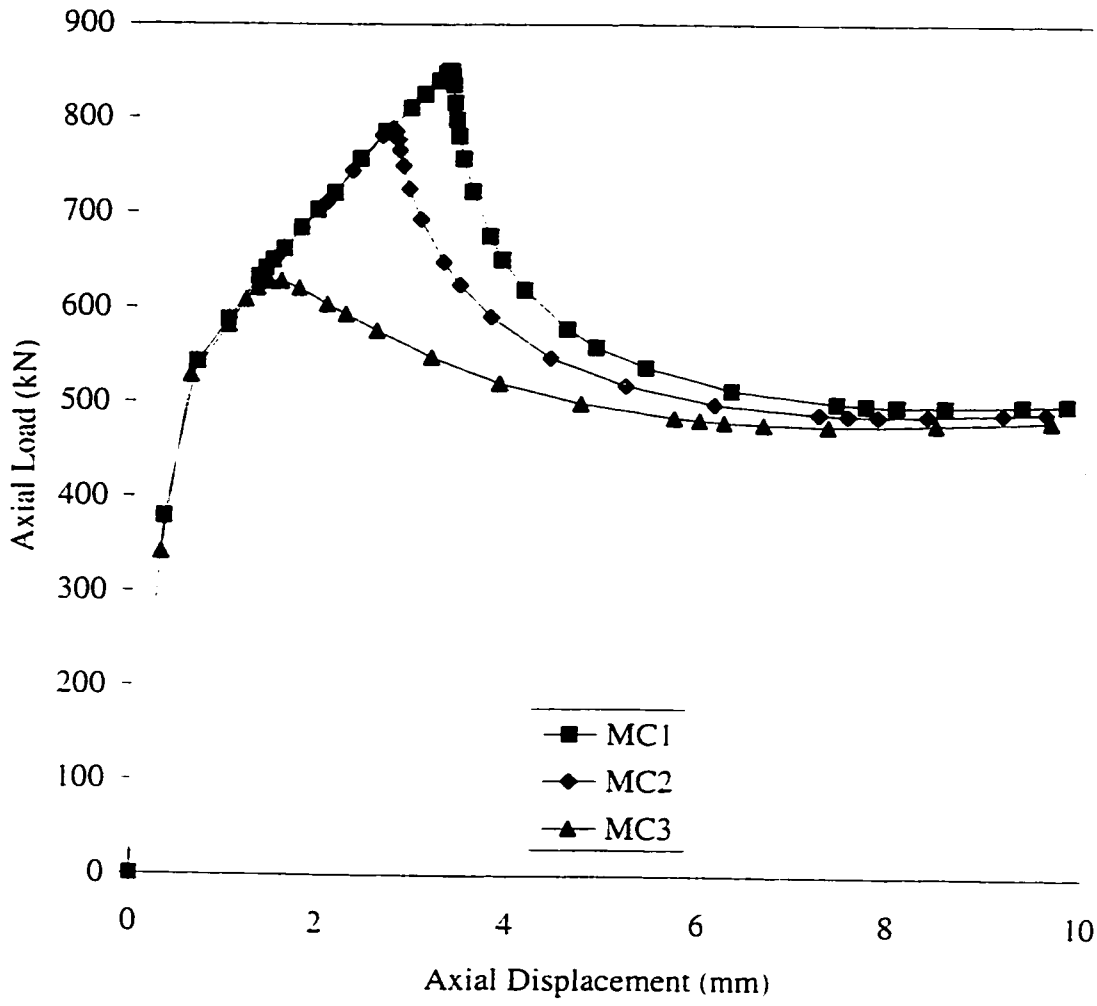

Model Description:

MC1 - *shape (1), 0.05 mm imperfection magnitude*
MC2 - *shape (1), 0.5 mm imperfection magnitude*
MC3 - *shape (1), 5.0 mm imperfection magnitude*

Figure 4.10 - Monotonic compression loading – effect of initial imperfection magnitude.

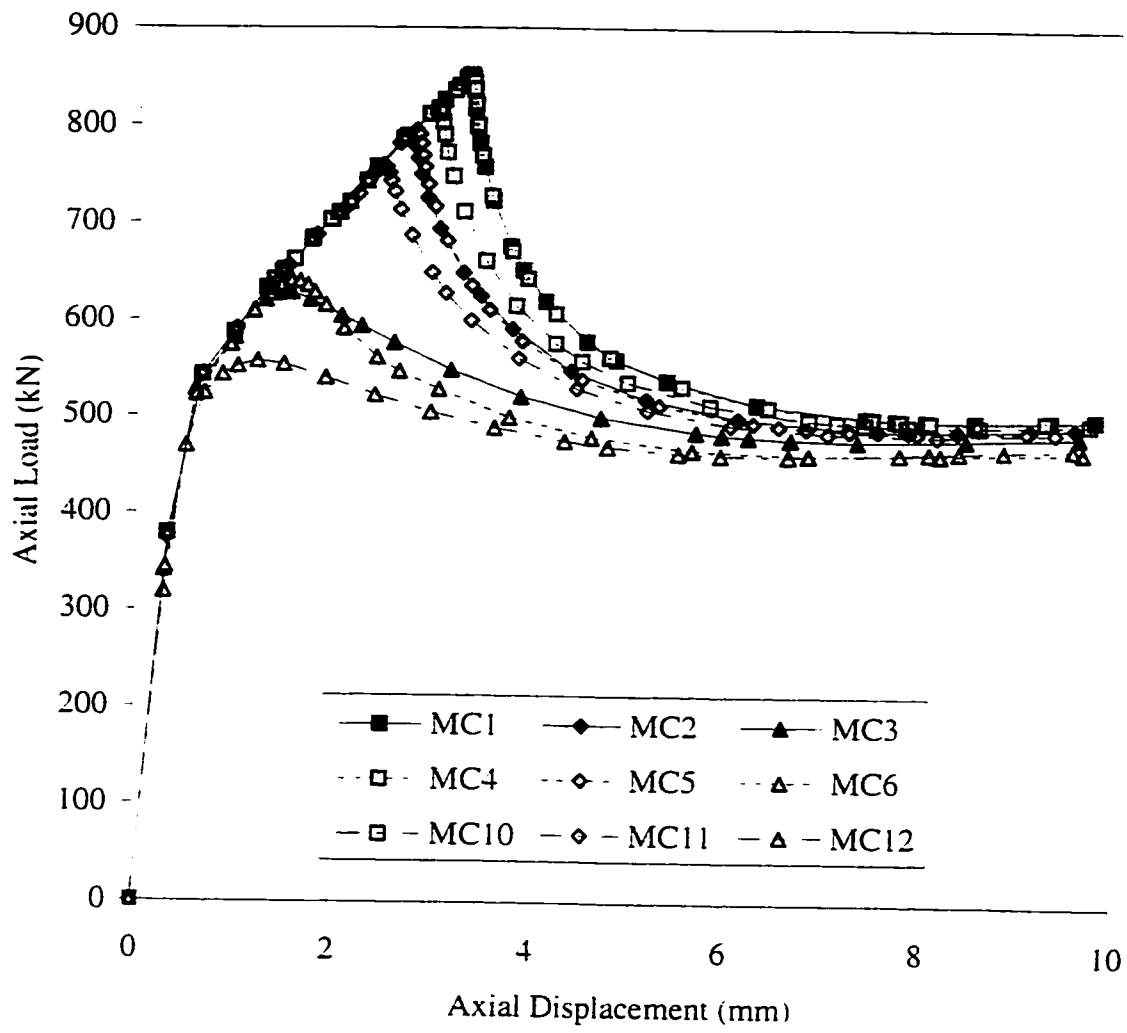

Model Description:

MC1	*- shape (1), 0.05 mm imperfection magnitude*
MC2	*- shape (1), 0.5 mm imperfection magnitude*
MC3	*- shape (1), 5.0 mm imperfection magnitude*
MC4	*- shape (2), 0.05 mm imperfection magnitude*
MC5	*- shape (2), 0.5 mm imperfection magnitude*
MC6	*- shape (2), 5.0 mm imperfection magnitude*
MC10	*- shape (3), 0.05 mm imperfection magnitude*
MC11	*- shape (3), 0.5 mm imperfection magnitude*
MC12	*- shape (3), 5.0 mm imperfection magnitude*

Figure 4.11 - Monotonic compression loading – effect of initial imperfection shape.

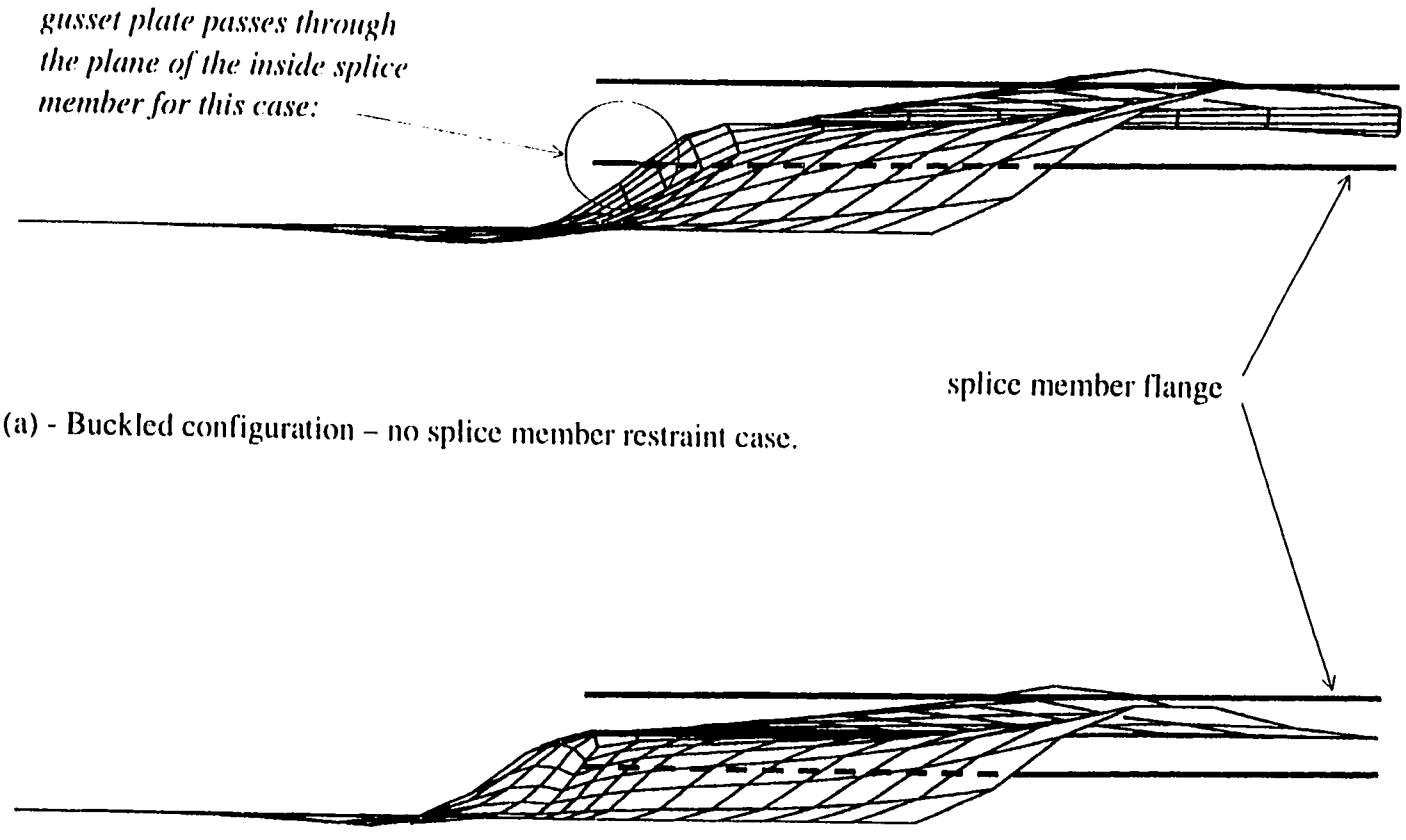

(a) - Buckled configuration – no splice member restraint case.

(a) - Buckled configuration – full splice member restraint case.

Figure 4.12 - Effect of splice member out-of-plane (clamping) restraint on buckled configuration.

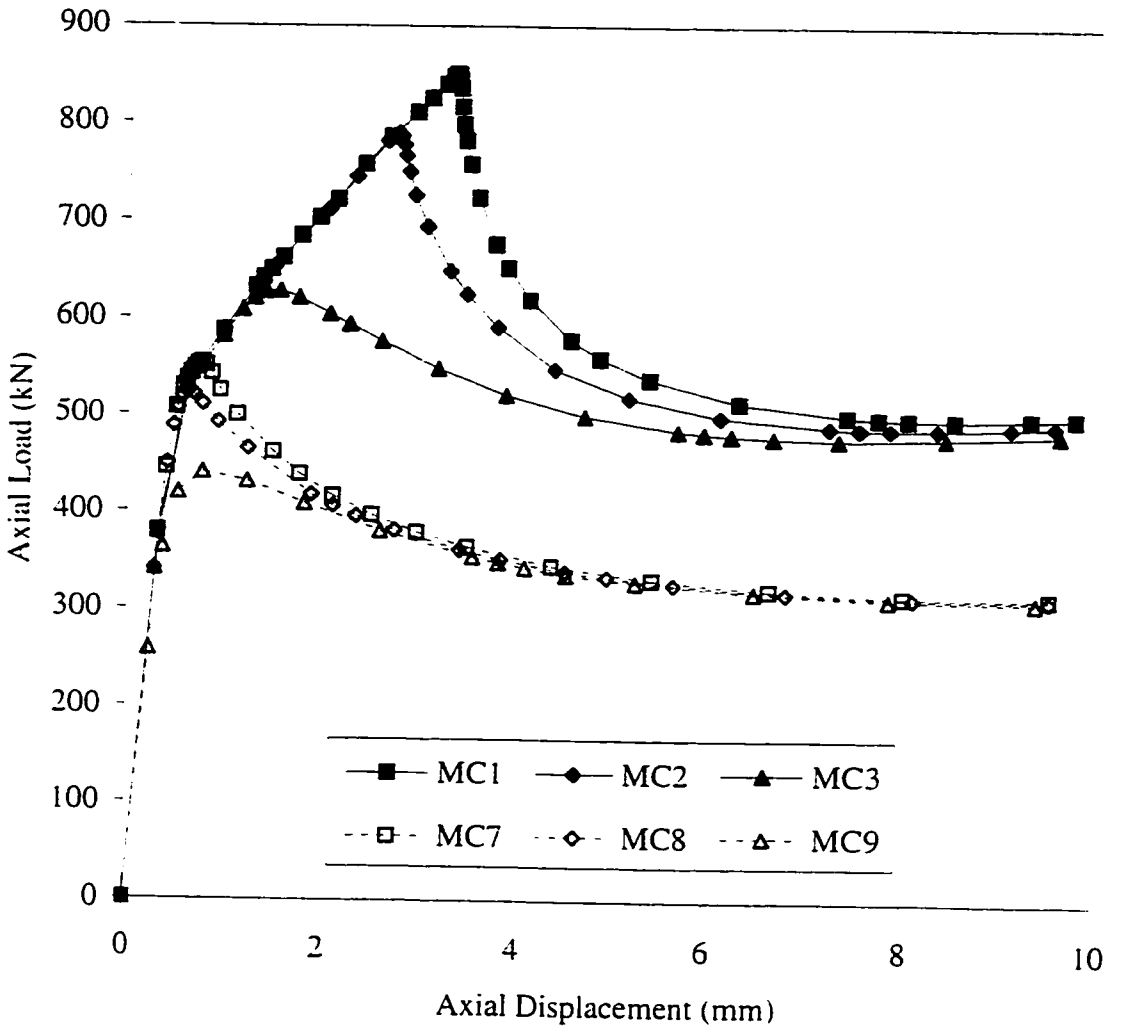

Model Description:

MC1	*- 0.05 mm imperfection magnitude, full restraint*
MC2	*- 0.5 mm imperfection magnitude, full restraint*
MC3	*- 5.0 mm imperfection magnitude, full restraint*
MC7	*- 0.05 mm imperfection magnitude, no restraint*
MC8	*- 0.5 mm imperfection magnitude, no restraint*
MC9	*- 5.0 mm imperfection magnitude, no restraint*

Figure 4.13 - Monotonic compression loading – effect of out-of-plane (clamping) restraint imparted by splice members.

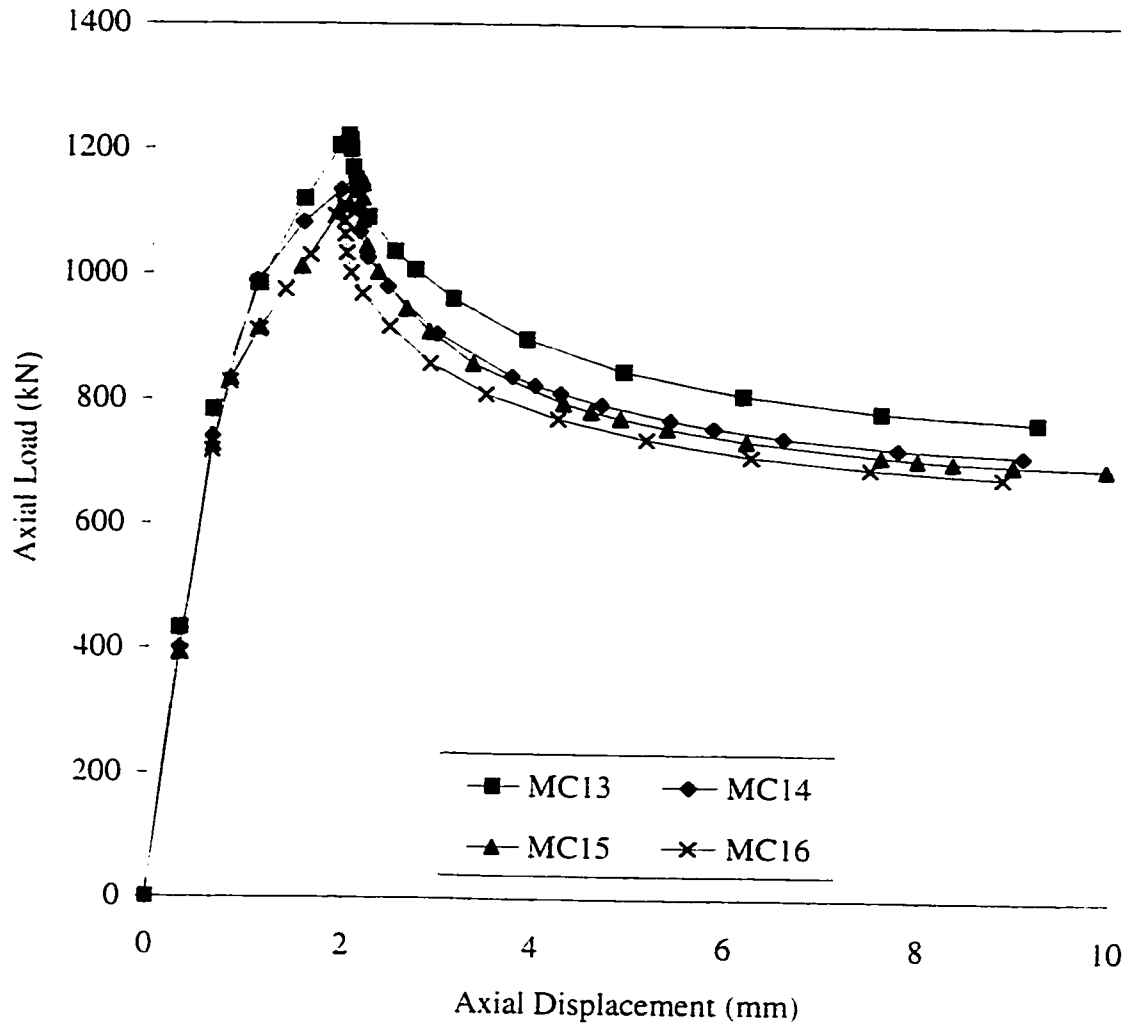

Model Description:

MC13 - *shape (1), 0.5 mm imperfection magnitude, Mesh 1*
MC14 - *shape (1), 0.5 mm imperfection magnitude, Mesh 2*
MC15 - *shape (1), 0.5 mm imperfection magnitude, Mesh 3*
MC16 - *shape (1), 0.5 mm imperfection magnitude, Mesh 4*

Figure 4.14 - Monotonic compression loading – effect of mesh refinement.

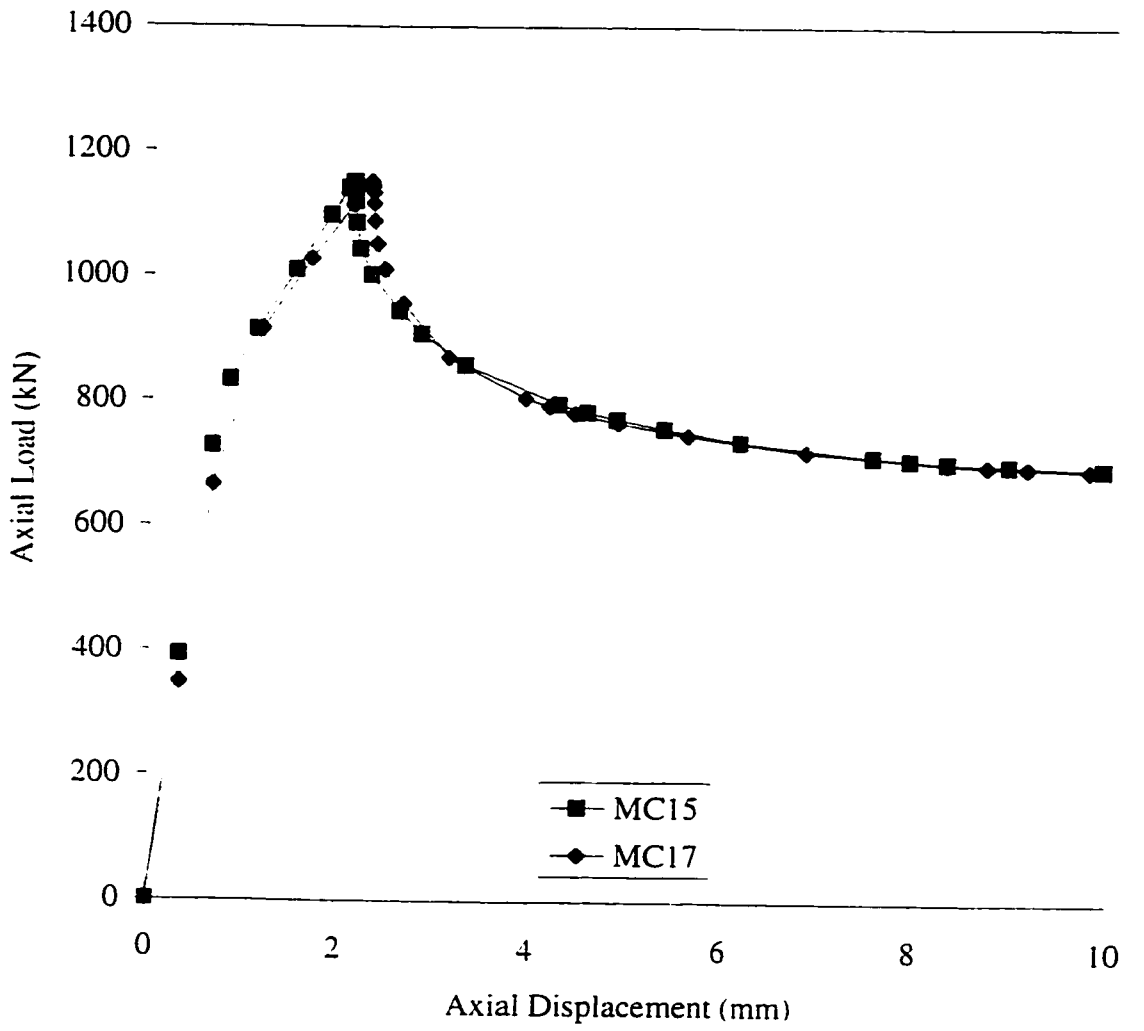

Model Description:

MC15 - *shape (1), 0.5 mm imperfection, rigid framing members*
MC17 - *shape (1), 0.5 mm imperfection, flexible framing members*

Figure 4.15 - Monotonic compression loading – effect of framing member stiffness.

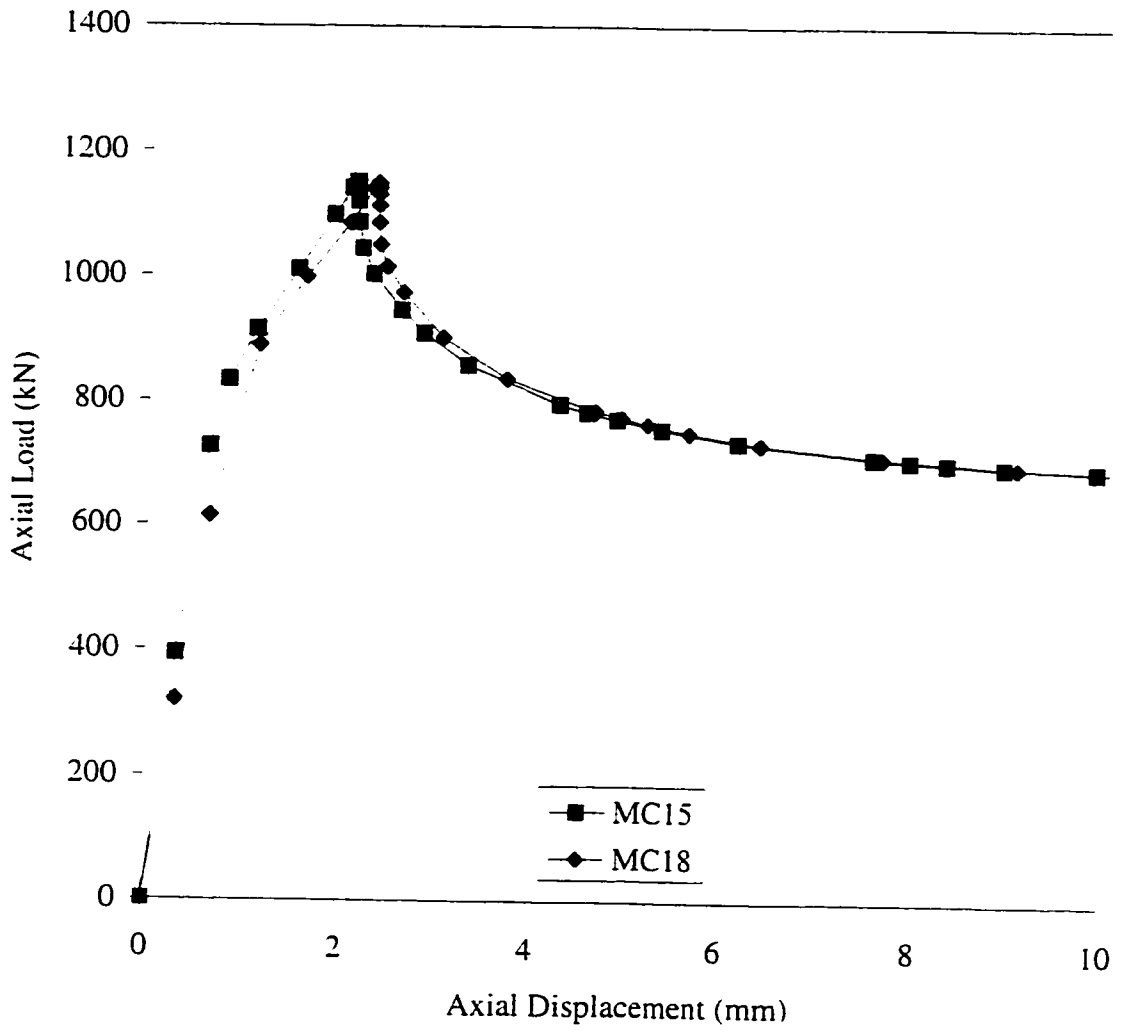

Model Description:

MC15 - *shape (1), 0.5 mm imperfection, rigid bolt model*
MC18 - *shape (1), 0.5 mm imperfection, elastic bolt model*

Figure 4.16 - Monotonic compression loading – effect of fastener (bolt) model.

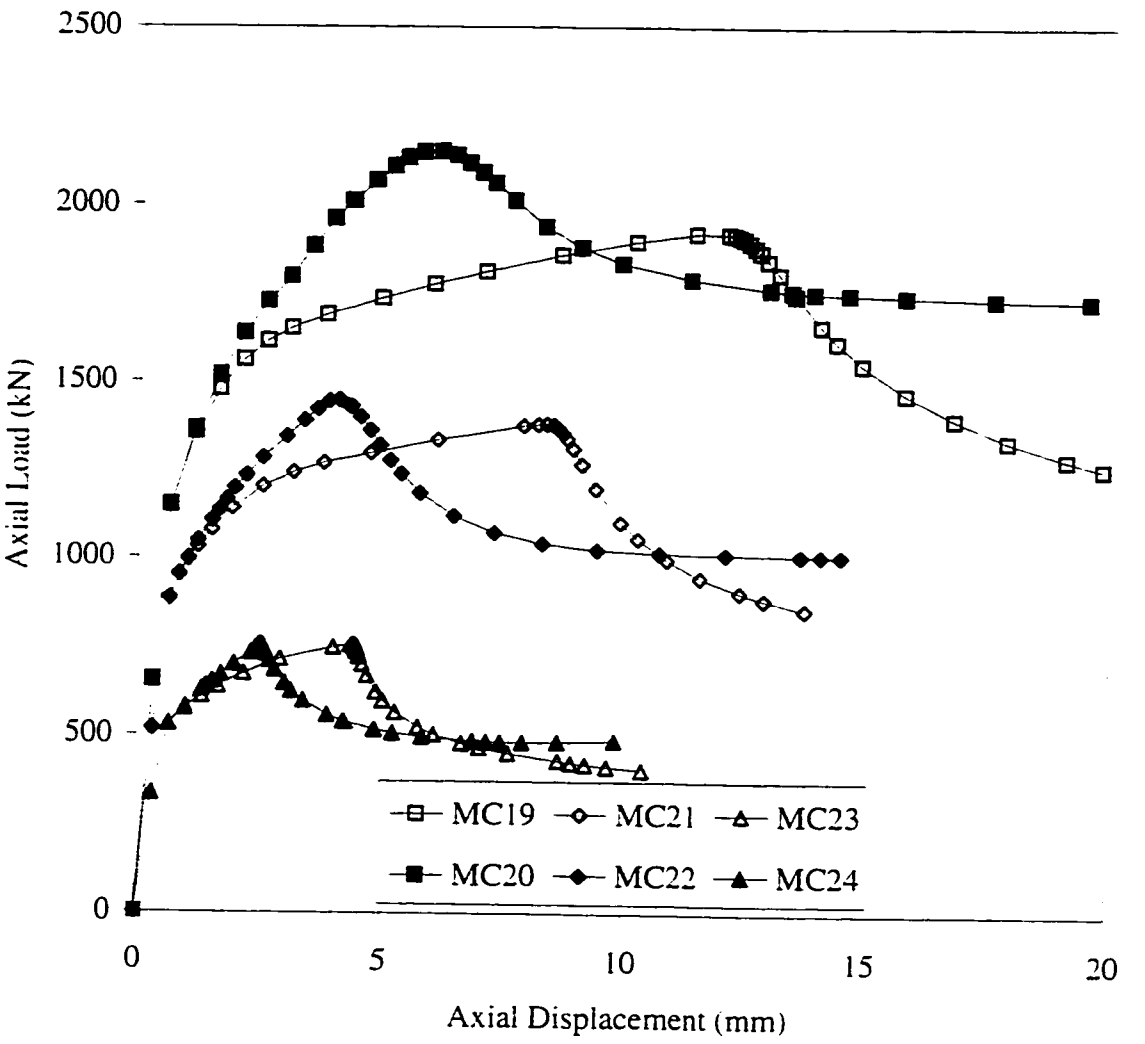

Model Description:

MC19	*- Yam and Cheng specimen GP1, elastic - perfect plastic*
MC20	*- Yam and Cheng specimen GP1, isotropic strain hardening*
MC21	*- Yam and Cheng specimen GP2, elastic - perfect plastic*
MC22	*- Yam and Cheng specimen GP2, isotropic strain hardening*
MC23	*- Yam and Cheng specimen GP3, elastic - perfect plastic*
MC24	*- Yam and Cheng specimen GP3, isotropic strain hardening*

Figure 4.17 - Monotonic compression loading – effect of material model.

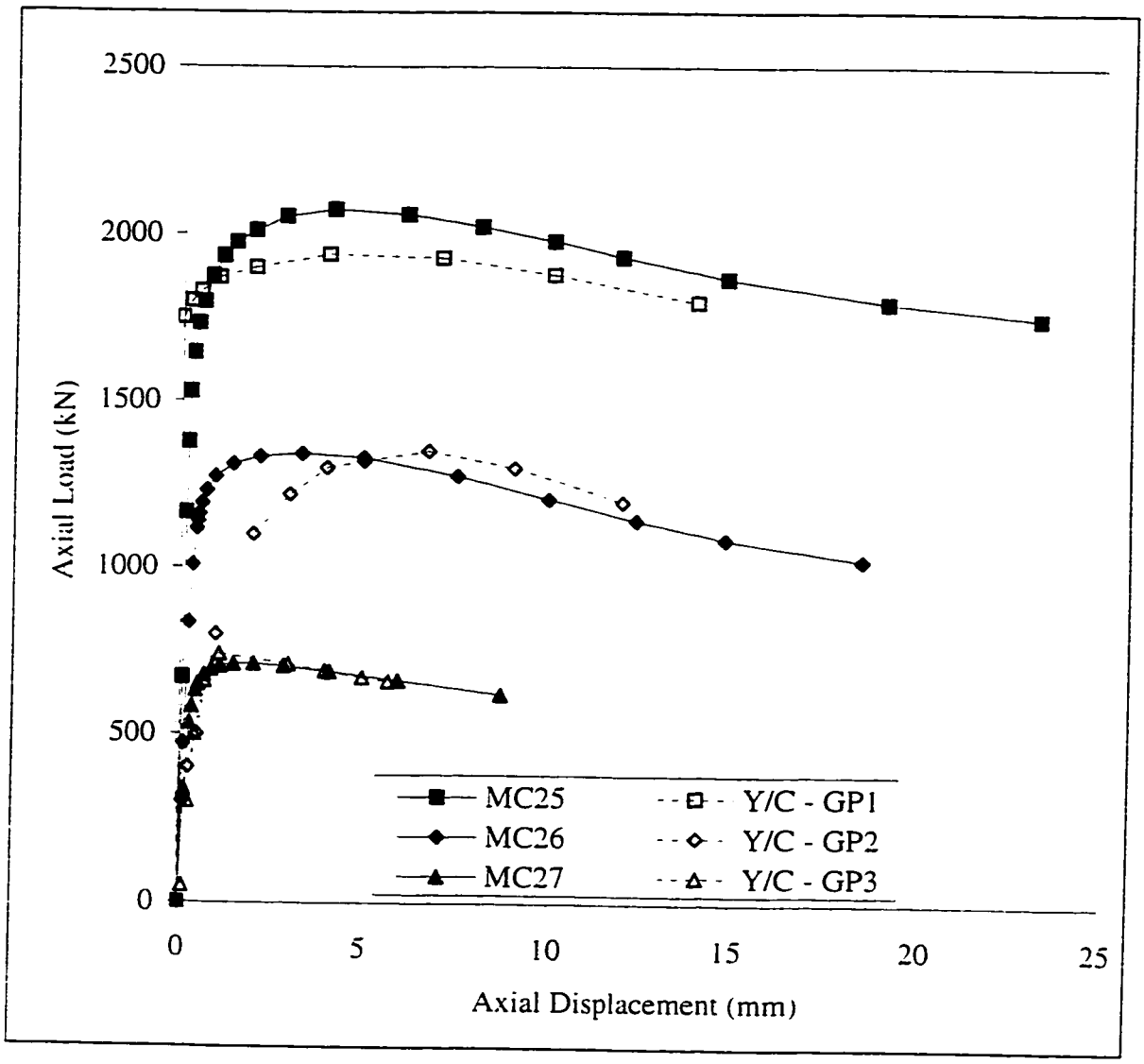

Model Description:

MC25 - *Y/C - GP1 (13.3 mm plate), isotropic strain hardening*
MC26 - *Y/C - GP2 (9.8 mm plate), isotropic strain hardening*
MC27 - *Y/C - GP3 (6.5 mm plate), isotropic strain hardening*

Figure 4.18 - Monotonic compression loading – comparison with Yam and Cheng specimens.

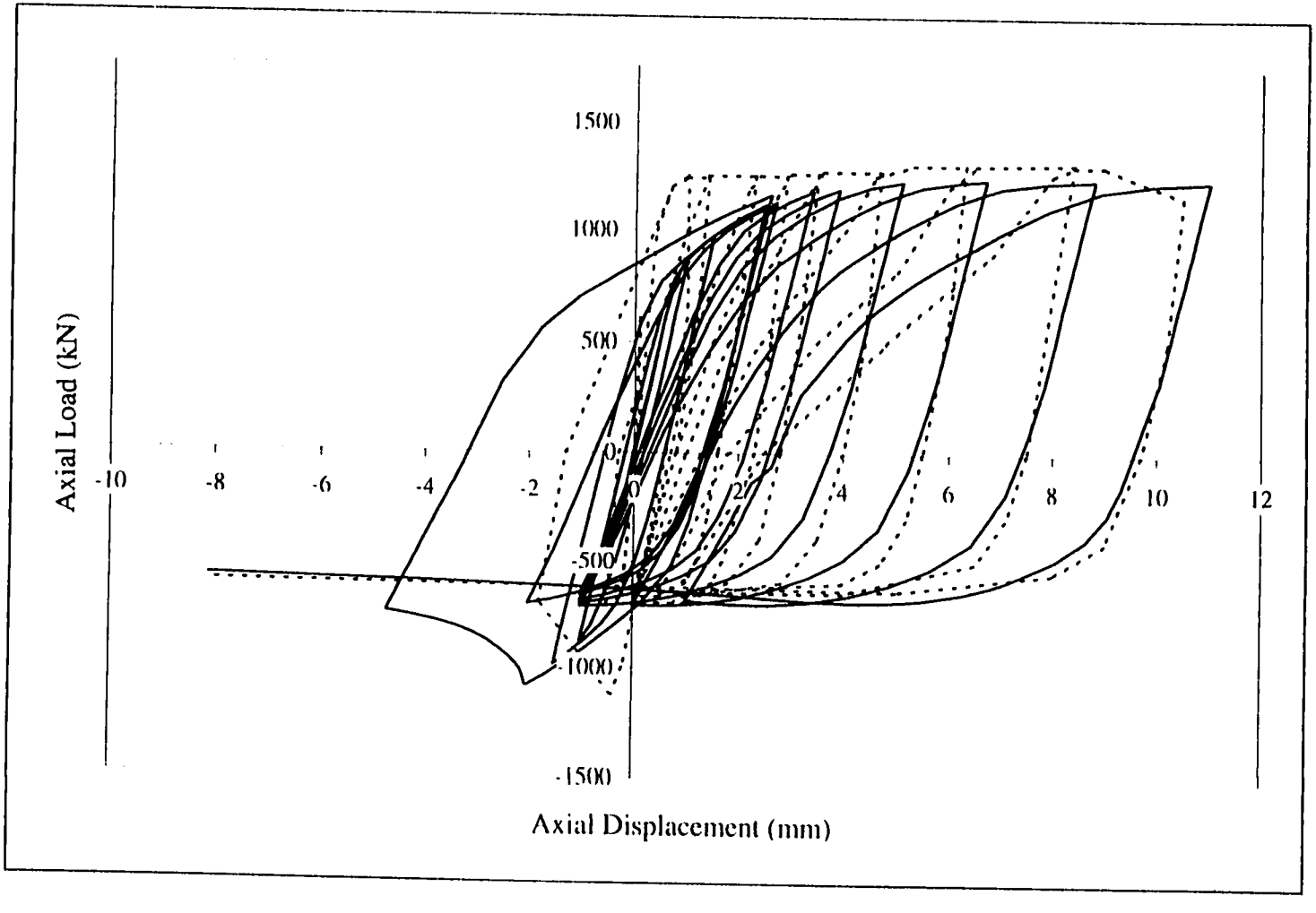

** Note:* - *Dashed line = test specimen hysteresis (Rabinovitch and Cheng Specimen A2)*
- *Solid line = finite element model CL2 hysteresis*

Figure 4.19 - Axial load versus displacement hysteresis for finite element model CL2.

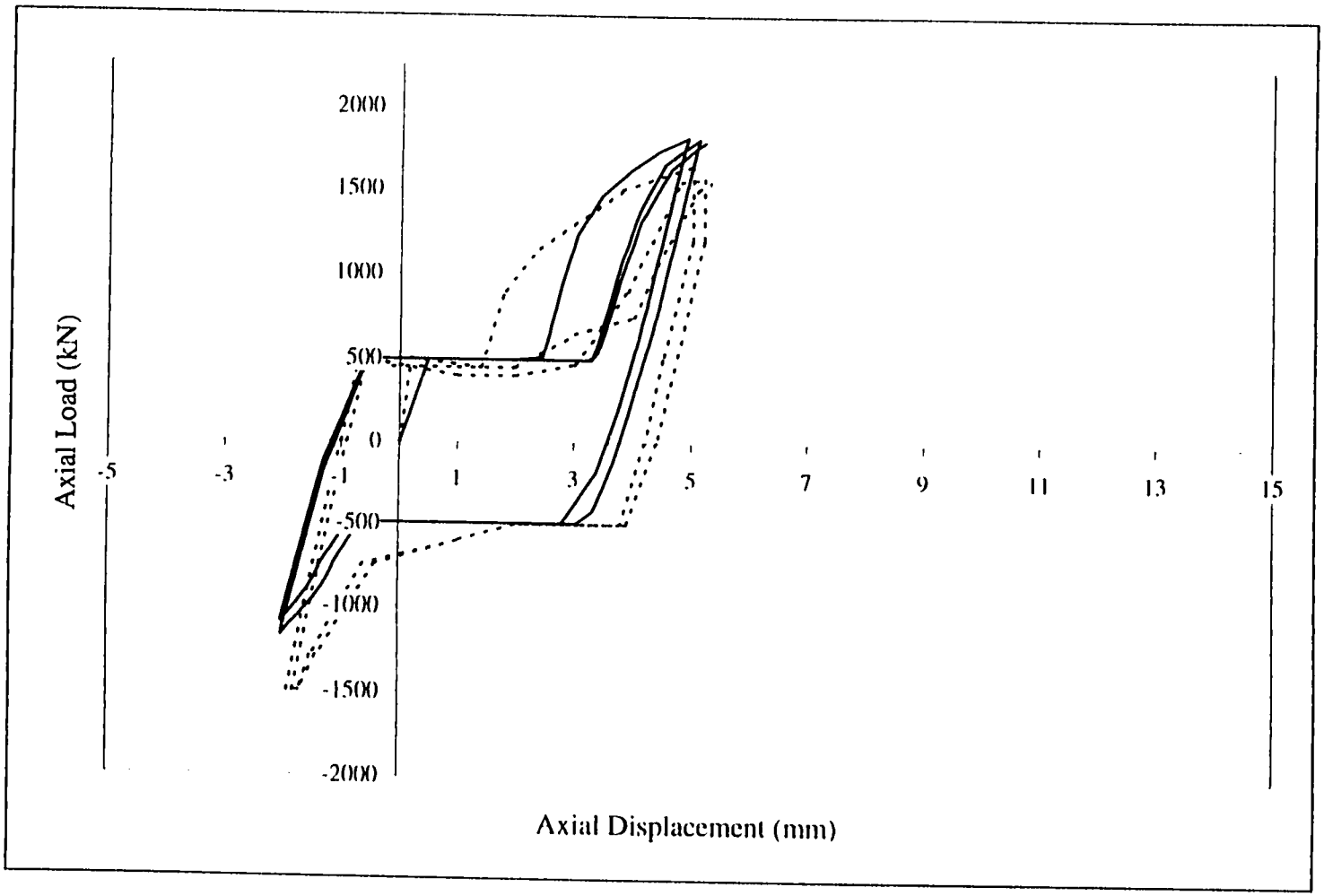

* *Note:* - *Dashed line = test specimen hysteresis (Rabinovitch and Cheng Specimen A1)*
- *Solid line = finite element model CL1 hysteresis*

Figure 4.20 - Axial load versus displacement hysteresis for finite element model CL1.

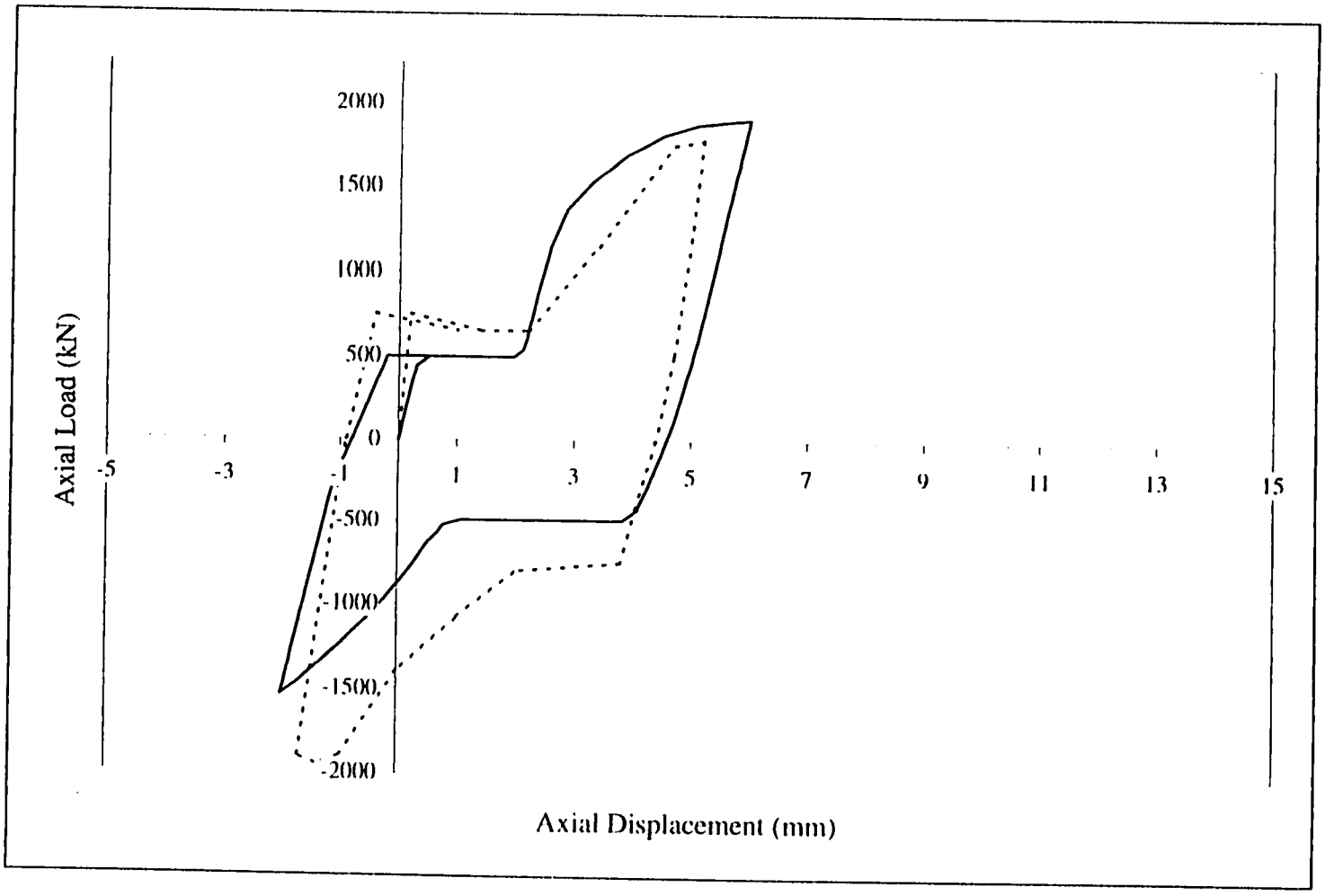

** Note:* - *Dashed line = test specimen hysteresis (Rabinovitch and Cheng Specimen A3)*
- *Solid line = finite element model CL3 hysteresis*

Figure 4.21 - Axial load versus displacement hysteresis for finite element model CL3.

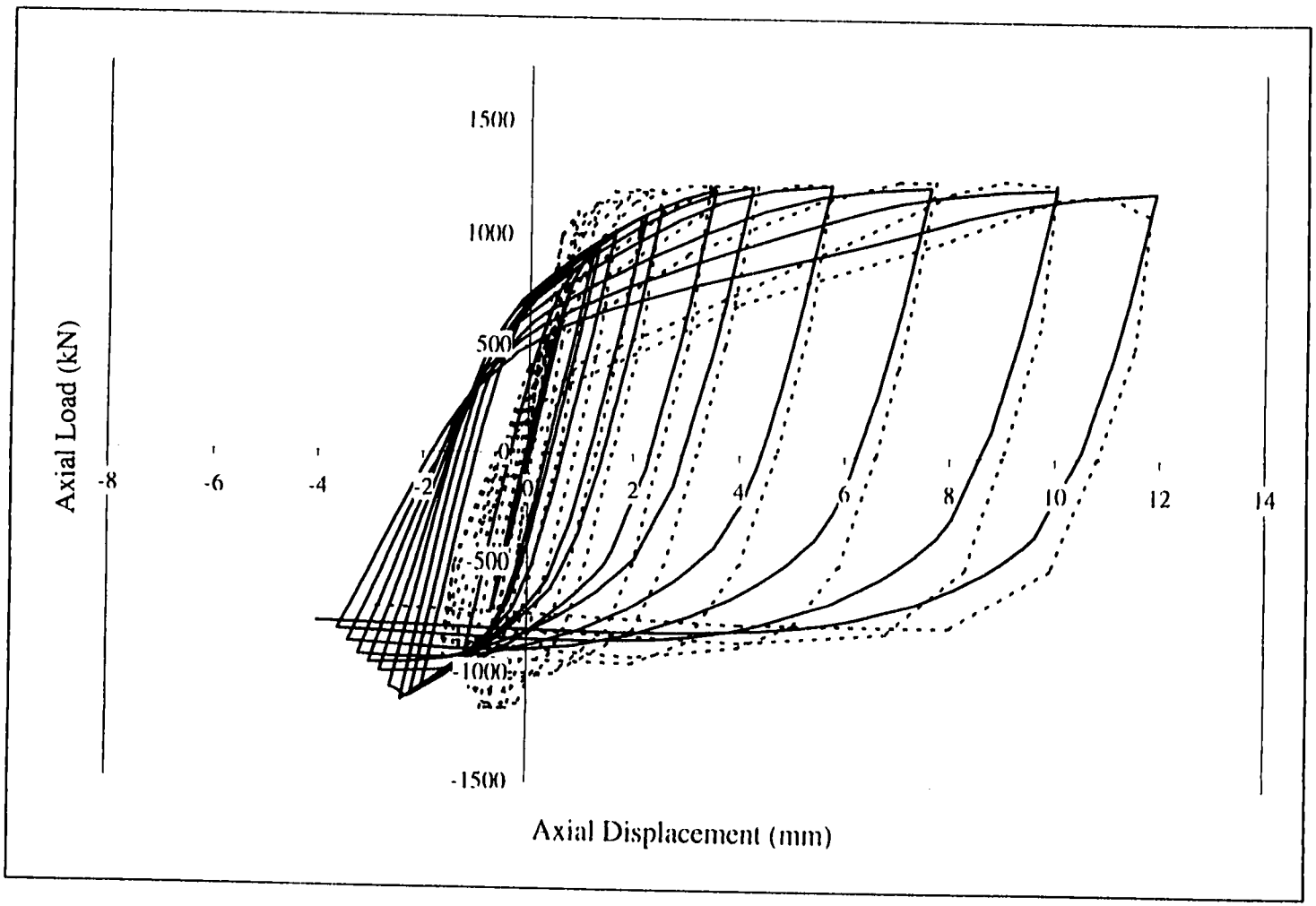

* *Note:* - *Dashed line = test specimen hysteresis (Rabinovitch and Cheng Specimen A4)*
- *Solid line = finite element model CL4 hysteresis*

Figure 4.22 - Axial load versus displacement hysteresis for finite element model CL4.

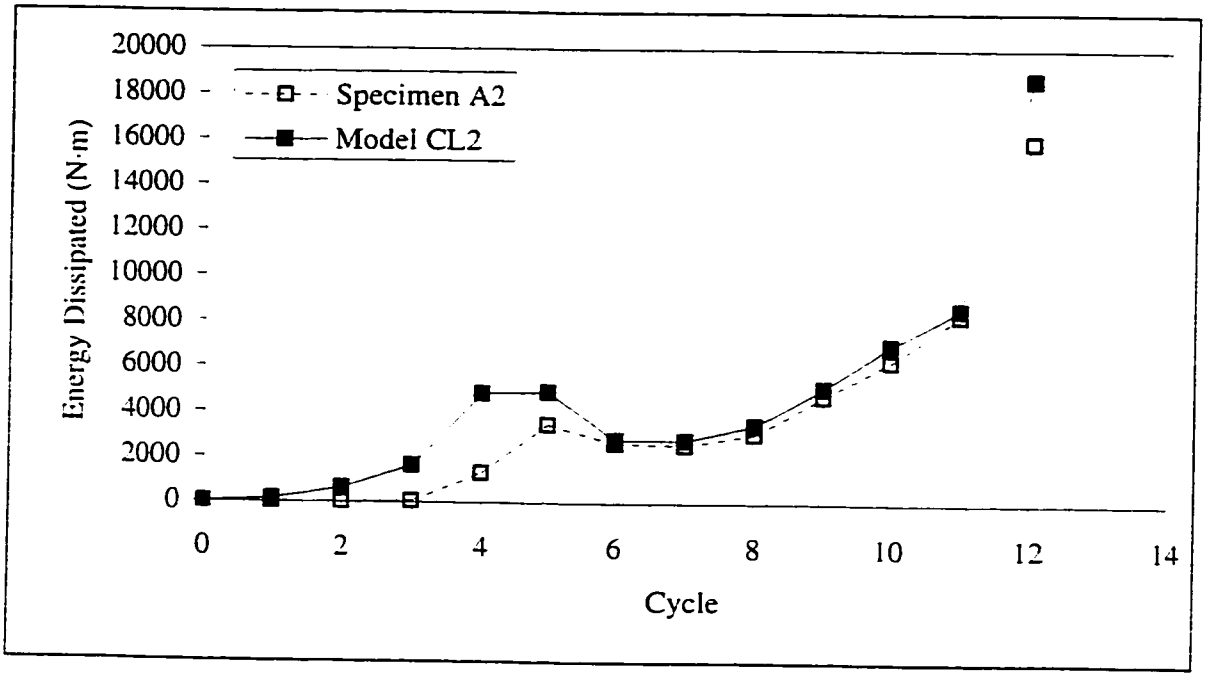

Figure 4.23 - Energy dissipated (per cycle) for finite element model CL2 / Rabinovitch and Cheng Specimen A2.

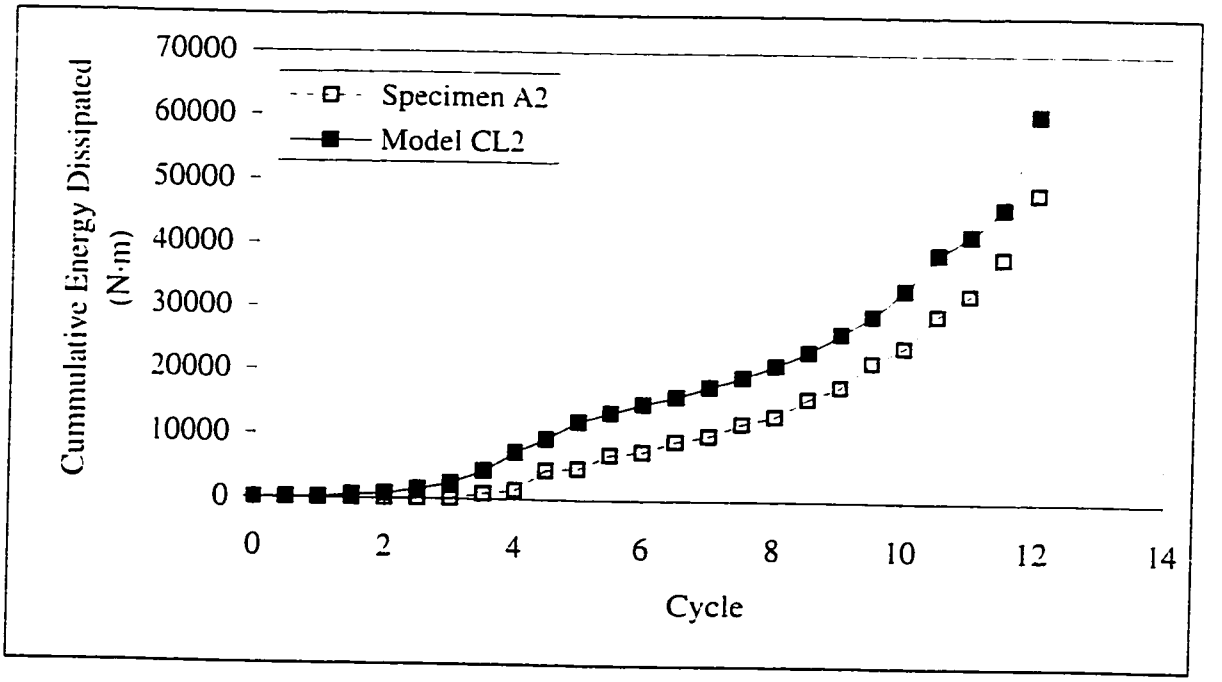

Figure 4.24 - Cummulative energy dissipated for finite element model CL2 / Rabinovitch and Cheng Specimen A2.

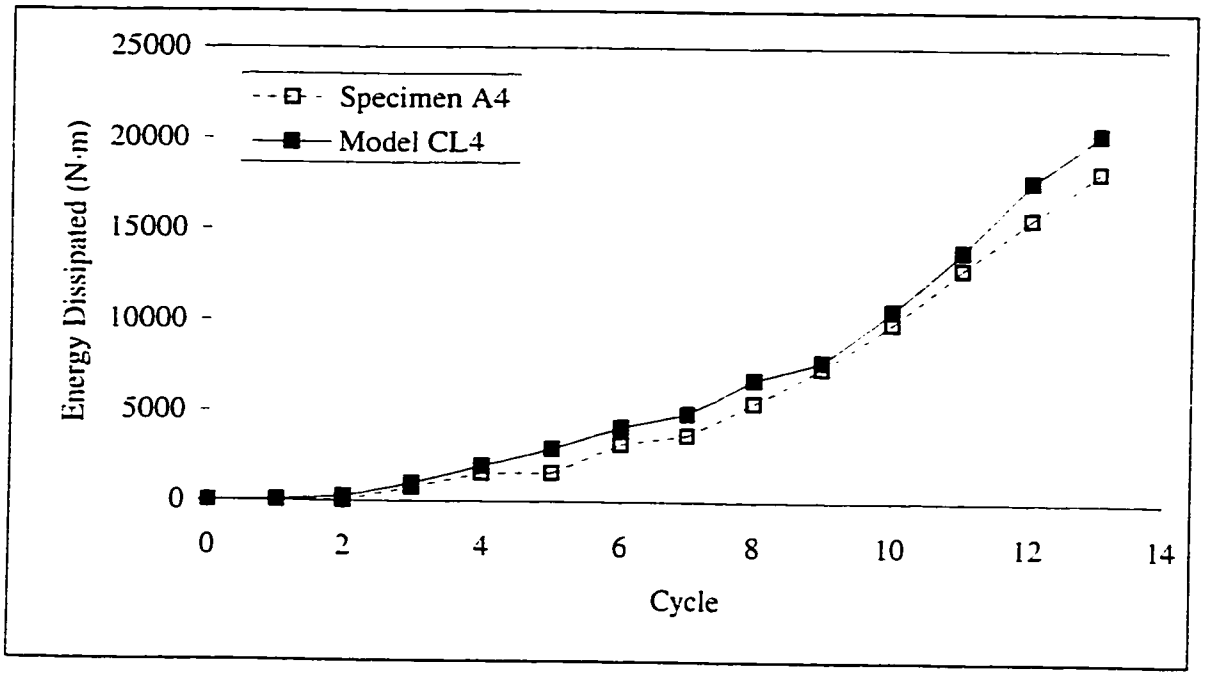

Figure 4.25 - Energy dissipated (per cycle) for finite element model CL4 / Rabinovitch and Cheng Specimen A4.

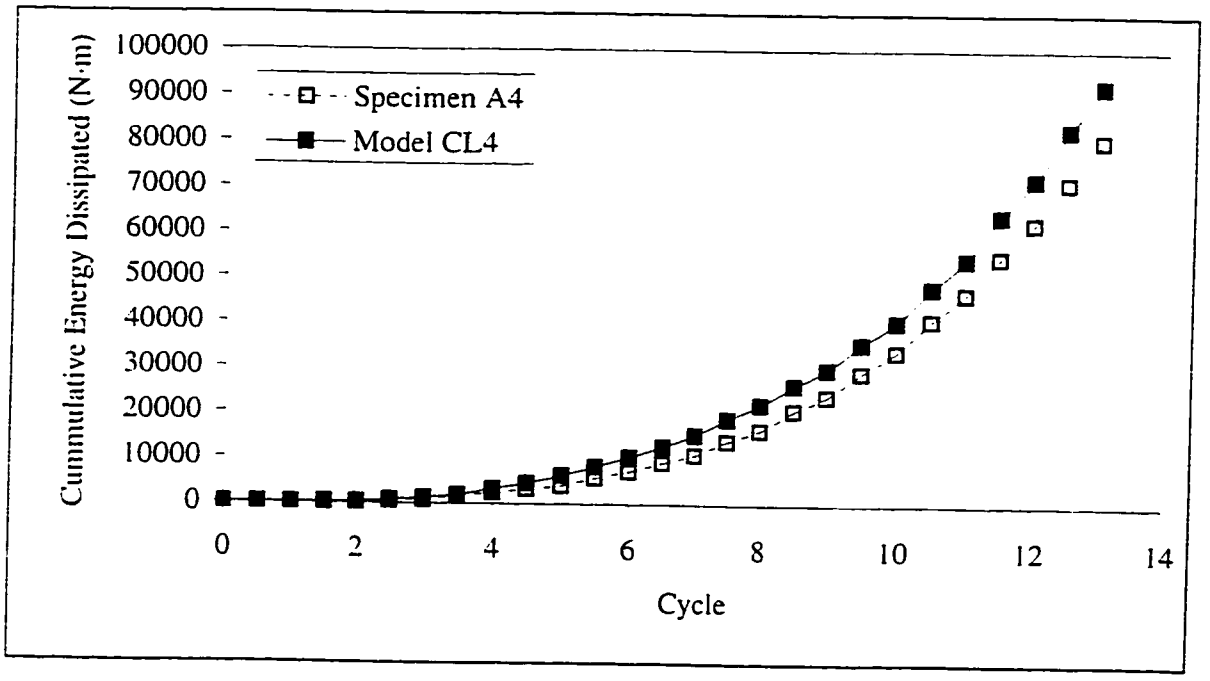

Figure 4.26 - Cummulative energy dissipated for finite element model CL4 / Rabinovitch and Cheng Specimen A4.

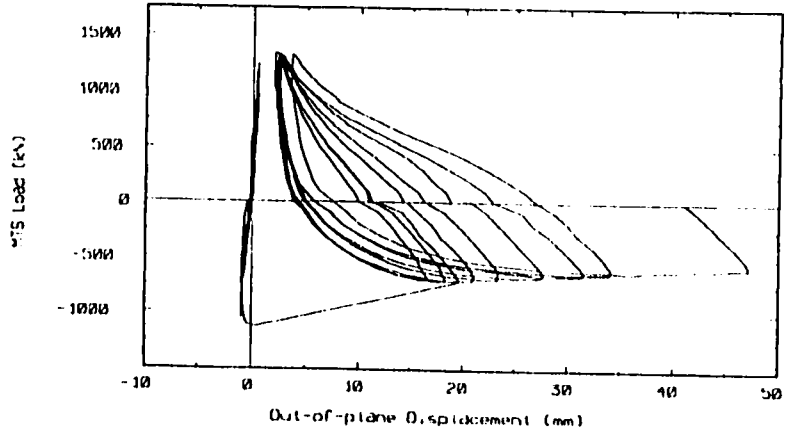

(a) - Specimen A2 out-of-plane hysteresis.

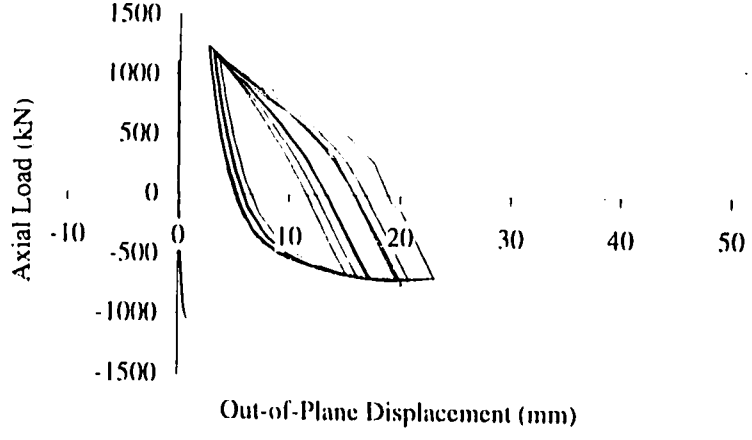

(b) - Model CL2 out-of-plane hysteresis.

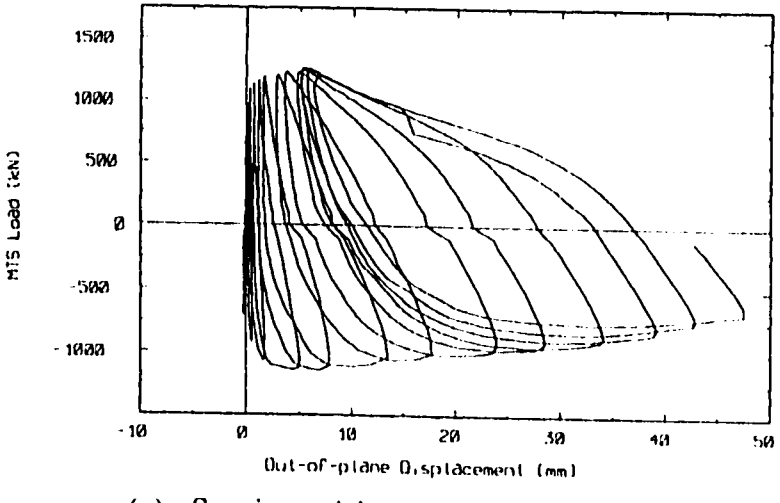

(c) - Specimen A4 out-of-plane hysteresis.

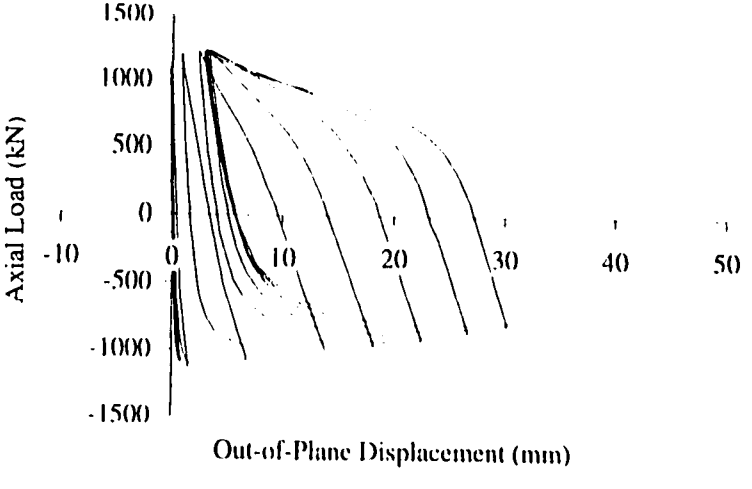

(d) - Model CL4 out-of-plane hysteresis.

4.27 - Out-of-plane cyclic behaviour - comparison with test results of Rabinovitch and Cheng (1993).

5. PARAMETRIC STUDY

5.1 Introduction

The test programs conducted by Yam and Cheng (1993) and Rabinovitch and Cheng (1993) focused uniquely on the behaviour of the gusset plate, either under monotonic compressive or cyclic loading. The interaction between the gusset plate and the brace member was not considered in either investigation. Instead, for the design of the test setup, the brace member was assumed to be much stiffer than the gusset plate, so that the gusset plate buckled essentially as though it were a fixed-guided column. Yam and Cheng (1993) studied the effects of gusset plate thickness, size, brace angle, out-of-plane restraint, and frame action on the behaviour of gusset plate connections loaded in monotonic compression. Rabinovitch and Cheng (1993) studied the effects of gusset plate thickness, bolt slip, and free edge stiffeners on the cyclic behaviour of gusset plates. In the cyclic loading tests performed by Rabinovitch and Cheng, only one cyclic load test was performed for each specimen configuration. No attempt was made to assess the effect of the load sequence on the behaviour of the gusset plate connections under cyclic loading.

The development of finite element models of the gusset plate specimens tested by Yam and Cheng (1993) and Rabinovitch and Cheng (1993) was described in Chapter 3. In Chapter 4 it was demonstrated that these finite element models can accurately predict the behaviour of gusset plates under monotonic and cyclic loading.

The purpose of the parametric study described in this chapter is to use the finite element models developed in the previous chapters to expand the investigations performed experimentally by Yam and Cheng (1993) and Rabinovitch and Cheng (1993), to include parameters that were not investigated experimentally. Namely, the parametric study will look at the effects of gusset plate – brace member interaction and loading sequence on the behaviour of gusset plates under monotonic and cyclic loading.

5.2 Finite Element Model

Figure 5.1 shows a mesh for a typical gusset plate – brace member subassembly. The splice member to brace member connection and the gusset plate to splice member connection were modeled with rigid links to simulate the fasteners. The out-of-plane (clamping) restraint imparted to the brace member web by the splice members was assumed to be infinite. The same connection length was used for all splice member to brace member connections. The selected connection length was such that in no case would the splice member to brace member connection govern the capacity of the subassembly.

The brace members were modeled with the S4R shell element. A half sine wave, out-of-plane initial imperfection was incorporated into the brace, with a magnitude (i.e. peak initial imperfection at the brace member midlength) of L/1400. This magnitude is

generally considered to be representative of initial imperfections typically found in wide flange sections (Bjorhovde, 1972).

An elastic – perfect plastic material model with a yield strength of 300 MPa was used for the gusset plate, the splice members, and the brace member. An elastic material model was used for the framing members, so that yielding in these members could be precluded. An elastic modulus of 200 000 MPa was used in both material models.

The restrained edges of the gusset plate were modeled using the "flexible" boundary condition model described in Chapter 3. One end of the brace member was connected to the gusset plate with the splice members as described above. The other end of the brace was pinned, i.e. free to rotate and to displace in plane, but restrained from out-of-plane displacement. In terms of the coordinate system shown in Figure 5.1, the restrained node at the end of the brace member opposite the gusset plate was free to displace in the 1-2 plane, but not in the coordinate 3 direction. In a real structure, this boundary condition would correspond to the point of intersection of two bracing members in a cross-bracing system. The load was applied by imposing an in-plane displacement at the restrained node. In order to ensure that the cross-section at the pinned end of the brace member would remain plane, beam elements were used to join the nodes on that cross-section (see Figure 5.1). These beam elements were stiff in bending and shear in order to transfer the load from the displaced node uniformly over the brace member cross section, but axially weak in order to allow lateral contraction and expansion of the cross-section due to Poisson ratio effect and to allow necking of the cross-section in tension.

5.3 Investigated Parameters and Specimens Description

A number of parameters were investigated in this study. Of primary interest, was the effect of gusset plate – brace member interaction on the behaviour of gusset plates under monotonic and cyclic loading. Also of interest, was the effect of load sequence on the behaviour of gusset plates loaded cyclically. In selecting gusset plate – brace member combinations for the parametric study, an effort was made to capture each of the following failure modes:

1) Yielding of gusset plate in tension (YGT);
2) Yielding of brace member in tension (YBT);
3) Buckling of gusset plate in compression (BGC); and,
4) Buckling of brace member in compression (BBC).

Gusset plate – brace member subassemblies were analyzed under monotonic tensile and compressive loading. Three load sequences were also developed to study cyclic behaviour. Of some interest in this phase of the investigation, was the degree to which the in-plane monotonic plots tend to delineate the envelope of the in-plane hysteresis.

For this parametric study, 450 x 550 mm gusset plates, similar in geometry to the specimens tested by Rabinovitch and Cheng (1993), were modeled. Three gusset plate thicknesses were used in the study, namely, 6 mm, 9 mm, and 12 mm. For each thickness, two brace sections were selected, namely, one that would result in failure due

to yielding of the gusset plate (when the gusset plate – brace member subassembly was loaded monotonically in tension), and one that would result in failure due to yielding of the brace member. For each brace member section, two brace lengths were modeled, namely, one corresponding to a slenderness, kL/r, of 50 and one corresponding to a slenderness of 100. It should be noted that these kL/r values were computed assuming an effective length factor, k of 1.0 (i.e. pin-pin). In actuality, the gusset plate does not act as a perfect pin, even out-of-plane. For most of the gusset plate – brace member combinations studied, the shorter brace member had a predicted capacity in compression higher than that of the gusset plate, whereas the longer brace member had a predicted capacity lower than that of the gusset plate. All gusset plate – brace member combinations were designed so that buckling (of either the gusset plate or the brace member) occurred out-of-plane, as this was the case for all of the test specimens. For each gusset plate thickness investigated, a gusset plate only (no brace member) case was analyzed to aid in assessing the effects of the gusset plate – brace interaction.

Table 5.1 and Table 5.2 summarize the descriptions and designations of the gusset plates and brace members used in the parametric study. The gusset plates were designated GP1, GP2 and GP3 corresponding to 6, 9 and 12 mm plate thickness, respectively. The brace members were each given a designation from B1 to B12. Brace members B1 to B4 were used with gusset plate GP1, brace members B5 to B8 were used with gusset plate GP2, and brace members B9 to B12 were used with gusset plate GP3. In Table 5.3 each of the gusset plate – brace member combinations are listed. The predicted capacities of each gusset plate and each brace member in tension and in compression are also presented in

Table 5.3. These predictions were obtained using the simplified methods described in Chapter 2. and they formed a basis for selecting gusset plate – brace member combinations which would cover the full range of desired failure modes.

5.4 Loading

The analysis of the gusset plate – brace member subassemblies for the parametric study was conducted under monotonic and cyclic loading. The monotonic loading analysis was conducted first. Each gusset plate – brace member combination was loaded in monotonic tension and compression, well beyond the yield (or buckling) displacement.

For the cyclic loading analysis, three load sequences were developed. Applied Technology Council Guideline (ATC24, 1992) was used as a guideline in developing these load sequences. As suggested in ATC24, increments of displacement for each cycle were multiples of the yield displacement, δ_y, obtained from monotonic tension loading analysis. In order to be able to compare the various subassemblies, a common value of yield displacement, δ_y, was desirable. This common value of δ_y was taken as the yield displacement from the gusset plate only (no brace member) case. This value seemed to be independent of gusset plate thickness. Figure 5.2 shows the monotonic tension load versus displacement plots for gusset plates GP1, GP2 and GP3. From these plots, a value of δ_y = 2.5 mm was computed based on the method suggested in ATC24. ATC24 recommends a minimum of three cycles at each displacement increment. It was felt that

three cycles would not be practical for this parametric study due to the number of models being analyzed. A load sequence that met this criterion (LS3) was developed however, to study the effect of repeated cycling at each displacement increment.

The basic load sequence, load sequence 1 (LS1), loaded the model in tension first. One cycle of loading was imposed at each displacement increment, up to a maximum axial displacement of 15 mm. Load sequence 2 (LS2) was identical to LS1, except that the model was loaded in compression first. Load sequence 3 (LS3) was identical to LS1, except, as explained above, three cycles were imposed at each displacement increment. Because of time constraint, only two models were analyzed with loading sequence LS3, namely, GP2B5 and GP2B7. Table 5.4 identifies which gusset plate – brace member subassemblies were analyzed under which load sequences.

5.5 Results of the Parametric Study

5.5.1 Monotonic Loading

A total of 12 gusset plate – brace member subassemblies were analyzed for the monotonic loading portion of this parametric study. As mentioned in the previous section, three models of the gusset plates without brace members were also analyzed, and the monotonic tension results for these models were used in the development the cyclic load sequences. Figures 5.2 and 5.3 show the monotonic tensile and compressive behaviour for the gusset plate only (no brace member) models.

Figures 5.4 to 5.9 summarize the tensile load versus displacement behaviour of the gusset plate – brace member subassemblies. Two load versus displacement plots are shown for each subassembly. Figures 5.4, 5.6, and 5.8 show axial load versus total axial displacement. Total axial displacement refers to the in-plane, axial displacement of the loaded brace member node (see Figure 5.1). Figures 5.5, 5.7, and 5.9 show axial load versus the axial displacement of the gusset plate. The axial displacement of the gusset plate refers to the in-plane displacement of the gusset plate measured at the free edge of the gusset plate as shown in Figure 5.1. As can be seen from Figures 5.4 to 5.9, if the axial displacement of the gusset plate is isolated, the slope of the resulting load versus deflection plot is unaffected by the inclusion of the bracing member. If the total displacement is studied however, it can be seen that in the elastic range, the stiffness of the subassembly is affected by the displacement due to elastic strain in the bracing member. As expected, the longer brace members resulted in lower total axial displacement stiffnesses.

In Figures 5.4 to 5.9, models with the same gusset plate thickness have been shown together. For each gusset plate thickness, two categories of curves can be established: those for which the capacity of the subassembly is limited by the tensile capacity of the gusset plate, and those for which the capacity of the subassembly is limited by the tensile capacity of the brace member. For example, from Figures 5.6 and 5.7, it can be seen that the capacity of the subassembly was limited by yielding of the brace member for models GP2B5 and GP2B6, since plastic deformation is observed in Figure 5.6 but no plastic

deformation is observed in the gusset plate as shown in Figure 5.7. In contrast, Figure 5.6 and Figure 5.7 show that the capacity of models GP2B7 and GP2B8 was limited by yielding of the gusset plate. Figure 5.6 indicates that when the brace member yields, the ultimate tensile load is lower than the gusset plate only (no brace member) case (shown by the dashed line). When the gusset plate yields, the inclusion of the brace member appears to have no effect on ultimate tensile capacity.

Figures 5.10 to 5.15 summarize the monotonic compressive behaviour of the models. Again, for each gusset plate thickness, two limiting conditions are identified: buckling of the brace member and buckling of the gusset plate. In these figures, it can be seen that the addition of the brace member resulted in a reduction in compressive capacity for all models, regardless of whether gusset plate buckling or brace member buckling governed the behaviour.

Once again, two load versus displacement plots are shown for each gusset plate thickness. Figures 5.10, 5.12, and 5.14 show axial load versus total axial displacement while Figures 5.11, 5.13, and 5.15 show axial load versus the axial displacement of the gusset plate. These figures indicate that for the models with lower capacities, buckling of the brace dominated the total displacement; whereas for the models with higher capacities, buckling of the gusset plate dominated the total displacement. Figures 5.16 and 5.17 show typical buckled configurations for both observed buckling modes (buckling of gusset plate and buckling of brace member).

Table 5.5 summarizes the capacities of the gusset plate – brace member subassemblies in tension and in compression. The capacities predicted using the simplified methods described in Chapter 2 are presented along with the results of the finite element analysis. From the model / prediction (M/P) ratios listed in the table, it appears that on the tension side, the capacities of the subassemblies were predicted quite closely with the simplified methods (M/P ratios range from 0.96 to 0.99). On the compression side, the simplified methods were conservative (M/P ratios range from 1.15 to 1.68).

5.5.2 Cyclic Loading

As mentioned earlier, three gusset plates were modeled with four different brace members each. Three load sequences were developed for the cyclic loading portion of this parametric study (see Figure 5.18). This means that it would have been possible to analyze 36 different subassembly – load sequence combinations. Due to time constraints, not all 36 possible combinations were investigated. Table 5.4 outlines the subassemblies that were analyzed for each load sequence. The results for each of these subassembly – load sequence combinations are presented in this section.

As was done for the monotonic loading investigation, gusset plate only (no brace member) models were analyzed first. Figures 5.19 and 5.20 summarize these results. In Figure 5.19 the effect of load sequence can be seen for gusset plate model (GP2). In this figure, it can be seen that the effect of load sequence (i.e. tension first versus compression first) on the hysteresis envelope is minimal. The effect of repeating cycles at each

displacement increment appears to be a deterioration of tensile and compressive capacity with each repeated cycle. This deterioration is small and appears to diminish with consecutive repeated cycles for a given displacement increment. In Figure 5.20 the effect of gusset plate thickness can be seen for load sequence LS1. In this figure, it can be seen that the effect of increasing gusset plate thickness is an increase in tensile and compressive capacity. The hysteresis plots for the thicker gusset plates also appear to exhibit less pinching behaviour. Axial load versus out-of-plane displacement hysteresis plots for the gusset plate only (no brace member) models can be found in Appendix A (Figures A.1 to A.6).

Figures 5.21 to 5.40 show the hysteresis loops for the gusset plate GP2 subassembly models. In general, it is apparent that the difference between imposing load sequence LS1 ("tension first") and LS2 ("compression first") on any given gusset plate – brace member subassembly is small. The hysteresis envelopes for the subassembly models are basically the same regardless of the load sequence used (this can be seen by comparing adjacent figures, which show results for the same subassembly under different load sequences, i.e. Figures 5.21 and 5.23 show GP2B5LS1 and GP2B5LS2 respectively). Models cycled under load sequence LS3 can be compared with those cycled under load sequence LS1 to study the effects of repeated cycling at each displacement increment. Comparing GP2B5LS1 and GP2B5LS3 (Figures 5.21 and 5.25, respectively), it can be seen that the effects of increasing the number of cycles for each displacement increment are a deterioration of the capacity of the gusset plate (in tension and compression) and a small amount of "softening", or loss of stiffness upon reloading with each cycle. Due to

the significant increase in the time required to analyze a model under LS3, only two models were analyzed under this load sequence.

For the cyclic loading study, as with the monotonic loading study, axial load versus total axial displacement hysteresis plots and axial load versus axial displacement of the gusset plate hysteresis plots were produced for each analysis. Comparing these figures (for the same subassembly – load sequence combination), it is possible to observe the cyclic behaviour of the gusset plate – brace member subassembly, as well as the axial load versus displacement history of the gusset plate. For example, comparing Figures 5.21 and 5.22, total axial displacement can be compared with the axial displacement of the gusset plate for GP2B5LS1. Figure 5.21 shows the behaviour of the entire subassembly. With this information, one can determine the total energy dissipated by the subassembly over the complete loading history. With Figure 5.22, it is possible to ascertain the contribution of the gusset plate.

Comparing the cyclic loading hysteresis plots for the various subassemblies, some qualitative conclusions can be drawn regarding the effects of gusset plate – brace member interaction on cyclic behaviour. Figures 5.21, 5.27, 5.31, and 5.37 show total axial displacement hysteresis plots for models GP2 – B5, B6, B7, and B8 under load sequence LS1. Figures 5.22, 5.28, 5.32, and 5.38 show hysteresis plots isolating the behaviour of the gusset plate for these same models. These figures indicate that the gusset plate contribution is significantly greater than the brace member contribution for subassembly GP2B7, the gusset plate is contributing somewhat to the total behaviour for GP2B5 and

GP2B8 (it appears to be buckling partially for GP2B5 and yielding significantly for GP2B7), and the gusset plate is making almost no contribution to the total behaviour for GP2B6 (i.e. only elastic displacement is taking place in the gusset plate). The total axial displacement plots indicate that when compressive axial displacement is accommodated primarily through gusset plate buckling (GP2B7 in Figures 5.31, 5.33, and 5.35), the total axial displacement hysteresis is generally well behaved (i.e. stable post buckling behaviour with minimal "pinching"). Conversely, when compressive axial displacements are accommodated primarily through buckling of the brace member (GP2B6 in Figures 5.27 and 5.29, GP2B8 in Figures 5.37 and 5.39), a less desirable behaviour is apparent (namely, rapid deterioration of the post buckling capacity with noticeable "pinching" of the hysteresis loops). A comparison of GP2B6 with GP2B8, shows that yielding of the gusset plate in tension versus yielding of the brace member has less effect on the cyclic behaviour of the subassembly.

Figures 5.41 and 5.42 show plots of energy dissipation during cyclic loading for the gusset plate GP2 subassemblies. Figure 5.41 shows energy dissipated per cycle, and Figure 5.42 shows cumulative energy dissipated. Energy dissipation plots for subassemblies subjected to the same load sequence have been grouped together in order to facilitate comparison. Figure 5.41 shows that for all three cyclic loading sequences investigated, subassembly GP2B7 dissipated the most energy. This subassembly was designed with the gusset plate as the weak element in tension and in compression (see Table 5.3). Models for which brace member buckling dominated the compressive behaviour (GP2B6 and GP2B8) dissipated the least amount of energy. Figure 5.41(c)

shows the effect of repeated cycling on energy dissipation. For GP2B5LS3, cycling appears to result in a deterioration of the amount of energy dissipated in consecutive cycles at the same displacement increment. This is most noticeable at the higher displacement increments. The amount of energy dissipated in consecutive cycles appears to be fairly constant for model GP2B7LS3.

Figures 5.43 to 5.58 show hysteresis plots for gusset plate GP1 and GP3 subassembly models analyzed under load sequence LS1. Comparison of these figures confirms the qualitative observations made for the GP2 subassemblies. For the gusset plate GP1 subassemblies, the gusset plate was designed as the weak element in tension for GP1B3 and GP1B4. The gusset plate was designed as the weak element in compression for GP1B1 and GP1B3. Comparing total axial displacement hysteresis plots for GP1B1 and GP1B3 (Figures 5.43 and 5.47), it can be seen that in the displacement range studied, the cyclic behaviour of the subassembly is not significantly affected by which element governs the capacity in tension (i.e. the gusset plate or the brace member). Conversely, comparing Figures 5.43 and 5.47 with Figures 5.45 and 5.49 shows that the cyclic behaviour is generally better when the gusset plate is the weak element in compression (i.e. more stable post buckling behaviour and less "pinching"). Similar conclusions can be drawn by studying the load responses for the gusset plate GP3 subassemblies.

Figures 5.59 and 5.60 show energy dissipation plots for each subassembly under load sequence LS1. Subassemblies with the same gusset plate have been grouped together. In Figure 5.59(a) it can be seen that the energy dissipated by GP1B1 and GP1B3 is almost

identical. As mentioned above, the only difference between these two models is the weak element in tension. Capacity design philosophy suggests that it would be more desirable to have the brace member as the weak element in tension. Since these subassemblies were not cycled up to the ultimate load in tension, this suggestion cannot be validated or refuted based on this investigation. It is apparent from Figures 5.59 and 5.60, however, that subassemblies for which compressive behaviour is dominated by gusset plate buckling tend to dissipate more energy (for the displacement range investigated).

Figures 5.61 to 5.63 show total axial displacement hysteresis plots for subassemblies under load sequence LS1, superimposed on top of monotonic load – displacement plots. To develop a hysteretic model based on monotonic behaviour was beyond the scope of this investigation. However, Figures 5.61 to 5.63 show that the monotonic plots delineate the hysteresis plots well, for most gusset plate – brace member subassemblies.

Axial load versus out-of-plane displacement hysteresis plots can be found in Appendix A (Figures A.7 to A.24), for all of the cyclically loaded gusset plate – brace member subassembly models investigated in the parametric study.

5.6 Summary

In this chapter, a parametric study was presented in which factors affecting the behaviour of gusset plates were studied. The parametric study looked at the effects of gusset plate – brace member interaction and loading sequence on the behaviour of gusset plates under

monotonic and cyclic loading. The findings of this parametric study can be summarized as follows:

1. The effect of the interaction between the gusset plate and the brace member on the behaviour of gusset plate – brace member subassemblies loaded monotonically and cyclically can be significant. A method for taking this interaction into account will have to be developed if the energy dissipation potential of the gusset plate is to be exploited in the design of concentric braced frames.
2. The monotonic load versus displacement behaviour was found to provide a good envelope of the cyclic load versus displacement hysteresis plots. This may form a basis for the development of a simplified method for incorporating gusset plate behaviour into a frame model.
3. The effect of load sequence (i.e. "tension first" versus "compression first") on cyclic behaviour was found to be small. Repeated cycling does however appear to have a deteriorating effect on the cyclic behaviour of gusset plates. even when a simple elastic-perfect plastic material model is used (i.e. tearing and Bauschinger effect are ignored).
4. The gusset plate – brace member subassemblies that underwent gusset plate yielding or buckling show significant energy dissipation potential, supporting the strong brace – weak plate concept proposed by Rabinovitch and Cheng (1993).

Table 5.1 - Gusset plate description.

Gusset Plate	Dimensions (mm)	Thickness (mm)	Yield Stress (MPa)
GP1	550 x 450	6	300
GP2	550 x 450	9	300
GP3	550 x 450	12	300

Table 5.2 - Brace member description.

Brace	Section	Length (mm)	kL/r
B1	W200x21	1520	50
B2	W200x21	3040	100
B3	W200x27	1560	50
B4	W200x27	3120	100
B5	W200x27	1560	50
B6	W200x27	3120	100
B7	W200x42	2060	50
B8	W200x42	4120	100
B9	W200x31	1600	50
B10	W200x31	3200	100
B11	W200x59	2595	50
B12	W200x59	5190	100

Table 5.3 - Summary of parametric study: subassembly model combinations and predicted capacities

		Tension			Compression		
Plate	Brace	Plate (kN)	Brace (kN)	Failure Mode	Plate (kN)	Brace (kN)	Failure Mode
GP1	B1	866	813	YBT	659	672	BGC
GP1	B2	866	813	YBT	659	376	BBC
GP1	B3	866	1017	YGT	659	840	BGC
GP1	B4	866	1017	YGT	659	470	BBC
GP2	B5	1299	1017	YBT	1033	840	BBC
GP2	B6	1299	1017	YBT	1033	470	BBC
GP2	B7	1299	1593	YGT	1033	1316	BGC
GP2	B8	1299	1593	YGT	1033	736	BBC
GP3	B9	1732	1200	YBT	1404	991	BBC
GP3	B10	1732	1200	YBT	1404	555	BBC
GP3	B11	1732	2268	YGT	1404	1874	BGC
GP3	B12	1732	2268	YGT	1404	1048	BBC

** Note:* - *"plate" capacity in tension prediction with S16.1 block shear equations*
- *"brace" capacity in tension prediction with S16.1 net section equations*
- *"plate" capacity in compression prediction with Thornton method*
- *"brace" capacity in compression prediction with S16.1 column curves*
- *= limiting predicted capacity in tension or compression*

- *YGT = yielding of gusset plate in tension*
- *YBT = yielding of brace member in tension*
- *BGC = buckling of gusset plate in compression*
- *BBC = buckling of brace member in compression*

Table 5.4 - Summary of parametric study monotonic loading results.

Plate	Brace	Monotonic Tension					Monotonic Compression				
		Prediction		F.E. Model		M/P ratio	Prediction		F.E. Model		M/P ratio
		Capacity (kN)	Failure Mode	Capacity (kN)	Failure Mode		Capacity (kN)	Failure Mode	Capacity (kN)	Failure Mode	
GP1	B1	813	YBT	798	YBT	0.98	659	BGC	688	BGC	1.04
GP1	B2	813	YBT	799	YBT	0.98	376	BBC	476	BBC	1.27
GP1	B3	866	YGT	828	YGT	0.96	659	BGC	692	BGC	1.05
GP1	B4	866	YGT	828	YGT	0.96	470	BBC	540	BBC	1.15
GP2	B5	1017	YBT	1007	YBT	0.99	840	BBC	972	BBC	1.16
GP2	B6	1017	YBT	1007	YBT	0.99	470	BBC	746	BBC	1.59
GP2	B7	1299	YGT	1262	YGT	0.97	1033	BGC	1292	BGC	1.25
GP2	B8	1299	YGT	1255	YGT	0.97	736	BBC	948	BBC	1.29
GP3	B9	1200	YBT	1191	YBT	0.99	991	BBC	1163	BBC	1.17
GP3	B10	1200	YBT	1191	YBT	0.99	555	BBC	934	BBC	1.68
GP3	B11	1732	YGT	1697	YGT	0.98	1404	BGC	1793	BGC	1.28
GP3	B12	1732	YGT	1696	YGT	0.98	1048	BBC	1377	BBC	1.31

** Note:* - *see Table 5.3 for explanation of capacity predictions*
- *M/P ratio = finite element model to prediction ratio*
- *YGT = yielding of gusset plate in tension*
- *YBT = yielding of brace member in tension*
- *BGC = buckling of gusset plate in compression*
- *BBC = buckling of brace member in compression*

Table 5.5 - Parametric study: summary of model / load sequence combinations analyzed under cyclic loading.

		Load Sequence		
Plate	Brace	LS1	LS2	LS3
GP1	B1	x		
GP1	B2	x		
GP1	B3	x		
GP1	B4	x		
GP2	B5	x	x	x
GP2	B6	x	x	
GP2	B7	x	x	x
GP2	B8	x	x	
GP3	B9	x		
GP3	B10	x		
GP3	B11	x		
GP3	B12	x		

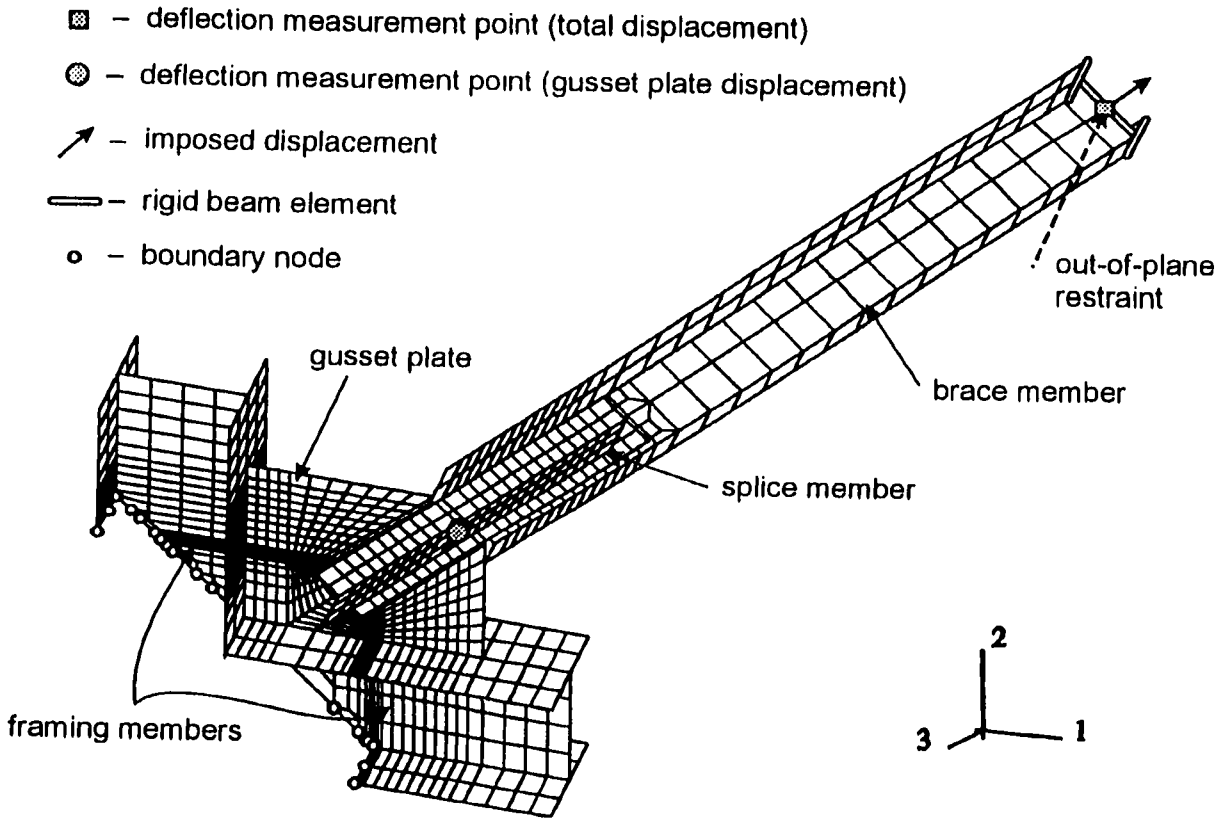

Figure 5.1 - Typical mesh for gusset plate - brace member subassembly.

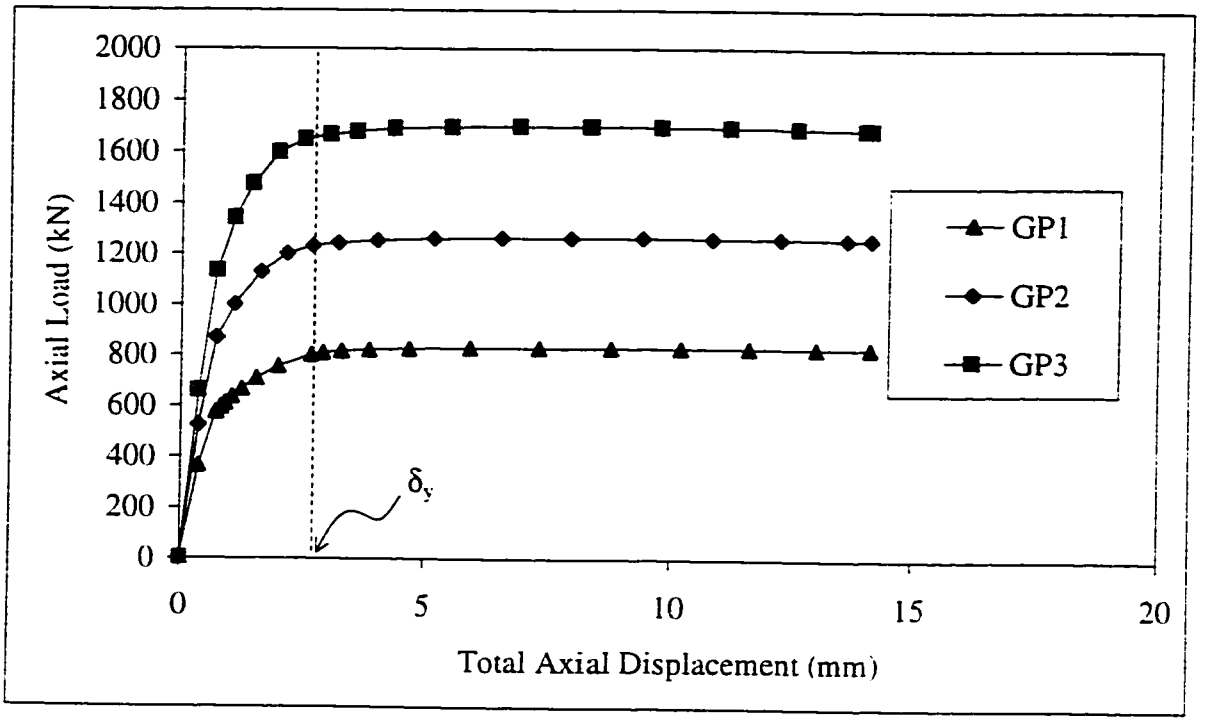

Figure 5.2 - Gusset plate only (no brace): in-plane behaviour under tension loading.

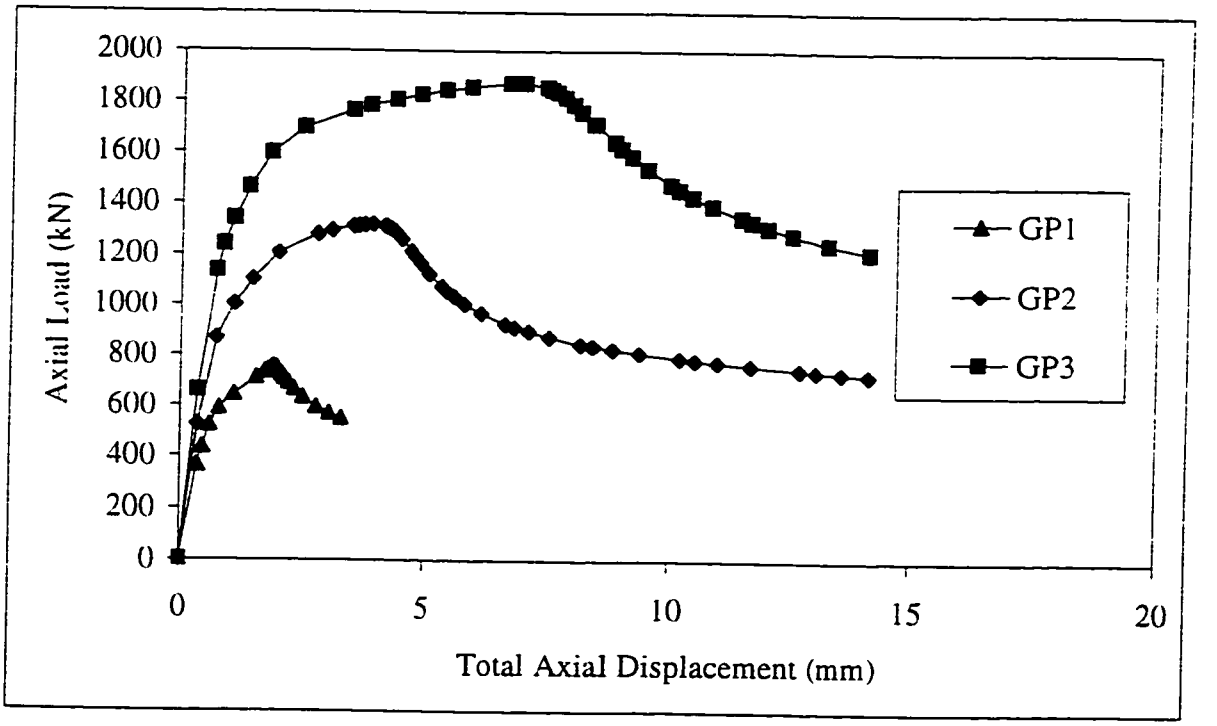

Figure 5.3 - Gusset plate only (no brace): in-plane behaviour under compression loading.

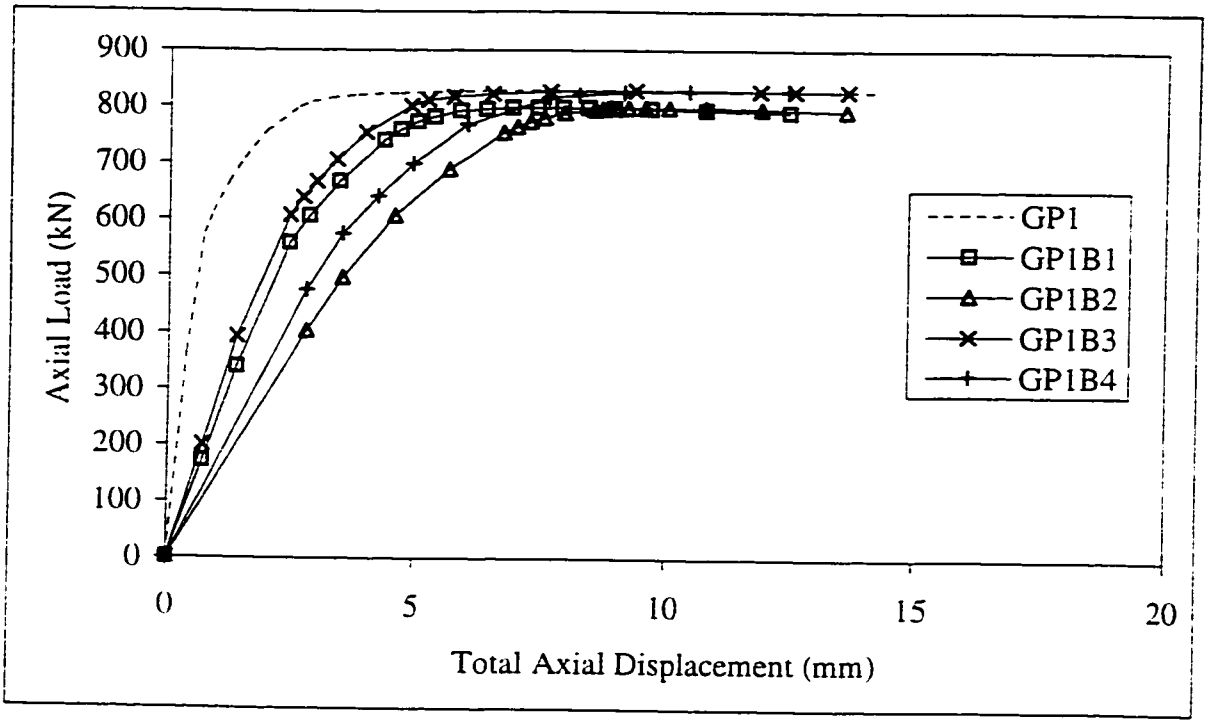

Figure 5.4 - Gusset plate GP1: total axial load versus displacement in tension.

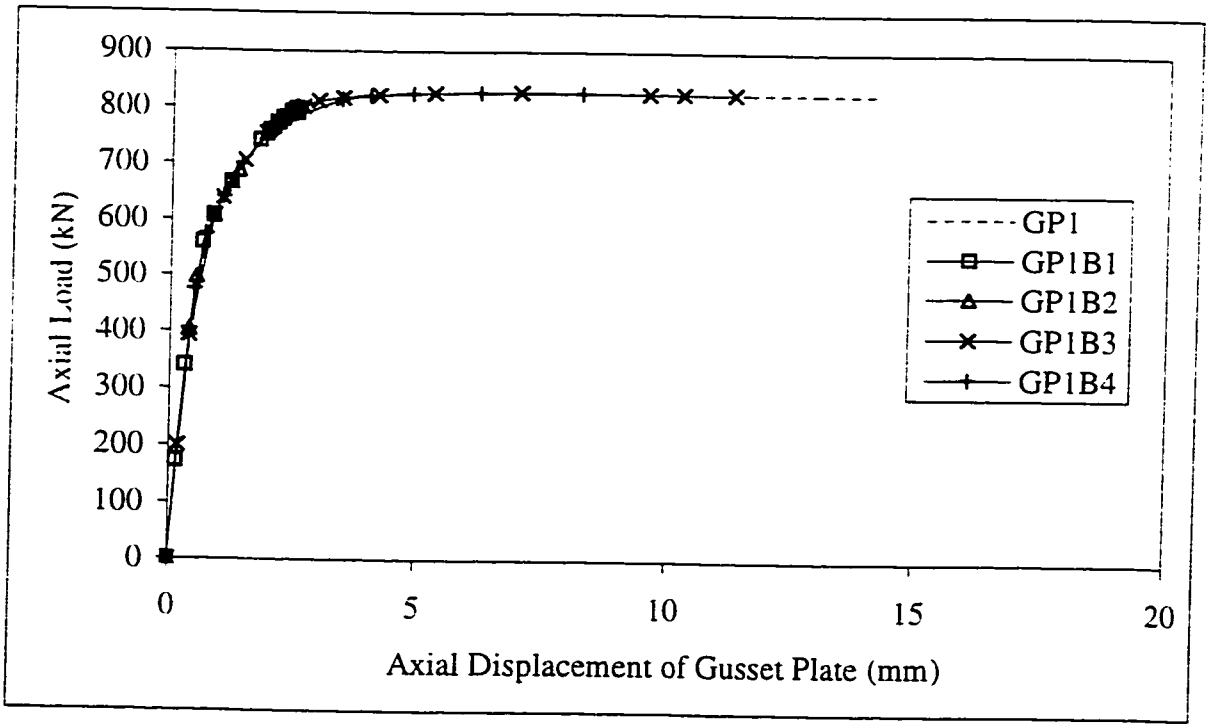

Figure 5.5 - Gusset plate GP1: gusset plate axial load versus displacement in tension.

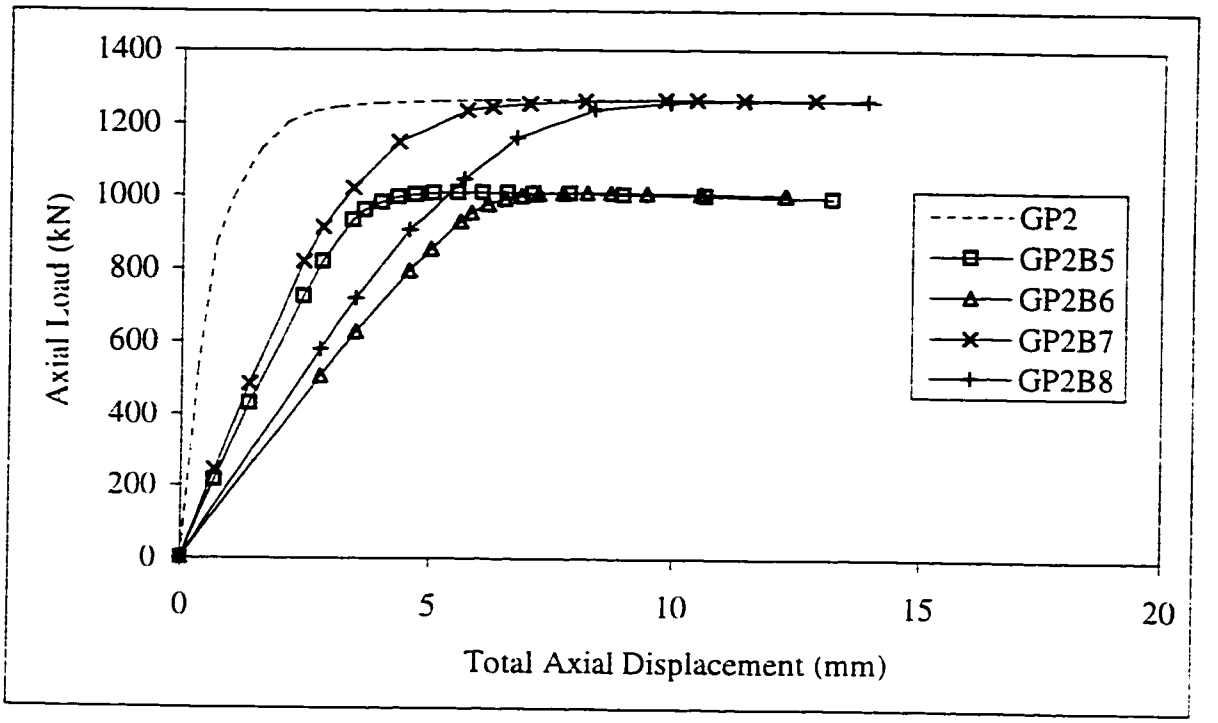

Figure 5.6 - Gusset plate GP2: total axial load versus displacement in tension.

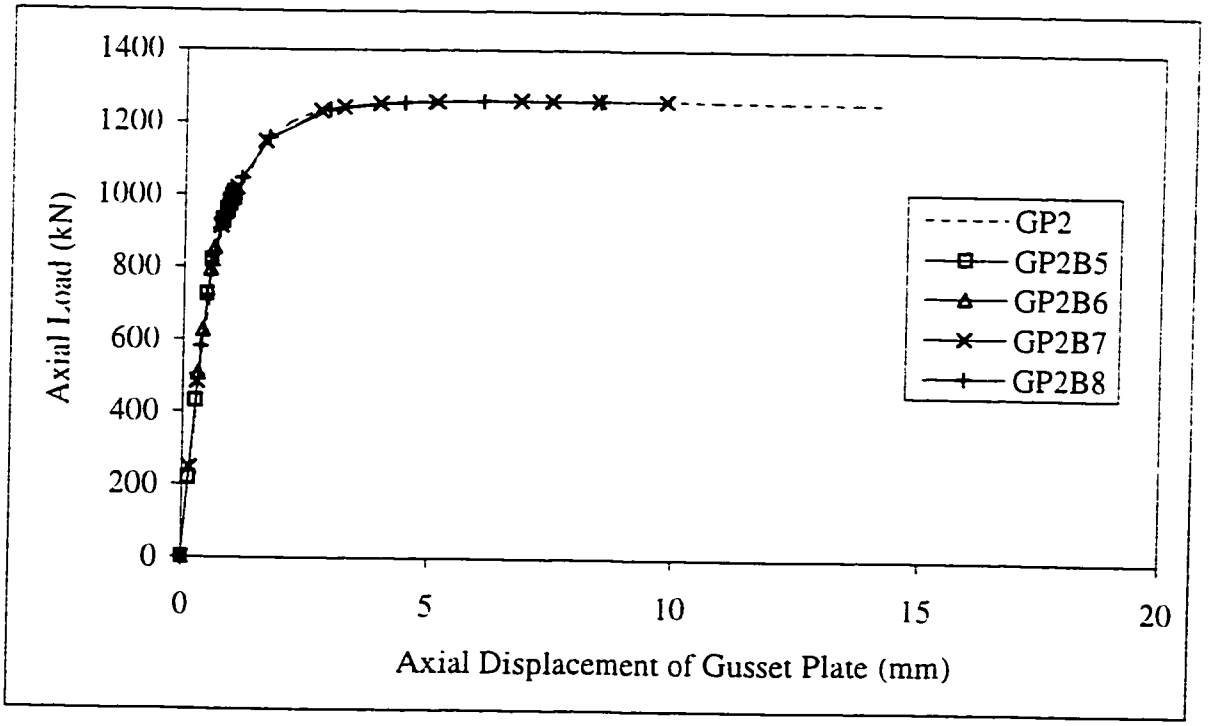

Figure 5.7 - Gusset plate GP2: gusset plate axial load versus displacement in tension.

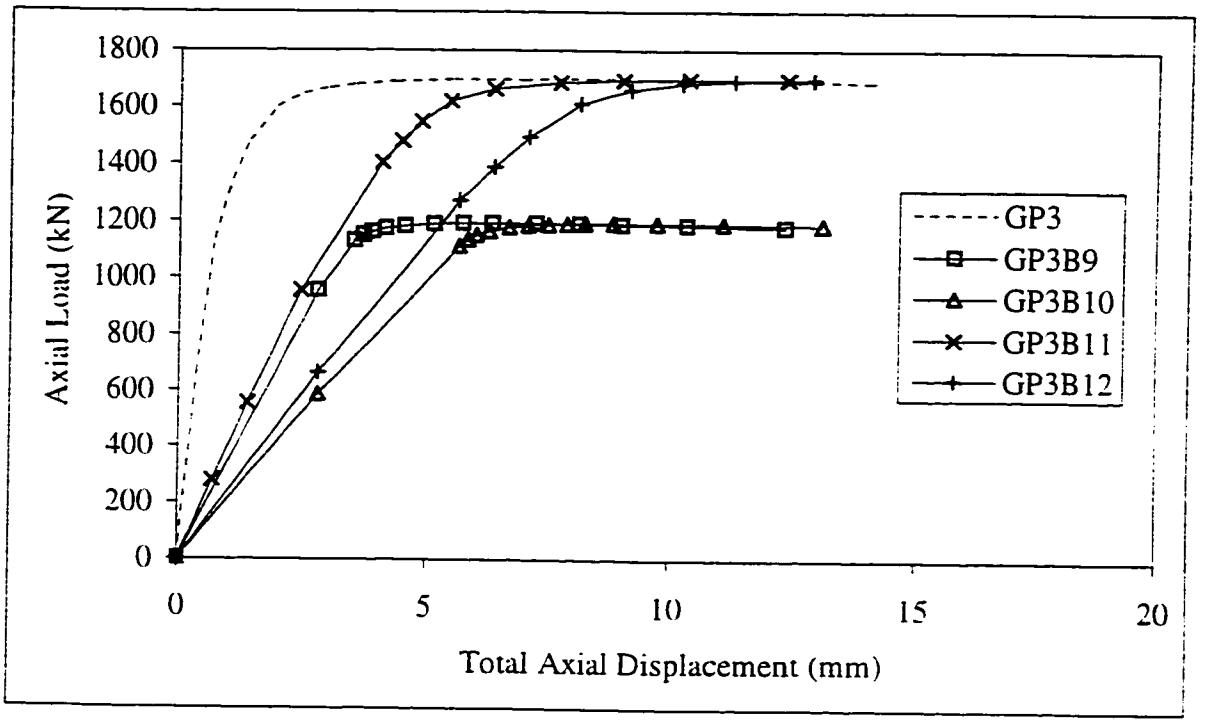

Figure 5.8 - Gusset plate GP3: total axial load versus displacement in tension.

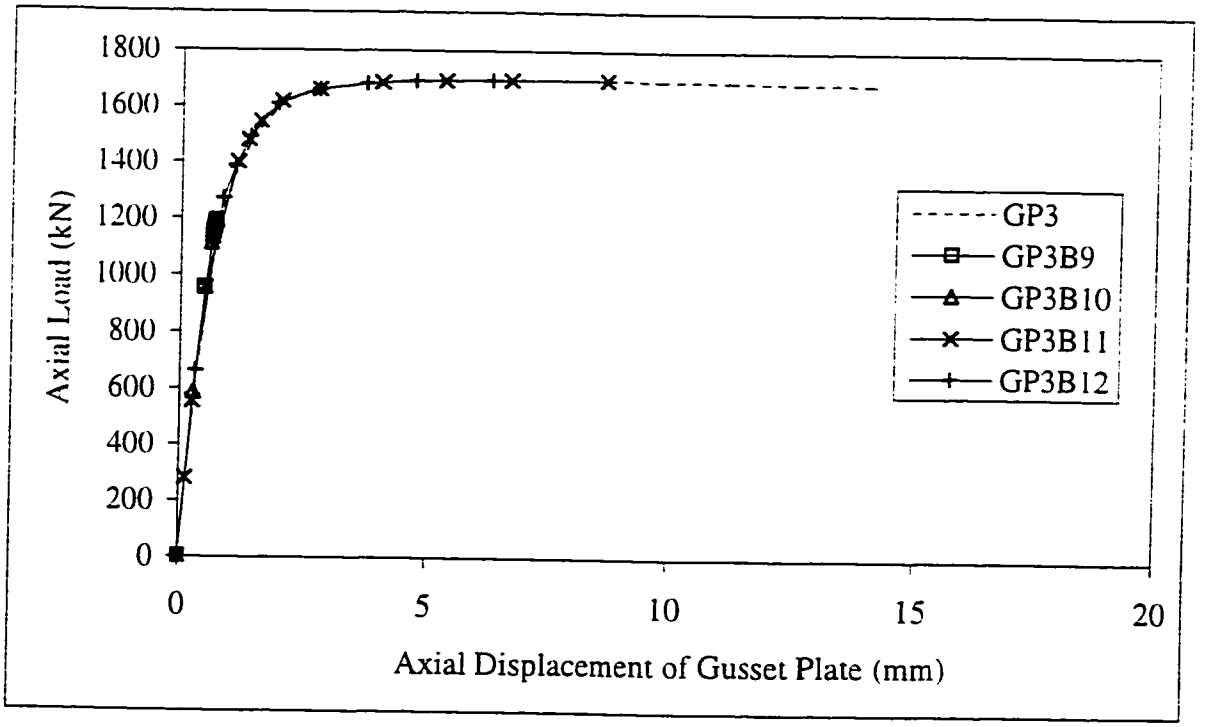

Figure 5.9 - Gusset plate GP3: gusset plate axial load versus displacement in tension.

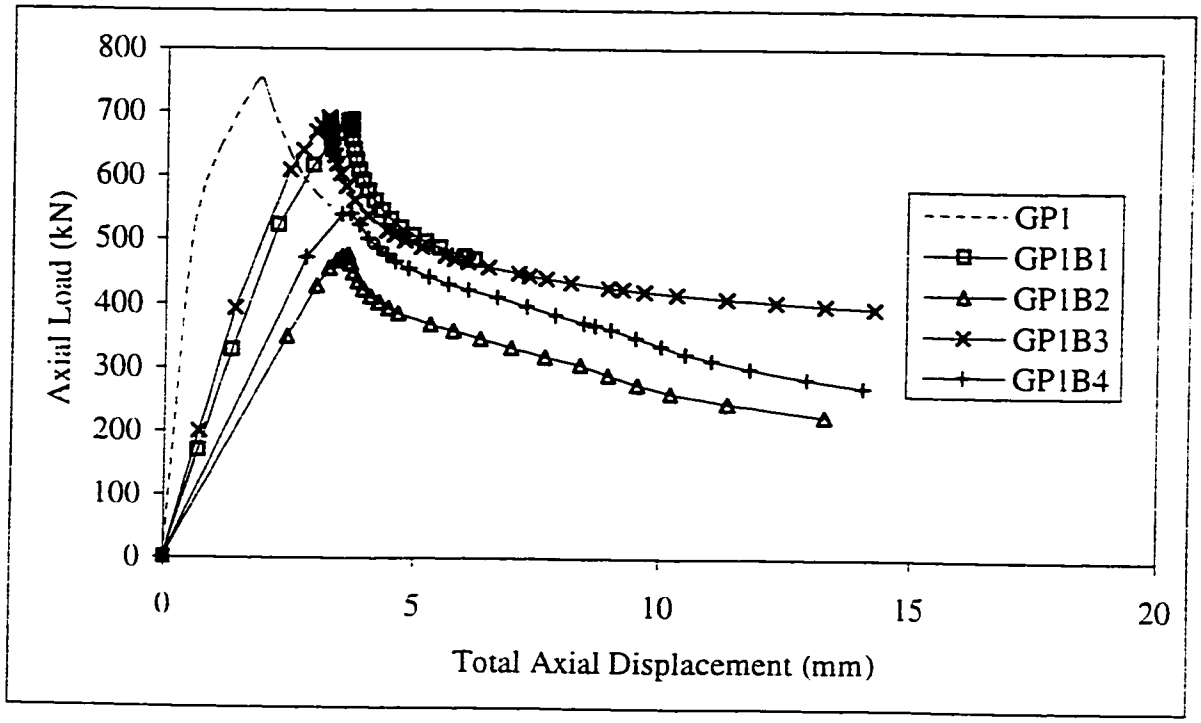

Figure 5.10 - Gusset plate GP1: total axial load versus displacement in compression.

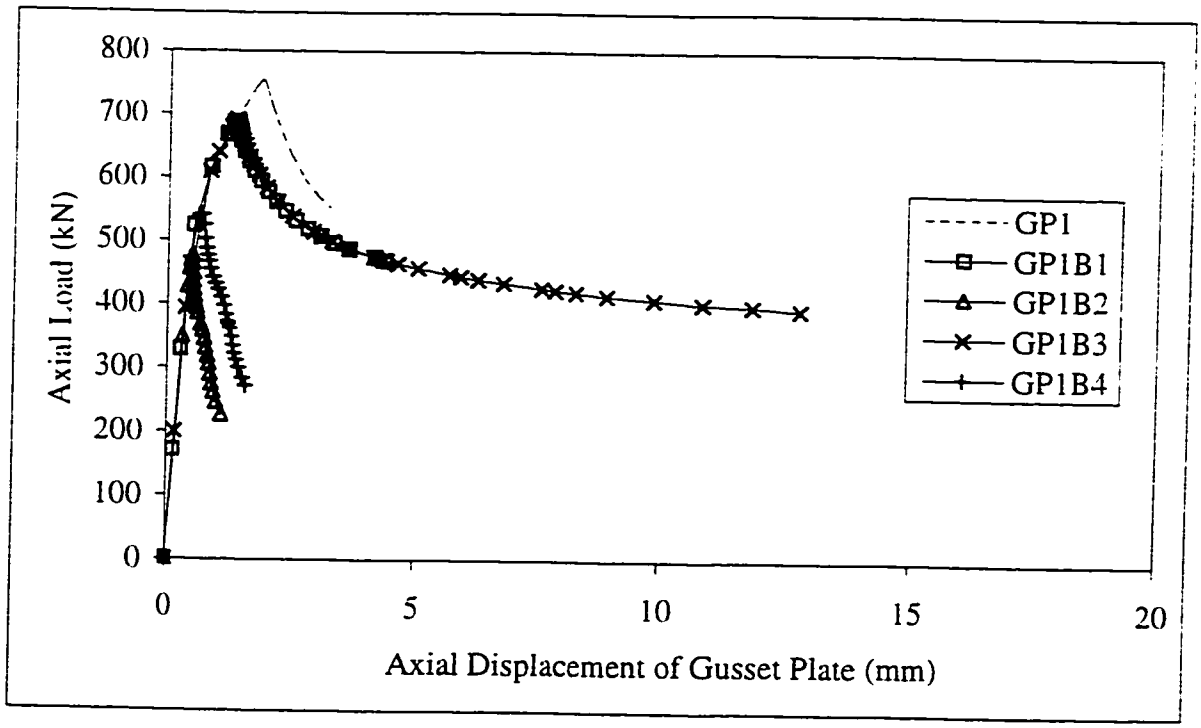

Figure 5.11 - Gusset plate GP1: gusset plate axial load vs. displacement in compression.

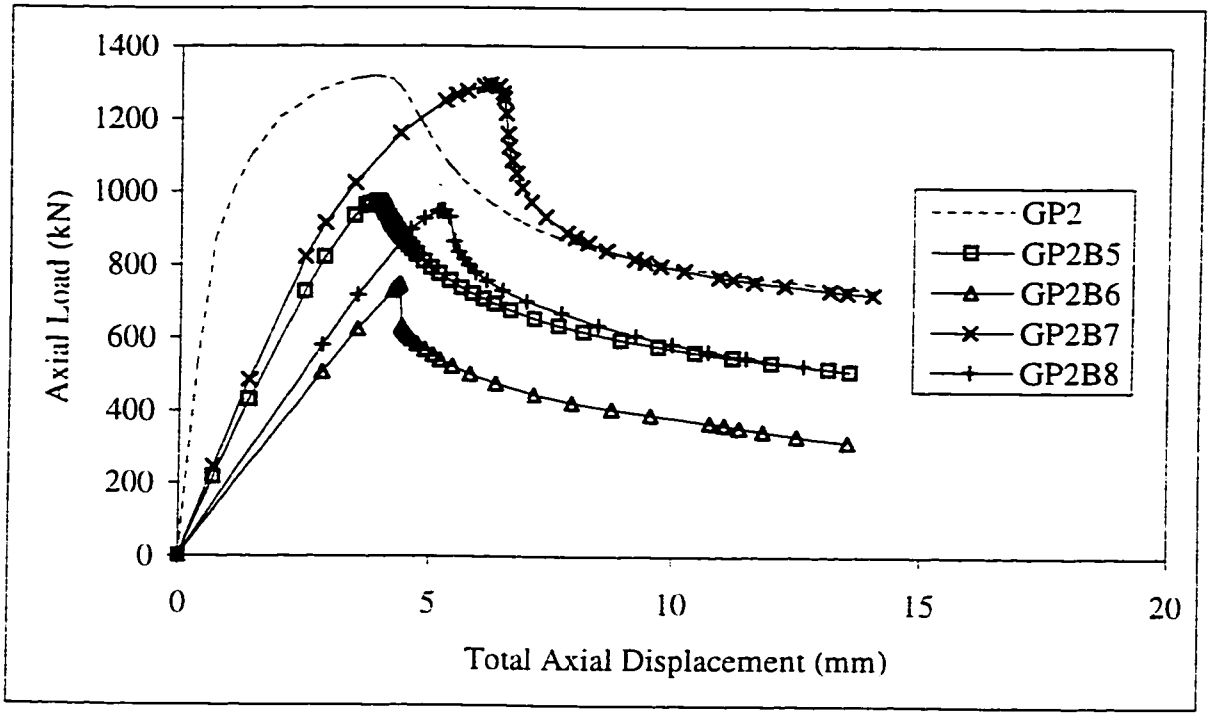

Figure 5.12 - Gusset plate GP2: total axial load versus displacement in compression.

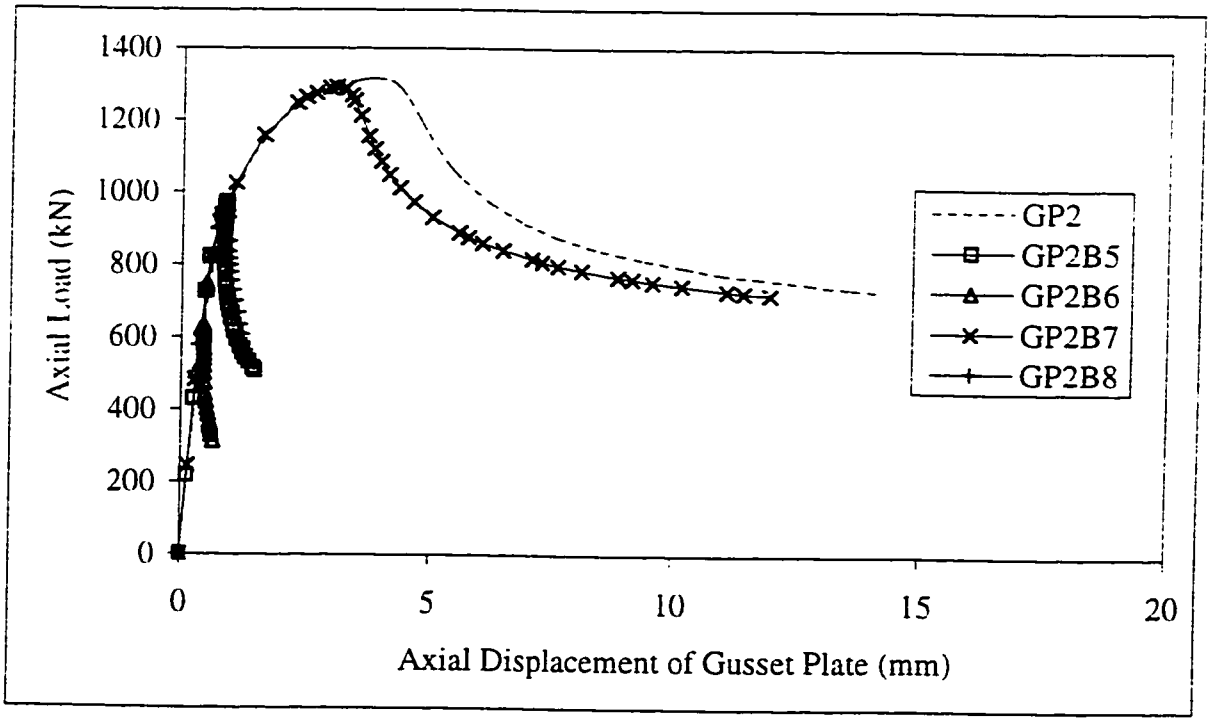

Figure 5.13 - Gusset plate GP2: gusset plate axial load vs. displacement in compression.

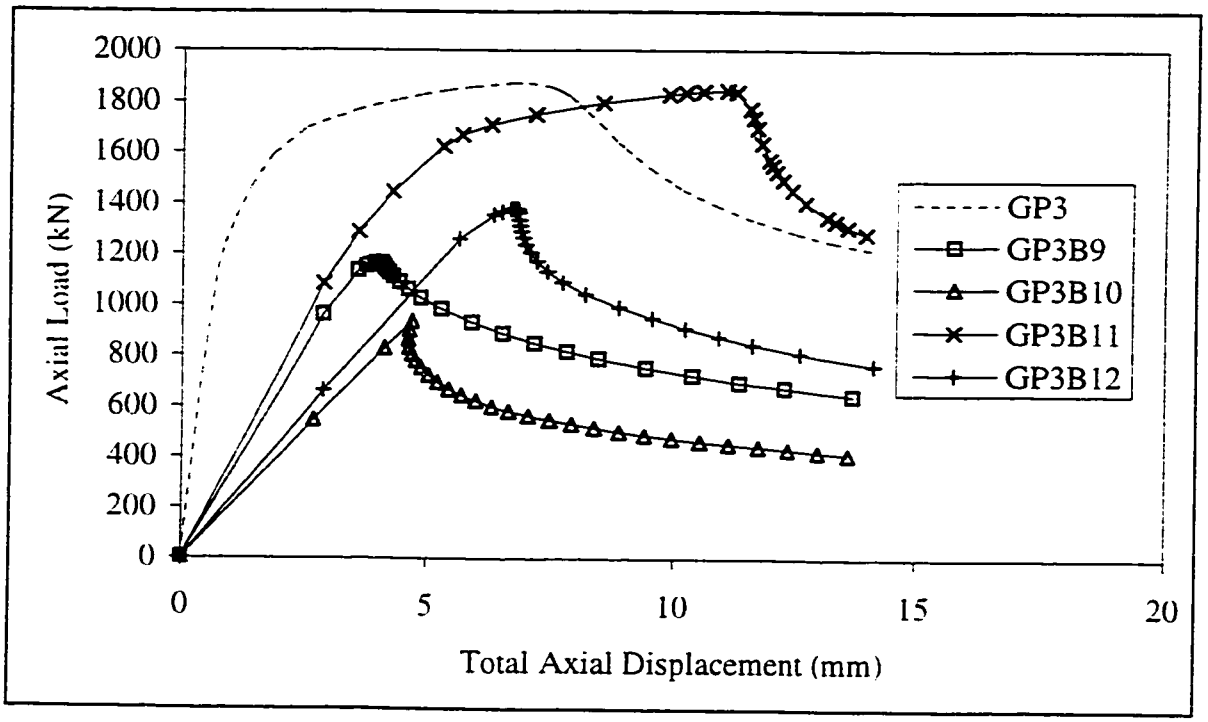

Figure 5.14 - Gusset plate GP3: total axial load versus displacement in compression.

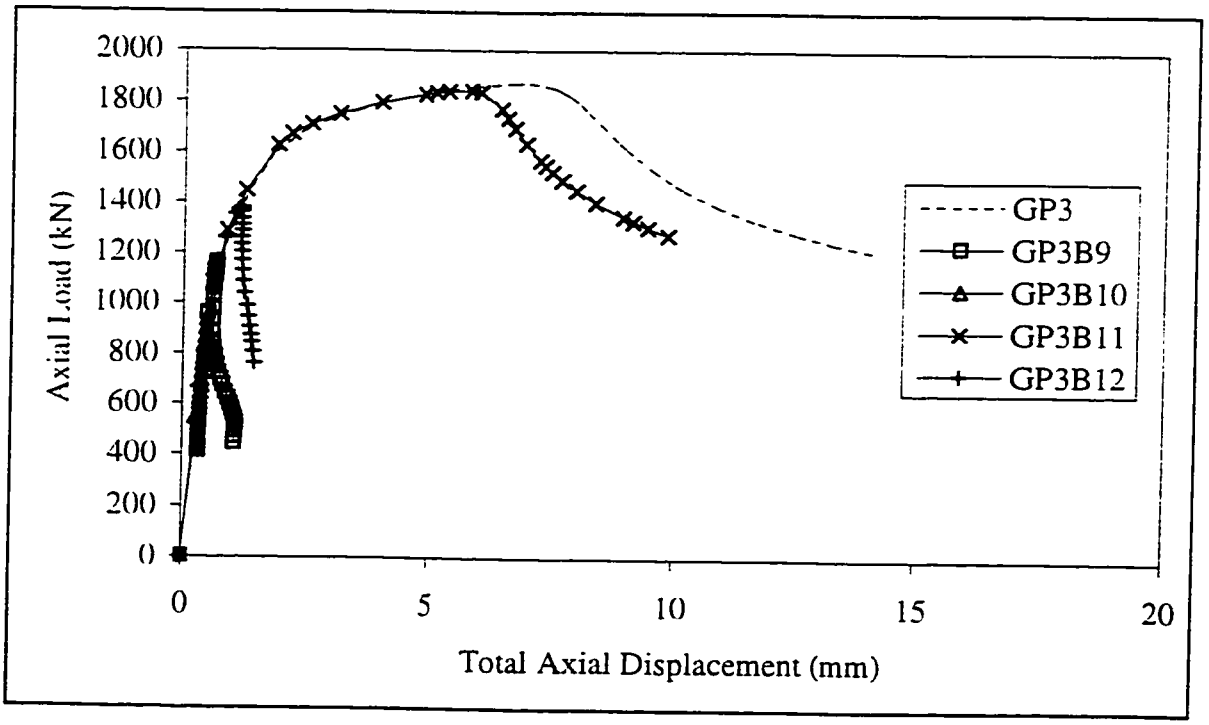

Figure 5.15 - Gusset plate GP3: gusset plate axial load vs. displacement in compression.

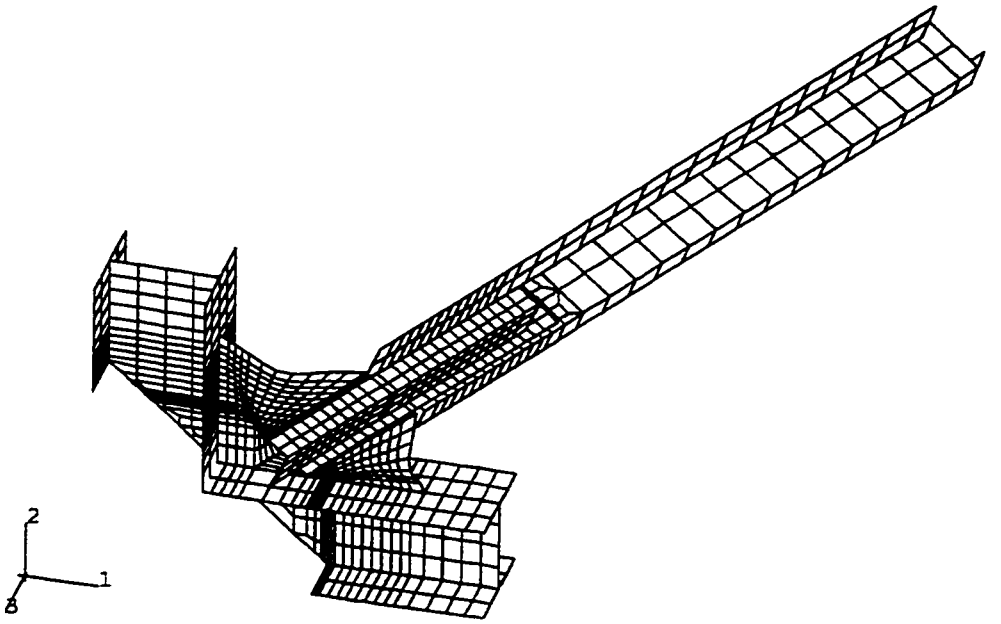

Figure 5.16 - Buckling of gusset plate.

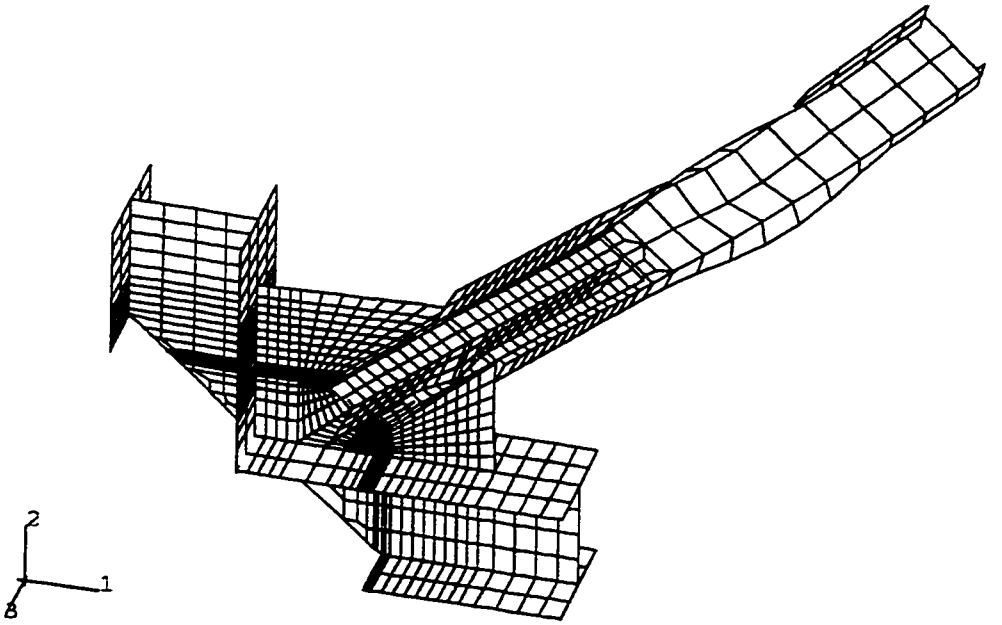

Figure 5.17 - Buckling of brace member.

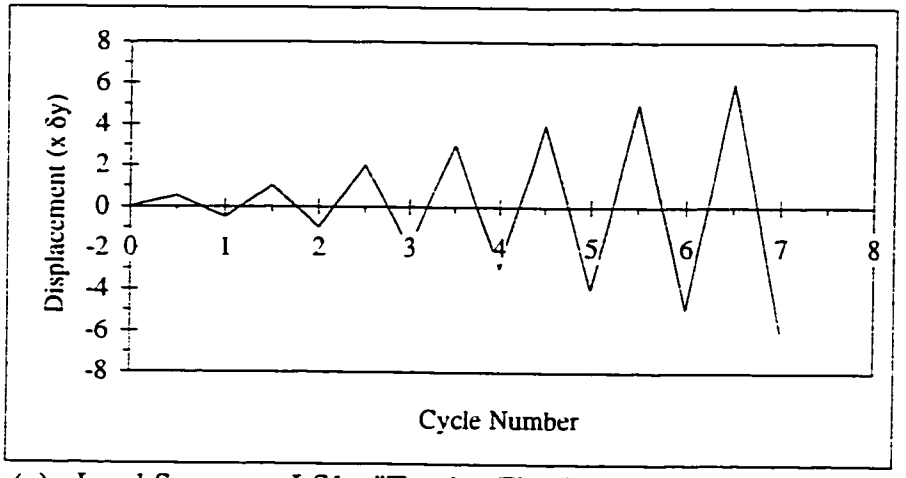

(a) - Load Sequence LS1 - "Tension First"

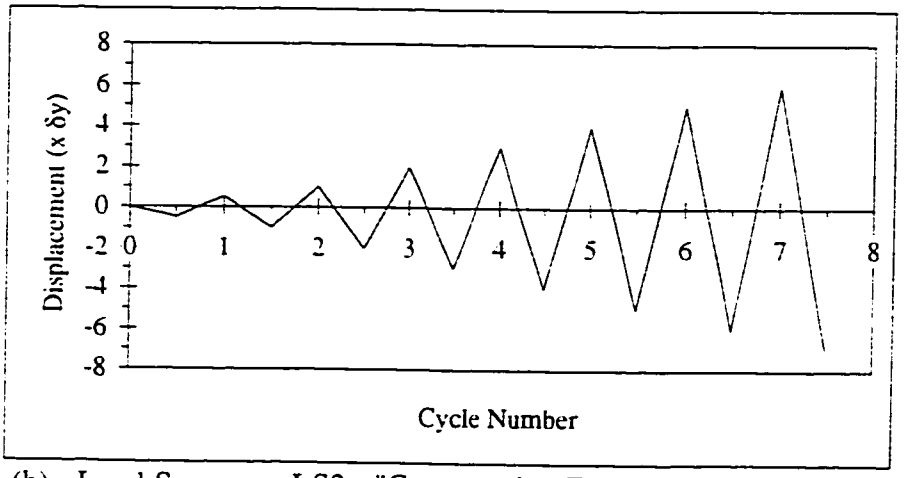

(b) - Load Sequence LS2 - "Compression First"

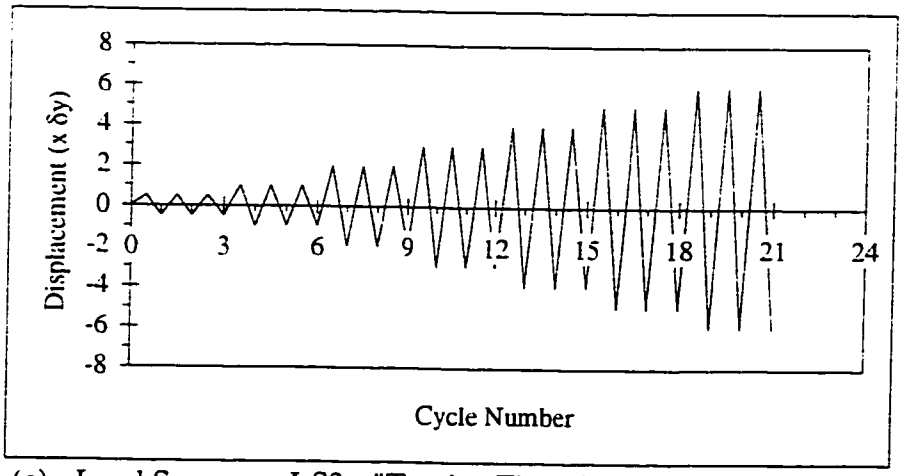

(c) - Load Sequence LS3 - "Tension First (3 cycles at each increment)"

Figure 5.18 - Summary of load sequences.

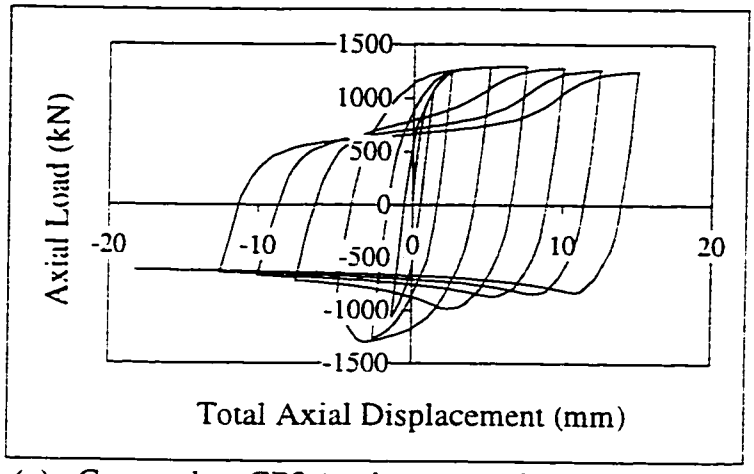

(a) - Gusset plate GP2 (no brace member): load sequence LS1 - hysteresis.

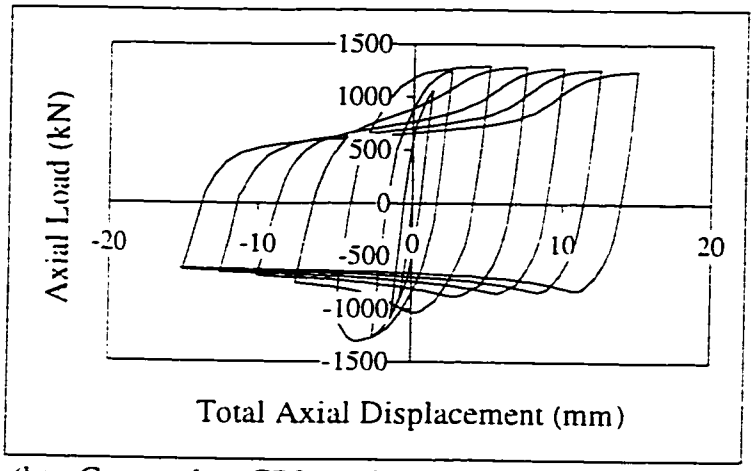

(b) - Gusset plate GP2 (no brace member): load sequence LS2 - hysteresis.

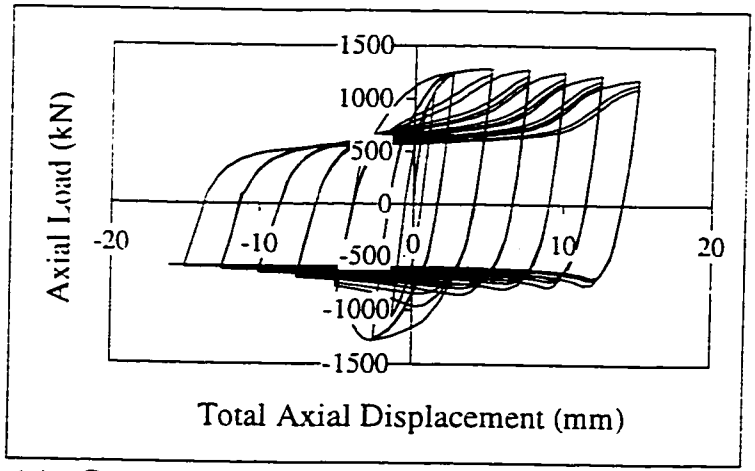

(c) - Gusset plate GP2 (no brace member): load sequence LS3 - hysteresis.

Figure 5.19 - Effect of load sequence on gusset plate only (no brace) in-plane behaviour.

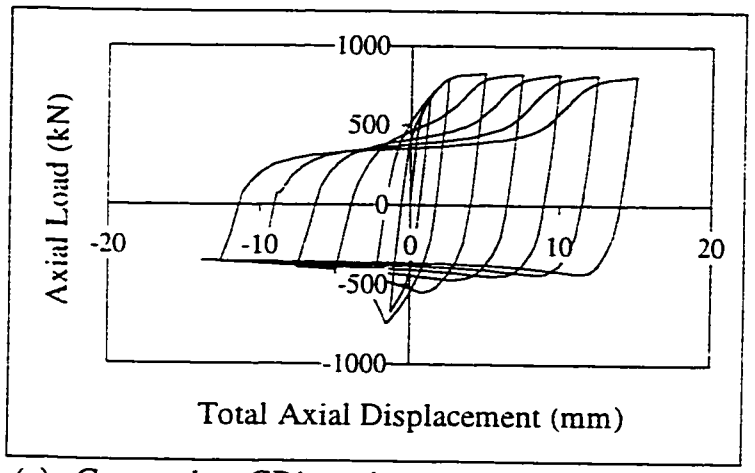

(a) - Gusset plate GP1 (no brace member): load sequence LS1 - hysteresis.

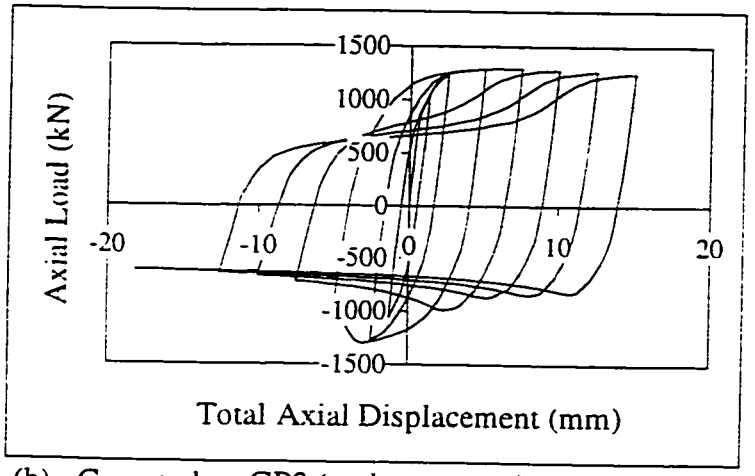

(b) - Gusset plate GP2 (no brace member): load sequence LS1 - hysteresis.

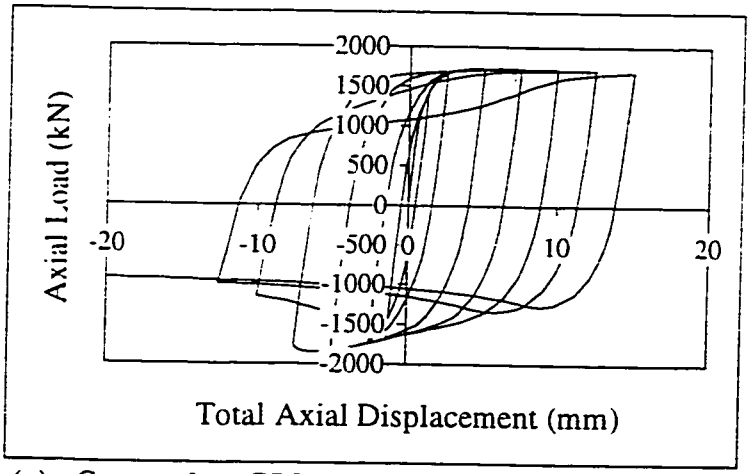

(c) - Gusset plate GP3 (no brace member): load sequence LS1 - hysteresis.

Figure 5.20 - Effect of plate thickness on gusset plate only (no brace) in-plane behaviour.

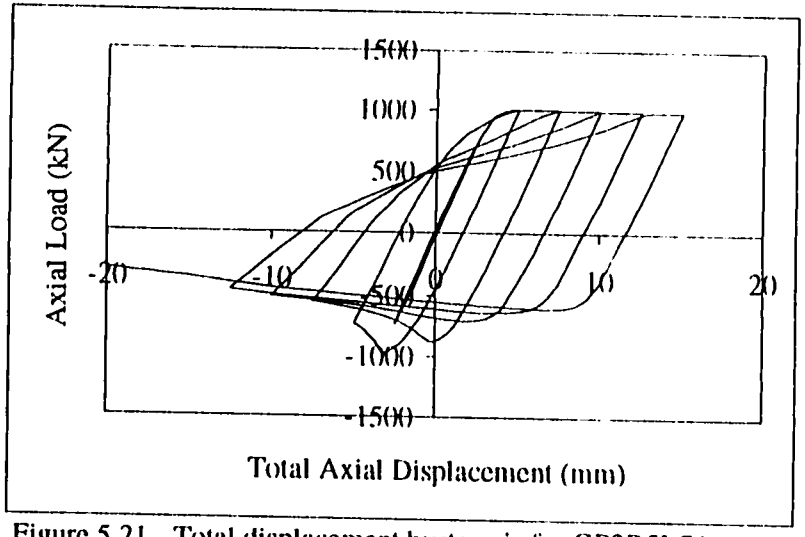

Figure 5.21 - Total displacement hysteresis for GP2B5LS1 .

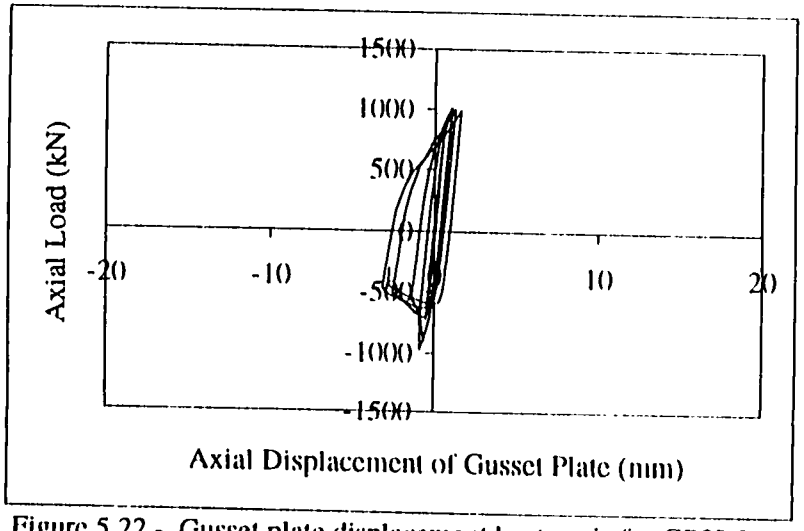

Figure 5.22 - Gusset plate displacement hysteresis for GP2B5LS1.

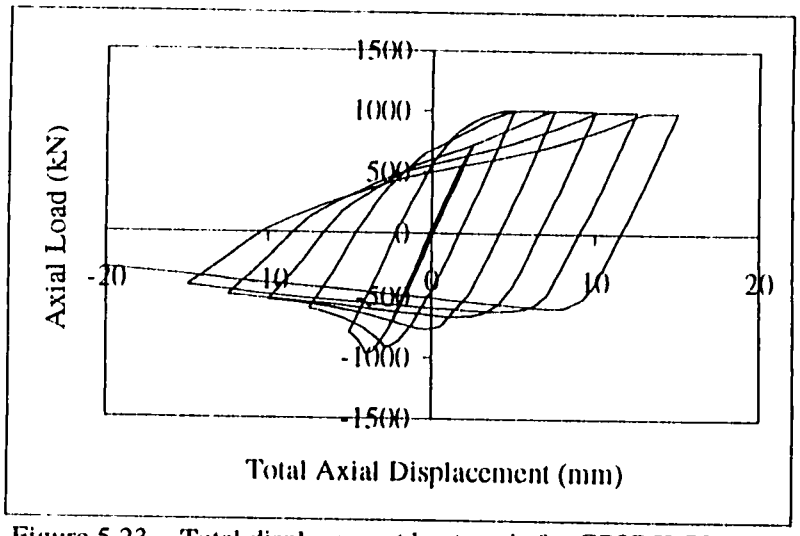

Figure 5.23 - Total displacement hysteresis for GP2B5LS2.

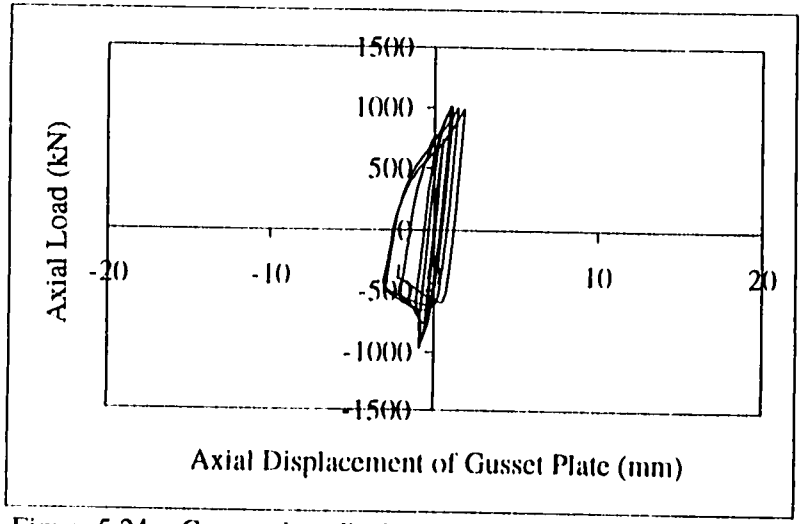

Figure 5.24 - Gusset plate displacement hysteresis for GP2B5LS2.

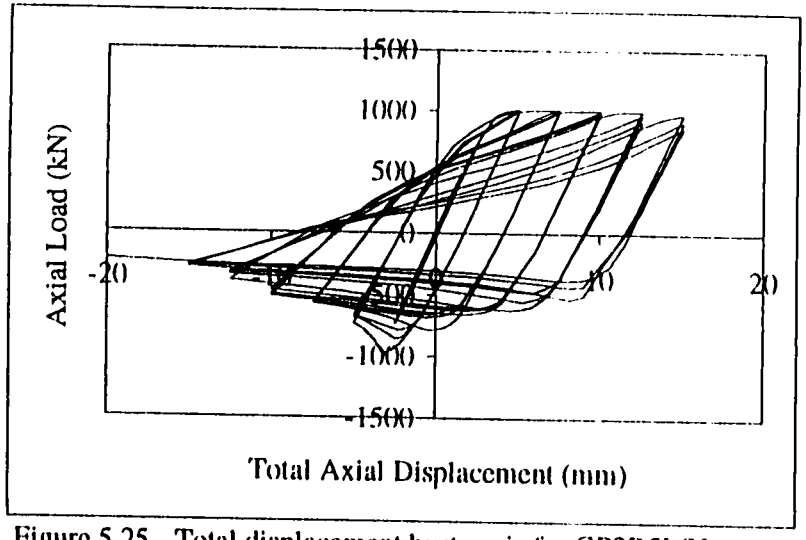

Figure 5.25 - Total displacement hysteresis for GP2B5LS3.

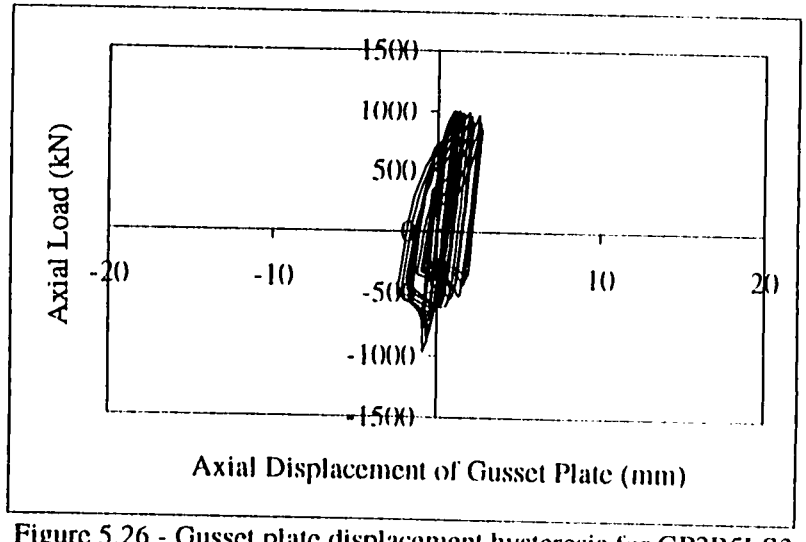

Figure 5.26 - Gusset plate displacement hysteresis for GP2B5LS3.

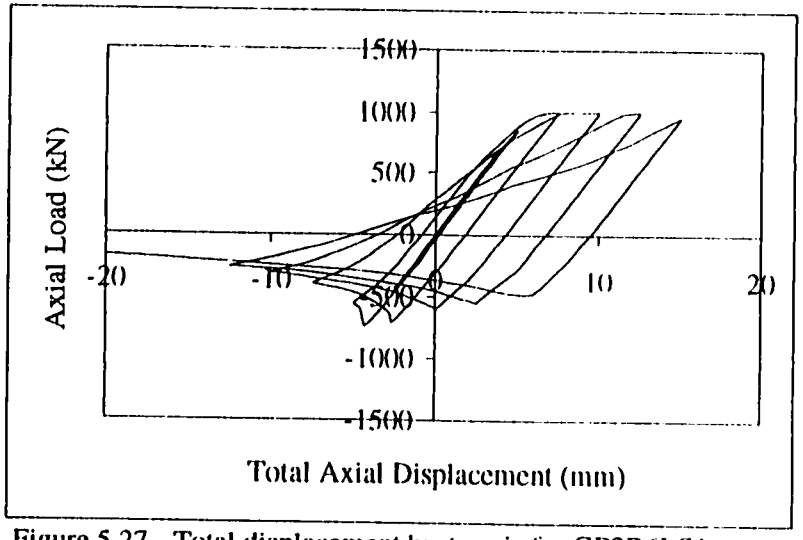

Figure 5.27 - Total displacement hysteresis for GP2B6LS1.

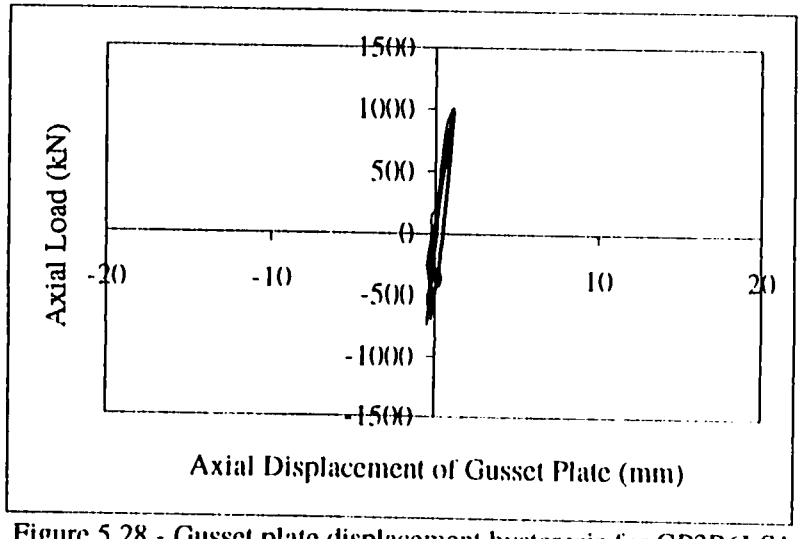

Figure 5.28 - Gusset plate displacement hysteresis for GP2B6LS1.

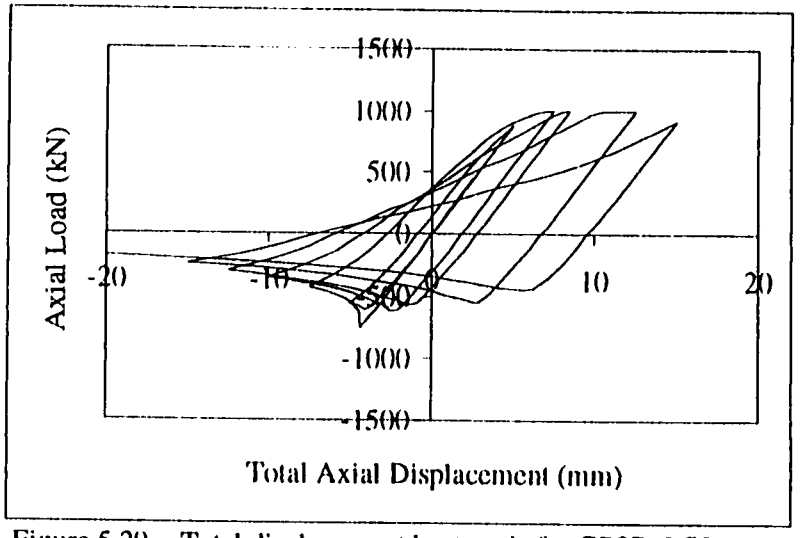

Figure 5.29 - Total displacement hysteresis for GP2B6LS2.

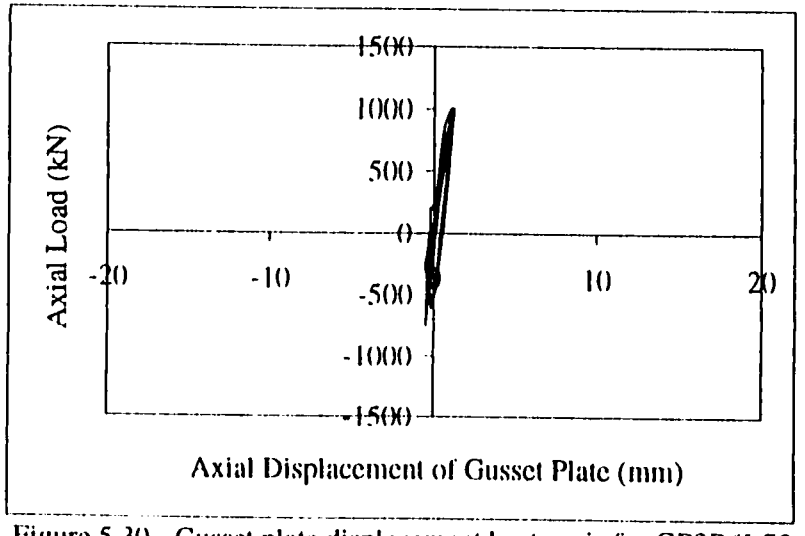

Figure 5.30 - Gusset plate displacement hysteresis for GP2B6LS2.

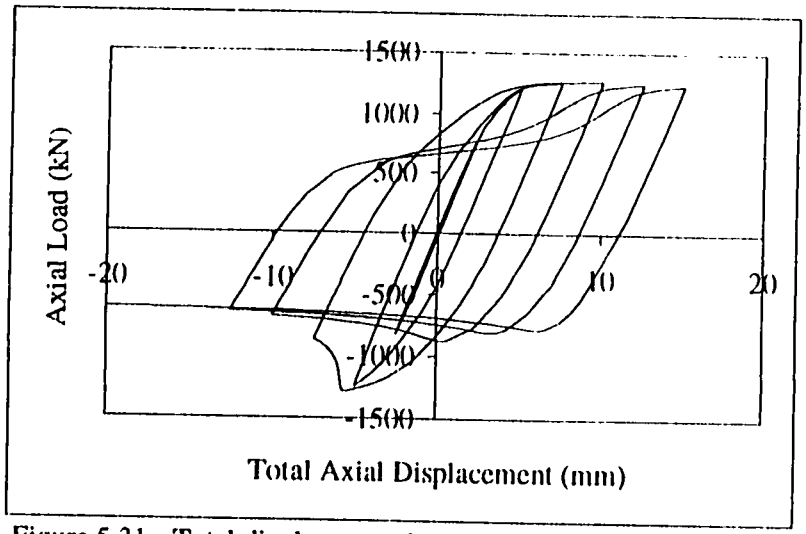

Figure 5.31 - Total displacement hysteresis for GP2B7LS1.

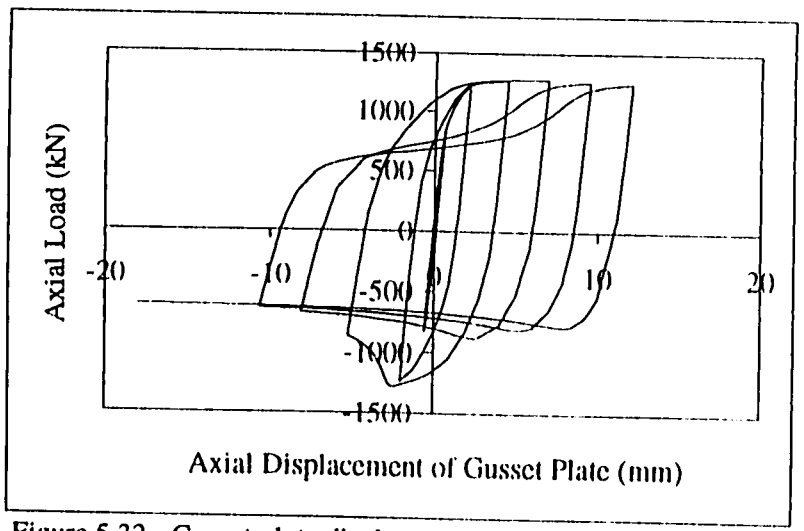

Figure 5.32 - Gusset plate displacement hysteresis for GP2B7LS1.

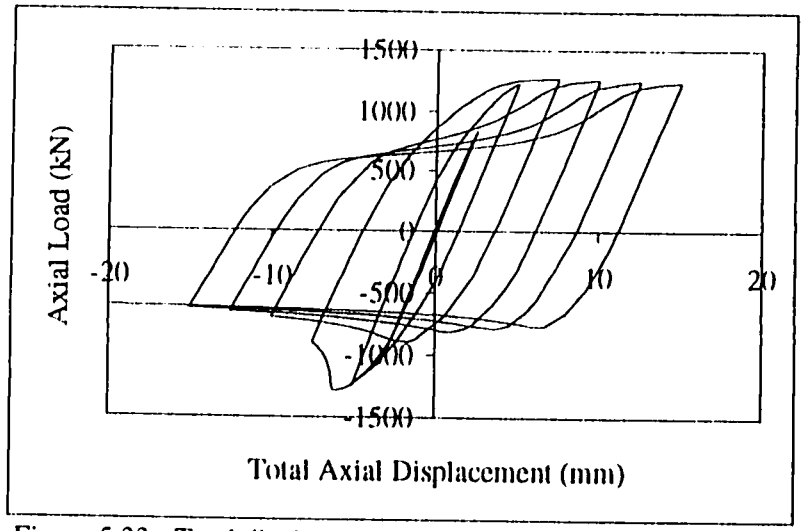

Figure 5.33 - Total displacement hysteresis for GP2B7LS2.

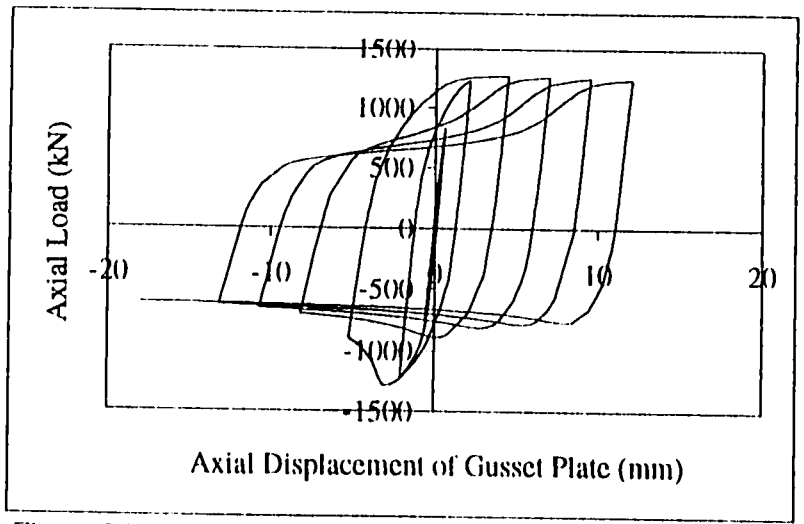

Figure 5.34 - Gusset plate displacement hysteresis for GP2B7LS2.

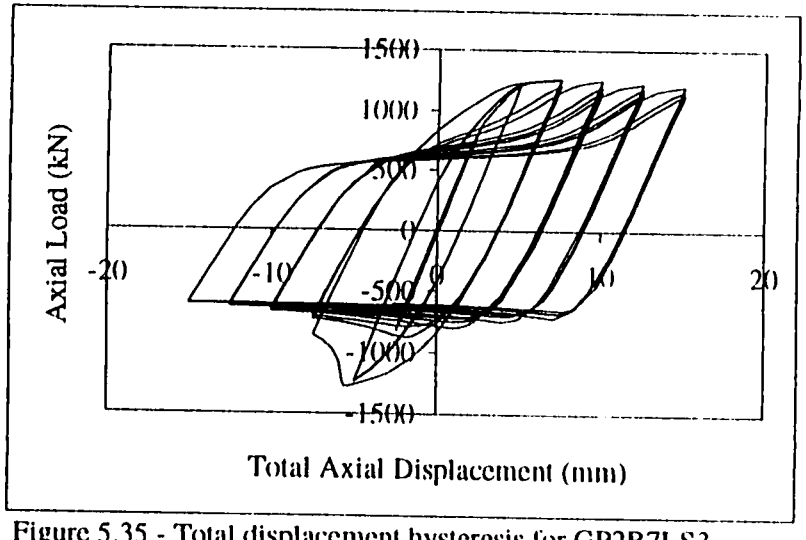

Figure 5.35 - Total displacement hysteresis for GP2B7LS3.

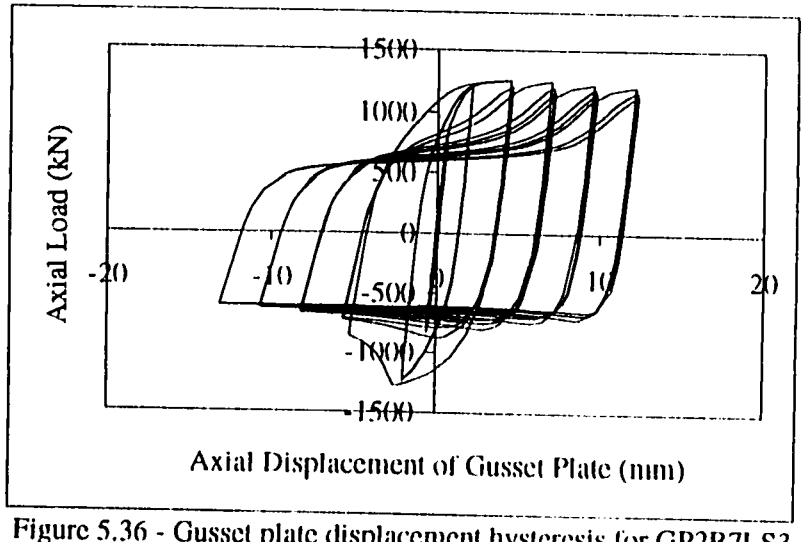

Figure 5.36 - Gusset plate displacement hysteresis for GP2B7LS3.

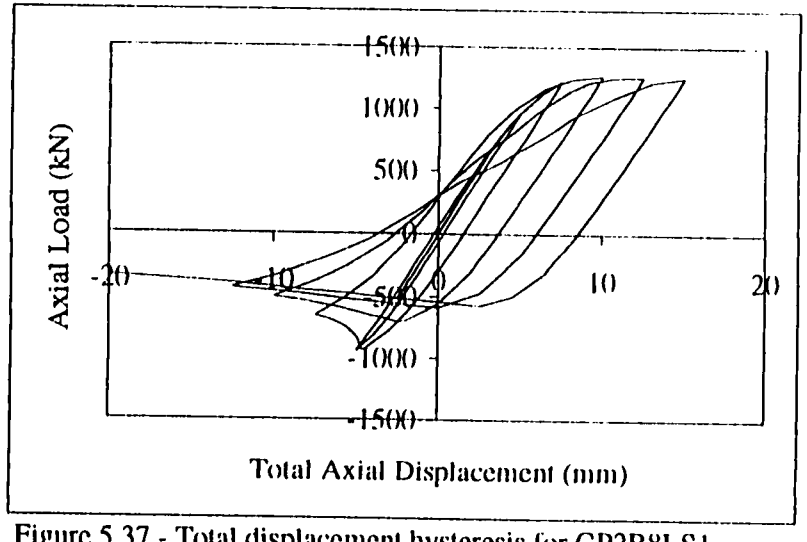

Figure 5.37 - Total displacement hysteresis for GP2B8LS1.

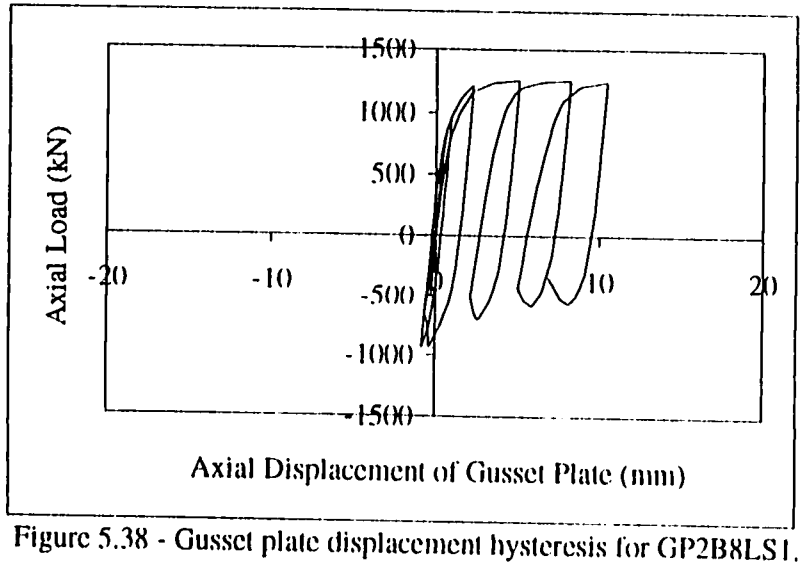

Figure 5.38 - Gusset plate displacement hysteresis for GP2B8LS1.

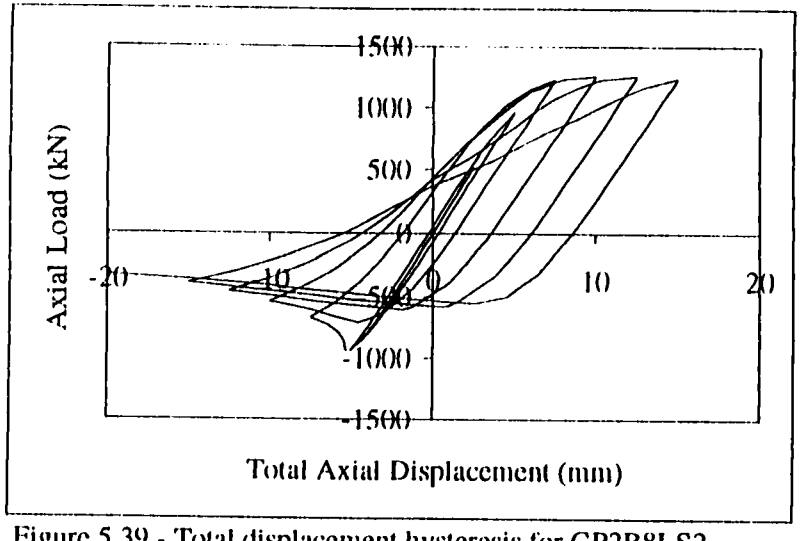

Figure 5.39 - Total displacement hysteresis for GP2B8LS2.

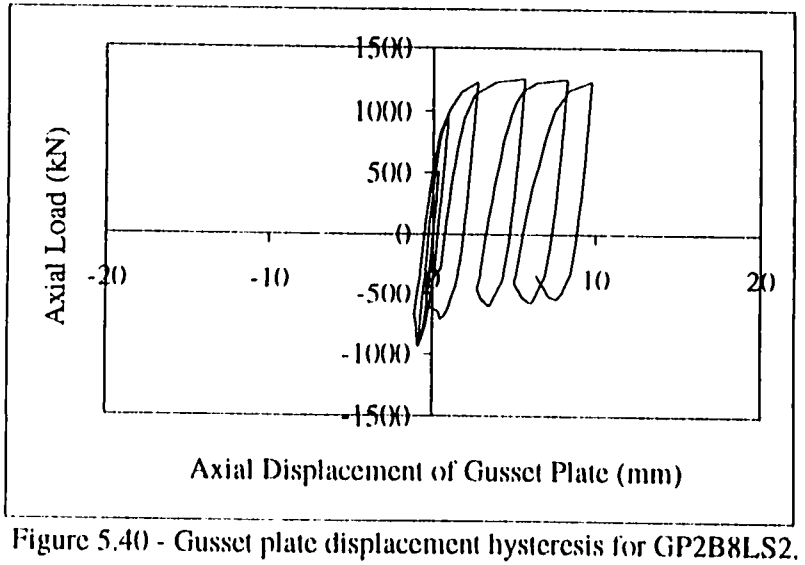

Figure 5.40 - Gusset plate displacement hysteresis for GP2B8LS2.

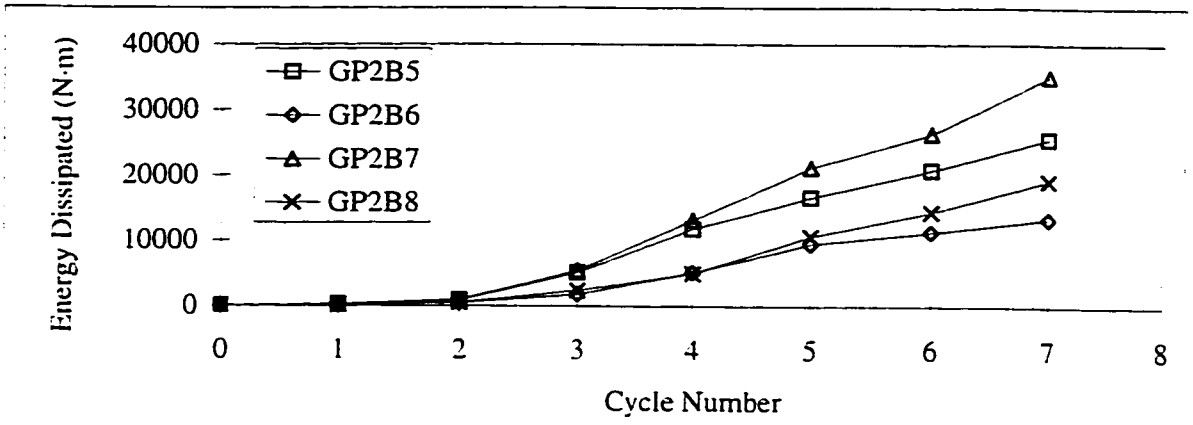

(a) - Load Sequence 1 - "Tension First"

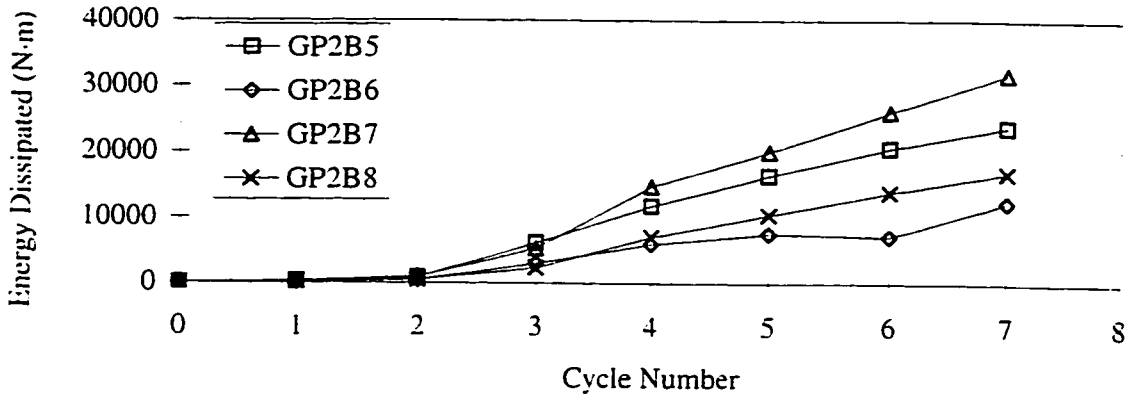

(b) - Load Sequence 2 - "Compression First"

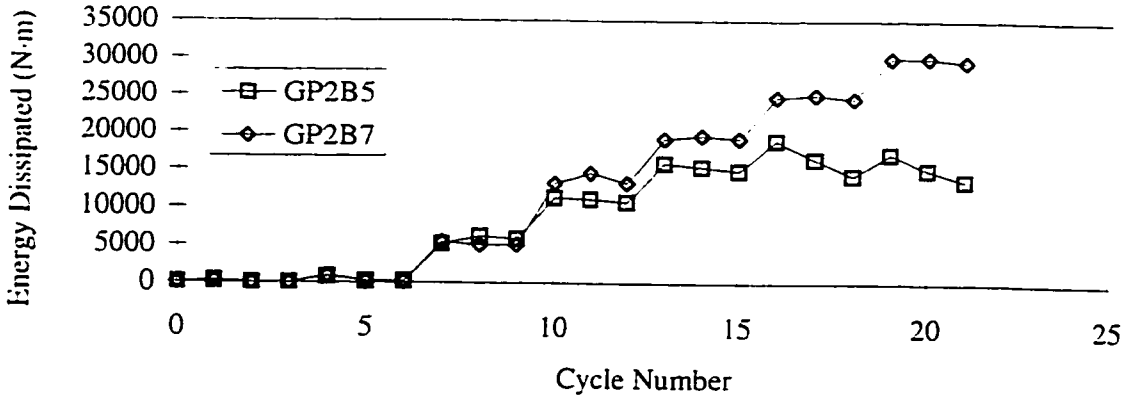

(c) - Load Sequence 3 - "Tension First (3 cycles at each increment)"

Figure 5.41 - Gusset plate GP2: energy dissipated (per cycle) for different brace members and load sequences.

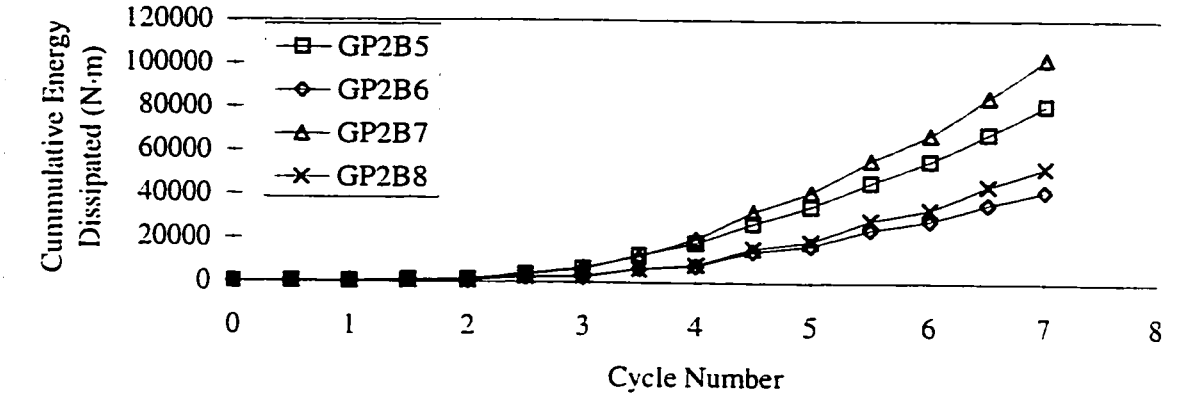

(a) - Load Sequence 1 - "Tension First"

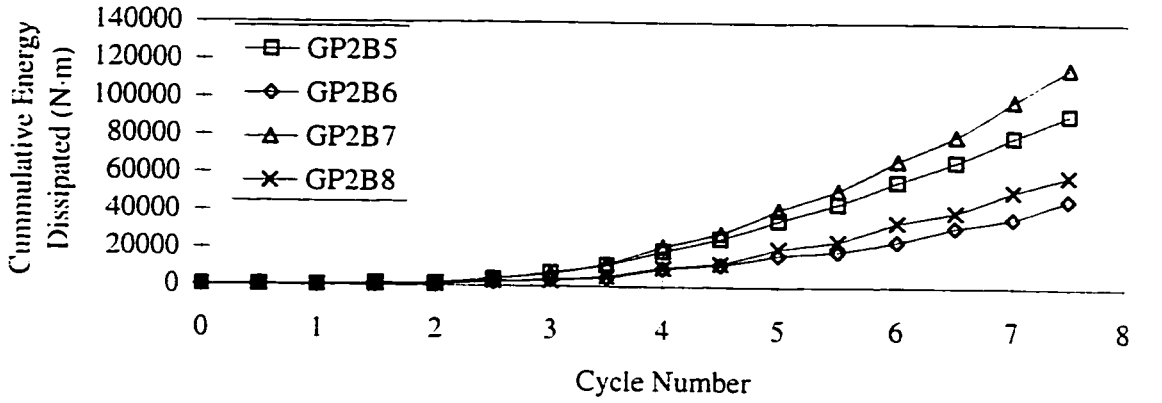

(b) - Load Sequence 2 - "Compression First"

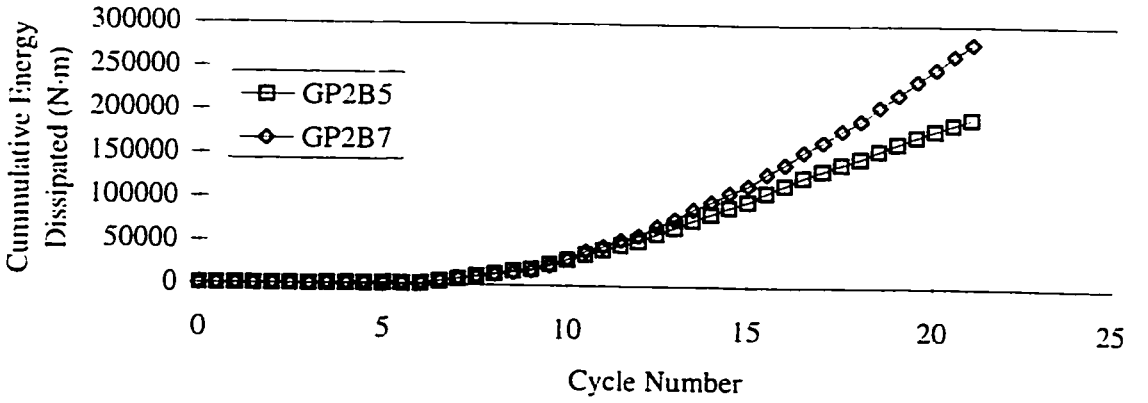

(c) - Load Sequence 3 - "Tension First (3 cycles at each increment)"

Figure 5.42 - Gusset plate GP2: cumulative energy dissipation for different brace members and load sequences.

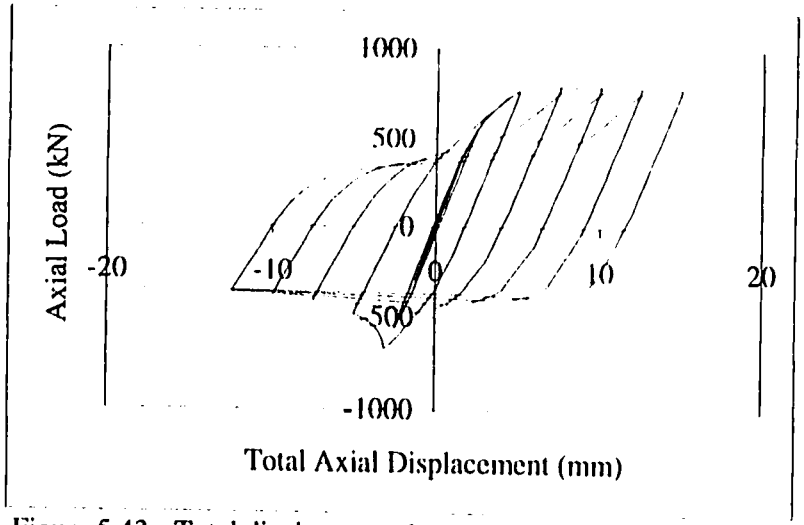

Figure 5.43 - Total displacement hysteresis for GP1B1LS1.

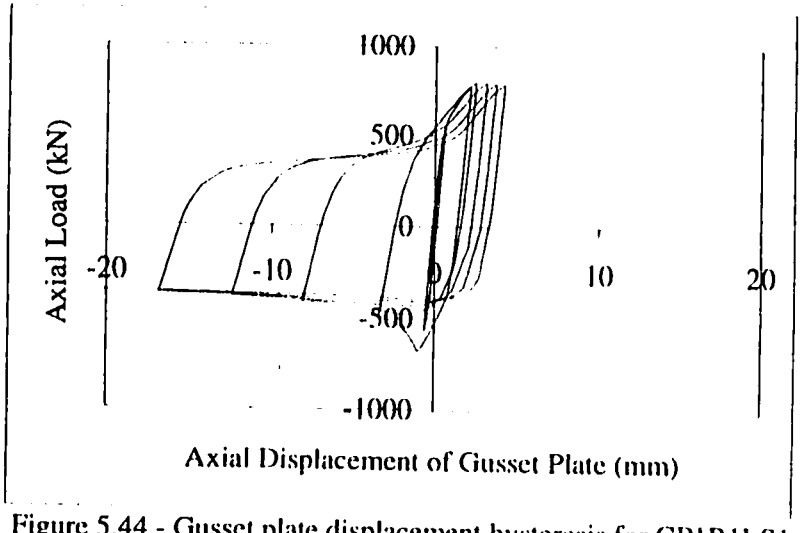

Figure 5.44 - Gusset plate displacement hysteresis for GP1B1LS1.

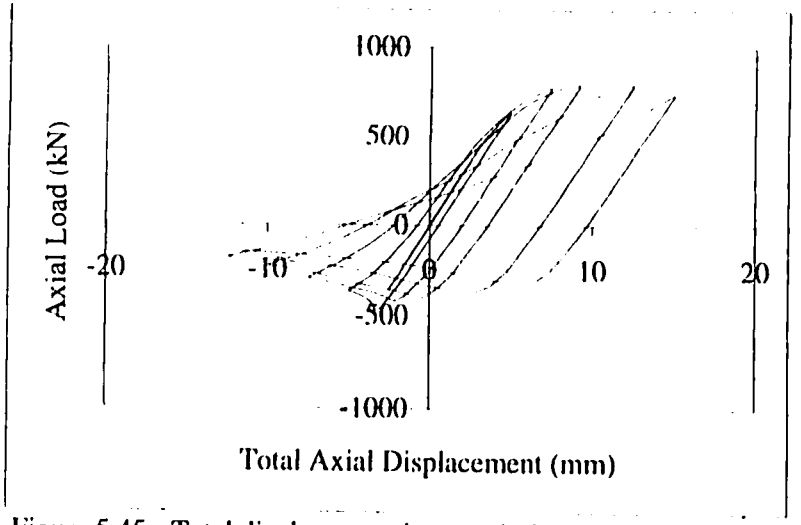

Figure 5.45 - Total displacement hysteresis for GP1B2LS1.

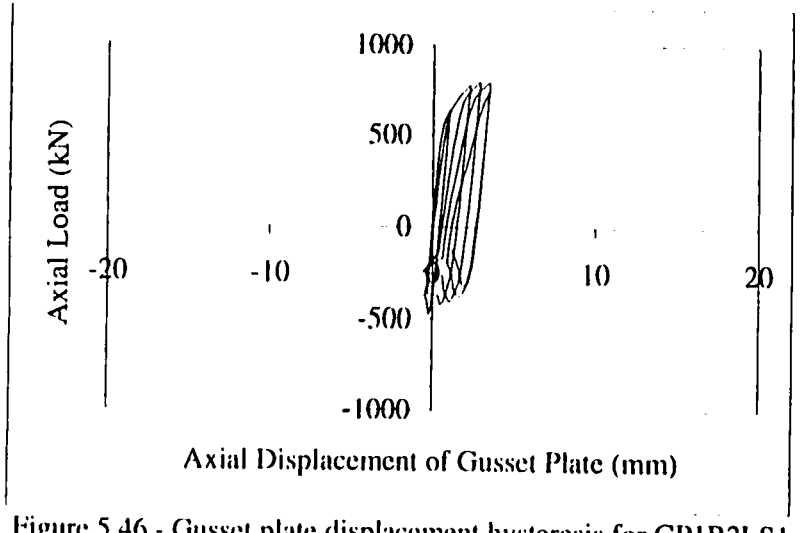

Figure 5.46 - Gusset plate displacement hysteresis for GP1B2LS1.

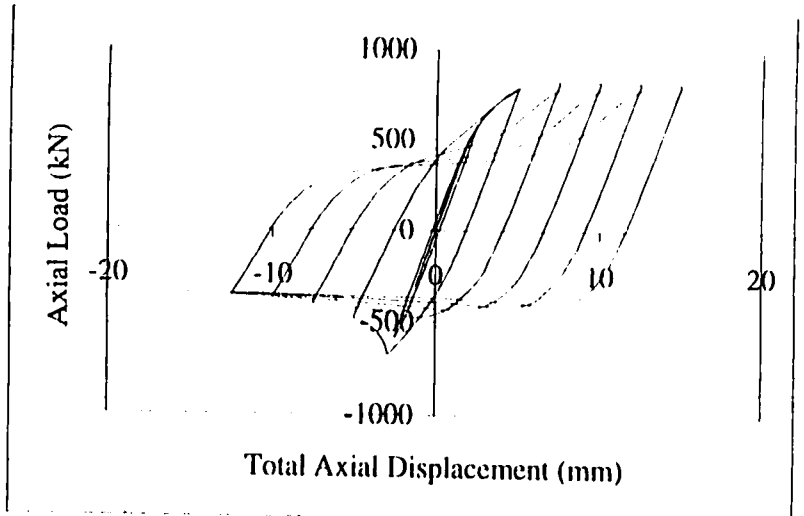

Figure 5.47 - Total displacement hysteresis for GP1B3LS1.

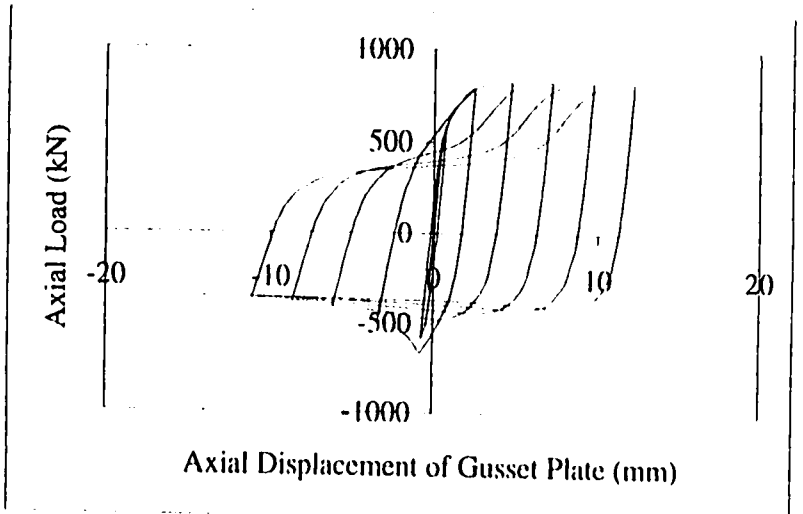

Figure 5.48 - Gusset plate displacement hysteresis for GP1B3LS1.

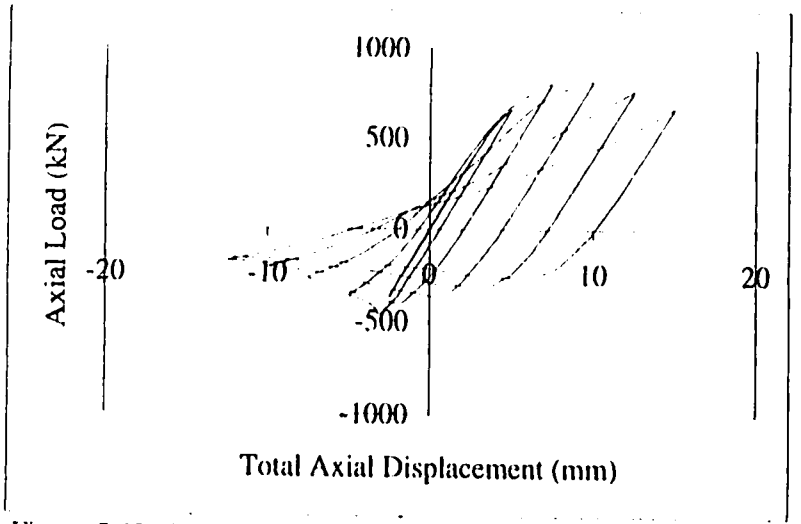

Figure 5.49 - Total displacement hysteresis for GP1B4LS1.

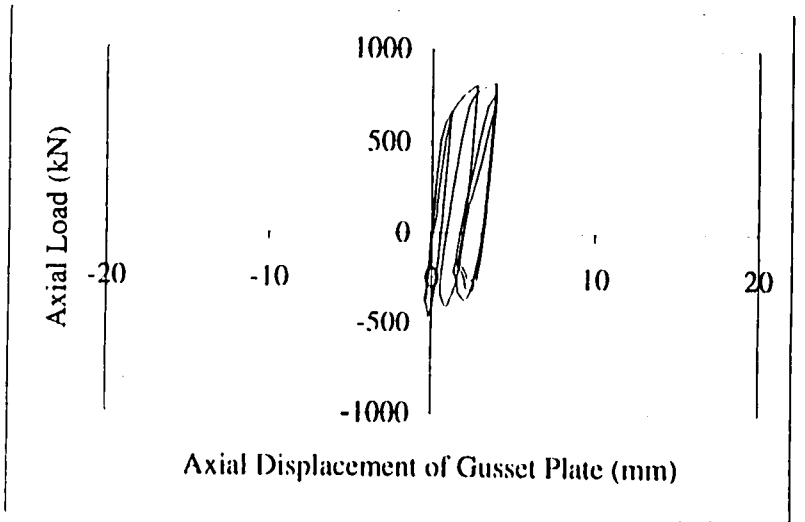

Figure 5.50 - Gusset plate displacement hysteresis for GP1B4LS1.

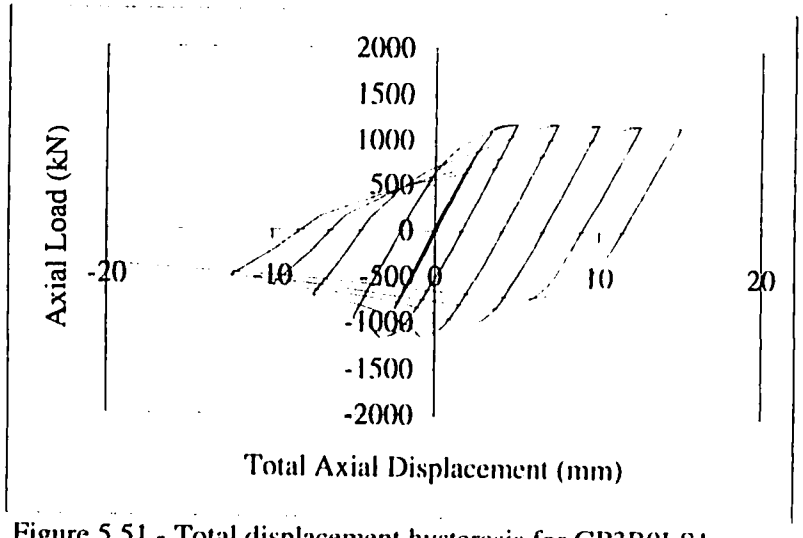

Figure 5.51 - Total displacement hysteresis for GP3B9LS1.

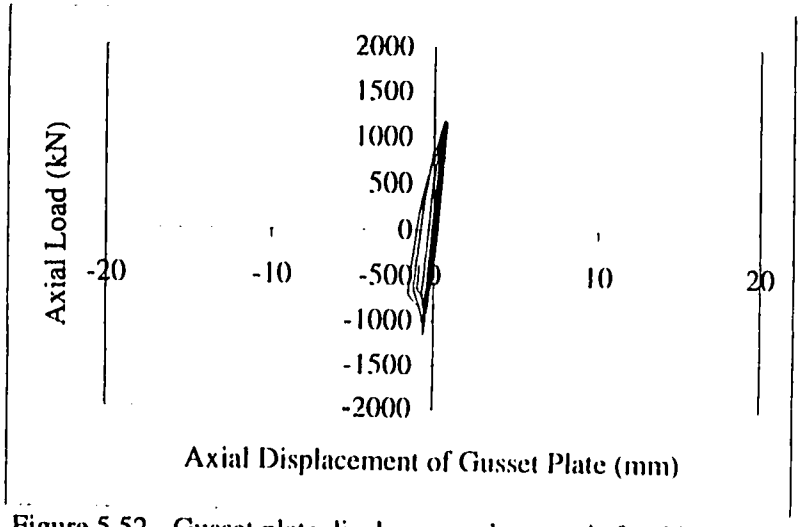

Figure 5.52 - Gusset plate displacement hysteresis for GP3B9LS1.

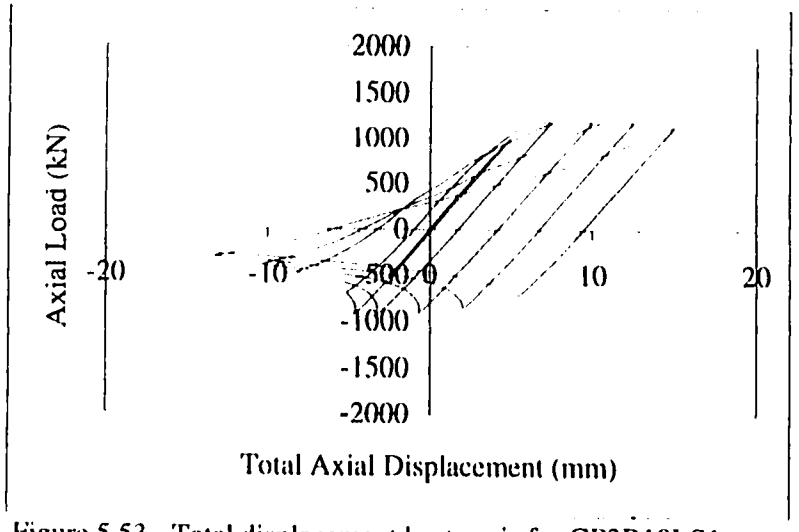

Figure 5.53 - Total displacement hysteresis for GP3B10LS1.

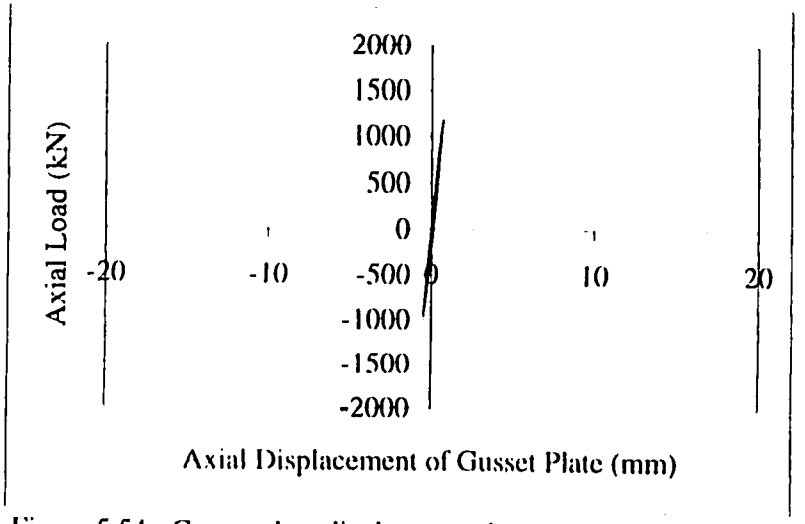

Figure 5.54 - Gusset plate displacement hysteresis for GP3B10LS1.

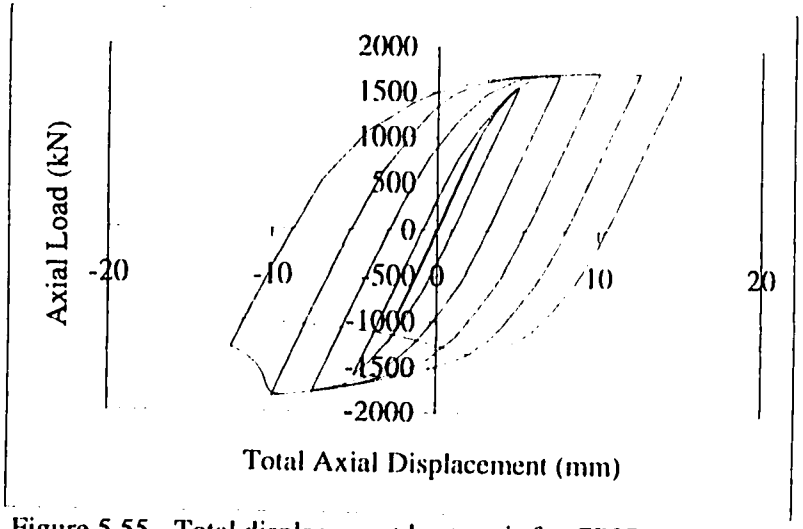

Figure 5.55 - Total displacement hysteresis for GP3B11LS1.

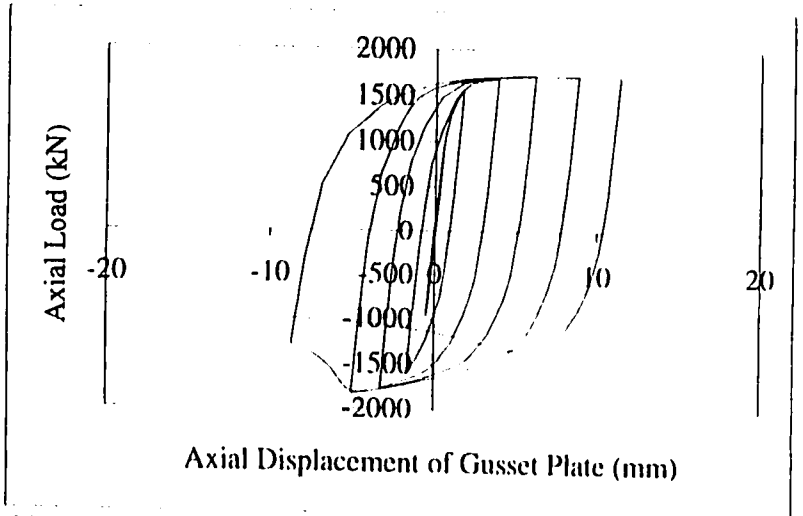

Figure 5.56 - Gusset plate displacement hysteresis for GP3B11LS1.

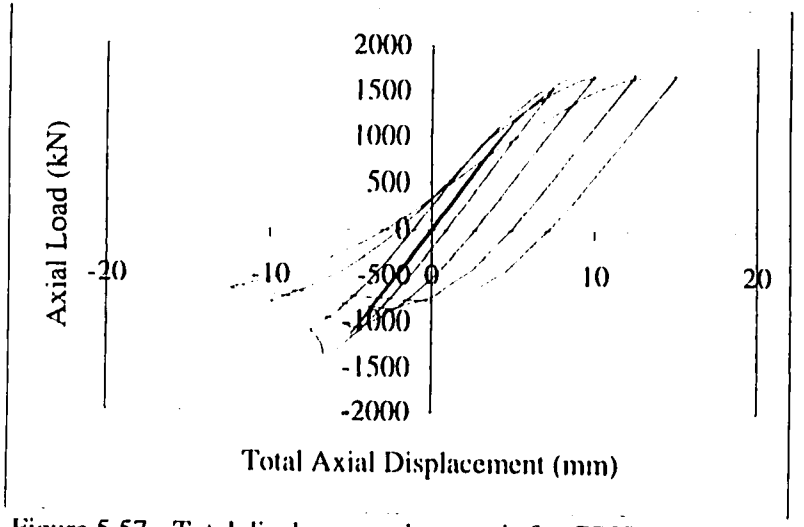

Figure 5.57 - Total displacement hysteresis for GP3B12LS1.

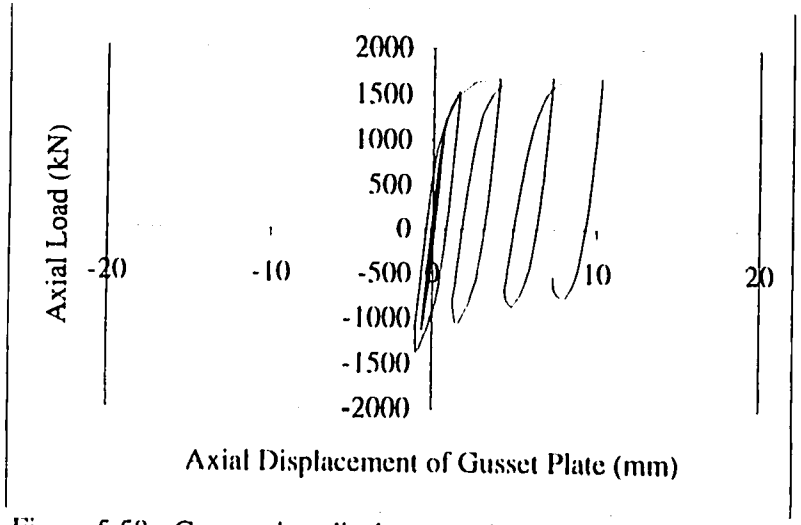

Figure 5.58 - Gusset plate displacement hysteresis for GP3B12LS1.

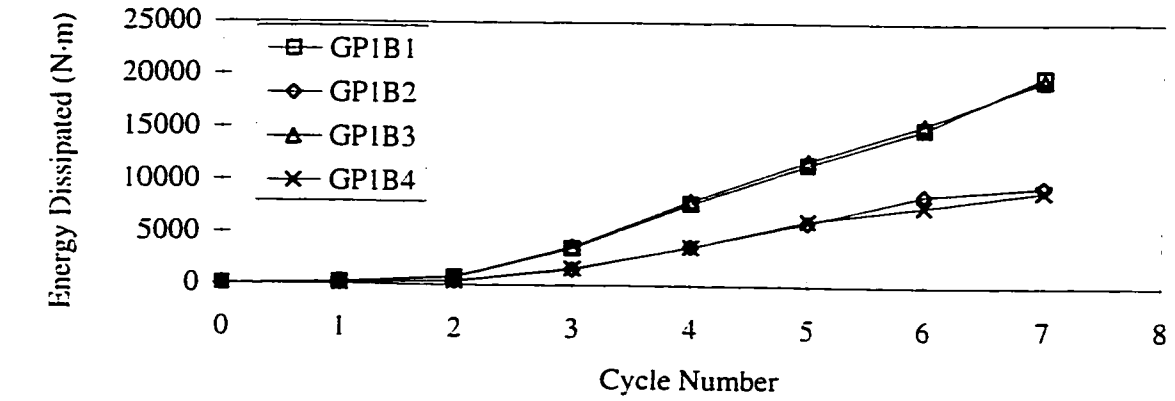

(a) - Gusset Plate GP1.

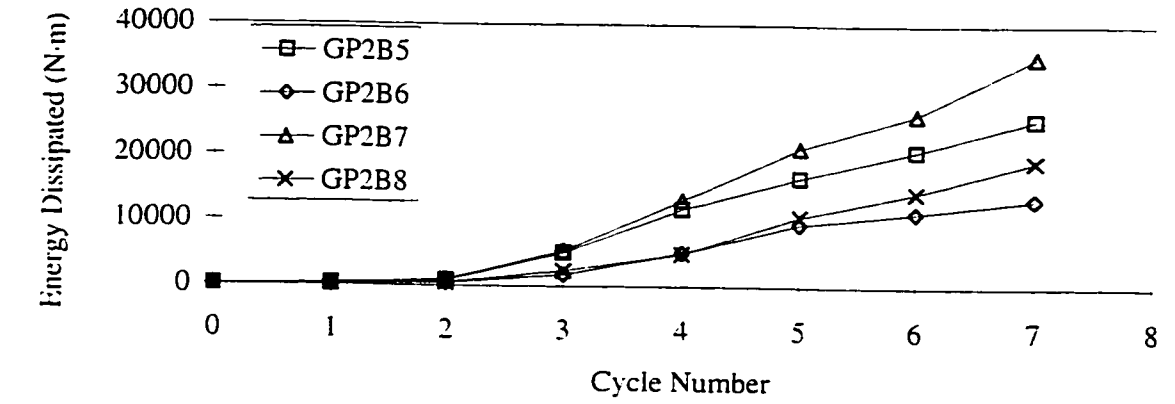

(b) - Gusset Plate GP2.

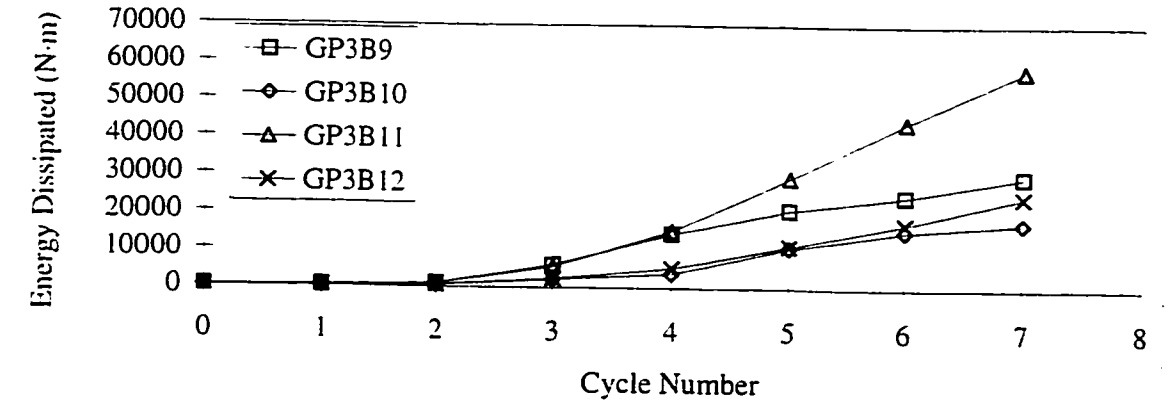

(c) - Gusset Plate GP3.

Figure 5.59 - Load sequence LS1: energy dissipated (per cycle) for different gusset plates and brace members.

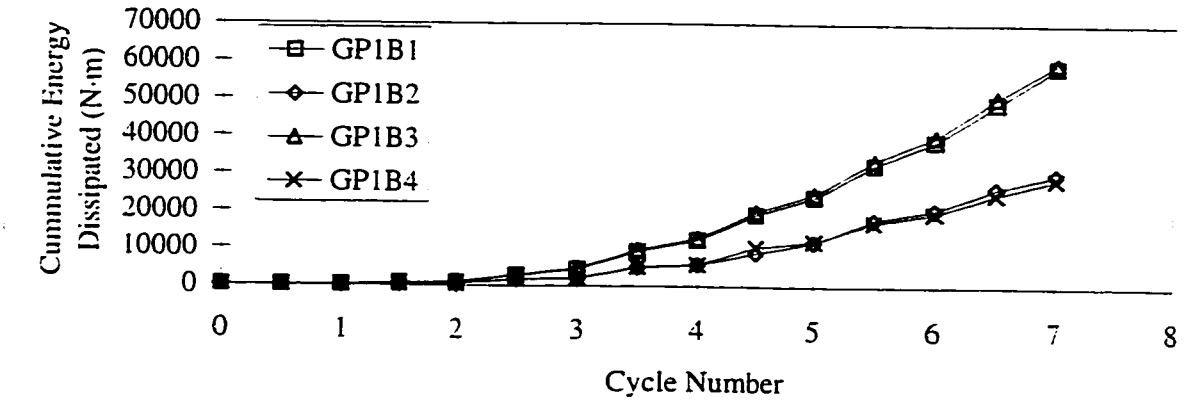

(a) - Gusset Plate GP1.

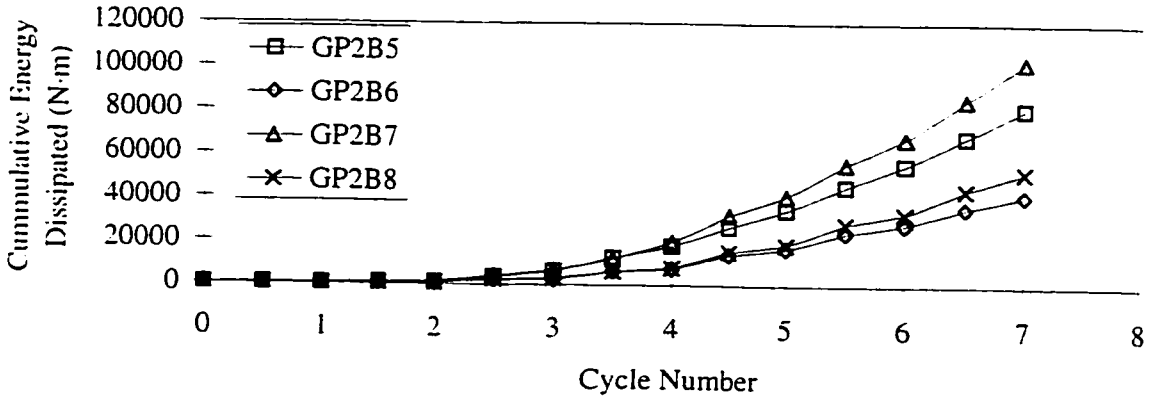

(b) - Gusset Plate GP2.

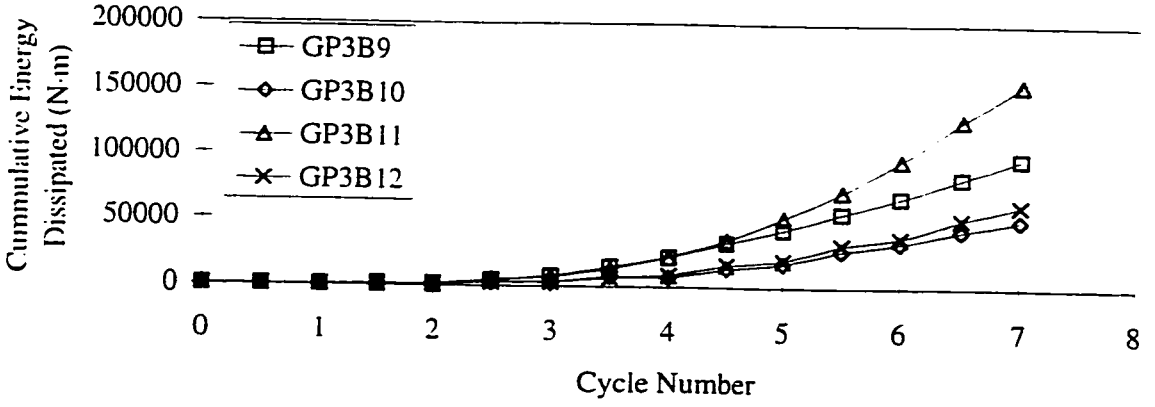

(c) - Gusset Plate GP3.

Figure 5.60 - Load sequence LS1: cummulative energy dissipation for different gusset plates and brace members.

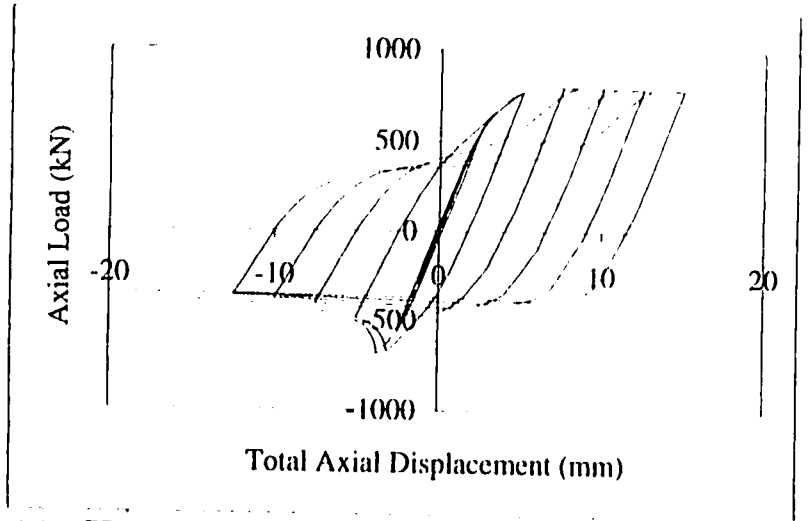

(a) - GP1B1LS1 total axial displacement behaviour.

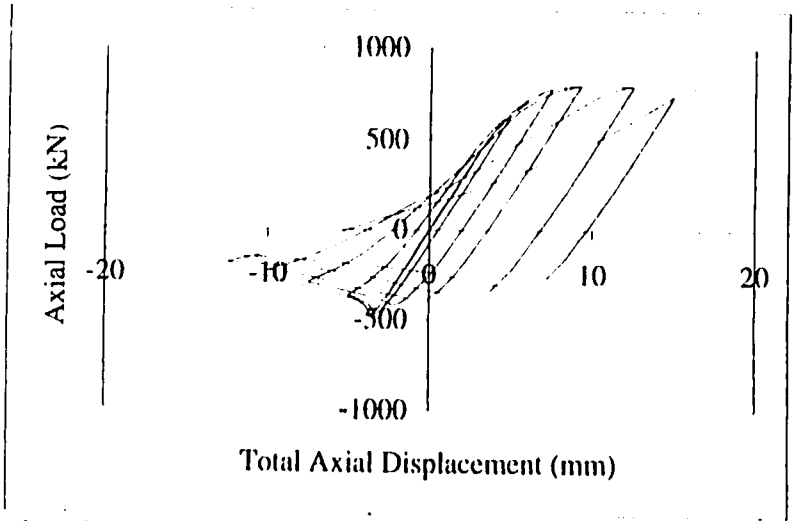

(b) - GP1B2LS1 total axial displacement behaviour.

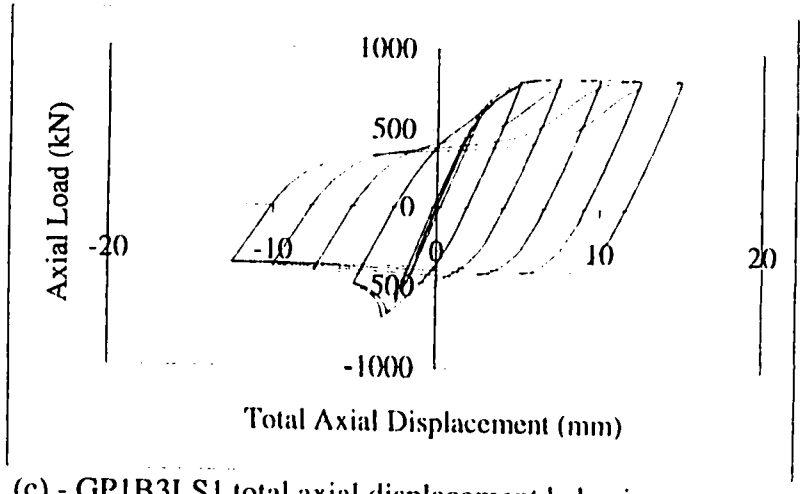

(c) - GP1B3LS1 total axial displacement behaviour.

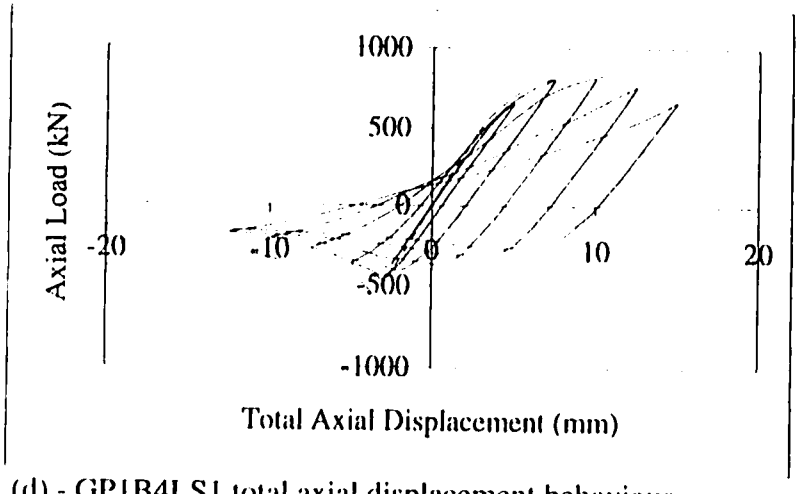

(d) - GP1B4LS1 total axial displacement behaviour.

Figure 5.61 - Comparison between monotonic loading curves and cyclic loading hysteresis for gusset plate GP1 subassemblies.

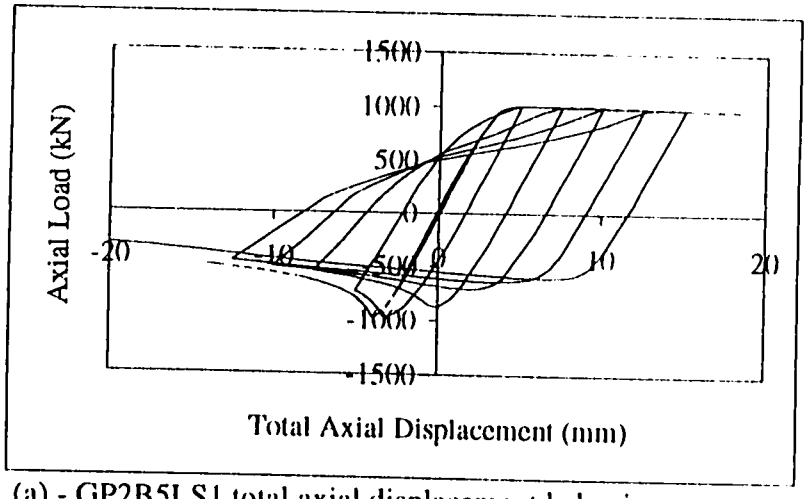

(a) - GP2B5LS1 total axial displacement behaviour.

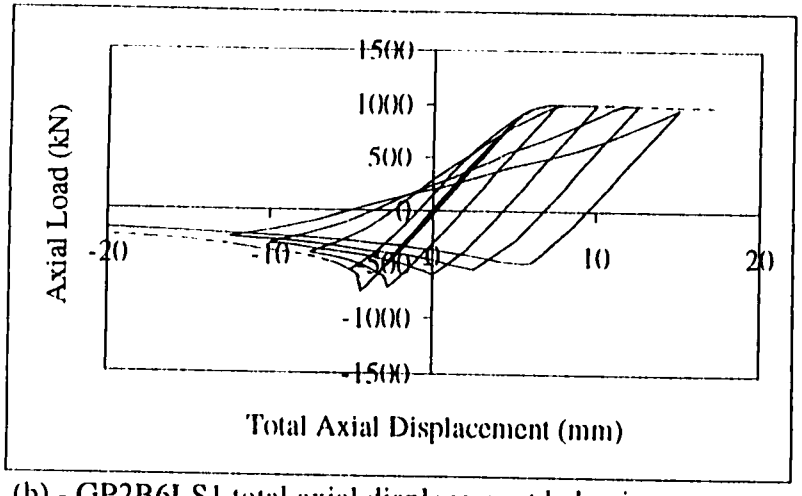

(b) - GP2B6LS1 total axial displacement behaviour.

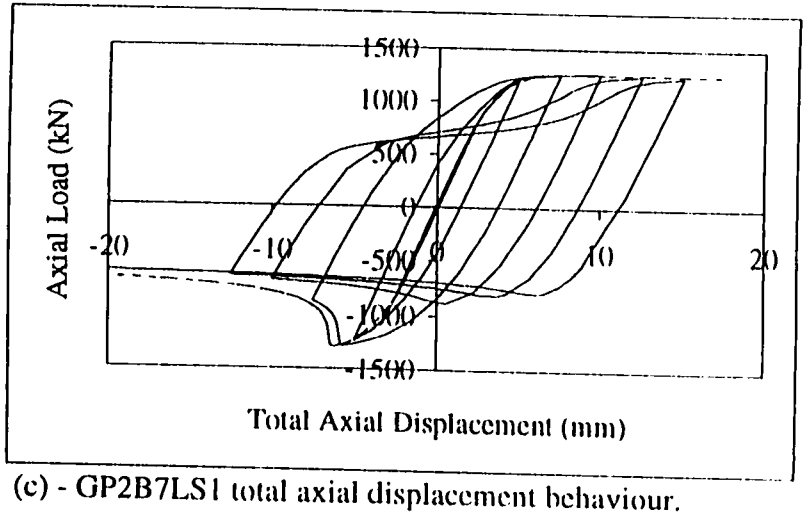

(c) - GP2B7LS1 total axial displacement behaviour.

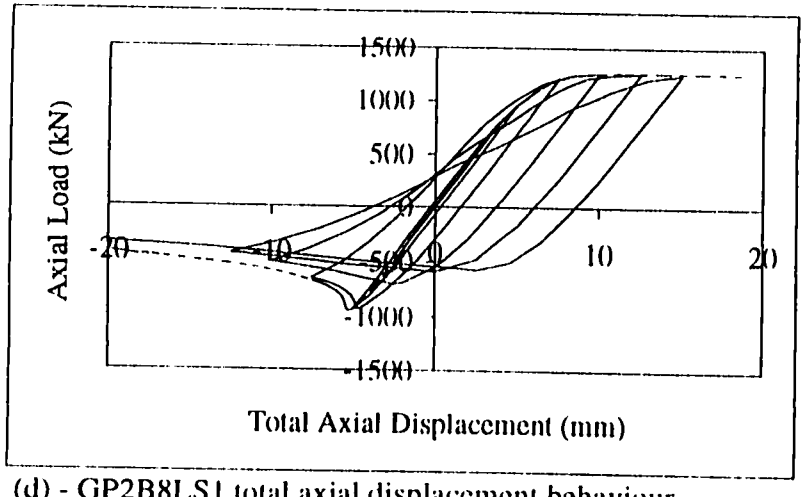

(d) - GP2B8LS1 total axial displacement behaviour.

Figure 5.62 - Comparison between monotonic loading curves and cyclic loading hysteresis for gusset plate GP2 subassemblies.

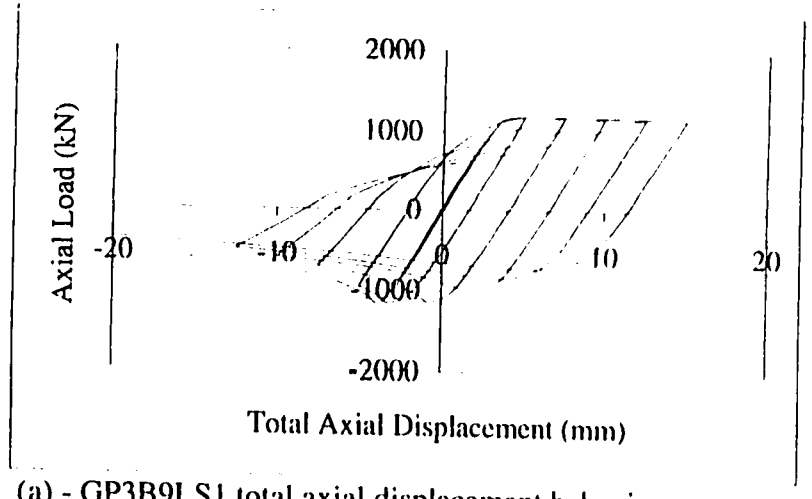

(a) - GP3B9LS1 total axial displacement behaviour.

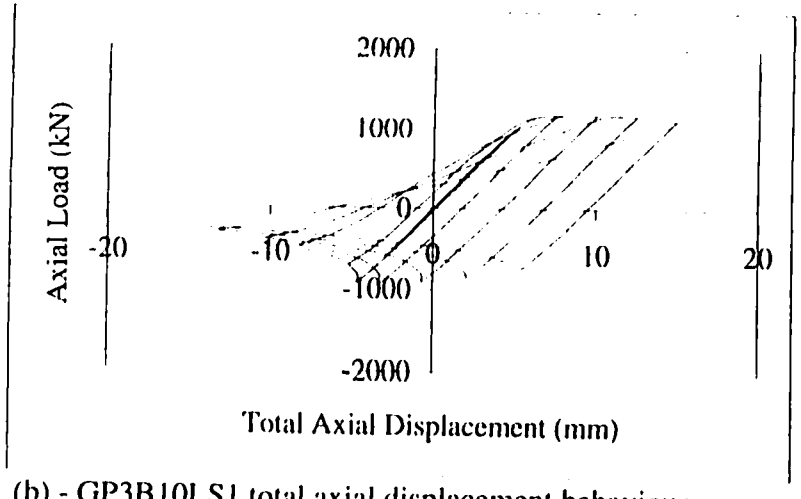

(b) - GP3B10LS1 total axial displacement behaviour.

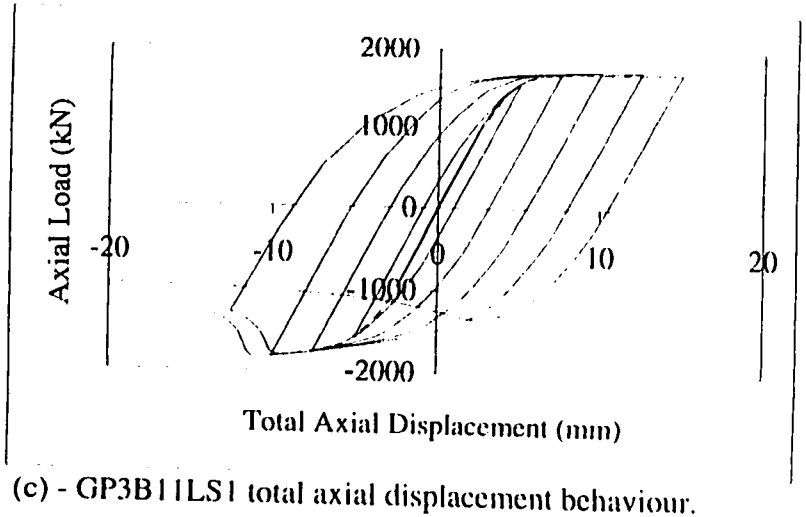

(c) - GP3B11LS1 total axial displacement behaviour.

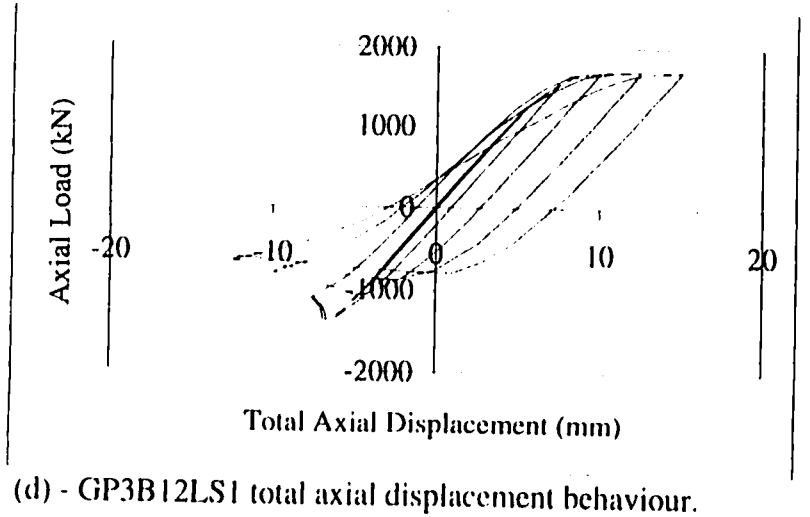

(d) - GP3B12LS1 total axial displacement behaviour.

Figure 5.63 - Comparison between monotonic loading curves and cyclic loading hysteresis for gusset plate GP3 subassemblies.

6. CONCLUSIONS AND RECOMMENDATIONS

6.1 Introduction

In this chapter, conclusions and recommendations are presented, based on the results of the numerical investigation presented in Chapters 3, 4, and 5.

6.2 Conclusions

In the first phase of this investigation, gusset plate models were developed and validated using the test results of Yam and Cheng (1993) and Rabinovitch and Cheng (1993). For this phase, a linear elastic mesh study was conducted, the behaviour of gusset plate connections under monotonic tension and compression loading was investigated, and the cyclic behaviour of several gusset plate specimens was modeled.

The linear elastic mesh study was performed to determine the level of mesh refinement required to ensure sufficient convergence. Gusset plate models were constructed with increasing levels of mesh refinement, elastic stress distributions were investigated, and axial displacements were compared. The results of the linear elastic mesh study can be summarized as follows:

- Axial displacements converged after several mesh refinements. The third finest mesh (Mesh 2 in Figure 3.1(b)) was determined to be adequate for predicting displacement.

- Principal stress contour plots confirmed that the peak principal stress and the highest principal stress gradients occur near the last row of bolts in the gusset plate to splice member connection. Although convergence of the peak principal stress was not achieved. convergence of the overall stress behaviour was apparent after several mesh refinements

To investigate gusset plate behaviour under monotonic tension loading. the models developed for the linear elastic mesh study were modified to incorporate inelastic material behaviour. In this step. the effects of mesh refinement. material model. framing member stiffness. and fastener model were investigated. The following conclusions can be drawn regarding the modeling of gusset plate behaviour under monotonic tension loading:

- The effects of material model (i.e. elastic – perfect plastic versus isotropic strain hardening) and framing member stiffness on the behaviour of the gusset plate models under monotonic tension loading are significant. Less significant is the effect of the fastener model (i.e. elastic versus rigid). The effect of mesh refinement on the behaviour of the gusset plate model under monotonic tension loading was small for the range of mesh refinements investigated. This effect was seen to diminish as the level of mesh refinement was increased.
- Models incorporating the elastic – perfect plastic material model and flexible framing members closely predicted the behaviour of gusset plates, under monotonic tension loading.

To investigate gusset plate behaviour under monotonic compression loading, the gusset plate models were modified to incorporate initial imperfections. In this step, the effects of mesh refinement, material model, framing member stiffness, fastener model, initial imperfection shape and magnitude, and the level of in-plane (clamping) restraint imparted by the splice members were investigated. The following conclusions can be drawn regarding the modeling of gusset plate behaviour under monotonic compression loading:

- The effects of initial imperfection magnitude and the level of out-of-plane (clamping) restraint imparted to the gusset plate by the splice members on the gusset plate model behaviour under monotonic compression loading are significant. The effects of framing member stiffness, fastener model and initial imperfection shape are much less significant. The effect of the material model (i.e. elastic – perfect plastic versus isotropic strain hardening) on ultimate capacity under monotonic compression loading is small, however, the effect of the material model on the model stiffness in the inelastic range can be significant.
- Models constructed with a 2 mm quarter sine wave initial imperfection, full splice member restraint, flexible framing members and an isotropic strain hardening material model accurately predicted the behaviour of gusset plates loaded monotonically in compression.

Based on the results of the linear elastic and monotonic loading studies, models were constructed to study the cyclic behaviour of gusset plates. For this step, a simple bolt slip model and a gusset plate edge stiffener model were developed. The following

conclusions can be drawn regarding the modeling of gusset plate behaviour under cyclic loading:

- Since the elastic – perfect plastic material model lead to better results under monotonic tension loading, and since the effect of material model on ultimate compressive load was not significant, the elastic – perfect plastic material model was deemed to be most appropriate for modeling cyclic behaviour.
- Using the elastic – perfect plastic material model along with flexible framing members, a 2 mm quarter sine wave initial imperfection and full splice member restraint, the behaviour of gusset plates under cyclic loading was accurately predicted.
- The use of a bolt slip fastener model was demonstrated to work well for modeling the behaviour of a cyclically loaded gusset plate for a couple of cycles. However, in its current form, the bolt slip model was not considered practical for modeling an entire load displacement hysteresis.

For the parametric study, the finite element models developed in the first phase were expanded to include brace members. The effects of gusset plate – brace member interaction and load sequence on monotonic and cyclic gusset plate behaviour were investigated in this phase. The following conclusions can be drawn based on the results of the parametric study:

- The effect of load sequence (i.e. tension first vs. compression first) on the gusset plate axial load versus displacement hysteresis envelope is small.

- The effects of repeating cycles at each displacement increment are: (1) a small deterioration in the peak compressive and tensile loads with each cycle, and (2) softening of the reloading (compression to tension) portion of the cycle. This results in a decrease in the energy dissipated with each cycle at a given displacement.
- Monotonic load versus displacement plots tended to delineate the cyclic load versus displacement hysteresis envelope.
- The effect of brace member stiffness on the gusset plate load versus displacement hysteresis is small when the gusset plate is the weak element. Gusset plate load versus displacement hysteresis plots can, however, deviate significantly from the "no brace" hysteresis when the brace member buckles or yields.
- Subassemblies for which the brace member is the weak element dissipate less energy than those for which the gusset plate is the weak element (at least in the displacement range studied). In general, hysteresis plots for the weak gusset – strong brace member models exhibited less pinching and sustained higher post buckling compressive loads than the conventionally designed subassemblies.

6.3 Recommendations.

The following recommendations can be made based on the results of this investigation:

- The following improvements could be made to the modeling procedure: (1) the results could be improved with the use of an "effective" material model to account for parameters not considered in these gusset plate models such the loss of gusset plate

material at the bolt hole locations, (2) the friction effects due to in-plane clamping could be modeled, and (3) initial imperfection measurements could be made on actual gusset plate specimens. Before such efforts are undertaken, however, consideration should be given to what benefit they would be to our general understanding of the cyclic behaviour of gusset plates.

- In this study, subassemblies were cycled until displacements similar to those achieved in the Rabinovitch and Cheng (1993) tests were reached. To compare the behaviour of weak gusset – strong brace subassemblies with conventional subassemblies over their full range of usefulness, a rational failure criterion would need to be developed for both elements (the gusset plate and the brace member).
- The parametric study should be expanded to include stiffeners. Rabinovitch and Cheng (1993) demonstrated that free edge stiffeners improve the cyclic behaviour of gusset plates. The inclusion of these stiffeners should improve the behaviour of subassemblies designed with the weak gusset – strong brace member concept.
- Cyclic loading tests should be conducted on gusset plate – brace member subassemblies similar to those modeled in this investigation to verify the findings of the parametric study.
- Efforts should be made to develop a simple gusset plate model to facilitate an investigation into the effects of gusset plate behaviour on overall frame behaviour.

7. REFERENCES

Astaneh-Asl, A., Goel, S.C., and Hanson, R.D., 1981. "Behaviour of Steel Diagonal Bracing." ASCE Conference, October 26-31, St. Louis, Missouri.

ATC (1992). Guidelines for Cyclic Seismic Testing of Components of Steel Structures. Report No. 24m Applied Technology Council, Redwood City, Ca.

Bjorhovde, R., 1972. "A Probabilistic Approach to Maximum Column Strength." Proceedings, ASCE Conference on Safety and Reliability of Metal Structures.

CAN/CSA-S16.1-94. 1995. Limit States Design of Steel Structures. Canadian Standards Association, Rexdale, Ontario.

Chakrabarti, S.K. and Bjorhovde, R., 1983. "Tests of Full Size Gusset Plate Connections." Research Report, Department of Civil Engineering, University of Arizona-Tucson, Arizona.

Davis, C.S., 1967. "Computer Analysis of the Stresses in a Gusset Plate." Thesis presented to the University of Washington, in Seattle, in partial fulfillment of the requirements for the degree of Masters of Science.

Gross, J.L., 1990. "Experimental Study of Gusseted Connections." Engineering Journal, AISC, Vol. 27, No. 3, Third Quarter, pp. 89-97.

Hardash, S.G. and Bjorhovde, R., 1984. "Gusset Plate Design Utilizing Block-Shear Concepts." Research Report, Department of Civil Engineering, University of Arizona-Tucson, Arizona.

Hardin, B.O., 1958. "Experimental Investigation of the Primary Stress Distribution in the Gusset Plates of a Double Plane Pratt Truss Joint with Chord Splice at the Joint." University of Kentucky Engineering Experiment Station, Bulletin No. 49.

Hibbitt, Karlsson and Sorenson Inc. 1995. "ABAQUS/Standard." User's Manual Volumes I and II, Version 5.5m Oatucket, R.I..

Hu, S.Z. and Cheng, J.J.R, 1987. "Compressive Behaviour of Gusset Plate Connections." Structural Engineering Report No. 153, Department of Civil Engineering, University of Alberta, Edmonton, Alberta.

Irvan, W.G., 1957. "Experimental Study of Primary Stresses in Gusset Plates of a Double Plane Pratt Truss." Bulletin No. 49, University of Kentucky Engineering Experiment Station.

Jain. A.K.. Goel. S.C.. and Hanson. R.D.. 1978. "Inelastic Response of Restrained Steel Tubes." Journal of the Structural Division. Proceedings of the American Society of Civil Engineers. Vol. 104. ST6. pp. 897-910.

Kulak. G.L.. Fisher. J.W.. and Struik. J.H.A.. 1987. Guide to Design Criteria for Bolted and Riveted Joints. John Wiley and Sons. Second Edition. New York.

NRCC. 1995. National Building Code of Canada 1995. Associate Committee on the National Building Code. National Research Council of Canada. Ottawa. Ontario.

Rabinovitch. J.S. and Cheng. J.J.R.. 1993. "Cyclic Behaviour of Steel Gusset Plate Connections." Structural Engineering Report No. 191. Department of Civil Engineering. University of Alberta. Edmonton. Alberta.

Redwood. R.G. and Jain. A.K.. 1992. "Code Provisions for Seismic Design for Concentrically Braced Steel Frames." Canadian Journal of Civil Engineering. April. pp. 1025-1031.

Thornton. W.A.. 1984. "Bracing Connections for Heavy Construction." Engineering Journal. AISC. Vol. 21. No.3. pp. 139-148.

Varsarelyi. D.D.. 1971. "Tests of Gusset Plate Models." Journal of the Structural Division. Proceedings of the American Society of Civil Engineers. February. pp. 665-678.

Wallaert. J.J. and Fisher. J.W.. 1965. "Shear Strength of High-Strength Bolts." Journal of the Structural Division. Proceedings of the American Society of Civil Engineers. Vol. 91. ST3. pp. 99-125.

Whitmore. R.E.. 1952. "Experimental Investigation of Stresses in Gusset Plates." Bulletin No. 16. Engineering Experiment Station. University of Tennessee.

Williams. G.C. and Richard. R.M.. 1986. "Steel Connection Design Based on Inelastic Finite Element Analysis." Report of the Department of Civil Engineering and Engineering Mechanics. The University of Arizona.

Yam. C.H.M. and Cheng. J.J.R.. 1993. "Experimental Investigation of the Compressive Behaviour of Gusset Plate Connections." Structural Engineering Report No. 194. Department of Civil Engineering. University of Alberta. Edmonton. Alberta.

8. APPENDIX

Included in this chapter are the axial load versus out-of-plane displacement hysteresis plots for the models investigated in the parametric study. Figures A.1 to A.6 show the hysteresis plots for the gusset plate only (no brace member) models. Figures A.7 to A.24 show the hysteresis plots for the gusset plate – brace member subassembly models.

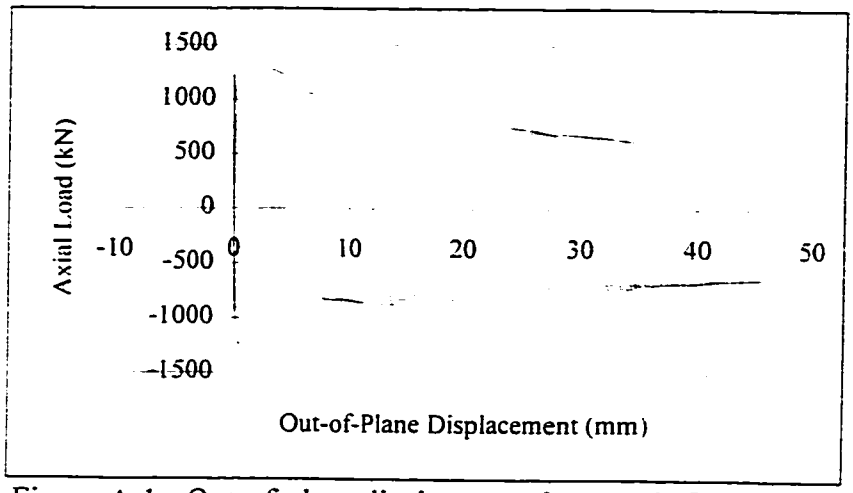

Figure A.1 - Out-of-plane displacement hysteresis for GP2LS1.

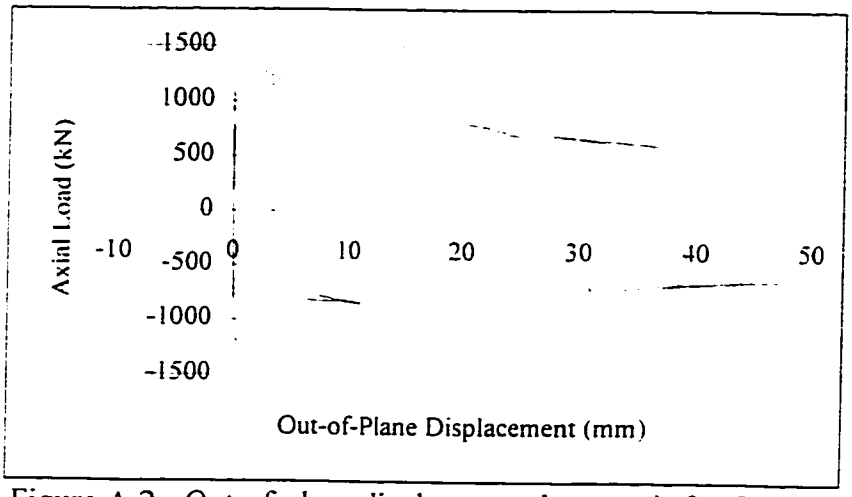

Figure A.2 - Out-of-plane displacement hysteresis for GP2LS2.

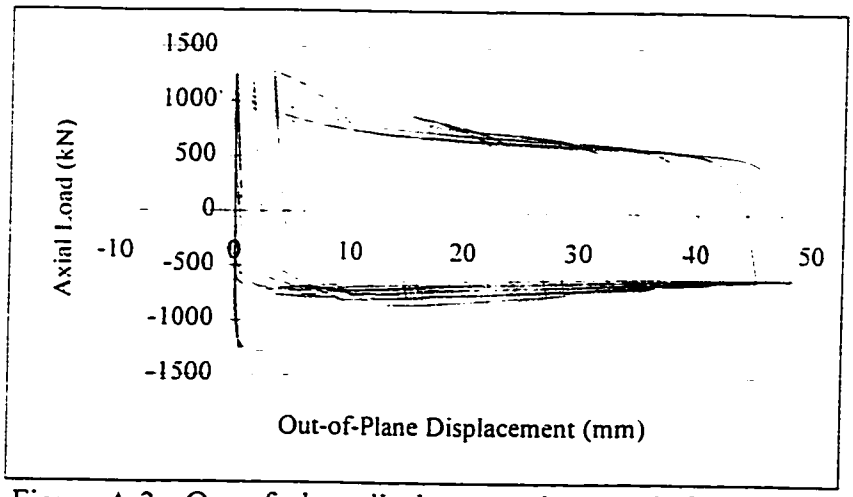

Figure A.3 - Out-of-plane displacement hysteresis for GP2LS3.

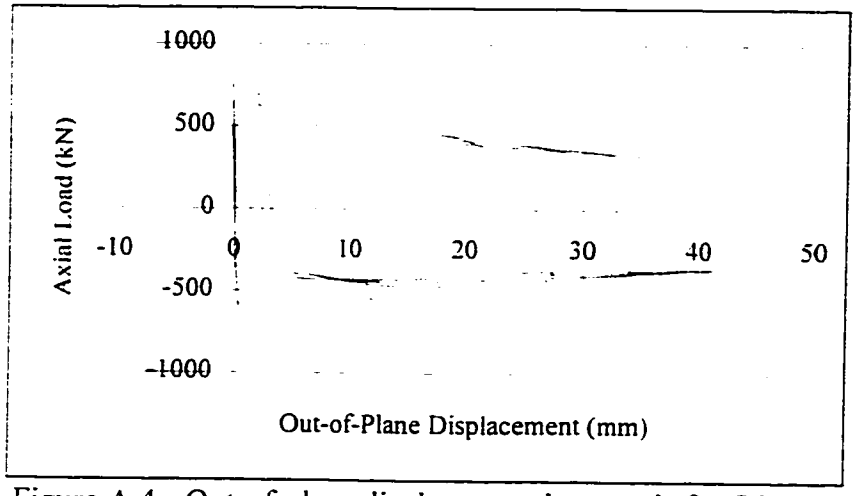

Figure A.4 - Out-of-plane displacement hysteresis for GP1LS1.

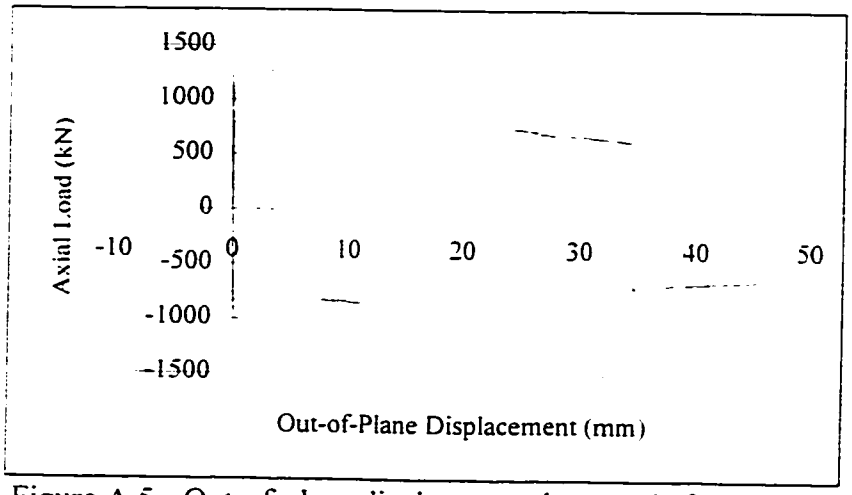

Figure A.5 - Out-of-plane displacement hysteresis for GP2LS1.

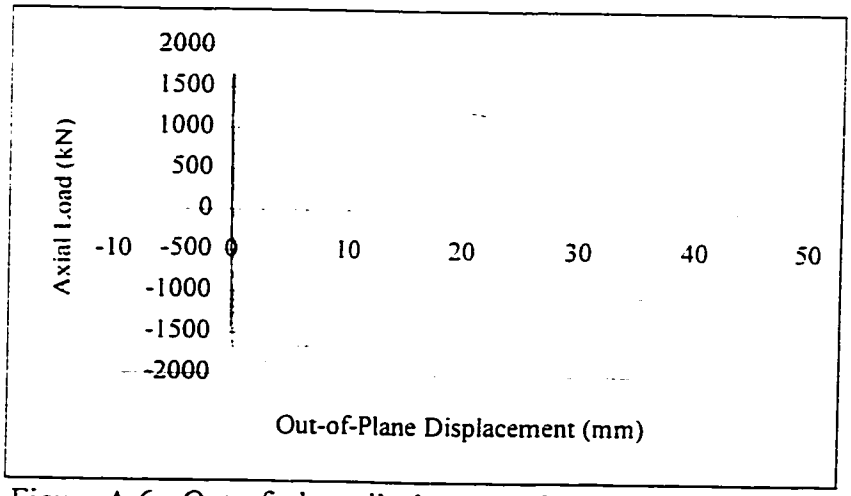

Figure A.6 - Out-of-plane displacement hysteresis for GP3LS1.

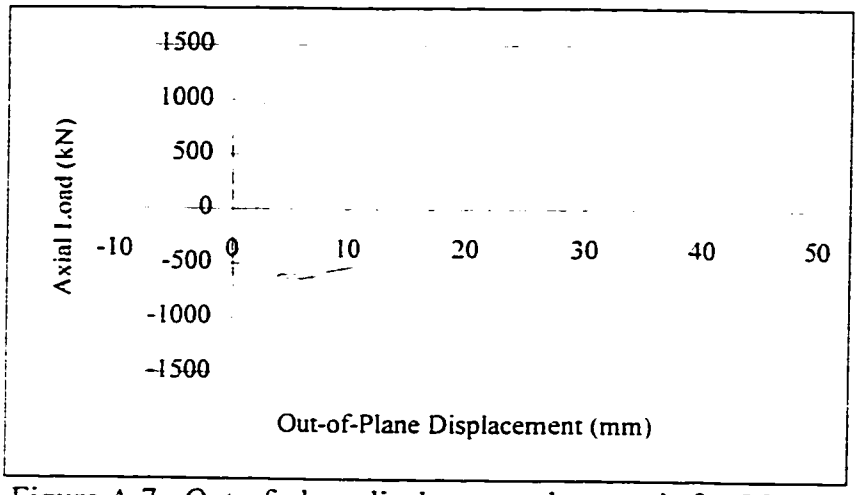

Figure A.7 - Out-of-plane displacement hysteresis for GP2B5LS1.

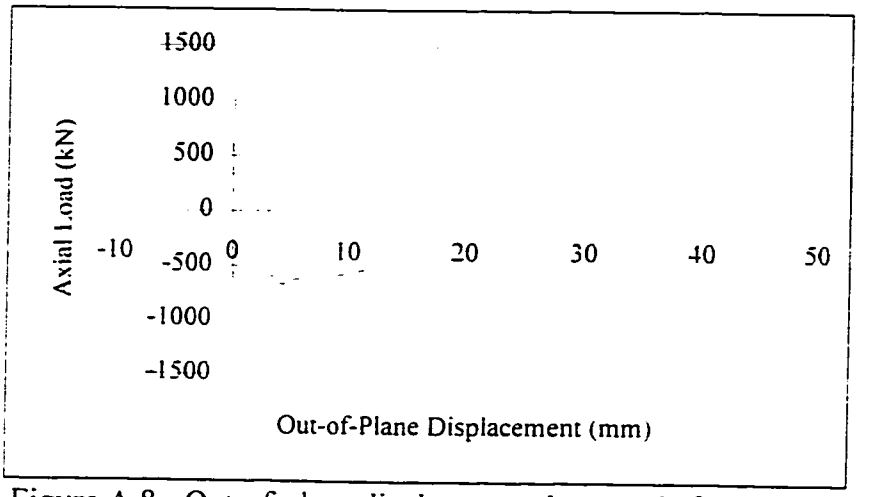

Figure A.8 - Out-of-plane displacement hysteresis for GP2B5LS2.

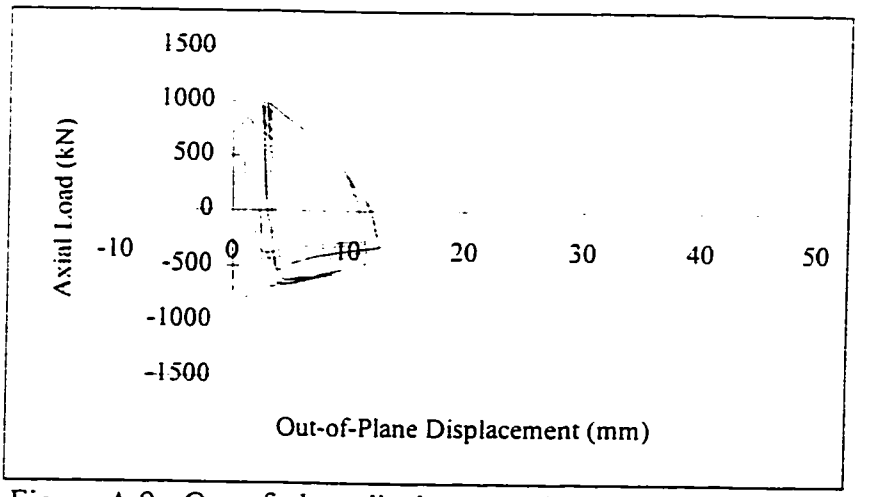

Figure A.9 - Out-of-plane displacement hysteresis for GP2B5LS3.

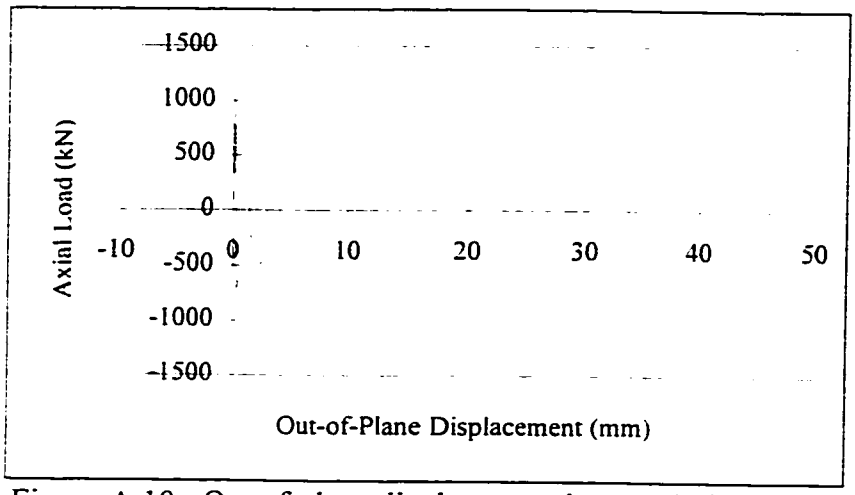

Figure A.10 - Out-of-plane displacement hysteresis for GP2B6LS1.

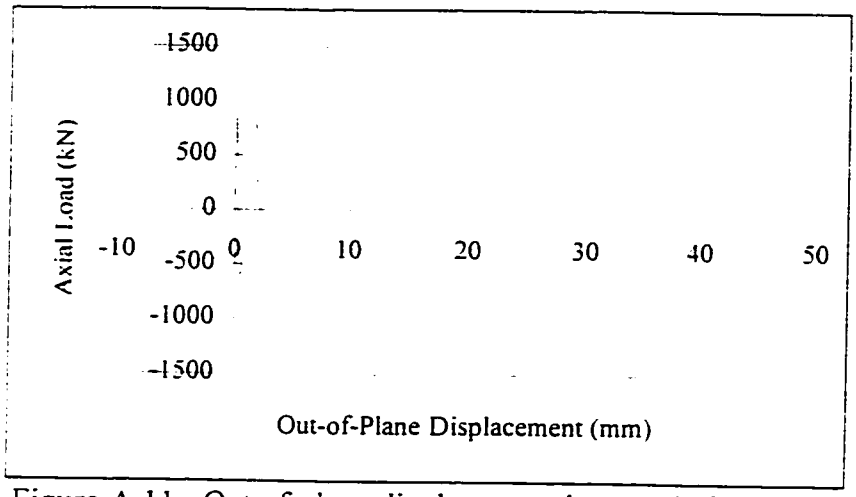

Figure A.11 - Out-of-plane displacement hysteresis for GP2B6LS2.

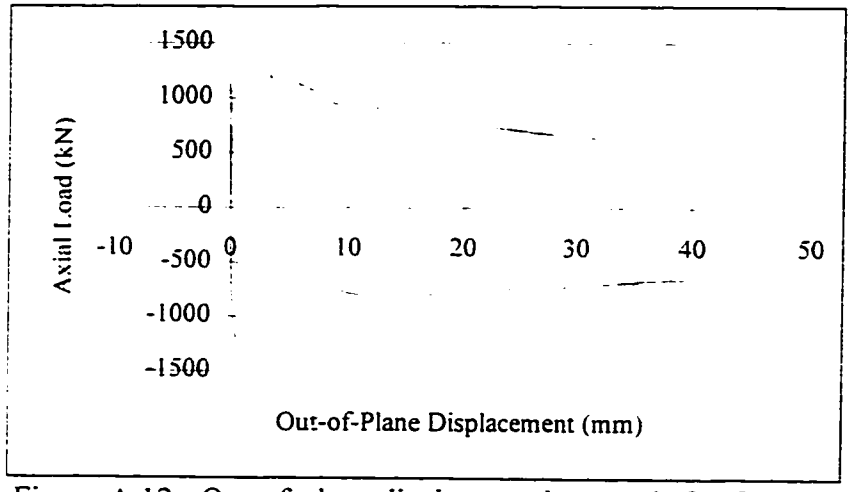

Figure A.12 - Out-of-plane displacment hysteresis for GP2B7LS1.

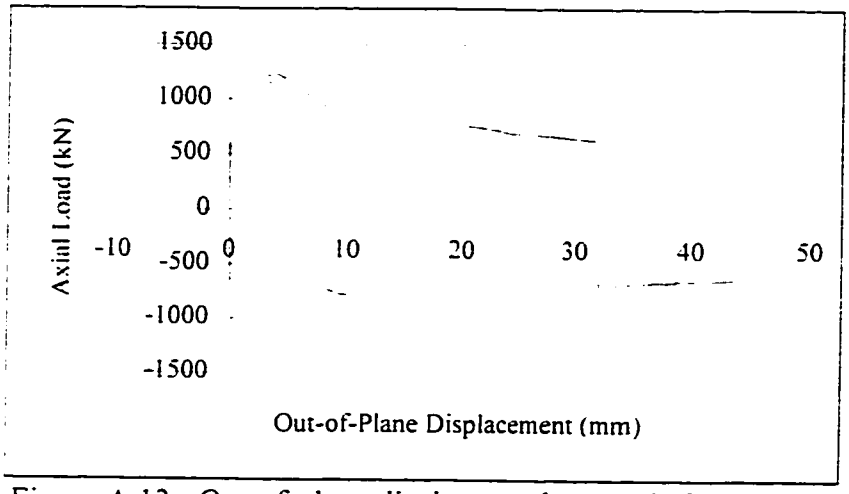

Figure A.13 - Out-of-plane displacment hysteresis for GP2B7LS2.

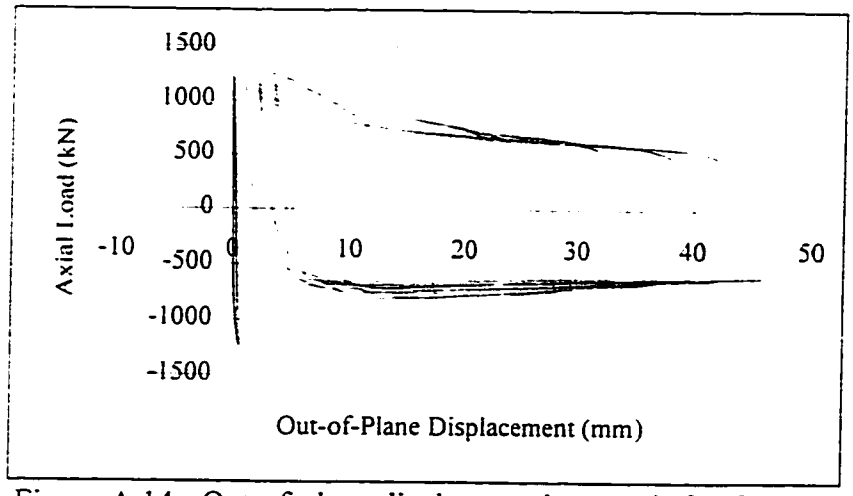

Figure A.14 - Out-of-plane displacment hysteresis for GP2B7LS3.

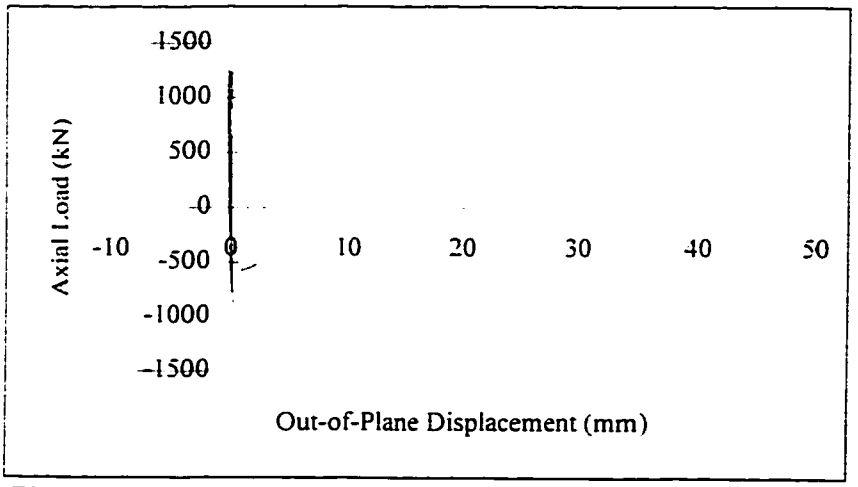

Figure A.15 - Out-of-plane displacment hysteresis for GP2B8LS1.

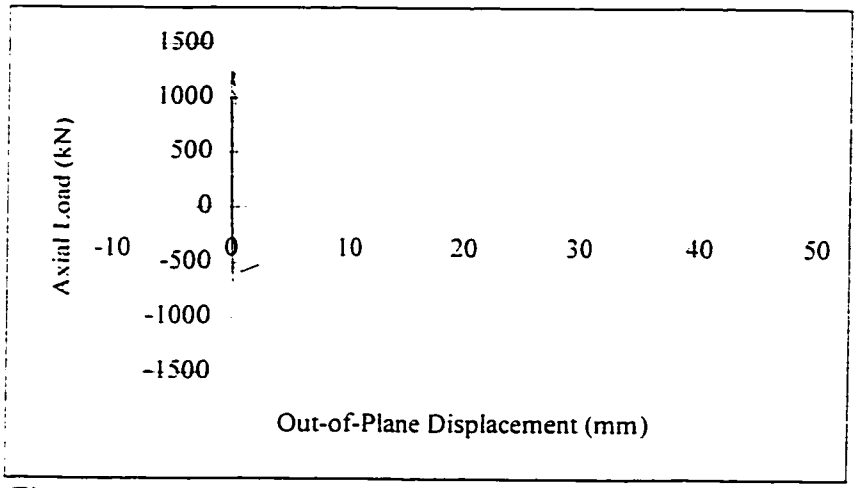

Figure A.16 - Out-of-plane displacment hysteresis for GP2B8LS2.

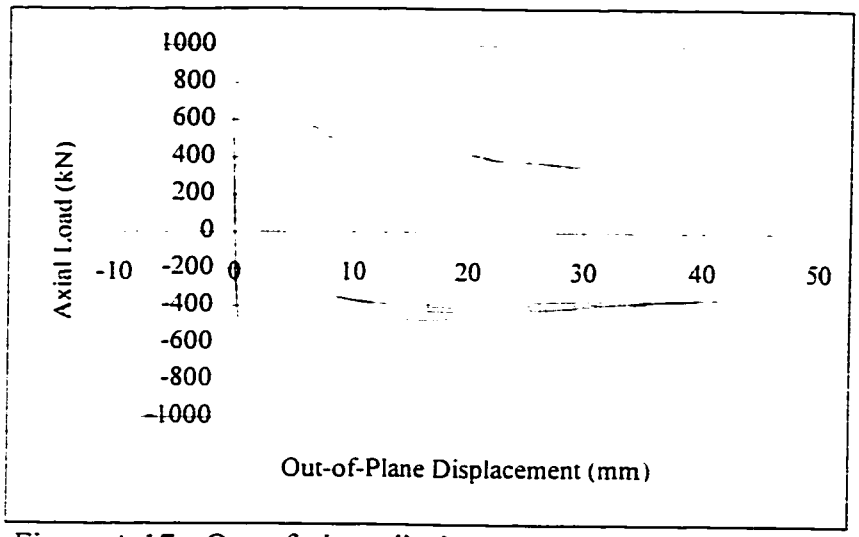

Figure A.17 - Out-of-plane displacement hysteresis for GP1B1LS1.

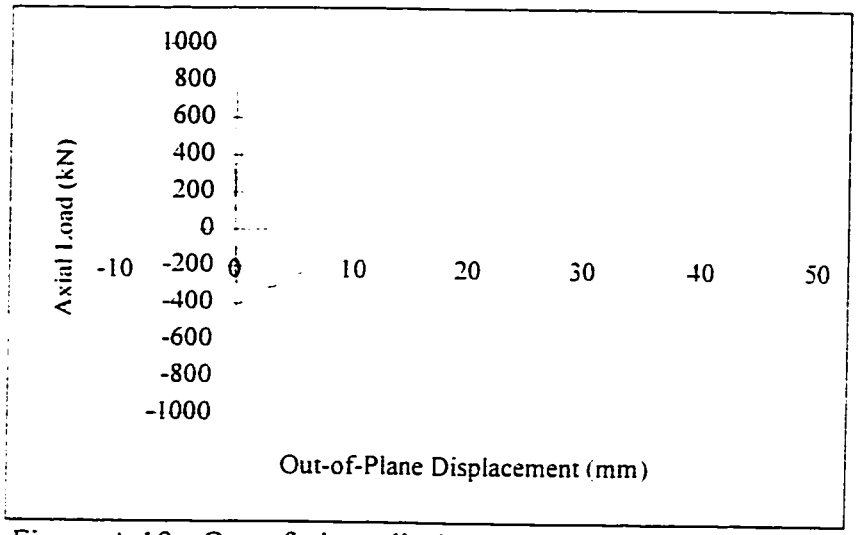

Figure A.18 - Out-of-plane displacement hysteresis for GP1B2LS1.

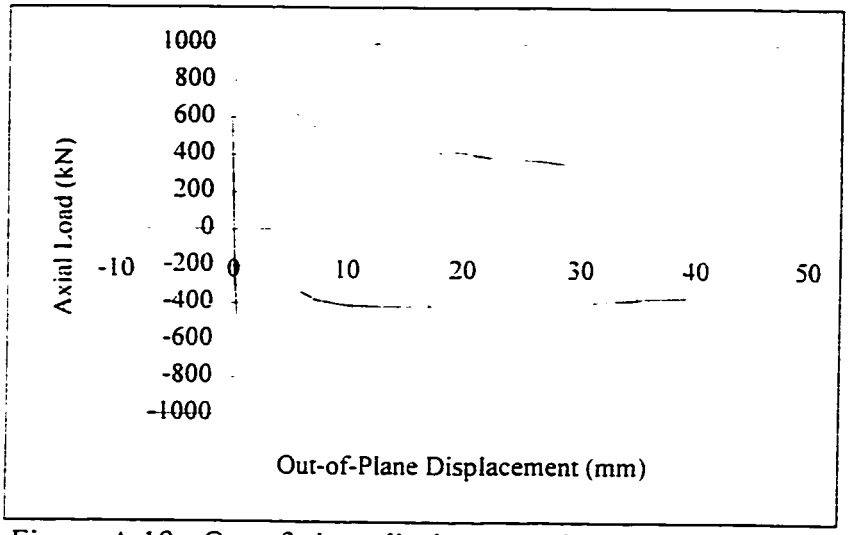

Figure A.19 - Out-of-plane displacement hysteresis for GP1B3LS1.

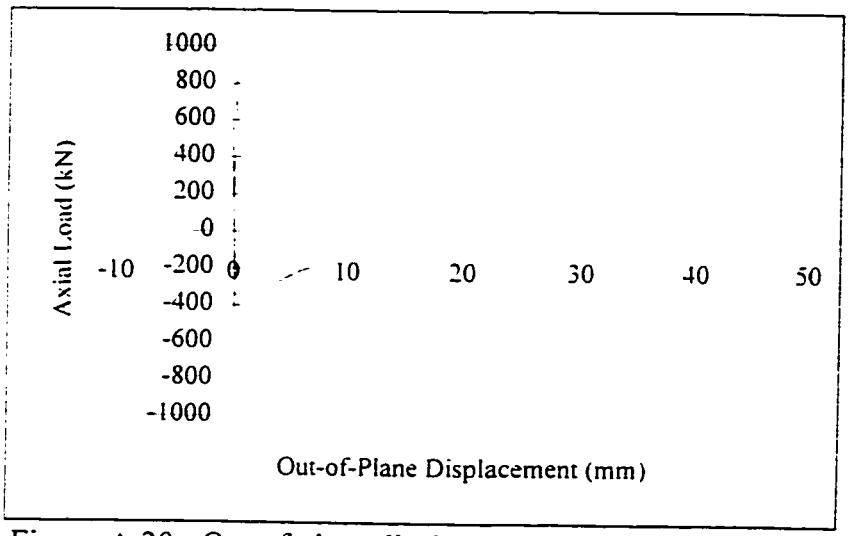

Figure A.20 - Out-of-plane displacement hysteresis for GP1B4LS1.

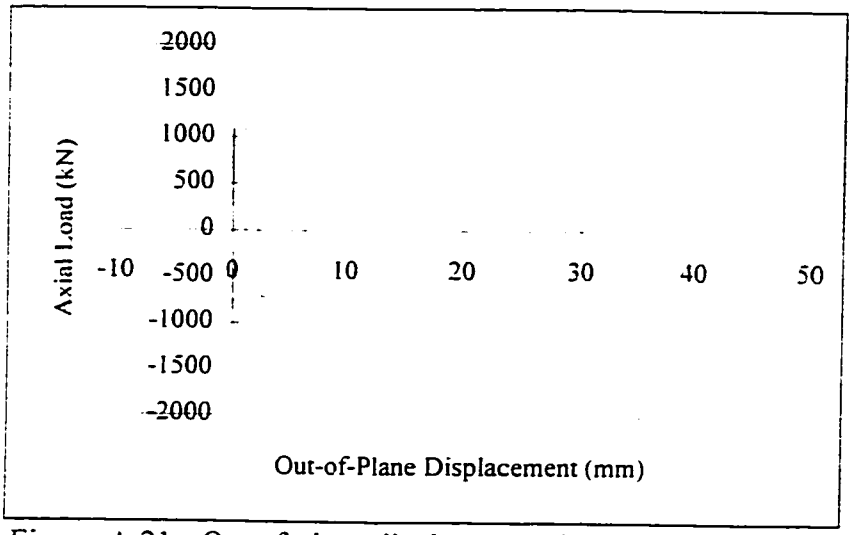

Figure A.21 - Out-of-plane displacement hysteresis for GP3B9LS1.

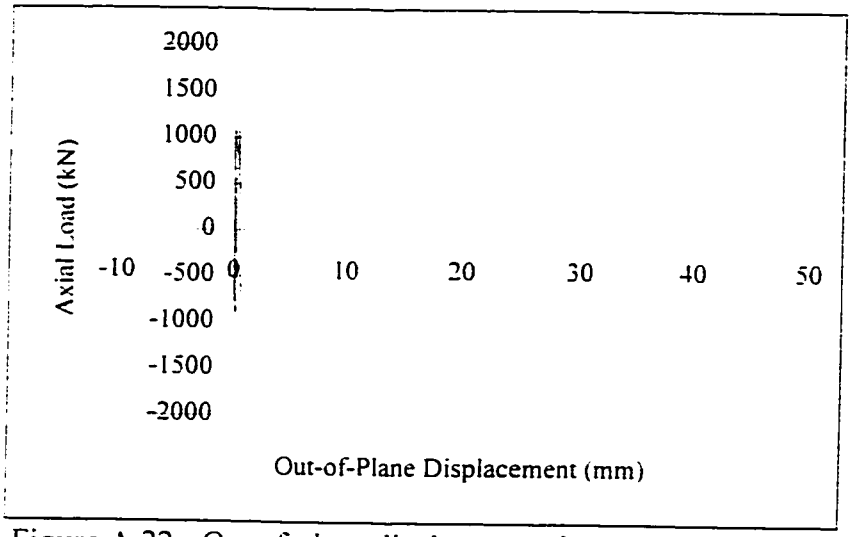

Figure A.22 - Out-of-plane displacement hysteresis for GP3B10LS1.

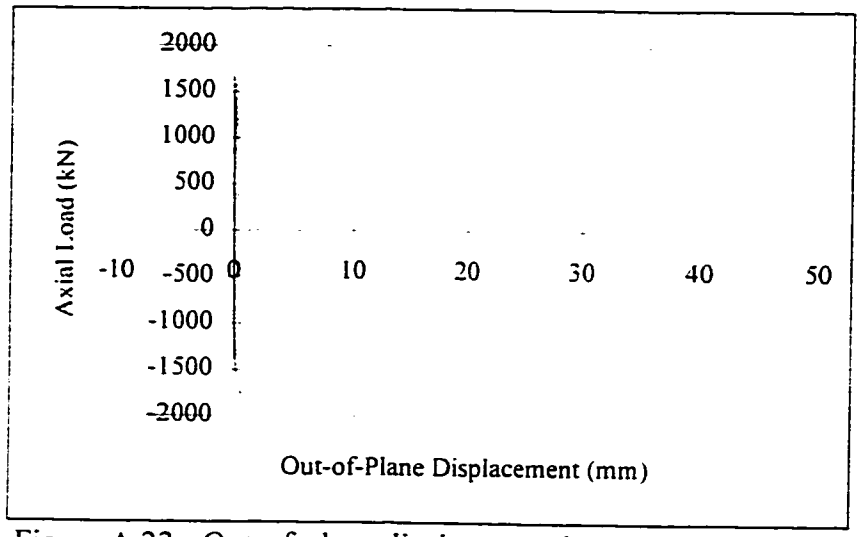

Figure A.23 - Out-of-plane displacement hysteresis for GP3B11LS1.

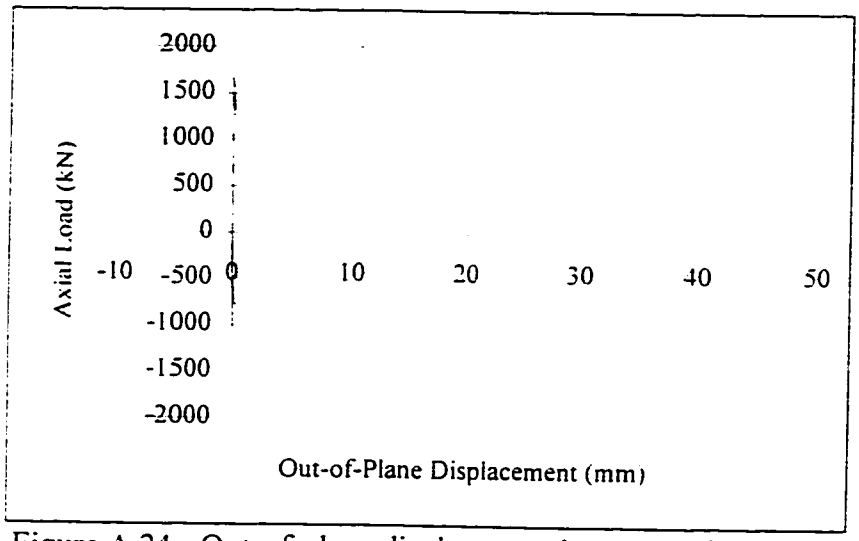

Figure A.24 - Out-of-plane displacement hysteresis for GP3B12LS1.

IMAGE EVALUATION
TEST TARGET (QA-3)

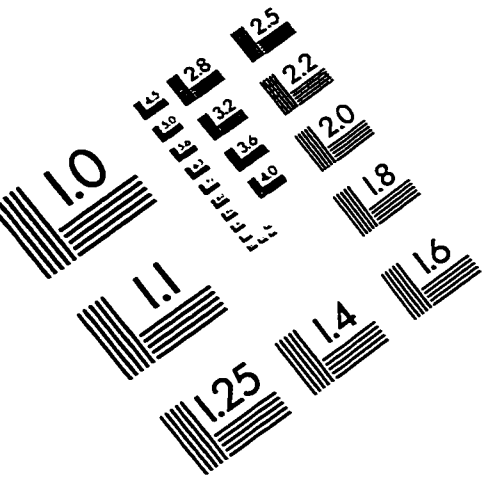

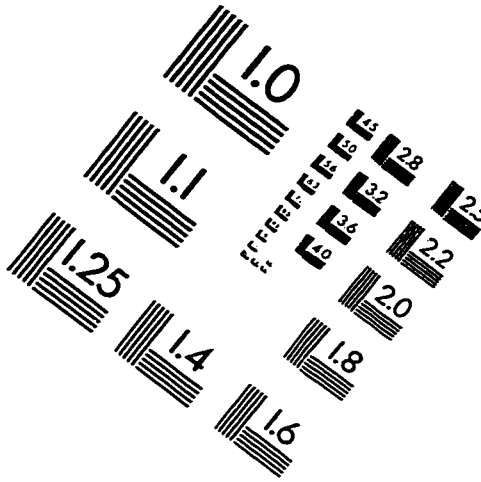

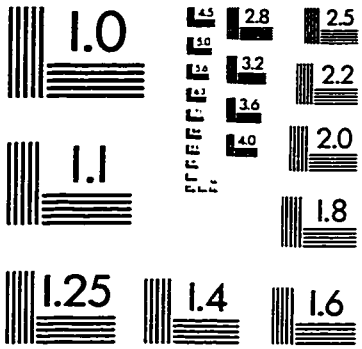

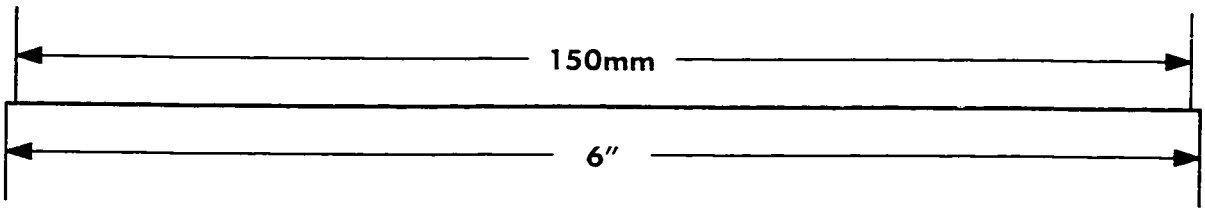

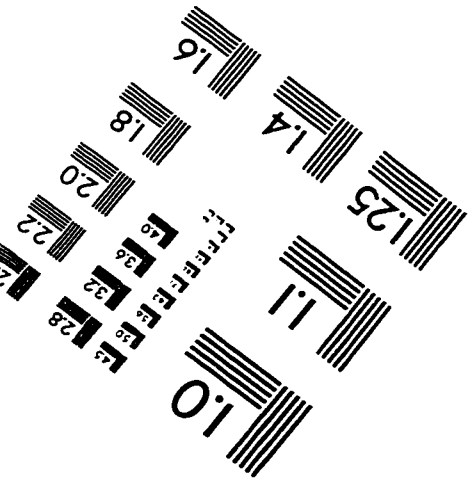

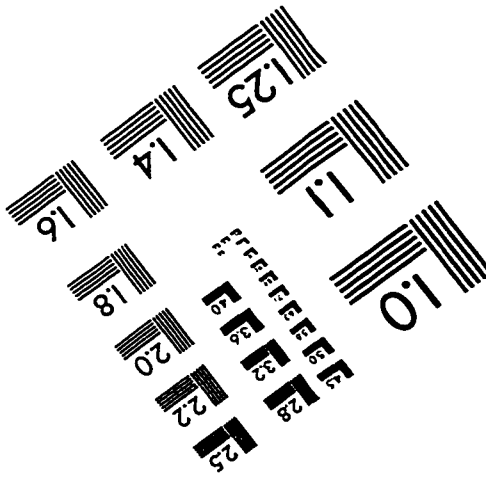

APPLIED IMAGE, Inc
1653 East Main Street
Rochester, NY 14609 USA
Phone: 716/482-0300
Fax: 716/288-5989